UNIVERSITÀ DI FOGGIA

Dipartimento di Scienze Agrarie, degli Alimenti e dell'Ambiente

Doctoral Thesis in
Management of Innovation in the Agricultural and Food Systems of the Mediterranean Region
– XXXI cycle –

Innovative and non-destructive technologies to evaluate quality of rocket leaves for ready to eat salads

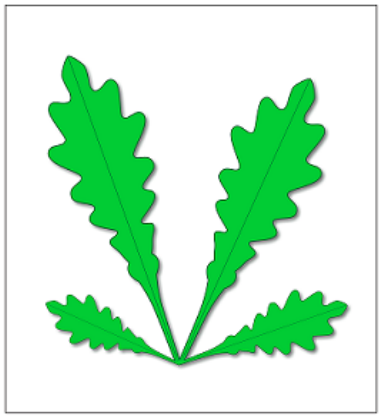

Candidate:
Muhammad Mudassir Arif Chaudhry

Tutor:
Dr. Maria Luisa Amodio

UNIVERSITÀ DI FOGGIA

Dipartimento di Scienze Agrarie, degli Alimenti e dell'Ambiente

Doctoral Thesis in
Management of Innovation in the Agricultural and Food Systems of the Mediterranean Region
– XXXI cycle –

Innovative and non-destructive technologies to evaluate quality of rocket leaves for ready to eat salads

Candidate:
Muhammad Mudassir Arif Chaudhry

Tutor:
Dr. Maria Luisa Amodio

UNIVERSITÀ DI FOGGIA

Dipartimento di Scienze Agrarie, degli Alimenti e dell'Ambiente

Doctoral Program in Management of Innovation in the Agricultural and Food Systems of the Mediterranean Region
– XXXI cycle –

Doctoral thesis on **"Innovative and non-destructive technologies to evaluate quality of rocket leaves for ready to eat salads"** discussed at the Universita di Foggia, 25 June, 2019

Candidate:
Muhammad Mudassir Arif Chaudhry

Tutor:
Dr. Maria Luisa Amodio (*Universita di Foggia, Italy*)

Committee members:

Prof. Antonio Ippolito (*Università degli Studi "Aldo Moro" di Bari*)

Prof. Stella Novella (*Università degli Studi della Basilicata*)

Prof. Ingunn Burud (*Norwegian University of Life Sciences*)

ACKNOWLEDGEMENT

I pay my deepest gratitude to the God Almighty who is the entire source of all knowledge and wisdom bestowed to mankind and who granted me the strength and the composure to complete my research and thesis.

First and foremost, I feel utmost pleasure to express my heartiest gratitude at deep sense of obligation to my supervisor **Dr. Maria Luisa Amodio**, Department of the Science of Agriculture, Food and Environment (SAFE), Università degli studi di Foggia, Italy under whose dynamic supervision, vital instructions, skillful guidance, constructive criticism, affection and kind sympathetic attitude, I am able to complete this difficult task quite easily.

I offer my sincere appreciation and thanks on the contribution of **Prof. Giancarlo Colelli,** Department of the Science of Agriculture, Food and Environment (SAFE), Università degli studi di Foggia Italy, who can never be forgotten to create comfortable and friendly behavior and for his valuable suggestions and guidance for completion of my research work.

I cannot forget my sincere friends who helped me at the first day in my university as well as throughout my degree program, **José Manuel Amigo Rubio**, Associated Professor, Department of Food Science, University of Copenhagen. I am very thankful to my friends for their support, cooperation and guidance, prayers, encouragement and love during all my study period, whenever I need May Almighty Allah bless all above mentioned persons and reward them the best returns for their piousness (Ameen).

Finally, I must express my very deep gratefulness to my parents, Brothers, Sisters and to my teachers for providing me with trustworthy support and unceasing encouragement during my years of study and through my research work. This accomplishment would not have been possible without them.

Muhammad Mudassir Arif Chaudhry,
PhD Course in Managing the Changes in Agricultural and Food Systems in the Mediterranean Area
Dipartimento di Scienze Agrarie, Degli Alimenti e Dell'Ambiente Universita di Foggia
Via Napoli 25, 71121 Foggia – Italy

Contents

PART I: INTRODUCTION

EXTENDED ABSTRACT

'Rocket' is a collective name to indicate many species of green leaves belonging to Brassicacea family and are significantly consumed in the Mediterranean countries either as stand-alone salads or mixed with other vegetables. They are well known for their pungent smell, bitter flavor and high nutritional value. Rocket leaves are commercially grown as perennial and annual species, the former known as perennial wall rocket also known as wild rocket (*Diplotaxis tenufolia(L.) DC.)* and the latter named annual garden rocket (*Eruca satvia Mill.*). The *Diplotaxis tenufolia* plant can achieve a height of 80 centimeters (cm) and is characterized by a tap root and lengthy leaves. A typical leaf of *Diplotaxis tenufolia* is fleshy, oblong and deeply lobed, possessing sharp apexes. On the other hand, *Eruca satvia Mill.* grows to achieve a height of 40 cm possessing lyrate-pinnatifid leaves, having an enlarged terminal lobe and smaller lateral lobes with a rosette shaped arrangement of the leaves. *Eruca satvia Mill.* species as compared to the *Diplotaxis tenufolia* possesses a thin tap root and is characterized by a rigid unbranched stem. Both the species manifest similar morphological and nutritive aspects possessing a characteristic bitter taste based on the account of glucosinolates present.

In the modern era, the consumer awareness regarding food safety, origins of the produce, nutritional value and demand for minimally processed fresh produce has led the food industry to explore rapid, reliable and cost effective methods for the evaluation of food products and their shelf-life since the conventional destructive analysis methods are time consuming, expensive, targeted and labor intensive. In this regard, non-destructive methods are gaining significant popularity which are assisting the food industry for the early fruits defect detection, fruits and vegetable classification on the basis of variety, maturity stage and origin and for the prediction of main internal constituents, mainly soluble solids and acids, and physical properties like firmness. On the industrial scale a significant weightage is given towards achieving fresh produce with superior quality in terms of vitamins, antioxidant activity, phenols and secondary metabolites.

Rising concerns regarding the nutritional composition led many research works to evaluate the feasibility of the spectral profiles in the visible near infrared range (Vis-NIR), near infrared range (NIR) and hyperspectral images (HSI) for prediction and mapping of desired compounds in fresh produce. It is important to mention that non-destructive techniques cannot completely replace the conventional

methods but can serve to assist these techniques saving time, expenses and labor. On the other hand, the non-destructive methods need no sample preparation once the model is developed making the prediction process quick. In this research work non-destructive techniques have been illuminated with respect to their potentiality in rocket leaves with special emphasis on hyperspectral imaging for the quality assessment of the fresh-cut rocket leaves accompanied by a basic introduction of the non-destructive image analysis techniques.

In the first research work the feasibility of using spectral profiles for the estimation of the shelf life of the rocket leaves was evaluated using a multivariate accelerated shelf life testing (MASLT) approach. Spectral changes over time were modeled by using principal component analysis (PCA) and as variation to the conventional method, partial least squares (PLS) method. Kinetic charts were built fitting the first principle component (PC1) and the first latent variable (LV1) scores versus time. In both cases, the kinetics were described by a first order reaction, and the model performance was evaluated by the R^2 values which ranged between 0.73 to 0.95 for samples stored at three different temperatures, one of them being the market temperature while the rest were categorized as accelerated temperatures which are usually higher than the market temperature. The cut-off value was calculated by judging the unacceptable spectra of samples at the accelerated temperature, as a result of which the shelf life of rocket leaves was estimated using the MASLT approach. The shelf life estimation was done using PCA based MASLT conventionally used as well as using a newly introduced methodology i.e. PLS based MASLT yielding encouraging results in both cases particularly in case of the PLS based MASLT.

On the other hand, since the literature regarding quality evaluation of rocket leaves or any other leafy vegetables over time shows that the potential of hyperspectral imaging in the visible and near infrared regions has not been investigated pursing the aim of prediction and mapping of internal constituents. Hence hyperspectral imaging data was evaluated employing Partial Least Squares regression (PLSR) for the prediction of Vitamin C, ascorbic acid (AA), dehydroascorbic acid (DHAA), antioxidant activity and phenols in wild rocket (*Diplotaxis tenuifolia*) over a storage span of 12 days at 5ºC. Hyperspectral images of the wild rocket leaves were acquired in the Vis-NIR (400-1000nm) and the NIR (900-1700nm) ranges using different data pretreatments and wavelength selection techniques. The model reliability was checked by the root mean square error (RMSE) and R^2 values. Among the predicted parameters Vitamin

C, AA, antioxidant activity and phenols were predicted satisfactorily in the NIR range. The prediction maps for the parameters were calculated to follow the changes over the storage period yielding more reliable results in the NIR range. All the results indicated that hyperspectral imaging combined with multivariate data possess the capability to provide reliable information regarding the shelf life estimation of the rocket leaves as well as for the prediction and mapping of the internal constituents.

Chapter 1

THE USE OF NON DESTRUCTIVE TECHNIQUES TO ASSESS NUTRITIONAL CONTENT OF FRUITS AND VEGETABLE

Maria L. Amodio, Muhammad M. A. Chaudhry, Giancarlo Colelli

Department of the Science of Agriculture, Food, and Environment, University of Foggia, Via Napoli 25, 71100 Foggia (Italy)

1. INTRODUCTION

The use of non-destructive methods is already widely developed for the early detection of fruit defects, for the classification of fruits and vegetable based on variety, maturity stage and origin and for the prediction of main internal constituents, mainly soluble solids and acids, and physical properties like firmness. In the last year, due to the increasing interest in nutritional compounds, different researches were conducted to study the feasibility of using non-destructive methods, mainly Middle, Near and Short Wavelength Infrared Spectroscopy for the prediction of nutritional compounds in fruits and vegetable. Among different classes of bioactive compounds, prediction models were developed for phenolics including anthocyanins, flavonoids and antioxidant activity in whole fruits and vegetables or in fruit extracts, and vitamin C or dietary fiber content in wheat. The advantage of using spectroscopic techniques even in the case in which better results are obtained preparing tissue extracts is still considerable, since the reference analytical methods normally require expensive equipment, people expertise and are time consuming. The latter may be the case of bigger fruits as summer squash or melons where the presence of a thick peel make difficult the internal prediction of nutritional constituents. On the other side, referring to compounds very sensitive to thermal or light degradation, when non-destructive techniques are applied on whole fruits and vegetables, the problem of the oxidation related to the process of extraction is over passed. Sample preparation time in this case greatly decreases and the requested time for the analysis is very short once a predictive model has been developed.

2. NON-DESTRUCTIVE TECHNIQUES FOR QUALITY EVALUATION OF FRUITS AND VEGETABLES

2.1. VIS-NIR spectroscopy

NIR spectroscopy is categorized among the simplest non-destructive techniques as it requires no sample preparation and permits several constituents to be measured simultaneously. NIR spectroscopy is based on the absorption of electromagnetic radiation in the wavelength range of 780–2500 nm (Huang et al., 2008). The sample is irradiated with a NIR source; as the irradiation passes through the sample, it gets absorbed and scattered causing a change in its spectral characteristics (McClure 2003; Cozzolino et al., 2006; Nicolai et al., 2007). This change is a function of the structure of the sample, the moisture content, the particle size, the temperature of the sample and, most importantly, of its chemical composition. The cell wall interfaces and suspended particles (mitochondria, chloroplasts and starch granules etc.) are one of the major causes of irradiation scattering in fruits and vegetables (McGlone et al., 1997; Lammertyn et al., 1998; Lammertyn et al., 2000; McGlone et al., 2002; Nicolai et al., 2007). Large sets of overtones and combination bands along with complex chemical composition result in highly convoluted NIR spectrum which, if properly elaborated, may allow to extract relevant information about the sample (Massart et al., 1988). The overtones can be considered as harmonics in which a series of absorptions are produced by every fundamental as a multiple of frequency. Factors such as tissue heterogeneity, instrumental noise, wavelength dependent scattering effects and ambient effects increase the complexity of the spectra.

To understand the concept of NIR one must be familiar with the phenomenon of energy absorption in the visible and mid-IR regions. The following Figure 1 shows the electromagnetic radiation spectrum of the visible, NIR and mid-IR region.

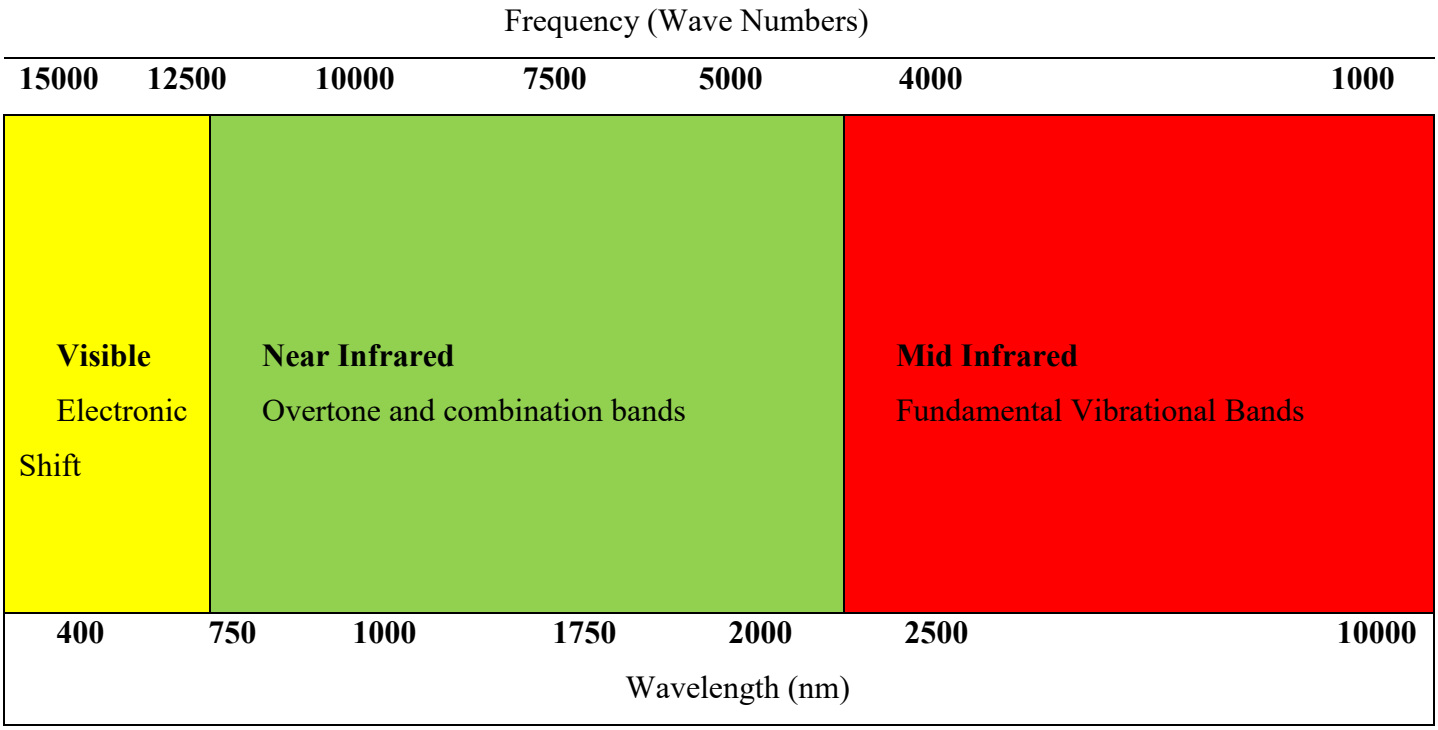

Figure 1. Electromagnetic radiation spectrum of the visible, NIR and mid-IR region.

When the light energy and the material come into contact, energy is absorbed at resonant frequencies due to atomic and molecular interactions; the electrons absorb energy and jump from a lower to higher orbit, in the visible region; energy is absorbed in the mid-IR region at the resonant frequencies by the bounded molecules who vibrate in different directions due to different movements as stretching, bending and rotation. Chemical bonds such as C-C, C-H, C-N, C-O, N-H and O-H can be suitably characterized by using the mid-IR region, after the sample is prepared to get sufficient light through it. Absorbance in the NIR spectra mostly occur due to the O-H (water, alcohol), N-H (protein) and C-H (oils, fats, hydrocarbons) chemical bonds whereas also some other bonds exhibit overtones in the region. The part of radiation that is not absorbed by the sample is in part reflected or transmitted; thus, depending on the instrument design and on the sample structure different applications using reflectance, transflectance, transmittance, and interactance may be developed.

For each acquisition mode, the position of the optical detector and the light source are different (see

Figure 2). In case of the reflectance mode, the detector captures the light reflected from the surface of the material and this technique is mostly utilized to detect the external quality features of the sample such as shape, size, color, texture and defects. This mode is advantageous when less penetration is required, for example, if the chemical to be analyzed lies just beneath the peel as in case of anthocyanin in blueberries. Diffuse reflectance infrared Fourier transform spectroscopy is used for powder samples without preparation.

The transflectance mode is used for the measurement of spectra of very thin and clear samples whose characteristics are very different from that of fruits and vegetables. A demonstration of the transflectance phenomenon is given in the Figure 2.

In transmittance mode, the internal information of the sample is acquired; the detector is placed in the opposite direction with respect to the light source to capture the light transmitted through the sample, hence detecting the concentration of materials or internal defects in the sample (Schaare and Fraser 2000). The region of 800-1100nm in the spectrum is usually utilized for diffuse transmission measurement acquisition.

The light source and the detector are parallel to each other in interactance mode, enhancing its capability to detect deeper information of the sample with reduced surface effects. Interactance is preferred over transmittance due to the reason that it is less effected by thickness of the sample as compared to the latter for which a special set up is also required for preventing specular reflection to enter into the detector (Nicolai et al., 2007).

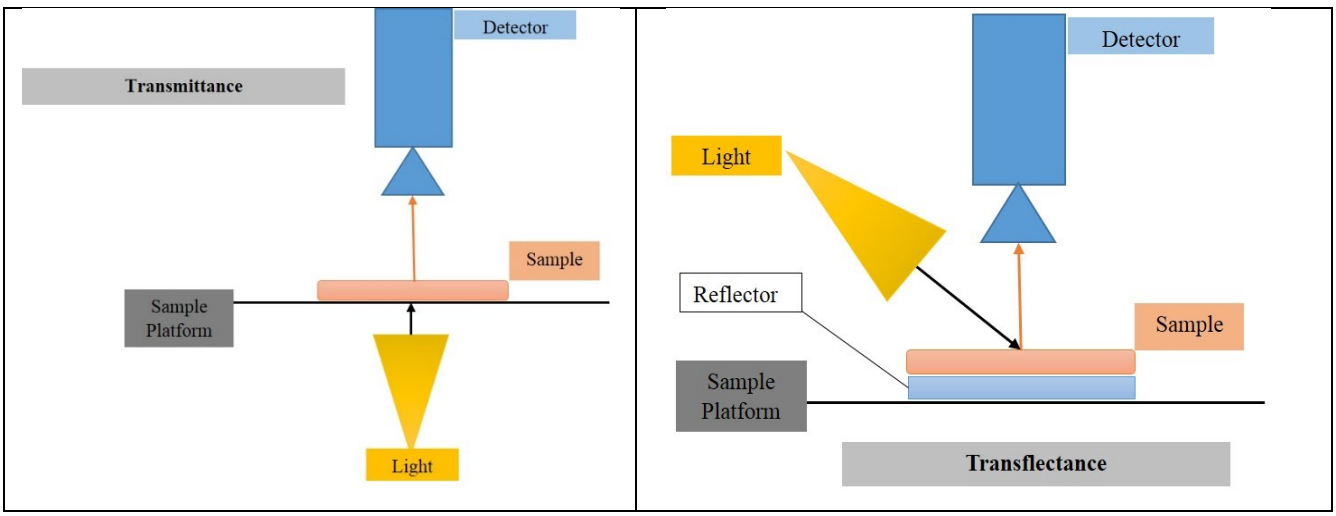

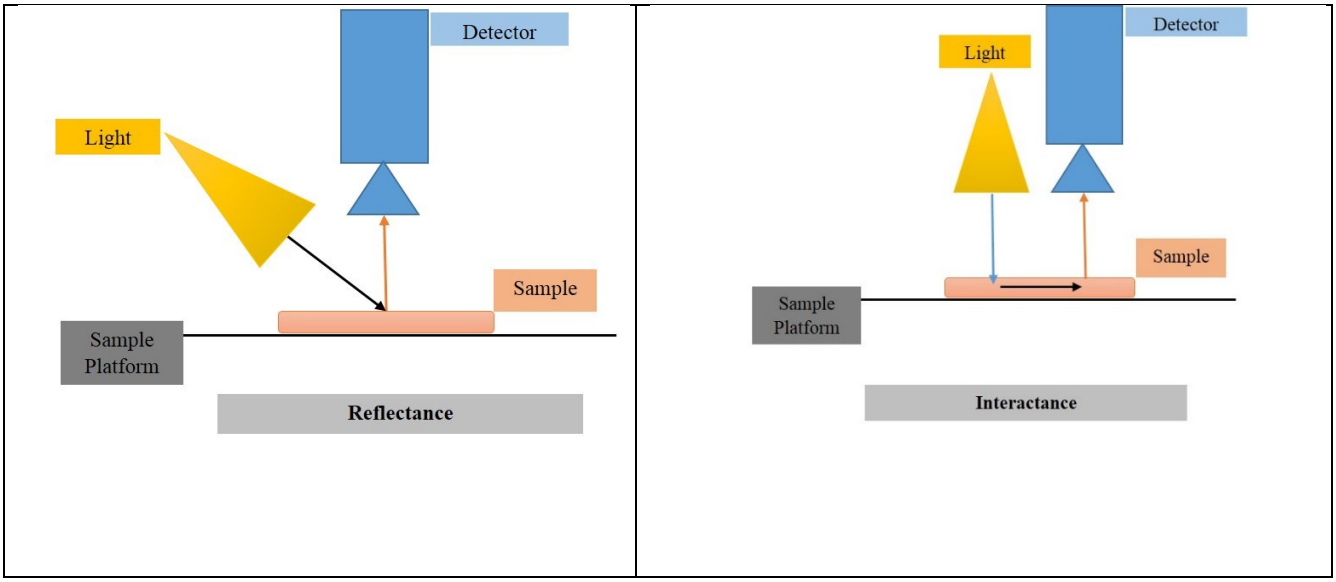

Figure 2: Examples of reflectance, transflectance, transmission and interactance configurations

2.2 Hyperspectral imaging

Hyperspectral imaging is a combination or integration of imaging and spectroscopic techniques for the quantitative prediction of physical and chemical characteristics of the food samples as well as their spatial distribution. Researchers working on the non-destructive analysis of food are interested in attaining spectral information, and spatial information, as to know a distribution of a quality attribute or of multi-constituents, or to detect small size objects not visible in the RGB. Out of these desired factors, spectroscopy if taken alone has the capacity to measure spectral and multi-constituent information only, whereas conventional imaging exclusively provides data regarding spatial information and detectability of objects with small size. Combined hyperspectral imaging serves to provide information of all the aforementioned factors simultaneously. The spectral measurement tells us 'what' is in the food sample, whereas, the image provides us the answer to the question 'where'; the hyperspectral image provides us the entire picture, i.e. 'what and where' at the same time (Wu and Sun 2013).

Hyperspectral images consist of a stack of images of the same object at different spectral wavelength bands, known as multispectral imaging, hyperspectral imaging and ultra-spectral imaging, according to the considered number of wavelengths (spectral range and resolution) (Ariana and Lu 2008). A spectral cube is a three dimensional cube that contains spectral and spatial information simultaneously. The

information of the wavelengths i.e. the spectral information, is contained in the form of voxels (vector pixels) and the spatial information exists in a two dimension-image of *x* rows and *y* columns Figure 3.

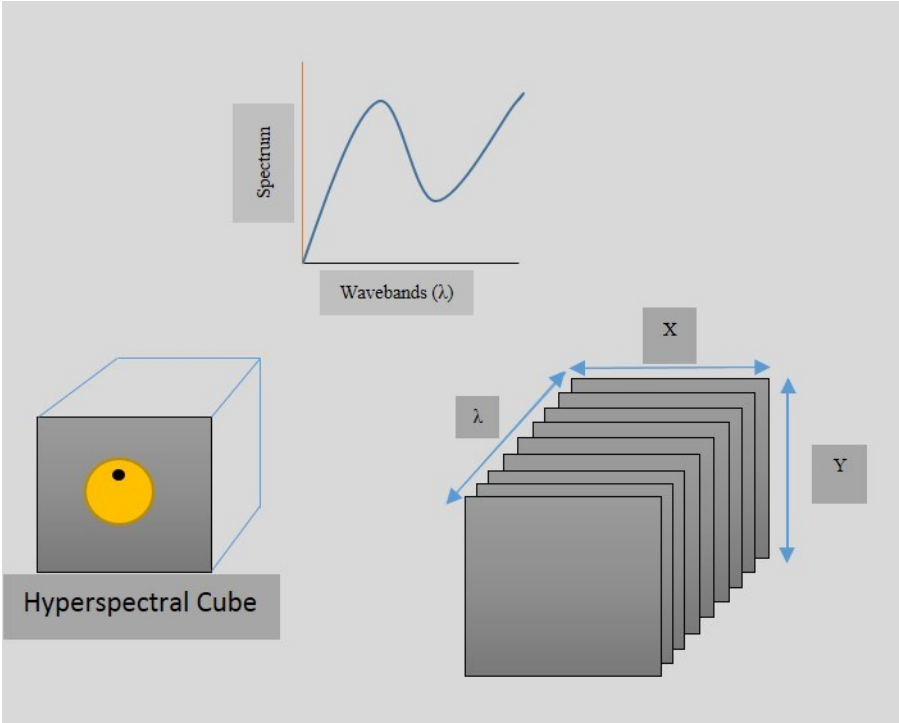

Figure 3. Example of hypercube showing the stack of λ images (dimension *x* x *y*).

In this hypercube, each spectral pixel corresponds to a spectral signature (or spectrum) of the corresponding spatial region, recording the entire measured spectrum of the imaged spatial points (Figure 4). Therefore, the measured spectrum indicates the ability of the sample in absorbing or scattering the exciting light, representing the inherent chemical properties of a sample. As a result, the technology provides us with unprecedented detection capabilities, which otherwise cannot be achieved with either imaging or spectroscopy alone. Hyperspectral imaging techniques have received much attention for food quality and safety evaluation and inspection. Many approaches and applications have shown the usefulness of hyperspectral imaging in the food industry (Sun 2010).

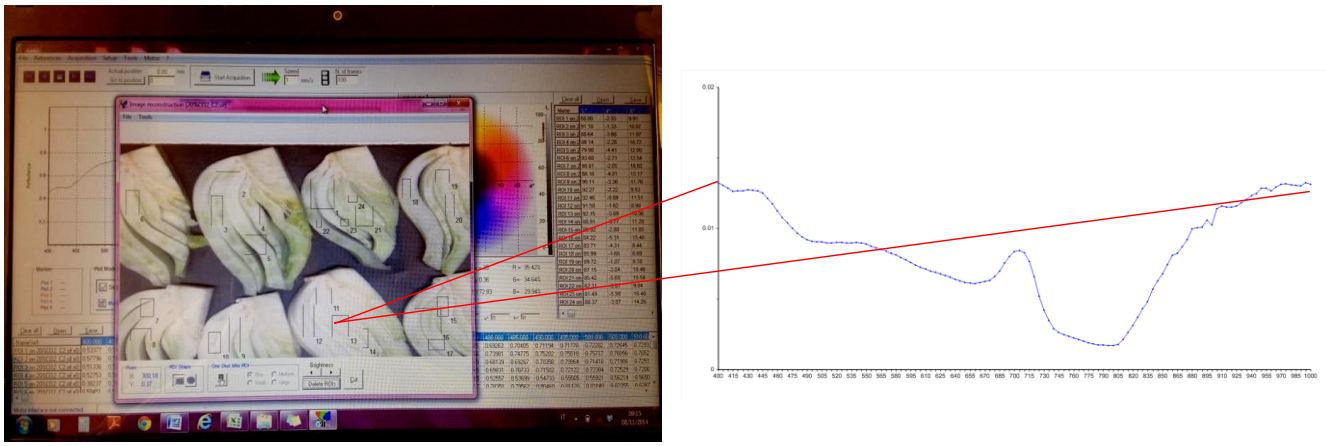

Figure 4. Reconstructed hyperspectral image and representation of the spectra extracted by a region of interest (by Amodio et al., unpublished).

The imaging instruments used for the hyperspectral imaging consist of a light source, a wavelength dispersion device, area detector and then a storing device for further processing. The light sources are different depending upon the type of samples to be tested and can be recognized as halogen lamps, light emitting diodes (LEDs) and lasers. Halogen lamps are mostly used to illuminate the Vis-NIR and NIR spectral regions. The light emitting diodes are considered to be an excellent light source due to low cost, small size, low energy consumption, low heat generation, robustness and insensitivity to vibration. Lasers are also used as a light source due to the reason that they are directional monochromatic light sources which are mostly used for the purpose of excitation in the application of fluorescence and Raman spectroscopic measurements. The tunable light sources allow the direct area scanning to obtain both spectral and spatial information of sample by setting the wavelength dispersion device in the illumination light path instead of the imaging light path.

The wavelength dispersion devices contain filter wheels, imaging spectrographs, tunable filters, Fourier transform imaging spectrometers and single shot imagers. The wavelength dispersion devices disperse the broadband light into different wavelengths. The light is efficiently transmitted by the bandpass filters at a particular wavelength whereas the light at the other wavelengths is eliminated. An imaging spectrograph most commonly operates in the line scanning mode (Figure 5), instantaneously disperses the broadband light into different wavelengths using a diffraction grating and generates a

spectrum for each point on the scanned line. Point scanning and area scanning are other examples of scanning mode (Figure 5). Detectors include charge coupled devices (CCD) detectors and complementary metal oxide semiconductor (CMOS) detectors. They quantify the intensity of the received light by converting the incident photons into the electrons (Wu and Sun 2013).

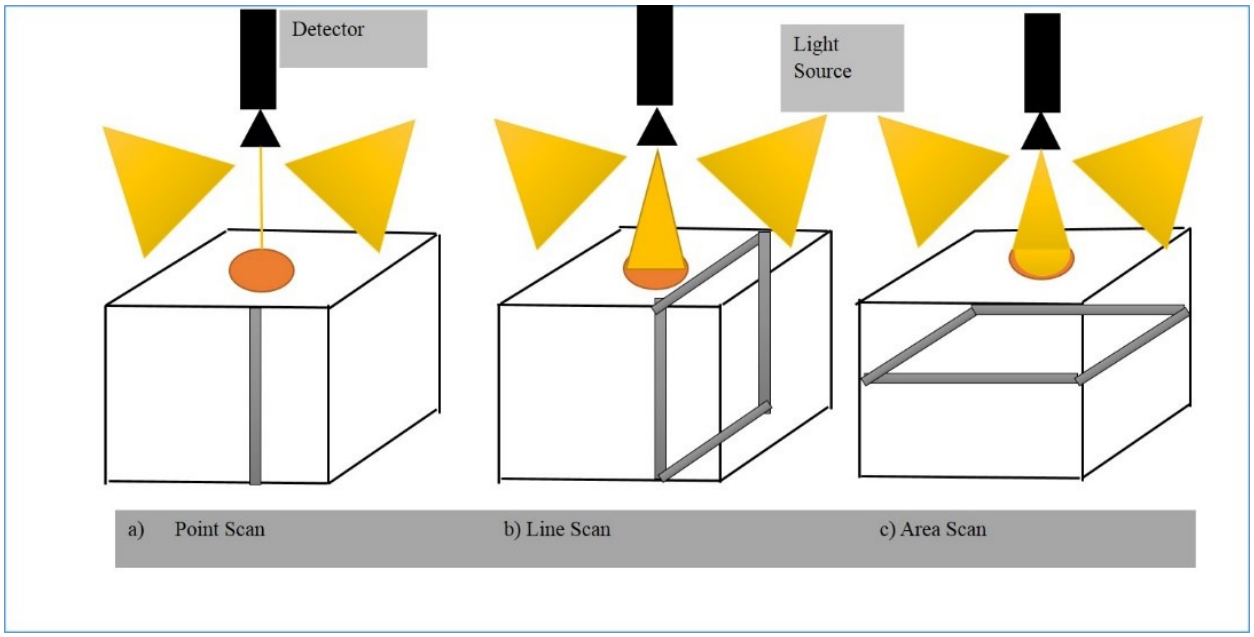

Figure 5. Types of scanning modality

Hyperspectral imaging technique has been used to detect defect and physiological disorders as bitter pit, bruises, surface defects and contaminations in apple fruits (Mehl et al., 2004; Peri et al., 2005; Xing et al., 2005;), and in pickling cucumber (Ariana and Lu 2010), for the citrus fruit inspection (Moltó et al., 2010.), to predict the sugar content distribution in melons (Sugiyama and Tsuta 2010), for measuring ripening of tomatoes (Polder and van der Heijden 2010), for quality evaluation of mushroom (Gowen et al., 2010.), to monitor ripening on banana (Rajkumar et al, 2012), to identify hidden bruise on kiwifruits and for many other applications requiring spatial information.

2.3 Chemiometric tools

The purpose of a NIR prediction model is to relate the spectral information of the learning samples to

their quality parameters as measured using a reference method. After the development and proper validation, the model can be used for further prediction of quality attributes of other unknown samples. The extraction of relevant information from the acquired spectra, requires a preliminary process to separate the chemical information from physical variations, obtained by applying mathematical pre-treatments of spectral signals. The spectroscopic signals usually contain 'noise' (unwanted effects) which may be due to instrumentation used for spectral acquisition, changes in various environmental factors and signal variations due to sample nature. The most commonly used pretreatments to remove scattering, are multiplicative scatter correction (MSC), Standard Normal Variate (SNV), and Detrend (DT) (Shenk and Westerhaus 1995; Heise and Winzen 2002; Naes et al., 2002; Nicolai et al., 2007) and derivatives (Savitzky and Golay 1964).

The next step is the development of a calibration equation to relate spectral to chemical features for the prediction of quality parameters of unknown samples (Williams and Sobering 1996; Guthrie et al., 2005; Guthire et al., 2006). This process involves regression techniques in addition to spectral pre-processing methods (Baardseth et al., 1996; Naes et al., 2002; McClure 2003; Cozzolino et al., 2006; Nicolai et al., 2007; Cozzolino et al., 2009).

The techniques used for this purpose include, Principal Component Analysis (PCA), linear regression methods for calibration development (Martens and Naes 1989; Burns and Ciurczak 2007) such as Multiple Linear Regression (MLR), the Principal Component Regression (PCR) and the Partial Least Squares (PLS) (Perez-Marin et al., 2007).

The Principal Component Analysis (PCA) is used to reduce the large multivariate data into limited number of independent factors (Buning-Pfaue 2003) providing information about the spectra population in terms of variables, sample distribution and abnormal sample detection. This technique is aimed to describe the maximum variability of the samples by reducing the information contained in all the variables to a limited number of principal components (PCs) which can be also used to detect sample outliers (samples with different spectral behavior).

Researchers prefer to involve controllable and easy-to-measure factors to elaborate, regulate, or predict the behavior of responses. MLR is used to convert data into information when the factors (variables) are in a small number having no significant redundancy (collinearity) and also possessing

good relationship to responses. If in some cases where the number of factors are too large i.e. larger than the number of observations, the MLR can give a model that fits the sample data well but will fail to predict the new data, a phenomenon known as overfitting. Among these large number of factors, there are only a few underlying factors that contribute to the variation in the response to a large extent. The purpose of the PLS is to extract these underlying factors, so that from these extracted factors (X-scores), the Y-scores can be predicted. The regression model is then simplified as the relationship is concentrated on the smallest possible number of underlying variables. PLS is, in fact, used when the number of variables (factors) is large and possess high collinearity, and when there is a need to take into account the reference value of the parameter for each sample along with the spectral information (Westerhaus et al., 2004). Here the emphasis is on the prediction of responses rather than understanding the underlying relationship between them. PLS regression can be easily extended to simultaneously predict several quality attributes. In this case the algorithm is called PLS2 (Naes et al., 2002).

Normally an internal validation (cross validation) procedure is applied to test the predictive ability of the PLS (Shenk and Westerhaus 1995). The collective calibration sample is divided into several sub-groups (depending on the number of samples); once the equation is developed each validation group is predicted by using the model built on the remaining groups. This procedure also prevents model overfitting (Williams and Norris 1987; Shenk and Westerhaus 1995), which would give poor results with external calibration.

In Figure 6 are shown the required steps to build a calibration model.

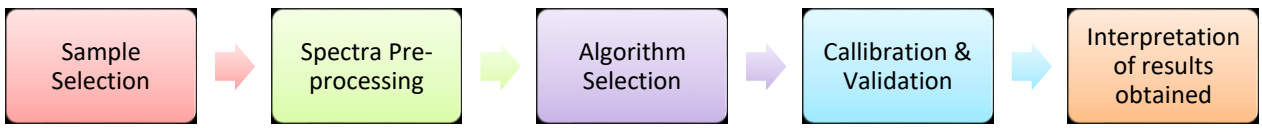

Fig. 6 Steps towards building a calibration model

The performance of the calibration model is then evaluated by comparing the following statistics as the standard error of calibration (SEC), the coefficient of determination between predicted and measured parameters (R^2), the standard error of cross validation (SECV) and coefficient of determination for cross validation (r^2) (Williams and Norris 1987). When a model is used for validation on external sample (test

set), errors refer to prediction performances, namely standard error of prediction (SEP).

Despite all this information, it must be taken into consideration that errors are always associated to the chemiometric method and can be only partially reduced. These errors may be due to sampling, sample preparation, and instrumental noise. Sampling errors are not a function of the underlying process but they are the real errors which are significant cause of deviation in the measurements. The sample preparation errors can occur during the various stages of the chemical process and errors in all these stages are often called ‘uncertainty’. Instrumental noise is another type of error that occurs due to the measurement process or instrument because of the various factors influencing instruments such as the effect of fluctuating voltages on filters and lamps.

For hyperspectral imaging the same kind of approach is used, normally a preprocessing of the hypercube is followed by the processing (Amigo et al., 2013), as the following example describes the data processing to predict phenol distribution in table grapes. In the first operation, image hypercube needs to be pre-processed in terms of spatial and spectral direction to eliminate undesirable noise to the signals (Brereton 2007) due to non-chemical biases and reduce data set dimensions; this is normally performed by applying compression techniques and mathematical pre-treatments to the spectra (a second derivative in the example of Figure 7).

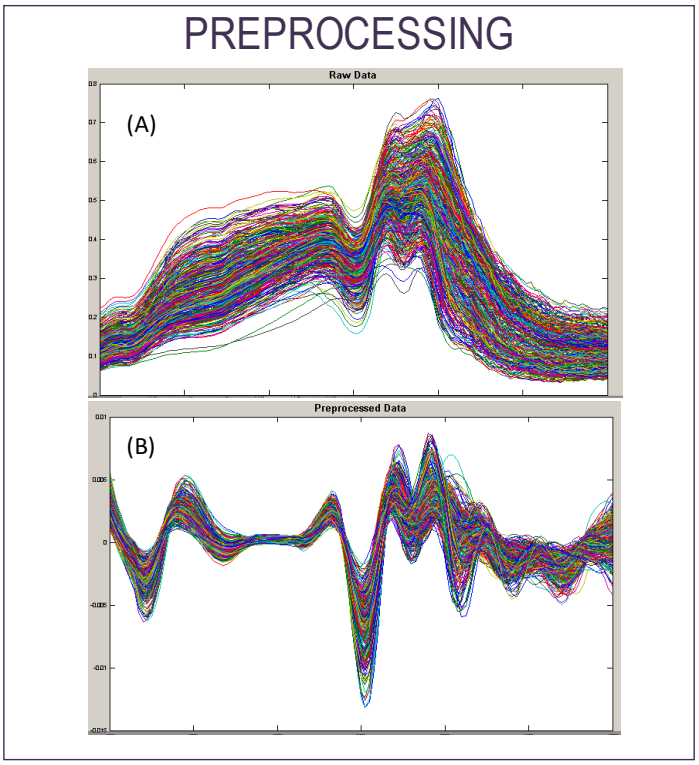

Figure 7. Example of spectra preprocessing: (A) raw spectra and (B) spectra after 2nd derivative transformation (by Amodio et al., unpublished).

On transformed spectra a thresholding algorithm, normally based on a PCA, can be applied in order to extract the spectral information related to the pixels of the object (Figure 8). On these spectra after the preprocessing, multivariate methods can be applied depending on the scope of the study. In this example a quantitative model was applied, whereas qualitative models are alternatively used when a discrimination among samples is the objective of the image processing. A PLS model relating spectral information to reference values of phenols measured analytically was tested (Figure 9). These models can be applied to further samples, including also the image of the whole bunch, as shown in Figure 10 where the phenol content is represented in a color map from 100 (blue) to 200 mg of Gallic acid. Equivalent 100 g^{-1} (red).

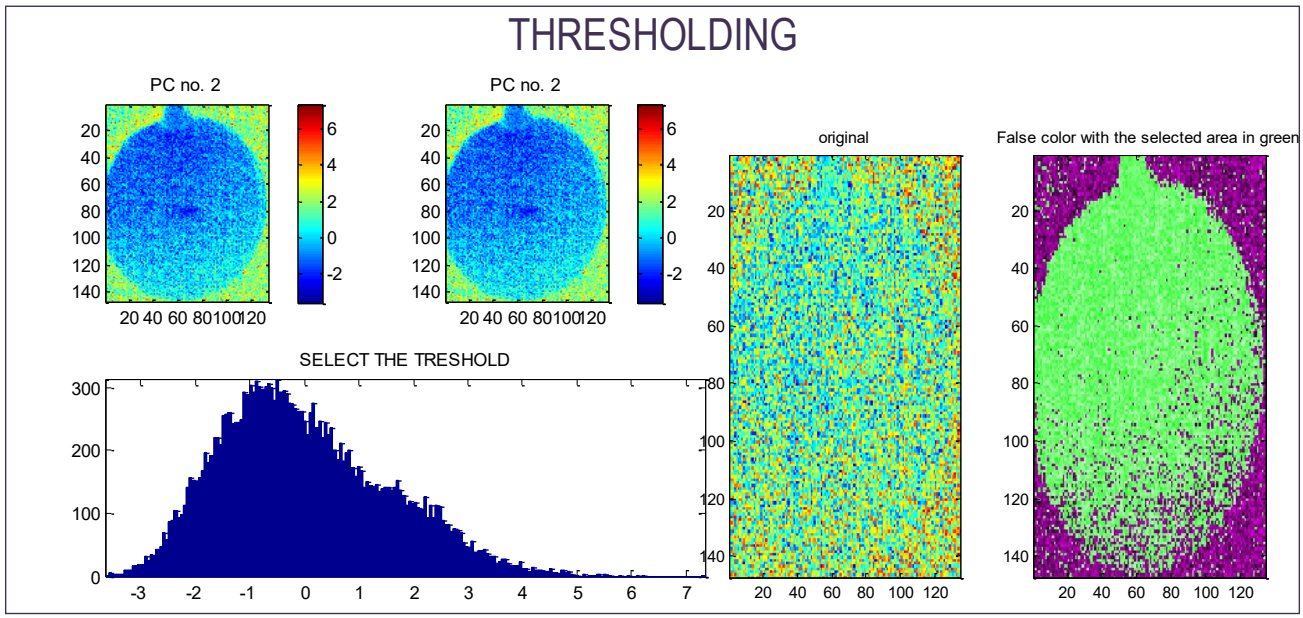

Figure 8. Example of image thresholding based on PCA (by Amodio et al., unpublished).

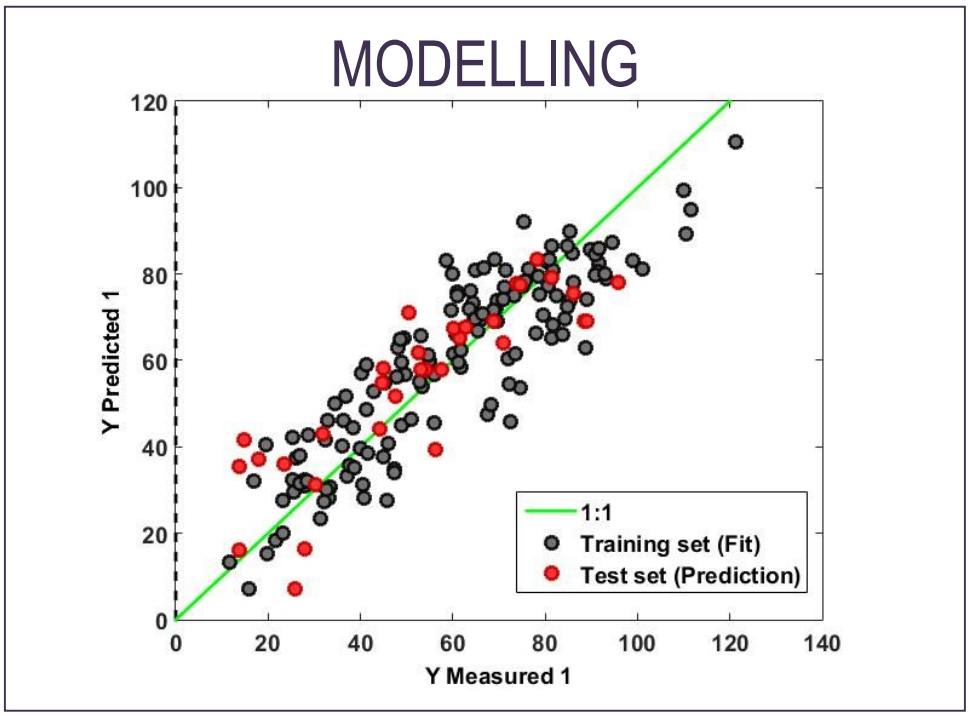

Figure 9. Example of output of a PLS model applied for prediction (by Amodio et al.,

unpublished).

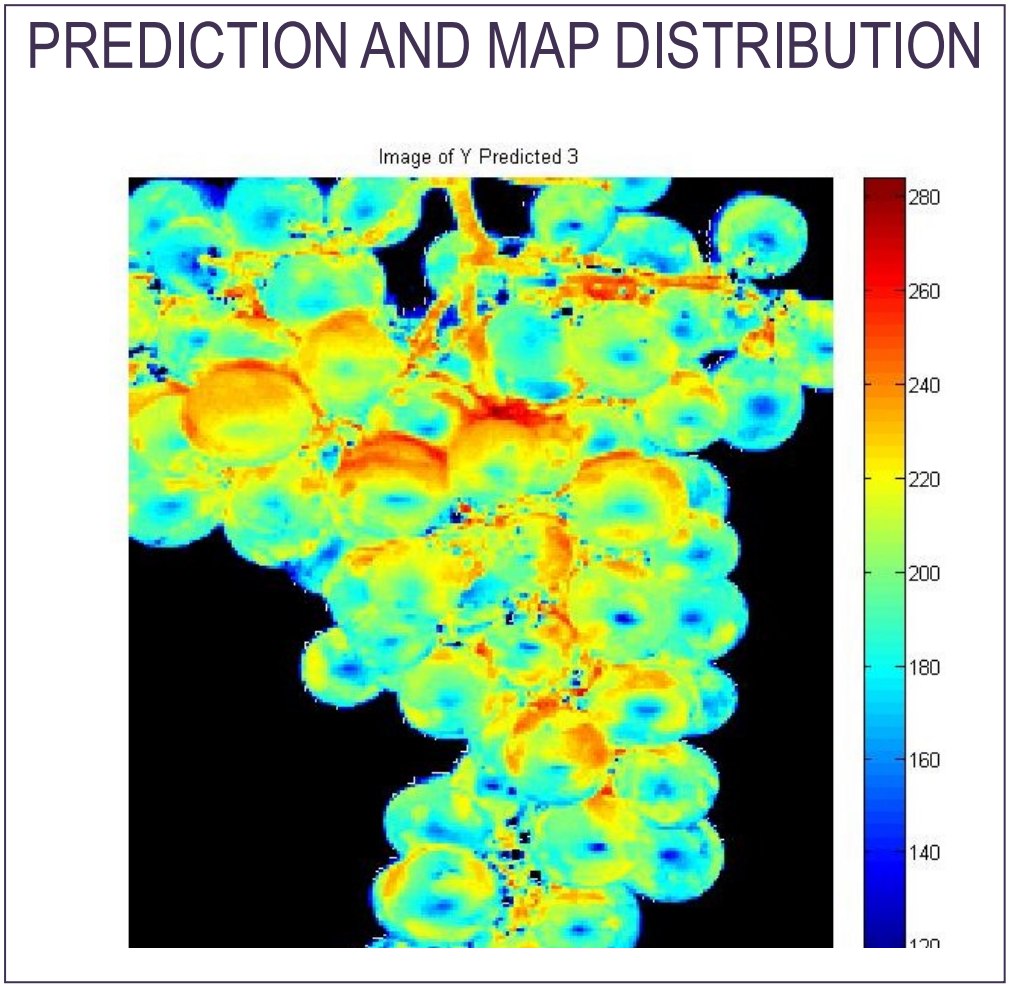

Figure 10. Distribution map of the phenol concentrations in the berries and in the stalk (by Amodio et al., unpublished).

3. PREDICTION OF NUTRITIONAL CONTENT OF FRUITS AND VEGETABLES

Near infrared (NIR) spectroscopy was used in the science of agriculture for the first time by Norris in 1964 for measurement of grain moisture content. Since then this technique has been successfully utilized for the measurement of moisture, protein and fat content of many food and agricultural products (Davies and Grant 1987; Irudayaraj et al., 2001). In the initial stage this technology was used mostly for the measurement of dry matter (DM) content of onions (Birth et al., 1985), soluble solids content (SSC) of

apples (Bellon-Maurel 1992) and water content of mushrooms (Roy et al., 1993), but at the moment current applications are quite different and include the estimation of nutritional compounds (Givens et al., 1997), the single organic acid (Ignat et al., 2012) and sugars detection (Rady et al., 2015) and have been also used to measure microstructure activities such as internal damage (Clark et al 2003), stiffness (Lammertyn et al., 1998) and sensory characteristics of fruits and vegetables (Mehinagic et al., 2004).

3.1 Prediction of Water content

IR is strongly absorbed by water and this absorption trend includes the NIR spectrum (730-2300nm). In high moisture foods with a water content ranging from 70-90% the absorption bands appear in close proximity to wavelengths of pure water (1400-1410nm being the strongest absorption band). For quantitative analysis of food water content the NIR bands in the ranges of 1400-1440nm and 1900-1950nm are mostly applied (Buning-Pfaue 2003). During water content analysis, beside free water molecules, there are one or two OH groups engaged in hydrogen bonds which influence the NIR absorption. Mixtures and continuum models are the two major classes of models to describe water structure (Wicke 1976).

Only a trace of absorption near 1430nm was observed for free water band in dry fruits such as soybean. In pear flesh a sharp absorption band was observed at 1406nm in a dehydrator which decreased in intensity as the dehydration process proceeded. The NIR spectrum of potato is in the range of 1100-2500nm (Buning-Pfaue 2003).

ElMasry *et al.,* (2007) used hyperspectral imaging in visible and near infrared regions i.e. 400-1000nm for the determination of moisture content (MC), SSC and pH in strawberry using PLS and multivariate calibration for spectral data analysis. The research concluded that as the strawberries ripened the moisture content and relative reflectance in 400-1000nm domain increased. For MC the correlation coefficient (R) was 0.90, with a SEC 6.1 and a SEP of 3.9.

Rajkumar *et al.,* (2012) investigated the relationship between banana maturity stage and MC using hyperspectral reflectance imaging (400-1000nm) at three different temperatures of 20, 25 and 30ºC and developed a linear correlation between the two parameters. They also found out that moisture content increased with growing maturity. The coefficient of determination for MC was found to be 0.87.

Huang *et al.,* (2014) developed regression models to simultaneously predict MC and color of soybeans during drying process using hyperspectral imaging technique in which mean reflectance and image

entropy parameters (related to the uniformity of pixel intensity in the image) were extracted. After establishing PLS models, it was found out that reflectance data provided more reliable results than the entropy data. The correlation coefficient valued $R_p = 0.97$ and RMSEP=4.7% was obtained for MC using reflectance data as compared to $R_p = 0.901$ and RMSEP= 9.2% using entropy data.

Pu and Sun (2015) used NIRS to show that the moisture in the central part of mango fruit is lower than in the surrounding flesh. For this purpose, two lab scale HSI systems were used and it was concluded that with the increase in MC the value of the mean relative reflectance decreased. Five feature wavebands at 908, 1076, 1153, 1405 and 1706 nm were used to develop PLS models (and showed best prediction results with $R_p^2 = 0.97$ and RMSEP=4.6%.

3.2 Soluble solids, acidity and assessment of the maturity stage

The soluble solids content (SSC) and total acidity (TA) can be predicted by using reflectance, transmittance and interactance modes of NIRS and Vis-NIRS. Good calibrations for different fruits can be obtained using transmittance mode. Reflectance mode also reaps satisfactory results for the fruit surface which is directly illuminated by the source (V Andrew McGlone et al., 2003). NIRS has successfully been brought to use for the determination of the soluble solids content (SSC) of many fruit species as apples (Iyo and Kawano 2001; Gomez 2001; Zude et al., 2006), kiwifruit (Ying et al., 2005), mushrooms (Roy et al., 1993) and citrus fruit (Guthrie et al., 2005; Gomez et al., 2006).

In case of tomatoes, SSC and TA are major internal quality indices contributing to the flavor (Kader 1984; Flores et al., 2009). Flores *et al.,* (2009) conducted a research to predict the internal quality parameters such as soluble solid content (SSC) and titratable acidity (TA) of the intact tomatoes (*Lycopersicum esculentum* Mill., cv. 'Raf') for two consecutive years. This variety is peculiar for its distinctive dark-green color and for its shape; moreover, due to its salinity resistance it possesses an exquisite flavor rarely found in other varieties. The study focused on the comparison of the new generation diode ray instruments with a laboratory scale NIR monochromator. The harvested fruit was stored at 10ºC and 95% RH. Different wavelength bands and different pretreatments were used to develop calibration models. The result concluded that the irregular shaped variety under study was accurately predicted by NIR using the spectra collected in the range of 400-1700nm excluding the

wavelengths above 1700nm, as they were found unnecessary for the application. The SECV for the prediction of SSC was in the range of 0.55-0.74 ºBrix and those of TA ranged in between 0.06% to 0.1% citric acid (Osborne et al., 1993; Lammertyn et al., 2000).

The soluble solid contents (SSC) of citrus fruits could be predicted by using partial least square (PLS) and modified PLS (MPLS) models.

V. McGlone *et al.,* (2003) conducted a research to predict the SSC and TA of *Citrus reticulata* (*cv.* "Miyagawa") known as Satsuma Mandarin using transmission, reflectance and interactance modes within spectral windows of 500-1100nm. Direct transmission mode with 700-930nm spectral window gave most accurate SSC predictions with R^2 value of 0.93 and RMSEP=0.32%. None of the three measurement modes provided accurate prediction of TA and the only predictive ability achieved (best values being R^2~0.65 and RMSEP~0.15%) was afforded indirectly through a correlation with the skin chlorophyll changes occurring with fruit maturity. In a more recent study on Satsuma mandarin, reflectance in a window of 400-2350nm was used obtaining an RMSEP value of 0.16 and an $R_c^2 = 0.94$ (Gomez et al., 2006).

Also other authors assessed internal quality parameters of mandarin fruit for total soluble solids (SSC) and dry matter (DM). By applying modified partial least square (MPLS) model using 720-950 nm window in 0^0 interactance spectroscopy with two scans they obtained an R_c^2 of 0.41 for SSC and 0.91 for DM and RMSEP of 0.22% and 0.45% for the above attributes respectively, for 17 different populations. They found out that the performance of the calibration model was very satisfactory for the prediction of SSC and DM whereas it was unacceptable for juiciness and TA (Guthrie et al., 2005).

Cayuela (2008) predicted the SSC and TA in oranges by developing PLS models using NIR spectrophotometer with a post dispersive reflectance configuration. According to these authors fruit samples were kept at 20ºC for 24 hours prior to measurements. Destructive techniques were used to get the values of SSC, TA and pH using digital refractometer, potentiometric titration of citrus juice and pH meter respectively prior to spectral analysis. Spectra were collected in two spectral windows of wavelength ranges 578-1090.2nm and 1110-1842.2nm respectively. For SSC the effect of spectral acquisition modalities on the efficacy of the model were also investigated and particularly by taking four and two spectral measurements along the fruit equator. The results were found to be more reliable for

the prediction of the SSC and not very consistent in case of TA and pH because of the low level of these parameters in citrus fruit. It was found that PLS models performed better than the MPLS models with the best results being $R_c^2 = 0.88$ and an internal validation SECV of 0.41 for SSC and that the acquisition of two spectral measurements gives better results as compared to four spectral measurements. Moreover, in this research the typical diffuse spectra of oranges were found in resemblance to those of Satsuma mandarins by Gómez *et al.,* (2006).

Some authors applied hyperspectral imaging in the range 400-1000 nm to predict the SSC, TA, pH, and DM in strawberries by selecting 6 wavelengths form the visible NIR region based on the β-coefficient of PLS analysis. Both PLS and MLR models gave same correlation coefficients of calibration i.e. $R_c =$ between 0.80 for SSC and 0.92 for DM (ElMasry et al., 2007). In the same work the images were also used to classify fruits according to their maturity stage. The same techniques and spectral range (500-1000nm) was also used to predict SSC and firmness of blueberries (Leiva-Valenzuela et al., 2013). For these high-value crops implementing a sorting line for soluble solids would, in fact be, highly desirable.

Schaare and Fraser (2000) compared the reflectance, interactance and interference modes of spectroscopic measurements for estimation of SSC of *Actinidia chinensis* (yellow fleshed Kiwifruits). According to this research the interactance mode spectra were found to give the most accurate results for SSC estimation (also the results were valid for estimation of flesh color and density). SSC were predicted with a SEP of $\pm$0.80°Brix with correlation coefficient R^2=0.93. Whole fruit densities and flesh hue angles were also predicted. Moreover on kiwifruits (Moghimi et al., 2010), combined Vis-NIR in the wavelength range of 400-1000nm and chemiometric techniques to predict SSC and TA. The prediction performance showed R^2values of 0.93 and 0.94 and RMSEP of 0.26°Brix and 0.076 for both parameters respectively.

Pu *et al.,* (2016) studied the prediction of SSC, pH and maturity discrimination in lychees by employing shortwave NIR in the range of 600-1000nm and longwave NIR in the range of 1000-2500nm. This research concluded that spectral set in the longwave NIR region performed better having values $R_p = 0.88$ and RMSEP=0.91 °Brix for SSC and $R_p = 0.74$ and RMSEP=0.29 for pH.

Some studies related to hard green mangos tried to index the eating quality of the fruits in terms of SSC (Subedi et al., 2007). PLSR models were optimized (for second derivative of absorbance spectra)

for SSC and DM in terms of short wave NIR wavelength range. The SSC models showed an $R_v^2 = 0.92$ with SEP of 0.67 and bias of 1.25%.

Moreover, another study by (Rungpichayapichet et al., 2016) developed calibration models for mango ripening index, SSC, TA, and firmness using diffuse reflectance spectra (700-1100nm) and PLSR. It was found out that using combined data of a few years for calibration greatly enhanced the prediction accuracy. All desired parameters were very suitably predicted by establishing prediction models from three year data with a R^2 value of 0.9 and SEP of 1.2% for SSC and R^2 =0.74 and SEP=0.38% for TA.

Marques *et al.,* (2016) conducted a study for the evaluation of hand held NIR spectrometer based on linear variable filter technology (LVF) for quality control analysis of mango 'Tommy Atkins' by building calibration models using PLSR for determination of SSC, TA, dry matter (DM) and pulp firmness. The spectrophotometer was found feasible to determine the quality parameters giving the coefficient of determination values 0.92 and 0.50 for SSC and TA respectively, and RMSEP of 0.55ºBrix for SSC and 0.17% citric acid.

These techniques may also be a valid support to enhance efficiency of cultivar breeding as for apple fruit phenotypes. Pre-storage and post-storage (0.5ºC, 6-10 weeks) NIR spectra of fruit were recorded and in the case of SSC and DM, the genetic correlation between observed and predicted performance was as high as 0.91 for SSC and 0.95 for DM (Kumar et al., 2015).

Moreover a desired objective of these predictive models is that they should be extended to as much pre-harvest conditions as possible, and therefore when testing different varieties, a multi-cultivar model is often compared to individual ones as in the case of plums (Louw and Theron 2010). These authors developed multivariate prediction models using FT-NIRS (800-2700nm) for SSC, TA, weight, sugar to acid ratio and firmness in three different cultivars of African plums. 'Pioneer' and 'Laetitia' cultivar specific models had a better predictability capacity as compared to 'Angeleno' model and it was concluded that multi cultivar models outperformed single cultivar models on R^2 values. Bureau *et al.,* (2009) used spectra of 598 fruits from 8 different cultivars of apricot at different maturity stages to predict a general model for SSC, TA and other attributes and found a high correlation for SSC and TA, whereas other quality attributes were not satisfactorily predicted. These models were, in fact, applied for the prediction of other 279 fruits giving a prediction error of less than 8% of fresh weight for SSC and about

15% for TA. Yang *et al.,* (2014) developed a robust model on sugar beet with 890 samples (820 in calibration and 79 in prediction) over 28 varieties which showed coefficient of determination value i.e. R^2 for calibration models of sugar content of 0.908 and RMSECV of 0.38.

On the other side in some cases the variety discrimination is also important, and therefore there are studies aimed to detect variety other than to predict other quality attributes as for pears where the authors discriminated 3 varieties by means of hyperspectral imaging (Li et al., 2016) and artichokes where 2 varieties were correctly classified (Amodio et al, unpublished). The results of this paper can be utilized to develop simple, low-cost and efficacious equipment in the further study.

In another study aimed to determining SSC and firmness of intact 'Aurora-1' peaches and to discriminate among harvest date and maturity stage the authors concluded that for SSC, the model obtained from validation set $RMSEP = 1.08\%$, $R^2 = 0.59$ showed better performance than when applied on independent data set ($RMSEP = 1.04\%$, $R^2 = 0.45$) and that no segregation of the samples was obtained for harvest season and maturity stage (Nascimento et al., 2016).

Generally, results on fruits demonstrate that soluble solids can be predicted with good accuracy encouraging the implementation of online systems to monitor this and eventually other quality attributes. In this case, it should be considered that other acquisition variables may affect the final results as for instance the distance from the light source and the position of the fruit as investigated on apple fruits for the prediction of SSC (Liu et al., 2007). The apples were equilibrated by placing them at 19ºC and 68% RH for two days. The distances of 0, 2, 4, and 6 mm were taken under consideration. Variance analysis was employed to obtain statistical analysis of FT-NIRS followed by development of calibration models using PLS. Best calibration model gave $R^2 = 0.84$ and SEP of 0.77. The research concluded that the different distances had different effect on the performance of the calibration models.

Moreover, in cases of cut products, model developed directly on the slices can give better prediction accuracy as found for sugar beet (Pan et al., 2015) for which SSC, moisture and sucrose content was predicted. With the same idea, Lu et al. (2000) developed a model after acquisition to predict the sugar content and firmness, finding that the prediction of sugar content for peeled apples was better than for unpeeled apples, where the RMSE increased by 0.17 ºBrix, on an average. Flores et al. (2008) conducted a study to access the SSC of the intact and cut melons and watermelons using a NIR diode array

spectrometer for data of two consecutive years. In case of cut melons the SECV was 0.60°Brix and $R^2 = 0.88$, whereas, in case of cut water melons, the values of above parameters were 0.49° Brix, with R^2 of 0.76, but some uncertainty in the prediction results may be accepted for a crop like this, where the prediction of internal sugar content would be very valuable.

Generally, for melons the variation of SSC along the longitudinal direction may be the major limitation in the robustness of the calibration models as pointed out for orange flesh netted melon fruits (*Cucumis melo* L. reticulatus group). The research found out that SSC in the outer mesocarp was 3 units higher at the stylar end of the fruit compared with the stem end, and that SSC in the inner mesocarp was higher than in the outer tissue, showing higher uniformity at spatial positions. With increasing maturity of the fruit, the linear relationship between the outer 10 millimeter and subsequent middle 10 millimeters of thickness of tissue also varied as different R^2 values were observed, affecting the performances of the calibration model. So for these fruits this variability should be taken into account to set up a performing acquisition set-up.

In addition to SSC and TA, NIR spectroscopy have also been successfully used for prediction of sugar and organic acid composition of fruits and vegetables.

The presence of glucose and sucrose in potatoes was predicted by Rady et al. (2015) using visible NIR spectroscopy. Each sample to be tested was a slice of 12.7mm thickness uniformly cut from all tubers. PLSR demonstrated that strongly correlated models were built for glucose (correlation coefficient as high as 0.97 for 'Russet Norkotah' and 0.81 for 'Frito Lay' cultivar as compared to those of sucrose which showed less correlation performance. The results depicted high classification errors for sucrose (30% for RN and 34% for FL).

Fernández-Novales *et al.,* (2009) concluded NIR spectroscopy as a promising technique for determination of reducing sugar content during grape ripening, winemaking and aging. NIR spectra of 146 samples were collected in the region of 800-1050nm. Spectra were interpreted and calibrations were developed using PCA, PLS and MLR regression. The values of R^2, SECV and RMSECV for the PLS model in full spectral range were 0.98, 13.62g/l and 13.58g/l, respectively.

3.3 Macro and micronutrients: vitamins, phenolic, antioxidant activity

Despite the high content of water in fruits and vegetables, whose peaks predominated over the ones of low concentration constituents causing reduction in prediction accuracy, as their spectra may overlap with water (Nicolai et al., 2007), many studies have been conducted to estimate the content of minor constituents including phytochemicals.

Research has been conducted to estimate the total antioxidant activity using infrared spectroscopy coupled with chemiometric predictive models. In context of antioxidant activity, infrared spectroscopy has garnered interest due to the reduced time required for the analysis, the enhanced precision and the simple sample preparation, no requirement for reagents and extraction steps (Lu and Rasco 2012). Various spectroscopic methods have, in fact, been used for the determination of the Vitamin C content, carotenoids, folates, phenols, and generally for the antioxidant capacity of fruits and vegetables, as also for fiber content. Liu *et al.,* (2015) Liu *et al.,* (2015)

Liu *et al.,* (2015) used multispectral imaging in combination with chemiometric methods for measurement of lycopene and phenolic compounds content in intact tomatoes and concluded that the models developed with back propagation neural network (BPNN) gave the best performance. For lycopene and total phenolic content prediction, the residual predictive content (RPD) was 4.59 and 9.33, respectively.

Rungpichayapichet *et al.,* (2015) compared the NIRS and color measurement to predict β-carotene content in Mango and found out that long wave NIR served the prediction purpose better as compared to the short wave NIR. The coefficient of determination $R^2 > 0.8$ and standard error of prediction of 11.6-20.2 retinol equivalents *RE* 100g^{-1} edible part *EP* were obtained by NIRS calibration.

De Nardo *et al.,* (2009) declared attenuated total reflectance (ATR) spectroscopy combined with multivariate analysis as a reliable and effective technique for rapid quantification of lycopene and β-carotene in tomato juices. High performance liquid chromatography (HPLC) was used as a reference method. Unique marker bands were shown by infrared spectra at 968cm^{-1} for β-carotene and 957cm^{-1} for lycopene. Multivariate spectral data analysis gave *r* values of >0.9 between the ATR-IR predicted and HPLC reference values. Standard error of cross-validation (SECV) values of 0.5 and 0.04 mg/100g of juice for lycopene and β-carotene were given.

Yang *et al.,* (2015) used various models for the development of relationship between anthocyanin

content in pericarp and HSI information. 3-D images of lychee were acquired in the range of 350-1050nm from HSI system. For data dimensionality reduction and selection of optimal wavelength in relation to anthocyanin content, successive projection algorithm (SPA) and stepwise regression (SWR) algorithm was used. To develop a quantitative relationship between the anthocyanin content in the pericarp and HSI information in both optimal wavelength sets, radial basis functional neural network (RBF-NN) was used to fuse together SPA-RBF-SVR and SWR-RBF-SVR models.

Ferrer-Gallego *et al.,* (2011) measured the phenolic compounds in the grapes and grape skin using NIR spectroscopy technique in the wavelength range of 1100-2498nm. The ratio performance deviation (RPD) was found to be 4.8, 2.1, 5.8 and 4.2 for anthocyanins, phenolic acids, flavanols, and flavonols in intact grapes, respectively. RPD values for the same parameters in case of grape skin were found to be 4.4, 6.3, 13.6, and 12.7 respectively. The study concluded that in order to obtain best results the use of a fiber-optic probe is recommended for directly recording the spectra of intact grapes.

Hyperspectral imaging and FT-NIR have also been used to predict phenolic content and antioxidant activity of fresh-cut artichokes, with FT-NIR giving more accurate results particularly for phenols which were predicted with an RMSEP of 18 mg/100g (Amodio et al., unpublished).

Ignat *et al.,* (2012) conducted a study to non-destructively estimate the ascorbic acid content of bell peppers during various stages of growth in reflectance mode obtaining Vis-NIR (477-950nm) and NIR (850-1888nm) spectra. The destructive analysis of the three cultivars showed that the 'Ever Green' variety possessed the highest content of ascorbic acid of 148.1mg/100g as compared to 'No.117' and 'Celica'. The PLS models predicted the ascorbic acid contents of all three cultivars with a cross validation error of 15.1-18.9mg/100g (RPD=2-2.4). In the same way another work evaluated the ability of NIR to predict ascorbic acid, chlorophyll a and b, and total phenolic compounds in the exocarp and mesocarp tissues, respectively of summer squash concluding that NIRS could be used for screening purposes (Blanco-Diaz et al., 2014).

Pissard *et al.,* (2013) collected the spectra of three different varieties of apples collected for three consecutive years in the range of 400-2500nm using NIR reflectance mode for the prediction of Vitamin C and polyphenolic content. The research concluded that good prediction precision for vitamin C was achieved using NIR with a SEP of 4.9mg 100^{-1}g FW and $R^2 = 0.8$. In case of total polyphenol content

these values were obtained to be 140µg g^{-1} FW and $R^2 = 0.94$. Therefore, the quality of the apples was successfully predicted using NIRS.

Also for nutritional compounds NIR spectroscopy can be used to screen different genotypes with the purpose of selecting cultivar with high nutritional values. One example is a study on Cassava root where more than 3000 samples were used to predict total carotenoids, and β-carotene and dry matter, with determination coefficients higher than 0.92. In the same study NIRS also distinguished the roots with high or low cyanogenic potential (R2: 0.86).

Sinelli *et al.,* (2008) developed predictive models for blueberry to evaluate the content of total phenols (RMSEP = 0.18mg catechin/g), total flavonoids (RMSEP = 0.25mgcatechin/g) and total anthocyanins (RMSEP= 0.22mg catechin/g), whereas for ascorbic acid model performance were lower. Also for nutritional compounds NIR spectroscopy can be used to screen different genotypes with the purpose of selecting cultivar with high nutritional values. One example is a study on Cassava root where more than 3000 samples were used to predict total carotenoids, and β-carotene and dry matter, with determination coefficients higher than 0.92. In the same study NIRS could also distinguish roots with high or low cyanogenic potential (R^2: 0.86).

Research work has also been done to predict the fiber content in various cereal products, barley cultivars and Brazilian soybean (Kays and Barton 2002; Kays et al., 2005; Ferreira et al., 2015).

Ferreira *et al.,* (2015) accessed the total dietary fiber in ground Brazilian soybeans employing FT-NIR spectroscopy in the range of 1000-2500nm using diffuse reflectance. The best prediction results were obtained using PLSR model and the R^2 value was found to be 0.80 with a RMSEP=0.86, conforming the reliability of NIRS technology for accurate prediction of total dietary fiber

Moreover, fiber content have been predicted on ground cereals. Kays *et al.,* (2005) investigated the total dietary fiber (TDF) content of barley cultivars using NIRS reflectance and transmission modes for whole polished and grounded grains. For polished whole grains, MPLS models were developed in the transmission spectral range of 850-1048nm obtaining SECV of 10.4 and R^2 value of 0.82. In case of ground barley samples, reflectance spectroscopy was employed in the wavelength range of 1104-2494 nm getting better prediction with SECV of 5.2 and an R^2 of 0.96. Hence, the reflectance mode gave better results than the transmission mode due to enhanced amount of information in the wavelength region

utilized. Also Kays and Barton (2002) used the NIRS to predict the soluble and insoluble dietary fiber grounded cereals. It was concluded by the research that insoluble dietary fibers were predicted more accurately as compared to the soluble dietary fibers. The values of SECV and R^2 for insoluble dietary fiber were 1.5% and 0.98, respectively, whereas the same values for soluble dietary fibers were 1.15% and 0.82.

Beside the application of spectroscopy on intact fruits and vegetable these techniques may also be used as destructive methods on juices, pastes and powders made from horticultural products or on chemical tissues extracts prepared as in the conventional analytical methods, since even in this way the measurement of nutritional content would be much faster and less expensive (in time and resources) than the conventional reference method. Interesting results on fruit paste have been reported for profiling tomato carotenoids having good accuracy for β-carotene content (R^2CV of 0.89 and RMSECV=0.174µg $g^{-1}$and for all-trans lycopene content ($R^2CV = 0.75$ and RMECV=6.88µg g^{-1}) (Deak et al., 2015).

Bureau *et al.,* (2013) tested attenuated total reflectance FT-IR on 284 and 483 samples from two successive years and of different cultivars possessing large phenotypic variability. Homogenates of all peach fruit samples were also analyzed using ATR-FTIR three methods were used to determine sugar and organic acid composition, namely, colorimetric enzymatic measurement (ENZ), high performance liquid chromatography and proton NMR spectroscopy, concluding that ENZ reference data provided best correlation with ATR-FTIR data, with best results giving RMSECV in range of 5.8-8.7% for SSC and 5.9-8.0% for TA.

Yang and Irudayaraj (2002) used six different spectroscopic techniques capable of detecting the vitamin C content in powdered mixture and solutions of food and pharmaceutical products by comparing the efficacy of NIR (0.988), FT-NIR (0.992), FTIR-ATR (0.999), diffuse reflectance (DRIFTS) (0.976), Fourier transform infrared-photoacoustic FTIR-PAS (0.988) and FT Raman spectroscopy (0.95). Overall prediction error ranged from 0.2 to 3 with best results obtained when using FT-NIR and FT Raman techniques. Another example regarding the prediction and localization of glucosinolates on freeze-dried broccoli by means of hyperspectral imaging demonstrated good potentiality on these samples (Hernandez-Hierro et al., 2014).

4. CONCLUSIONS

Further research perspectives in this field should be focused on simplifying existing models reducing the number of wavelength in order to facilitate the implementation of online sorting systems based on nutritional content and on exploiting the possibility of using these techniques to develop new methods for unexplored nutritional compounds and over a large number of species and cultivar, also to assess the impact of pre and postharvest factors on the fate of these compounds. Moreover, also the scope of using spectroscopic techniques to assess nutritional content on fruit extracts prepared as for the conventional analytic methods would be an interesting perspective to reduce the time of measurements and to allow to conduct the analysis without having a chemical laboratory with sophisticated equipment and expert technicians.

Finally, in this chapter the use of these techniques as a classification methods were not deeply commented, since the focus was on quantitative methods, but classification algorithms may be applied to discriminate fruits and vegetable for their origins, including also the growing practices or for quality discrimination with a particular regard to their nutritional quality.

REFERENCES

Amigo, J. M., I. Marti and A. Gowen (2013). "Hyperspectral imaging and chemometrics: a perfect combination for the analysis of food structure, composition and quality." Chemometric in Food Chemistry, Elsevier, Amsterdam: 343-370.

Ariana, D. P. and R. Lu (2008). "Quality evaluation of pickling cucumbers using hyperspectral reflectance and transmittance imaging: Part I. Development of a prototype." Sensing and Instrumentation for Food Quality and Safety **2**(3): 144-151.

Ariana, D. P. and R. Lu (2010). "Evaluation of internal defect and surface color of whole pickles using hyperspectral imaging." Journal of Food Engineering **96**(4): 583-590.

Baardseth, P., H. Helgesen and T. Isaksson (1996). "Multivariate techniques in the analysis of meat quality." Meat Science **43**: 135-149.

Bellon-Maurel, V. (1992). Application de la spectroscopie proche infrarouge au contrôle en ligne de la qualité des fruits et legumes.

Birth, G., G. Dull, W. Renfroe and S. Kays (1985). "Nondestructive spectrophotometric determination of dry matter in onions." Journal of the American Society for Horticultural Science (USA).

Blanco-Díaz, M. T., M. Del Río-Celestino, D. Martínez-Valdivieso and R. Font (2014). "Use of visible and near-infrared spectroscopy for predicting antioxidant compounds in summer squash (Cucurbita pepo ssp pepo)." Food chemistry **164**: 301-308.

Brereton, R. G. (2007). Applied chemometrics for scientists, John Wiley & Sons.

Büning-Pfaue, H. (2003). "Analysis of water in food by near infrared spectroscopy." Food Chemistry **82**(1): 107-115.

Bureau, S., B. n. d. Quilot-Turion, V. r. Signoret, C. Renaud, M. Maucourt, D. Bancel and C. M. Renard (2013). "Determination of the Composition in Sugars and Organic Acids in Peach Using Mid Infrared Spectroscopy: Comparison of Prediction Results According to Data Sets and Different Reference Methods." Analytical chemistry **85**(23): 11312-11318.

Bureau, S., D. Ruiz, M. Reich, B. Gouble, D. Bertrand, J.-M. Audergon and C. M. G. C. Renard (2009). "Rapid and non-destructive analysis of apricot fruit quality using FT-near-infrared spectroscopy." Food Chemistry **113**(4): 1323-1328.

Burns, D. A. and E. W. Ciurczak (2007). Handbook of near-infrared analysis, CRC press.

Cayuela, J. A. (2008). "Vis/NIR soluble solids prediction in intact oranges (Citrus sinensis L.) cv. Valencia Late by reflectance." Postharvest Biology and Technology **47**(1): 75-80.

Clark, C., V. McGlone and R. Jordan (2003). "Detection of Brownheart in 'Braeburn'apple by transmission NIR spectroscopy." Postharvest Biology and Technology **28**(1): 87-96.

Clark, C., V. McGlone, C. Requejo, A. White and A. Woolf (2003). "Dry matter determination in 'Hass' avocado by NIR spectroscopy." Postharvest Biology and Technology **29**(3): 301-308.

Cozzolino, D., W. Cynkar, N. Shah, R. Dambergs and P. Smith (2009). "A brief introduction to multivariate methods in grape and wine analysis." International Journal of Wine Research **1**(1): 123-130.

Cozzolino, D., R. Dambergs, L. Janik, W. Cynkar and M. Gishen (2006). "Analysis of grapes and wine by near infrared spectroscopy." J. Near Infrared Spectrosc **14**(5): 279-289.

Davies, A. and A. Grant (1987). "Review: Near infra-red analysis of food." International Journal of Food Science & Technology **22**(3): 191-207.

De Nardo, T., C. Shiroma-Kian, Y. Halim, D. Francis and L. E. Rodriguez-Saona (2009). "Rapid and Simultaneous Determination of Lycopene and β-Carotene Contents in Tomato Juice by Infrared Spectroscopy." Journal of Agricultural and Food Chemistry **57**(4): 1105-1112.

Deák, K., T. Szigedi, Z. Pék, P. Baranowski and L. Helyes (2015). Carotenoid determination in tomato juice using near infrared spectroscopy**. International Agrophysics. **29:** 275.

ElMasry, G., N. Wang, A. ElSayed and M. Ngadi (2007). "Hyperspectral imaging for nondestructive determination of some quality attributes for strawberry." Journal of Food Engineering **81**(1): 98-107.

Fernández-Novales, J., M.-I. López, M.-T. Sánchez, J. Morales and V. González-Caballero (2009). "Shortwave-near infrared spectroscopy for determination of reducing sugar content during grape ripening, winemaking, and aging of white and red wines." Food Research International **42**(2): 285-291.

Ferreira, D. S., R. J. Poppi and J. A. L. Pallone (2015). "Evaluation of dietary fiber of Brazilian soybean (Glycine max) using near-infrared spectroscopy and chemometrics." Journal of Cereal Science **64**: 43-47.

Ferrer-Gallego, R., J. M. Hernández-Hierro, J. C. Rivas-Gonzalo and M. T. Escribano-Bailón (2011). "Determination of phenolic compounds of grape skins during ripening by NIR spectroscopy." LWT-

Food Science and Technology **44**(4): 847-853.

Flores, K., Sánchez, M., D. Pérez-Marín, M. López, J. Guerrero and A. Garrido-Varo (2008). "Prediction of total soluble solid content in intact and cut melons and watermelons using near infrared spectroscopy." Journal of Near Infrared Spectroscopy **16**(2): 91-98.

Flores, K., M.-T. Sánchez, D. Pérez-Marín, J.-E. Guerrero and A. Garrido-Varo (2009). "Feasibility in NIRS instruments for predicting internal quality in intact tomato." Journal of Food Engineering **91**(2): 311-318.

Givens, D. I., J. De Boever and E. Deaville (1997). "The principles, practices and some future applications of near infrared spectroscopy for predicting the nutritive value of foods for animals and humans." Nutrition research reviews **10**(01): 83-114.

Gómez, A. H., Y. He and A. G. Pereira (2006). "Non-destructive measurement of acidity, soluble solids and firmness of Satsuma mandarin using Vis/NIR-spectroscopy techniques." Journal of food engineering **77**(2): 313-319.

Guthrie, J., C. Liebenberg and K. B. Walsh (2006). "NIR model development and robustness in prediction of melon fruit total soluble solids." Crop and Pasture Science **57**(4): 411-418.

Guthrie, J., K. B. Walsh, D. Reid and C. Liebenberg (2005). "Assessment of internal quality attributes of mandarin fruit. 1. NIR calibration model development." Crop and Pasture Science **56**(4): 405-416.

Heise, H. and R. Winzen (2002). "Chemometrics in Near-Infrared Spectroscopy." Near-infrared spectroscopy: Principles, instruments, applications: 125-162.

Hernández-Hierro, J. M., C. Esquerre, J. Valverde, S. Villacreces, K. Reilly, M. Gaffney, M. L. González-Miret, F. J. Heredia, C. P. O'Donnell and G. Downey (2014). "Preliminary study on the use of near infrared hyperspectral imaging for quantitation and localisation of total glucosinolates in freeze-dried broccoli." Journal of Food Engineering **126**: 107-112.

Huang, H., H. Yu, H. Xu and Y. Ying (2008). "Near infrared spectroscopy for on/in-line monitoring of quality in foods and beverages: A review." Journal of Food Engineering **87**(3): 303-313.

Huang, M., Q. Wang, M. Zhang and Q. Zhu (2014). "Prediction of color and moisture content for vegetable soybean during drying using hyperspectral imaging technology." Journal of Food Engineering **128**: 24-30.

Ignat, T., Z. Schmilovitch, J. Fefoldi, B. Steiner and S. Alkalai-Tuvia (2012). "Non-destructive measurement of ascorbic acid content in bell peppers by VIS-NIR and SWIR spectrometry." Postharvest Biology and Technology **74**: 91-99.

Irudayaraj, J., S. Gunasekaran and S. Gunasekaran (2001). "Optical methods: visible, NIR, and FTIR spectroscopy." Nondestructive food evaluation techniques to analyze properties and quality. New York: Marcel Dekker. p: 1-2.

Iyo, C. and S. Kawano (2001). "Predicitng brix values of stored apples using near infrared spectra." Journal of the Japanese Society for Horticultural Science (Japan).

Kader, A. (1984). Effects of postharvest handling procedures on tomato quality. Symposium on Tomato Production on Arid Land 190.

Kays, S. E. and F. E. Barton (2002). "Near-infrared analysis of soluble and insoluble dietary fiber fractions of cereal food products." Journal of agricultural and food chemistry **50**(10): 3024-3029.

Kays, S. E., N. Shimizu, F. E. Barton and K. i. Ohtsubo (2005). "Near-infrared transmission and reflectance spectroscopy for the determination of dietary fiber in barley cultivars." Crop science **45**(6): 2307-2311.

Kumar, S., A. McGlone, C. Whitworth and R. Volz (2015). "Postharvest performance of apple phenotypes predicted by near-infrared (NIR) spectral analysis." Postharvest Biology and Technology **100**: 16-22.

Lammertyn, J., B. Nicolaï, K. Ooms, V. De Smedt and J. De Baerdemaeker (1998). "Non-destructive measurement of acidity, soluble solids, and firmness of Jonagold apples using NIR-spectroscopy." Transactions of the ASAE **41**(4): 1089-1094.

Lammertyn, J., A. Peirs, J. De Baerdemaeker and B. Nicolaı (2000). "Light penetration properties of NIR radiation in fruit with respect to non-destructive quality assessment." Postharvest Biology and Technology **18**(2): 121-132.

Leiva-Valenzuela, G. A., R. Lu and J. M. Aguilera (2013). "Prediction of firmness and soluble solids content of blueberries using hyperspectral reflectance imaging." Journal of Food Engineering **115**(1): 91-98.

Li, B., B. Hou, D. Zhang, Y. Zhou, M. Zhao, R. Hong and Y. Huang (2016). "Pears characteristics

(soluble solids content and firmness prediction, varieties) testing methods based on visible-near infrared hyperspectral imaging." Optik-International Journal for Light and Electron Optics **127**(5): 2624-2630.

Liu, C., W. Liu, W. Chen, J. Yang and L. Zheng (2015). "Feasibility in multispectral imaging for predicting the content of bioactive compounds in intact tomato fruit." Food Chemistry **173**: 482-488.

Liu, Y.-d., Y.-b. Ying, X. Fu and H. Lu (2007). "Experiments on predicting sugar content in apples by FT-NIR Technique." Journal of Food Engineering **80**(3): 986-989.

Louw, E. D. and K. I. Theron (2010). "Robust prediction models for quality parameters in Japanese plums (Prunus salicina L.) using NIR spectroscopy." Postharvest Biology and Technology **58**(3): 176-184.

Lu, X. and B. A. Rasco (2012). "Determination of antioxidant content and antioxidant activity in foods using infrared spectroscopy and chemometrics: a review." Critical reviews in food science and nutrition **52**(10): 853-875.

Marques, E. J. N., S. T. de Freitas, M. F. Pimentel and C. Pasquini (2016). "Rapid and non-destructive determination of quality parameters in the 'Tommy Atkins' mango using a novel handheld near infrared spectrometer." Food Chemistry **197, Part B**: 1207-1214.

Martens, H. and T. Naes (1989). "Multivariate Calibration".—John Wiley and Sons, Chichester, UK."

Massart, D. L., B. Vandeginste, S. Deming, Y. Michotte and L. Kaufman (1988). "Chemometrics: a textbook."

McClure, W. F. (2003). "204 years of near infrared technology: 1800-2003." Journal of Near Infrared Spectroscopy **11**(6): 487-518.

McGlone, V., H. Abe and S. Kawano (1997). "Kiwifruit firmness by near infrared light scattering." Journal of Near Infrared Spectroscopy **5**: 83-90.

McGlone, V., D. Fraser, R. Jordan and R. Künnemeyer (2003). "Internal quality assessment of mandarin fruit by vis/NIR spectroscopy." Journal of Near Infrared Spectroscopy **11**(5): 323-332.

McGlone, V. A., D. G. Fraser, R. B. Jordan and R. Kunnemeyer (2003). "Internal quality assessment of mandarin fruit by vis/NIR spectroscopy." Journal of Near Infrared Spectroscopy **11**(5): 323-332.

McGlone, V. A., R. B. Jordan and P. J. Martinsen (2002). "Vis/NIR estimation at harvest of pre-and post-storage quality indices for 'Royal Gala'apple." Postharvest Biology and Technology **25**(2): 135-144.

Mehinagic, E., G. Royer, R. Symoneaux, D. Bertrand and F. Jourjon (2004). "Prediction of the sensory quality of apples by physical measurements." Postharvest biology and technology **34**(3): 257-269.

Mehl, P. M., Y.-R. Chen, M. S. Kim and D. E. Chan (2004). "Development of hyperspectral imaging technique for the detection of apple surface defects and contaminations." Journal of Food Engineering **61**(1): 67-81.

Moghimi, A., M. H. Aghkhani, A. Sazgarnia and M. Sarmad (2010). "Vis/NIR spectroscopy and chemometrics for the prediction of soluble solids content and acidity (pH) of kiwifruit." Biosystems engineering **106**(3): 295-302.

Naes, T., T. Isaksson, T. Fearn and T. Davies (2002). A user friendly guide to multivariate calibration and classification, NIR publications.

Nascimento, P. A. M., L. C. d. Carvalho, L. C. C. Júnior, F. M. V. Pereira and G. H. d. A. Teixeira (2016). "Robust PLS models for soluble solids content and firmness determination in low chilling peach using near-infrared spectroscopy (NIR)." Postharvest Biology and Technology **111**: 345-351.

Nicolai, B. M., K. Beullens, E. Bobelyn, A. Peirs, W. Saeys, K. I. Theron and J. Lammertyn (2007). "Nondestructive measurement of fruit and vegetable quality by means of NIR spectroscopy: A review." Postharvest Biology and Technology **46**(2): 99-118.

Osborne, B. G., T. Fearn and P. H. Hindle (1993). Practical NIR spectroscopy with applications in food and beverage analysis, Longman scientific and technical.

Pan, L., R. Lu, Q. Zhu, J. M. McGrath and K. Tu (2015). "Measurement of moisture, soluble solids, sucrose content and mechanical properties in sugar beet using portable visible and near-infrared spectroscopy." Postharvest Biology and Technology **102**: 42-50.

Pérez-Marín, D., A. Garrido-Varo and J. Guerrero (2007). "Non-linear regression methods in NIRS quantitative analysis." Talanta **72**(1): 28-42.

Peri, G., G. Colelli and R. Romaniello (2005). "Predizione del contenuto in solidi solubili delle mele mediante imaging iperspettrale." Proceedings of AIIA: 27-30.

Pissard, A., J. A. Fernández Pierna, V. Baeten, G. Sinnaeve, G. Lognay, A. Mouteau, P. Dupont, A. Rondia and M. Lateur (2013). "Non-destructive measurement of vitamin C, total polyphenol and sugar content in apples using near-infrared spectroscopy." Journal of the Science of Food and Agriculture

93(2): 238-244.

Pu, H., D. Liu, L. Wang and D.-W. Sun (2016). "Soluble Solids Content and pH Prediction and Maturity Discrimination of Lychee Fruits Using Visible and Near Infrared Hyperspectral Imaging." Food Analytical Methods **9**(1): 235-244.

Pu, Y.-Y. and D.-W. Sun (2015). "Vis–NIR hyperspectral imaging in visualizing moisture distribution of mango slices during microwave-vacuum drying." Food Chemistry **188**: 271-278.

Rady, A., D. Guyer and R. Lu (2015). "Evaluation of Sugar Content of Potatoes using Hyperspectral Imaging." Food and Bioprocess Technology **8**(5): 995-1010.

Rajkumar, P., N. Wang, G. EImasry, G. Raghavan and Y. Gariepy (2012). "Studies on banana fruit quality and maturity stages using hyperspectral imaging." Journal of Food Engineering **108**(1): 194-200.

Roy, S., R. C. Anantheswaran, J. S. Shenk, M. O. Westerhaus and R. B. Beelman (1993). "Determination of moisture content of mushrooms by Vis—NIR spectroscopy." Journal of the Science of Food and Agriculture **63**(3): 355-360.

Rungpichayapichet, P., B. Mahayothee, P. Khuwijitjaru, M. Nagle and J. Müller (2015). "Non-destructive determination of β-carotene content in mango by near-infrared spectroscopy compared with colorimetric measurements." Journal of Food Composition and Analysis **38**: 32-41.

Rungpichayapichet, P., B. Mahayothee, M. Nagle, P. Khuwijitjaru and J. Müller (2016). "Robust NIRS models for non-destructive prediction of postharvest fruit ripeness and quality in mango." Postharvest Biology and Technology **111**: 31-40.

Savitzky, A. and M. J. Golay (1964). "Smoothing and differentiation of data by simplified least squares procedures." Analytical chemistry **36**(8): 1627-1639.

Schaare, P. and D. Fraser (2000). "Comparison of reflectance, interactance and transmission modes of visible-near infrared spectroscopy for measuring internal properties of kiwifruit (Actinidia chinensis)." Postharvest Biology and Technology **20**(2): 175-184.

Shenk, J. and M. Westerhaus (1995). Analysis of agriculture and food products by near infrared reflectance spectroscopy. Monograph. 12101 Tech Road, Silver Spring, MD 20904, USA: NIRSystems, Inc.

Shenk, J. and M. Westerhaus (1995). "Analysis of agriculture and food products by near reflectance

spectroscopy. Foss NIRSystems." Inc, Silver Spring.

Sinelli, N., A. Spinardi, V. Di Egidio, I. Mignani and E. Casiraghi (2008). "Evaluation of quality and nutraceutical content of blueberries (Vaccinium corymbosum L.) by near and mid-infrared spectroscopy." Postharvest Biology and Technology **50**(1): 31-36.

Subedi, P., K. B. Walsh and G. Owens (2007). "Prediction of mango eating quality at harvest using short-wave near infrared spectrometry." Postharvest Biology and Technology **43**(3): 326-334.

Sun, D.-W. (2010). Hyperspectral imaging for food quality analysis and control, Elsevier.

Westerhaus, M., J. Workman, J. B. Reeves and H. Mark (2004). "Quantitative analysis." Near-infrared spectroscopy in agriculture(nearinfraredspe): 133-174.

Wicke, E. (1976). "WAP Luck (Ed.): Structure of Water and Aqueous Solutions, Proceedings of the International Symposium Marburg 1973, Verlag Chemie GmbH und Physik Verlag GmbH, Weinheim/Bergstraße 1974, XXX+ 590 Seiten mit 247 Abb. und 48 Tab., Preis: DM 94,–." Berichte der Bunsengesellschaft für physikalische Chemie **80**(7): 673-673.

Williams, P. and K. Norris (1987). Near-infrared technology in the agricultural and food industries, American Association of Cereal Chemists, Inc.

Williams, P. C. and D. Sobering (1996). "How do we do it: a brief summary of the methods we use in developing near infrared calibrations." Near infrared spectroscopy: The future waves: 185-188.

Wu, D. and D.-W. Sun (2013). "Advanced applications of hyperspectral imaging technology for food quality and safety analysis and assessment: A review — Part I: Fundamentals." Innovative Food Science & Emerging Technologies **19**: 1-14.

Xing, J., C. Bravo, P. T. Jancsok, H. Ramon and J. De Baerdemaeker (2005). "Detecting bruises on 'Golden Delicious' apples using hyperspectral imaging with multiple wavebands." Biosystems Engineering **90**(1): 27-36.

Yang, H. and J. Irudayaraj (2002). "Rapid determination of vitamin C by NIR, MIR and FT-Raman techniques." Journal of Pharmacy and Pharmacology **54**(9): 1247-1255.

Yang, Y.-C., D.-W. Sun, H. Pu, N.-N. Wang and Z. Zhu (2015). "Rapid detection of anthocyanin content in lychee pericarp during storage using hyperspectral imaging coupled with model fusion." Postharvest Biology and Technology **103**: 55-65.

Yang, Y., J. Ren, X. Zheng, L. Zhao and M. Li (2014). "[Rapid determination of beet sugar content using near infrared spectroscopy]." Guang pu xue yu guang pu fen xi= Guang pu **34**(10): 2728-2731.

Ying, Y., H. Lu, X. Fu, Y. Liu, H. Xu and H. Yu (2005). Application FT-NIR in rapid estimation of soluble solids content of intact kiwifruits by reflectance mode. Optics East 2005, International Society for Optics and Photonics.

Zude, M., B. Herold, J.-M. Roger, V. Bellon-Maurel and S. Landahl (2006). "Non-destructive tests on the prediction of apple fruit flesh firmness and soluble solids content on tree and in shelf life." Journal of Food Engineering **77**(2): 254-260.

Chapter 2

IMAGE ANALYSIS

Muhammad Mudassir Arif Chaudhry[1], Farahmand Babellahi[1], Maria Luisa Amodio[1], Amna Sahar[2], Giancarlo Colelli[1]

[1] Dip.to di Scienze Agrarie, degli Alimenti e dell'Ambiente, Universita di Foggia, Via Napoli, 25, 71122 Foggia (Italy)

[2]Deparetment of Food Engineering, Faculty of Agricultural Engineering & Technology, University of Agriculture, Faisalabad

1. NEED FOR IMAGE ANALYSIS

With the rapid changes in lifestyles in the modern era, the demand for the healthy, safe, nutritious, authenticated and fresh food products have boosted in the past few decades. The consumers prefer convenient, ready to eat (RTE) and high quality food products with known origins. Moreover, awareness and concerns of the modern food consumers regarding food fraud, safety scandals and a globalized food production have oriented the research in food industries to develop standards for effectively interconnecting the systems of food production and distribution (Trienekens and Zuurbier, 2008). Food fraud and adulteration, are becoming highly sophisticated, vitalizing the need for high standard control on an increasing number of samples. As for fresh fruit and vegetable, product authenticity is the major concern both from consumer and processors who are concerned about unfair competition in the market (Reid et al., 2006). Location of origin, varieties and system of production are some of the production factors that need to be certified. Different labels in Europe, are intended to protect the geographic provenience of a product, recognized for its peculiar characteristics, or use of a particular farming method; the most important among them being, the protected designation of origin (PDO), protected geographical indication (PGI) and traditional specialty guaranteed (TSG). Higher price is in fact paid for the guarantees derived from these labels, as for social certification of sustainable production or for organically produced crops, thus increasing the risk of frauds. With the rising demand of the fresh cut produce, the food processing industries are orienting their research towards finding ways for the rapid, cost effective, reliable, nondestructive and low environmental impact techniques for the assessment of

quality, adulteration and origin of the food products.

Traditional techniques, used for food authentication rely on the detection of trace elements (element profiling) and isotope ratio, particularly important for the authentication of geographical origin and growing system, since plants derive their composition from the soil and the production system applied and also the ratio of stable isotopes varies with climatic conditions, geographical origin, and soil type. Moreover, rare-earth elements are directly linked to the geology of the area and are a powerful discriminating factor for geographical origin. Liquid and gas chromatography (LC and GC), eventually coupled with mass spectroscopy (MS), Nuclear Magnetic Resonance (NMR), Isotope Ratio Mass Spectrometry (IRMS), Multi Collector – Inductively Coupled Plasma – Mass Spectrometry (MC-ICP-MS), Thermal Ionization Mass Spectrometry (TIMS), Inductively Coupled Plasma-Mass Spectroscopy (ICP-MS) and Inductively Coupled Plasma-Atomic Emission Spectroscopy (ICP-AES) are used for food authentication. Molecular tools as Polymerase Chain Reaction (PCR) are used for species and cultivar differentiation, for detection of Genetic Modified Organism (GMO) but also in other fields related to food origin and production.

Since the conventional destructive analysis methods are time consuming, expensive, targeted and labor intensive therefore, the nondestructive methods due to their reliability, rapidness and cost effectiveness are gaining popularity in the food industry with widely developed methods for the classification of fruits and vegetables, origin and variety, defect detection and internal composition prediction. Rising concerns regarding the nutritional composition led many research works to evaluate the feasibility of the spectral profiles in the visible near infrared range (Vis-NIR), near infrared range (NIR) and hyperspectral images (HSI) for prediction and mapping of desired compounds in fresh produce. These techniques hold significant advantages over the chemical analysis since the chemical analysis are more time consuming, costly, adversely impact the environment, need careful sample preparation and require skilled personnel to yield expected results. It is important to mention that non-destructive techniques cannot completely replace the conventional methods but can serve to assist these techniques saving time, expenses and labor. On the other hand, the non-destructive methods need no sample preparation once the model is developed making the prediction process quick. This chapter will focus on the nondestructive techniques with special emphasis on hyperspectral imaging for the quality assessment of the fresh produce and will

present a basic introduction of the nondestructive image analysis techniques.

2. IMAGE ACQUISITION METHODS IN FOOD TECHNOLOGY

2.1 Relationship between images, spectroscopy and hyperspectral imaging

Computer vision technology uses various image processing routines hence providing a reliable alternative for the transition of industry towards automation. A computer vision system typically comprise an illumination system connected to a personal computer further in connection with electrical and mechanical devices which operate as an alternative for the replacement of human manipulative efforts in process management and performance (Du and Sun, 2006). But there are a few limitations associated with the computer vision technology to be used for industrial applications, since they are only confined to the measurement of external attributes and are unable to define the internal features. Modern food industries require systems capable for the classification of the products having similar appearance, quantification of internal/chemical quality attributes, and detection of invisible internal defects.

In this regard for the measurement of optical properties based on reflectance, absorbance and transmittance modes, of the food products, using spectral devices have proved to be very reliable for evaluation of internal quality attributes, classification and defect detection. Most commonly the spectral devices measure the ultraviolet (UV), visible (VIS) and near infrared (NIR) regions along with their combinations in the electromagnetic spectrum (Jayas et al., 2010).

The energy released or absorbed by charged particles is known as electromagnetic radiation which possesses electric and magnetic field components which oscillate (troughs and crusts) perpendicular to the direction of the energy propagation as well as each other. The distance between two adjacent crests or two adjacent troughs is termed as *wavelength*. This electromagnetic radiation is associated with a particular wavelength range termed as 'electromagnetic spectrum' (see Figure 1). The electromagnetic spectrum is divided into seven major regions starting from higher frequency to lower frequency and difference in the size of the waves, since frequency is inversely proportional to the wavelength (Equation 1). Among these regions, the human eye can only detect 300nm of the electromagnetic field with bare eyes i.e. in a range of 400-700 nm known as the visible region.

$$v = f\lambda \qquad \text{(Equation 1)}$$

Where, v is the speed of the wave (3.0×10^8 ms^{-1} in case of vacuum), f is the frequency and λ is the wavelength. Quantitative and qualitative analysis of various materials are conducted on the basis of the

interaction of the light photons in the electromagnetic spectrum with the molecules of various materials under study. Therefore, in the food and agriculture industry the assessment of various physical and chemical properties of products is carried out on the basis of this interaction.

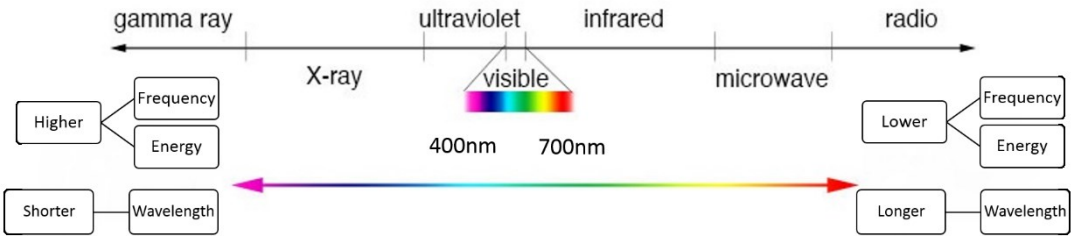

Figure 1. The Electromagnetic Spectrum

An image can be defined as a two dimensional function $f(x, y)$ where x and y represent the spatial coordinates and the amplitude of f at any given coordinate (x, y) is called the gray level or intensity of the image at that point. Each digital image comprises of a limited number of values or *pixels* each of which is located at a particular place along with a value assigned. Color images are formed by the combination of two or more 2-D images such as an RGB (red, green, blue) image (see Figure 2).

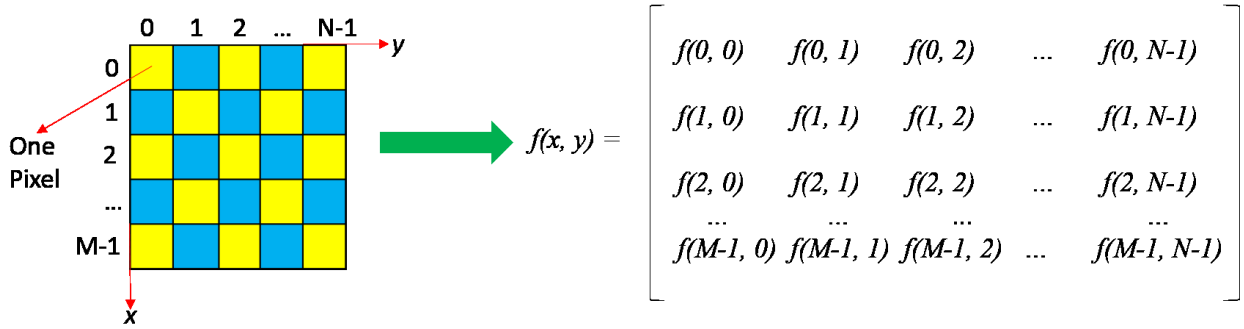

Figure 2. Coordinate convention for a simple 2-D spatial gray scale image and its matrix representation

In Figure 2 the 2D digital image conceptual representation is shown and $f(x, y)$ is by definition a digital image itself and whereas the array represents each element of the image known as image element, picture element or *pixel*.

Hence a gray scale image provides the intensity of reflected light over a single band from the electromagnetic spectrum. On the other hand, a color image constitute intensity over the red, green and blue bands of the electromagnetic spectrum. HSIs are composed of multiple continuous bands over a

specified range of wavelengths possessing different resolutions in the electromagnetic spectrum. Increasing the number of bands enhances the capability of the image to carry more information. The purpose for the development of the HIS systems was to integrate the spatial and spectral information to obtain desired results which would not have been possible neither with spatial nor spectral techniques, if used individually. Since, the spectroscopy techniques alone provide the spectral information resulting from the interaction of photons of light with the molecules of the material under study as reflected intensity at different wavelengths hence formulating an explicit 'fingerprint' of the product whereas the imaging technique provides spatial and temporal information in a 2D space. Integration of these two techniques results in a formulation of 3D data cube with the spatial dimensions along the *x* and *y* coordinates and a spectral dimension along the *z* coordinate (see Figure 3).

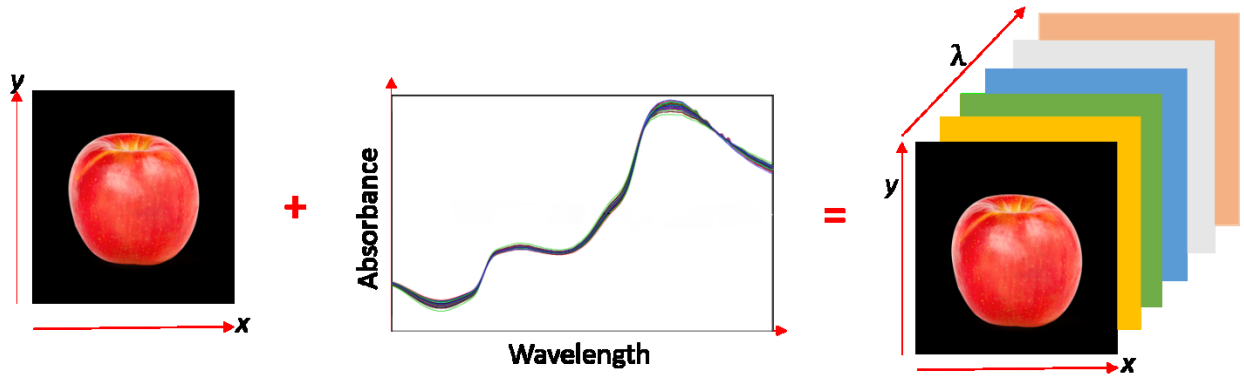

Figure 3. Phenomenon for the formulation of hyperspectral cube where *x* and *y* are the spatial dimensions and *λ* represents the spectral dimension

Hyperspectral imaging technique has proved to be reliable, rapid and economical; providing elaborative analysis results with the spatial dimension representing the spatial distribution of the chemical compounds in the food products along with the spectral dimension representing the type of chemical compounds present in the specimen under consideration. Simply stating, the spatial dimension. Image processing and analysis is an integrating approach of the principles of mathematics, computer science and programming resulting in the enhancement of the systems performance to evaluate several samples per second rather than several seconds per sample. Table 1 provides a brief picture of the major differences between imaging, spectroscopy and hyperspectral imaging.

Table 1. Overview of differences between imaging, spectroscopy and hyperspectral imaging

Analysis Goals	Imaging	Spectroscopy	Hyperspectral Imaging
Spatial information	✓	✗	✓
Spectral information	✗	✓	✓
Chemical composition and mapping	✗	✗	✓
Defect/damage detection	✗	✗	✓

2.2 Basic Terminology

Proceeding further a basic introduction of the commonly used terminology including important expressions, definitions and technical information regarding hyperspectral image analysis is inevitable to highlight the differences and grasp the concepts efficiently.

2.2.1 Spatial Resolution

The spatial resolution of an image is defined as the area in the image that is represented by one *pixel* of a 2-D image, mentioning more precisely, the spatial resolution refers to the number of pixels per unit length. Hence, in case of the hyperspectral images, the size of the smallest object that can be observed by the sensor on the sample as a distinct object refers to spatial resolution. Higher the spatial resolution the more detail the image carries.

2.2.2 Spectral Range

The number of wavelength regions in the electromagnetic spectrum covered by the hyperspectral imaging device is called the spectral range. Modern demands of chemical imaging and agricultural product analysis have led manufacturers to develop hyperspectral imaging devices covering different wavelength ranges of the electromagnetic spectrum depending on the types of analysis. In case of food analysis, the most commonly used spectral ranges are ultra violet (UV) (190-380nm), visible range (Vis) (380-700nm), Visible near infrared (Vis-NIR) (400-1000nm), and the near infrared (NIR) (800-1700nm) ranges. For more sophisticated applications, the devices in the short wave infrared (SWIR) range (900-2500nm) have also been developed but usually for the food applications near infrared (800-1700nm) is

most commonly used.

2.2.3 Spectral Resolution

It is the measure of the narrowest spectral feature that can be resolved by the spectrograph of the hyperspectral imaging device in the electromagnetic spectrum. Hence, the ultimate capability of the spectrograph in separating the two adjacent monochromatic features emitted by a particular point in an image refers to the spectral resolution. The magnitude of the spectral resolution is related to the wavelength dispersion of the spectrograph as well as the entrance and exit aperture sizes.

2.2.4 Band Numbers and Band Width

The number of bands usually can be referred to the number of images or number of wavelengths stacked to form a single hyperspectral image. In other words, in case of a multispectral image the band numbers are usually lower (>10) referring to the informative images at certain wavelengths while in case of the hyperspectral images the number of spectral bands may range from 100-250 depending upon the type of the hyperspectral imaging device being used.

2.2.5 Signal to Noise ratio (SNR)

The ratio between the measured radiance by the hyperspectral imaging device and the noise created by the electronic components and detector of the imaging system is defined as signal to noise ratio. In other words, SNR is a comparison of the level of signal desired to the level of background noise, hence, higher the ration the lower the interference of the noise. In case of the hyperspectral imaging the SNR is wavelength depended due to the reason that a decrease is seen in the overall radiance over the longer wavelengths along the electromagnetic spectrum.

2.2.6 Spectral Signature

Spectral signature can be defined as the pattern of electromagnetic energy reflected, absorbed or transmitted at a specific wavelength. All the materials possess distinctive chemical, physical and biological features that can be distinguished by observing the patterns of the reflection, absorbance, and emittance of light or electromagnetic energy at specific wavelengths which is the basic fact exploited by the hyperspectral imaging. This feature is known as spectral signature or spectral fingerprint. Each pixel in the hyperspectral image has its own spectral signature.

2.3 RGB Imaging

Color plays a significant role in human visual perception as well as in computer vision. Thousands of

color shades and intensities can be discerned by the human eyes compared with approximately 24 shades of grey. Natural scenes are recognized by computer vision based on color information. Color plays a role of an important descriptor in automated image analysis for simplification of object identification and extraction from a scene. Three factors are responsible for the perceived color of objects: the spectral reflectance from the sample (how surfaces reflect color), intensity of ambient illumination (the color content of light shining on a surface), and the spectral response of the sensors in the imaging system (Gunasekaran, 1996). A tremendous amount of spatial resolution is offered by color vision that is useful for the quantification of the ingredient color distribution and surface texture in a food system. There are two major categories of color image processing firstly, full-color processing with the images obtained from a full-color sensor; and secondly, pseudo-color processing, which works by the assignment of each color shade to a particular monochrome intensity or range of intensities.

Three primary colors red, green, and blue (RGB) constitute the color combination of the photographed image. This is known as additive color system since if equal amount of three colors are combined, they form white. Color images can be created by placing red, green, and blue filters over individual pixels on the image sensor which in most cameras is a charge coupled device (CCD). Interpolation is used by the camera for the computation of the actual color of each pixel by combining the color it captured directly through the filter with the other two colors captured by the pixels around it (Figure 4).

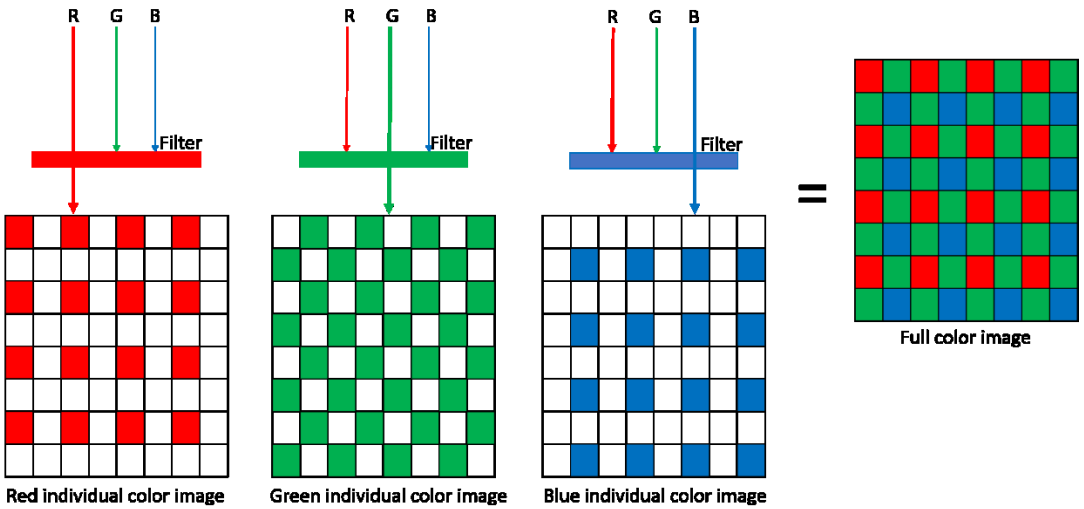

Figure 4. Working principle of RGB camera (Sensor red, green and blue color filtered pixels separately and full color image)

Currently, development of some smartphone applications are also under progress to access certain color related quality attributes. The devices that contain a charged coupled detector (CCD) usually use RGB coding in which the pixels are coded in the red, green and blue channels in between a range of 0-255, where 0 refers to black while 255 refers to white. These images can also be represented in other systems by conversion of the RGB variables to other color spaces such as Lab (or CIELab), where L represents lightness, and a and b mark the variations from red to green and yellow to blue; HSV (Hue, Saturation, Value) a cylindrical-coordinate system which is a representation of human vision; YCBCR, used for luma chroma JPEG conversion, where y represents the luminance component and both CB and CR the chromatic components and CMYK (cyan, magenta, yellow, key), which is used usually in color printing.

2.3.1 RGB model

Every color in an RGB model is represented in its primary spectral components of red, green, and blue based on a Cartesian coordinate system in which the cubical color subspace of which is shown in Figure 5. In this case the RGB primary values can be seen at three corners while the secondary colors (cyan, magenta, and yellow) formulate the rest of the three corners; the black color (value 0) lies at the origin and white (value 255) is at the corner farthest from the origin. In this model, the gray scale (points of equal RGB values) extends from black to white from the RGB values (0, 0, 0) to (255, 255, 255). The different colors in this model are basically defined with the help of vectors extending form the origin and can be seen on or inside the cube (Gonzales and Wintz, 1987). If all R, G and B possess zero values then the resulting color is black and when all these color values are maximum i.e. 255 each, the color in this case is white. Usually in computer vision systems, each the base-color intensities possess 8 bits of resolution thus, representing each point in the image by 24 bits of data. Moreover, for obtaining information on any point in the image, analysis of all 24 bits of data must be done (Gunasekaran, 1996). Also Figure 5 shows the splitting of an RGB image of grape wine leaf into separate red, green and blue colors.

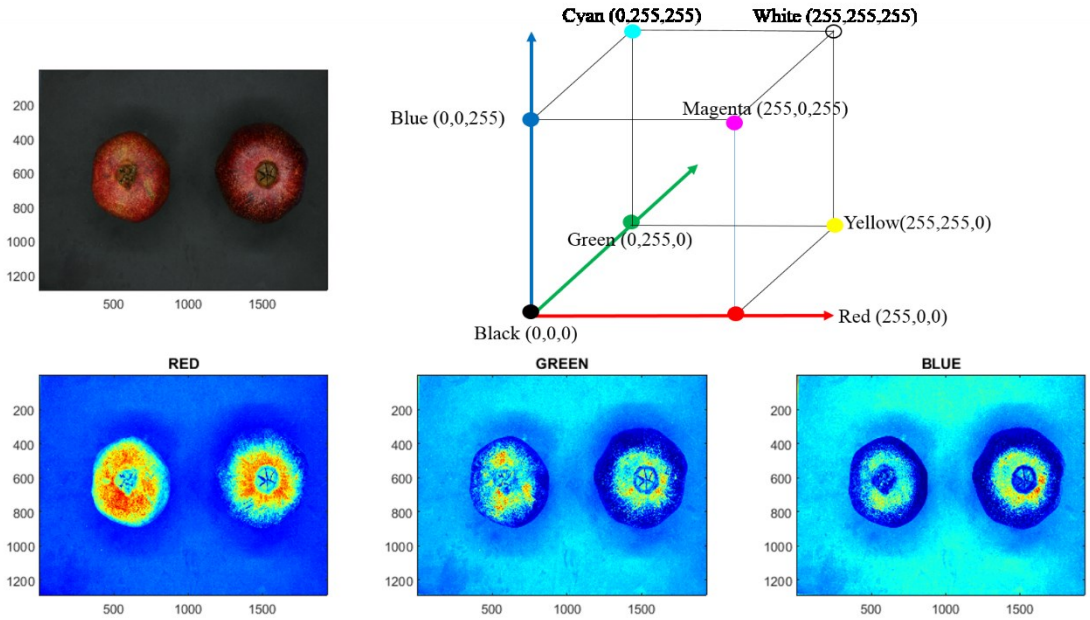

Figure 5. Schematic diagram of an RGB color cube and splitting of an RGB image of pomegranates into red, green and blue

2.3.2 CIE Lab color model

This color space was created by the International Commission on Illumination (CIE) in 1931 and was one of the first color spaces mathematically defined. It is also known as CIELAB color model. CIE L*a*b lies among the color spaces which were derived from CIE XYZ space in 1976. In L*a*b* color model the color is determined with respect to the position in a 3D color space. All the colors visible to the human eye were described and the creation of this model was aimed at serving a device-independent model. The Hunter and the CIE L*a*b* models use the following parameters, namely lightness represented as L*. Black color is yielded by an L* value of 0 while an L* value of 100 indicates diffuse white. In this case, a* represents the Chroma or position of a color between red/magenta and green. a* value with a negative sign indicates green color while magenta is indicated with a positive value. b* shows the position of the color between yellow and blue. Negative values on this case indicate blue color and positive values indicate yellow color.

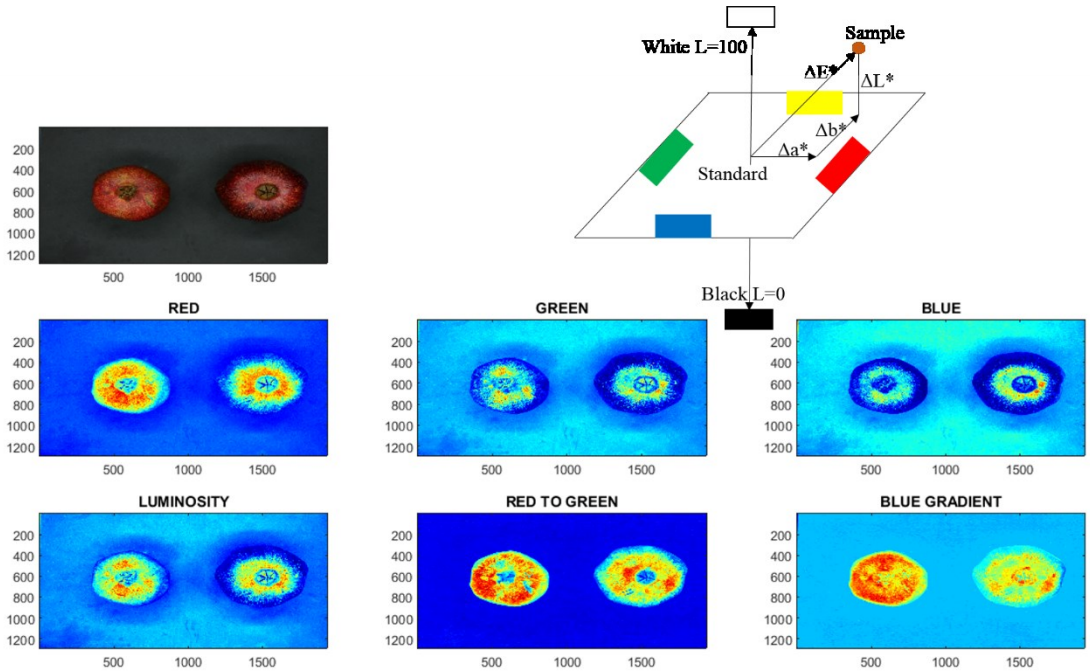

Figure 6. Schematic diagram of CIE Lab model and conversion from the RGB image of pomegranates to CIE Lab model

2.3.3 HSV model

The HSV model is composed of 3 components, namely hue, saturation and value. In cases where value is substituted by brightness the model is named as HSB. In this model the resemblance to the human color perception is higher as compared to other additive and the subtractive color models. Technically, in CIECAM02 model the hue, saturation and brightness, has been defined. Hue is defined as the degree to which a stimulus can be described as similar to or different from stimuli that are described as red, green, blue, and yellow (the unique hues). Intensity on the other hand is the total amount of light passing through a particular area and an attribute of a visual sensation according to which an area appears to emit more or less light is called brightness. The brightness that is related to the brightness of a similarly illuminated white is called lightness value. Moreover, the attribute of a visual sensation according to which the perceived color of an area appears to be more or less chromatic is called colorfulness. Colorfulness is the degree of difference between a color and gray. Furthermore, saturation is defined as the colorfulness of a stimulus relative to its own brightness.

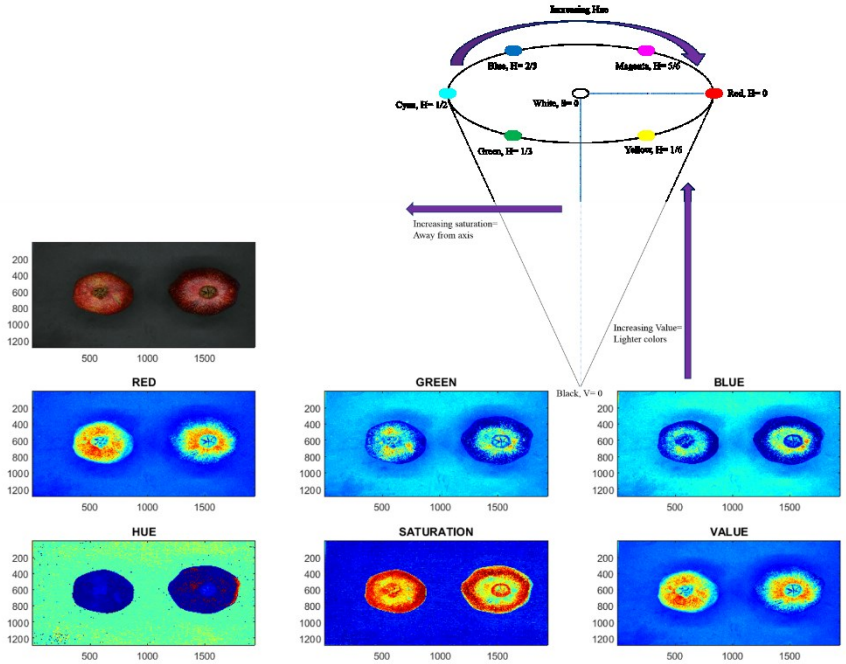

Figure 7. Schematic diagram of HSV model and conversion from RGB image of pomegranates to HSV color space

2.4 *Hyperspectral Imaging, Hyperspectral Data and Multispectral Imaging*

Hyperspectral imaging has proved to be a reliable chemical or spectroscopic imaging analytical tool, in a variety of fields such as agriculture, pharmaceuticals, astronomy and medicine. This emerging technique is an integration of imaging technique and spectroscopy, attaining both spatial and spectral information simultaneously in a data cube. Hyperspectral images consist of a stack of images of the same object over a large number of contiguous wavebands for each spatial position for a targeted study formulating a 3D data cube (Diwan P. Ariana and Lu, 2008). Since each pixel possesses its own spectra, these can be useful for the characterization of the composition of that specific position and the spatial images provide the surface feature information. The composition of the sample under consideration can be accessed by the spectral dimension whereas the spatial dimension helps in visualizing the location of a particular chemical compound, and both spectral and spatial dimensions integrated together provides an answer to "what and where" in the food sample the desired compound exists (Wu and Sun, 2013a). Voxels or vector pixels contain the spectral information, whereas the spatial information is contained in

an image with two dimensions having *x* rows and *y* columns. In the hypercube shown in figure 8, each spectral signature belongs to a pixel that corresponds to a specific spatial region, which records the entire spectrum of the measured spatial pixels. Hence, the resulting spectrum form an image is measured as the capability of the sample for scattering or absorbing of the exciting light, simultaneously presenting the characteristic chemical information and hence in this way the spatial images can be used for attaining surface-feature information.

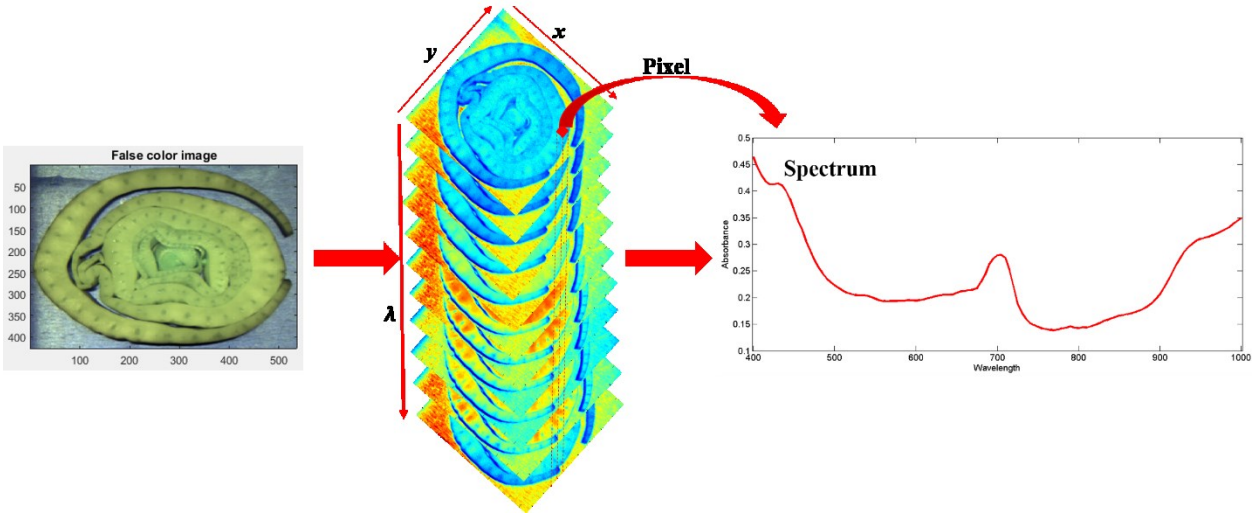

Figure 8. Hyperspectral image of fresh cut fennels and spectrum of a pixel

2.4.1 Components of Hyperspectral imaging system

Instrumentation plays a basic and important role for the acquisition of high quality and reliable hyperspectral images. The selection of the components, setup design and calibration of the images require a background knowledge of the configuration of the hyperspectral imaging devices. The integral components of hyperspectral imaging devices are excitation source (light), devices for wavelength dispersion and area detectors.

Light sources are aimed at excitation or illumination of the sample constituting an essential component of the optical system. In this regard the halogen lamps, light emitting diodes (LEDs), lasers and tunable light sources are most significantly used. Halogen lamps are a broadband illumination source and are frequently utilized in the visible and near-infrared spectral ranges. Usually, a tungsten lamp filament is enclosed in a halogen gas filled quartz glass bulb for the formulation of a halogen bulb or source. At higher temperatures the filament produces an incandescent emission generating a light source as an

output. In this case, the light is a smooth continuous spectrum in the visible and the near infrared regions without having any sharp peaks (Wu and Sun, 2013b). Halogen lamps have been used in the food applications as illumination sources for external and internal information acquisition (D P Ariana and Lu, 2008; Wu et al., 2012; Amodio et al., 2017). But in case of halogen lamps few drawbacks exist such as, a shorter life span, rapid heating, voltage fluctuations effecting output stability and sensitivity to vibrations. On the other hand, the LEDs can produce a narrow band light in different wavelengths of the ultraviolet, visible and near infrared regions along with producing high intensity broadband white light. LEDs are also prone to voltage fluctuations, temperature and certain intensity issues have been observed compared to halogens since LEDs have comparatively lower intensity and grainy light is produced by increasing the number of LEDs in bulbs. Presently, LEDs have not been frequently utilized in the food analysis research and are in development phase. Lasers are monochromatic sources of light mostly used in Raman and fluorescence applications (Yang et al., 2012; Jiménez-Carvelo et al., 2017). The major characteristics of laser light are monochromaticity, directionality and coherence. In case of tunable light sources, between the sample and the light source, a dispersion device is used which works on the basis of area scan mode and not used for the line scanning and point scanning. These light sources due to weak illumination are not suitable for the conveyor belts used in food industries.

An integral part of the hyperspectral imaging system is comprised of wavelength dispersion devices which are used for dispersion of the broadband light into various wavelengths. The most commonly used wavelength dispersion devices include filter wheels, imaging spectrographs, liquid crystal tunable filters, Fourier transform imaging spectrographs and single shot imagers. In this chapter only the imaging spectrographs will be emphasized since they are most commonly used with the line scan system. An imaging spectrograph comprising diffraction gratings is used for the dispersion of the broadband light that is incident on the sample into different wavelengths and generates a spectrum for each point on the scanned line. Equally spaced transmitting or reflecting elements separated from each other by a distance in order of light wavelength under study formulate a diffraction grating (Palmer, 2005). Image spectrographs are basically divided into two major categories named transmission gratings and reflectance gratings. In case of transmission gratings, the grating is superimposed on a transparent surface while as the name indicates, in case of the reflectance grating the surface is reflective with a grating

superimposed on it. Figure 9 shows the flowchart diagram of the components of a common push broom (line scan) hyperspectral imaging system.

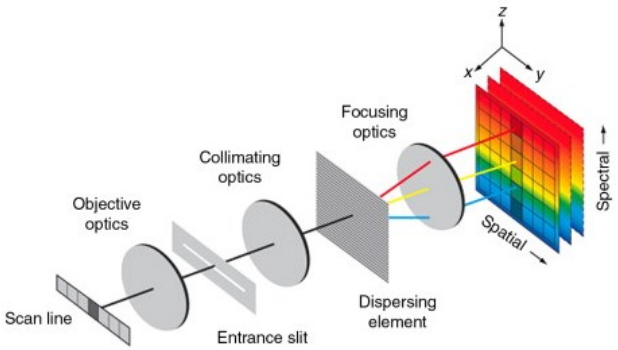

Figure 9. Optical chain of common push broom imaging spectrometer *adapted from* (Dell'Endice et al., 2009)

The transmission grating is seldom used due to limited properties of the resin and limited operability at higher diffraction angles. Therefore, reflectance gratings are most commonly used which possess greater advantages over the transmission grating such as high quality images with low distortion and larger field size (Bannon and Thomas, 2005). The components of a reflection grating comprises of an entrance slit, two spherical mirrors that are concentric, a convex reflection grating that is aberration-corrected, and a detector. As soon as the light ray enters the slit, it is reflected to the reflection grating by one of the two mirrors resulting in the dispersion of the incident beam in a way that the direction of the light propagation is a function of its wavelength (Sun, 2010). The other mirror reflects this dispersed light towards the detector forming a continuous spectrum at different pixels. The reflection spectrographs provide a high signal to noise ratio (*S/N*) and perform well in low light conditions.

Area detectors convert the incident light photons into electrons and hence quantify the intensity of the light acquired. In hyperspectral imaging systems the most commonly used area detectors are charge coupled devices (CCD) cameras comprising of photovoltaic semiconductor devices. These devices are semiconductor components for exploiting the semiconductor properties such as Silicon (Si), gallium arsenide (GaAr) and germanium (Ge). Due to their low cost, temperature range and simple processing silicon is mostly used in semiconductor devices. In most spectral imaging devices, the semiconductor line or area arrays used are silicon (Si), indium gallium arsenide (InGaAs) and indium antimonide (InSb)

most commonly. Silicon (Si) arrays possess sensitivity towards a wavelength range from 400-1000 nm while for the longer wavelengths (1000-5000 nm) the indium antimonide (InSb) and indium gallium arsenide (InGaAs) are sensitive (Figure 10). For sensitivity optimization in different wavelength regions instruments are developed with overlapping detector elements with cooling arrangements especially for the near infrared regions for the reduction of the dark current enhancing the efficiency of the hyperspectral imaging devices.

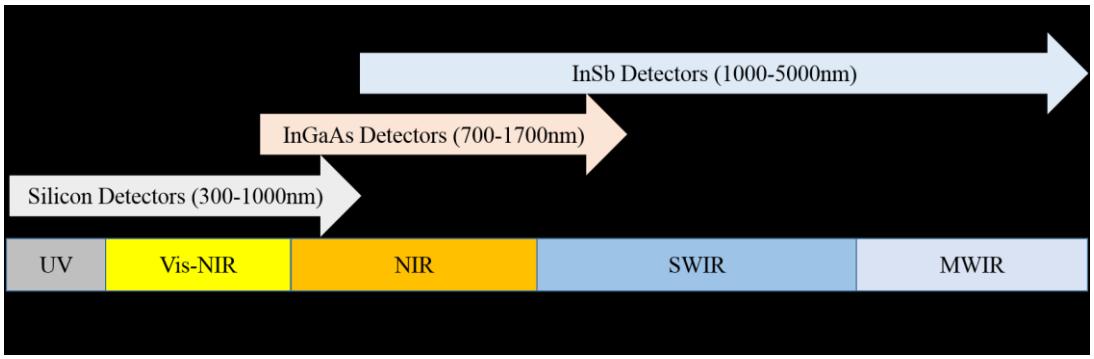

Figure 10. Detector materials and their sensitivity ranges over the electromagnetic spectrum

2.4.2 Hyperspectral Image Acquisition Modes

A spectral image can be acquired by three different modes conventionally used, namely, staring image, whiskbroom and push broom. Staring imaging is an area scanning mode also known as focal plane scanning imaging in which the image field of view is fixed and images are acquired wavelength by wavelength making it a wavelength scanning method. In case of whiskbroom method also known as point scan method the spectrum of a single point is measured and the next spectrum is acquired by moving the sample. The push broom or line scan method acquires a spectrum from a sample line which is further instantaneously recorded with the help of an array detector. The line scan method is highly compatible with the conveyor belt system and is the most used in the food industry for online applications. Therefore, in this chapter more details will be given regarding the line scan hyperspectral image acquisition mode.

In line scan devices a 2D grating and detector array are used to scan an entire line instead of a single pixel at a time. Out of the two dimensions of the sensor chip a single line of the sample at a time is scanned onto a pixel row and simultaneously on the second dimension a spectrum of each point on the line is generated by a spectrograph. Figure 9 shows the configuration of a line scan device. The line scan

configuration is usually used when the samples under study are moving with respect to the imaging system as in the food industry operations. The sensor detectors in a line scan system have a liner array arrangement hence capturing the entire scan line at once. In this case filter change is not required and the speed of image acquisition is a function of camera read out speeds. Conclusively, in a line scan system the 3D data cube is formed by capturing a line of spatial information possessing a full spectral range for each pixel of the spatial information which is the most suitable case of the real time evaluation of the samples in the conveyor belt system in the food industry (Kim et al., 2001; Sun, 2010).

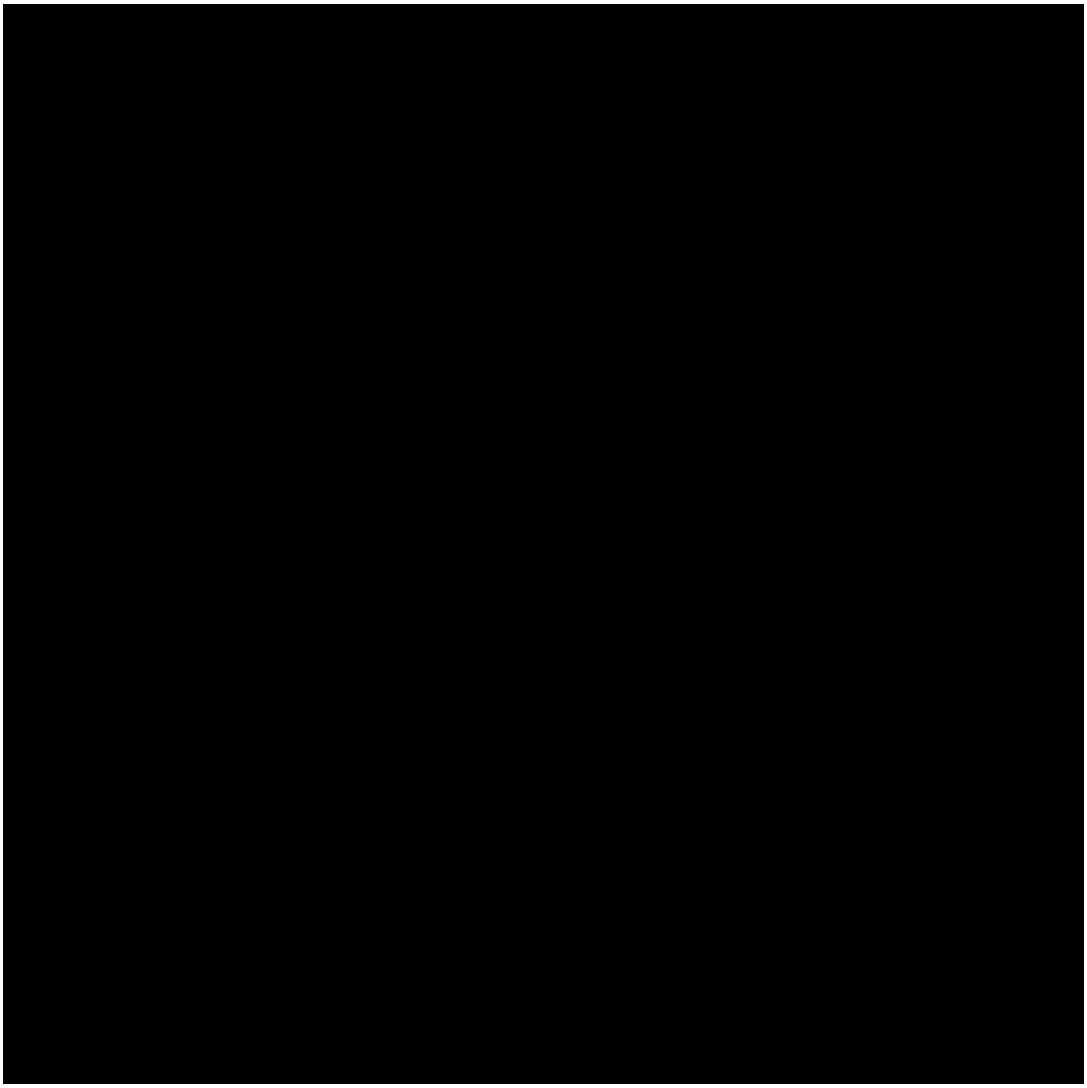

Figure 11. Flow chart diagram for Hyperspectral image processing

2.5 Calibration of Raw Hyperspectral Images

In order to secure the consistency of the hyperspectral system and for the reliability of the obtained results, the calibration of the hyperspectral imaging systems holds great importance. For this purpose mainly, wavelength, spatial and curvature calibration is done followed by reflectance calibration (Wu and Sun, 2013b). The major aims for the calibration of the hyperspectral imaging systems include the standardization of the spectral axis, determination of correct operation of the system, acquisition and validation of the spectral data and diagnosing the instrumental errors. Even under the controlled measurement conditions the reference spectra may vary in some systems hence putting forth the necessity for a standard calibration and validation procedure. Wavelength calibration is aimed at the identification of every pixel with a specific wavelength along the spectral dimension. In the calibration process, the calibration lamps including Argon (Ar), Mercury (Hg), Krypton (Kr), Mercury Argon (Hg/Ar), Xenon (Xe) and Neon (Ne) are scanned with the hyperspectral imaging devices resulting in the identification of the spectral peaks and corresponding pixel indices over the spectral dimension followed by the formulation of regression models between the two parameters. This regression is used for the identification of the wavelengths of all the pixels in the spectral dimension.

The dimensions and resolution of the field of view of hyperspectral imaging system are determined via spatial calibration. Since in the line scanning systems two spatial dimensions differ based on the phenomenon of their formulation hence resulting in two different resolutions of the spatial dimensions. In this case, the x direction pixels are acquired as a result of sample movement over the platform (stepwise) while the pixels in the y direction are obtained from the spectrograph. The x direction resolution is a function of step size of movement per pixel and the range is the distance of the movement while the calibration of the y direction is done by scanning thin parallel lines as a target. Resolution of the y direction is the ratio of the distance of a range on the thin parallel line target to the number of pixels on the range whereas the y direction range is a product of the number of pixels in the scanned image and the resolution (Wu and Sun, 2013b).

The hyperspectral imaging systems are calibrated for curvature for the analysis of the food products that possess a spherical geometry assuring the spectrum of pixels independent of the location. The amount of reflected light in this case is usually corrected based on the angle (ϕ or Θ) between the incident light and

normal to the direction of surface. For mandarins curvature calibration was proposed by (Gómez-Sanchis et al., 2008) as follows:

$$\rho(\lambda) = \frac{\rho_{xy}(\lambda)}{[\alpha_D \cos(\emptyset)+(1-\alpha_D)]} \quad \text{(Equation 2)}$$

Where, $\rho(\lambda)$ is the corrected spectrum in the spatial point (x, y) at the wavelength λ, whereas α_D represents the ratio between the direct light and the total average lights and the amount of reflected direct light at each pixel is given by $\cos(\phi)$. Similarly, in another study conducted by (Qin and Lu, 2008), the geometric relation between the fruit and the imaging system such as the fruit surface curvature effects in measured reflectance scattering were taken into account and the corrected reflectance was calculated by applying a correction factor C(r). Moreover, (Peng and Lu, 2008) introduced various modified Lorentzian distribution functions were applied the fitting of spectral scattering profiles at individual wavelengths for countering the scattering effects due to the spherical surface of golden delicious apples. (Gowen et al., 2008) proposed multiplicative scatter correction (MSC) was also proposed for the reduction of the spectral variability in mushrooms due to surface curvature.

Once the hyperspectral image is obtained the reflectance calibration is done using the black and the white reference images since the raw hyperspectral image is the intensity of the detector signal. The aim of the reflectance calibration is the removal of the dark current of the camera sensor. The same procedure is adopted to acquire white reference image (W_r) utilizing a white surface board which is smooth, uniform, stable and possessing a reflectance value of 99.9% while the black reference image (B_r) is acquired with the camera lens covered completely with an opaque cap and with the light source turned off. These black and white reference images are used according to the following equation for the correction of the raw hyperspectral image (I_{raw}).

$$I_c = \frac{I_{raw}-B_r}{W_r-B_r} x100 \quad \text{(Equation 3)}$$

Where, where I_c is the finally calibrated and corrected hyperspectral image in a unit relative reflectance, I_{raw} is the raw hyperspectral image, B_r is representing the black reference image and W_r is the white reference image.

2.6 Image Segmentation

Image segmentation is a process of dividing the image into different parts or regions, in other words into sets of pixels with an intention of simplified image analysis. Since an image is comprised of many pixels

so each pixel can be similar to the corresponding neighboring pixels with respect to a particular characteristic or property which may include intensity of the pixel, the color values, or textural characteristics. Image segmentation is practically employed for filtering noisy images, problems of feature extraction and recognition.

Determination of the technique of segmentation and the extent of the segmentation required is decided based on the aim or problem under consideration. Furthermore, another aim of matching the similar objects in two or more different images can be achieved using image segmentation. this is accomplished by pin pointing and segmenting the object of interest in the first image followed by matching of the segmentation result of the first image with the second image (Sapna Varshney et al., 2010).

2.6.1. Thresholding Methods

Thresholding is a procedure for the conversion of the multilevel images into binary images for image simplification. Converting an image into binary image means assigning a value of 0 to the background pixels and a value of 1 to the objects of interest or foreground pixels of an image. These values 0 and 1 are assigned on the basis of comparison with a threshold value T which can be intensity or a color value. A constant threshold value refers to global thresholding otherwise the thresholding is categorized as local thresholding. Background illumination plays a significant role in successful thresholding of the images since an unevenly illuminated background cannot be thresholded by the global thresholding methods and requires multiple thresholds for compensating the uneven illumination. Conventionally, image thresholding is done interactively but it is also possible to develop automated thresholding procedures (Kaur and Kaur, 2014; Gonzales and Wintz, 1987).

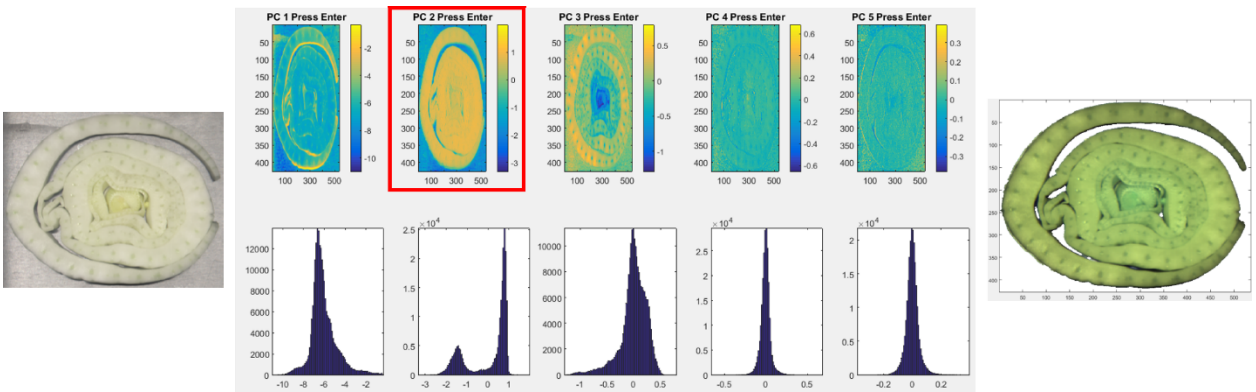

Figure 12. PCA based image segmentation

PCA is used for the simplification of the hyperspectral imaging data by making linear combinations of the original variables. Image thresholding can also be done using the PCA as shown in figure 12.

2.6.2. Edge-Detection Methods

One of the well-developed techniques for image processing includes edge detection methods which work on the basis of rapid variation in intensity values in the image under study, since a single intensity value does not provide good information about the edges. In case of edge detection methods, the edges are located where the first derivate of the intensity is higher than the threshold or where the second derivative has zero crossings. Firstly, after the detection of all the edges they are connected together for the formulation of object boundaries for the segmentation of the required regions. There are two commonly used edge based methods including, Gray histograms and Gradient based methods. Moreover, for the detection of the edges various techniques such as sobel operator, canny operator and Robert's operator are utilized resulting in the formulation of a binary image (Saleh Al-amri and Kalyankar, 2010).

2.6.3. Region-Based Methods

In case of the region based methods, the characteristics of an input image are used for the mapping of the individual pixels which are known as regions which possess correspondence to an object of interest or a meaningful part (see Figure 13). Various region based techniques including Local techniques, Global techniques and Splitting and merging techniques are commonly utilized. The determination of the region based method to be utilized is done based on the application area and the input image. For simple images local techniques can prove to be effective yielding the desired segmentation results whereas in case of complex images even the most sophisticated techniques cannot yield the required segmentation results (Gonzales and Wintz, 1987).

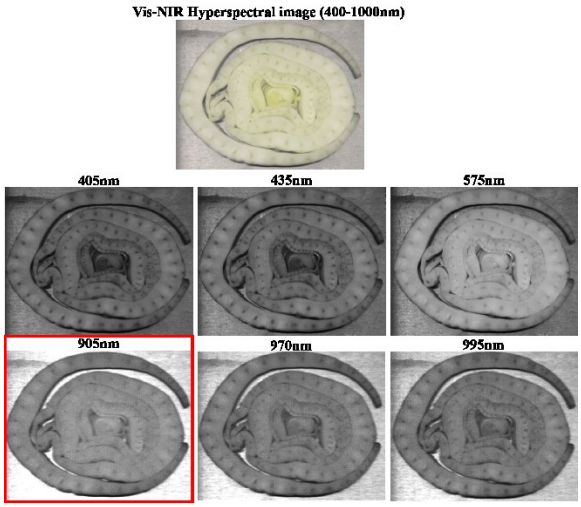

Figure 13. Otsu method for image segmentation (finding the best contrast between the image and the background) is a region based segmentation method

2.6.4. Clustering Methods

Clustering is an unsupervised learning phenomenon where the major aim for the formulation of clusters is to achieve a finite set of categories known as clusters for a proper visualization and description of the data. In case of clustering a training stage doesn't exist since it is utilized without any prior knowledge of the classes and hence in this way it differs from classification where the classes are analyzed with prior knowledge. Clustering functions by defining a similarity metric between the items of the data, hence grouping the similar items together in the form of clusters. Moreover, the identification of the attributes that provide the best clustering is significantly important to achieve reliable clusters. The clustering methods group the data on the principle of maximization of the intra class similarity and minimization of the inter class similarity. Clustering profiles which are responsible for the distinction among clusters are determined by analyzing the cluster properties. A new data instance is classified by assignment to the closest matching cluster, and is assumed to have characteristics similar to the other data in the cluster (Dehariya et al., 2010).

2.7 Data Exploration and Preprocessing

Hyperspectral images are data cubes with huge dimensionality and contained information. Therefore, data exploration techniques are a prerequisite for aim oriented image processing. Data exploration tools provide an insight of the image elements that cannot be accessed with simple observation providing the

sources of variability or co-variability in the image data. The most commonly used data exploration tool for preliminary investigation of hyperspectral imaging in the food industry is principle component analysis (from now on mentioned as PCA).

PCA is aimed at data dimensionality reduction, preserving maximum information by finding the principle components (PCs) which are the linear combinations of the original variables and each PC explains a direction of variance in the data with the first PC explaining the direction of the maximum variance. PCA is categorized as an unsupervised classification method. Mentioning simply, the information contained in 161 variables (wavelengths) can be explained by a few PCs, especially for pattern recognition and inner relationships in case of food analysis. Let **A** (XY x λ) be an unfolded hypercube with X and Y as the spatial dimensions and λ representing the spectral dimension, then the PCA formula can be given as:

$$X=TP^{T}+E \qquad \text{(Equation4)}$$

Where, T denote the loadings, P represents the scores and E is the error. Since the orthogonal PCs are projected in a new space the relationship between this new axis and the old axis is represented by the loadings plot. On the other hand, scores refer to the distance of the projected samples to the center of the new axis. The total variance explained can be given as:

$$Explained\ variance\ (\%) = \frac{\sum_{i=1}^{M}\sum_{j=1}^{N} \hat{x}_{ij}}{\sum_{i=1}^{M}\sum_{j=1}^{N} x_{ij}} \quad \text{where,} \quad \hat{x}_{ij} = \sum_{i=1}^{M}\sum_{j=1}^{N} t_{i1}p_{1j}^{T} \qquad \text{(Equation 5)}$$

As it can be clearly seen the scores samples plot give a clear variability of the PC scores with passage of time and also show that the variability changes rapidly with the increasing temperature i.e. the variability in the PC scores in the (blue block) which corresponds to the leaves stored at 15°C is the maximum. In this case the PC score variability corresponds to the quality degradation of the leaves.

Prior to application of the PCA data normalization is highly recommended which in case of the continuous variables (hyperspectral images) is mean centering and in case of the multispectral images auto scaling is used. The following equations correspond to the mean centering and auto scaling of the hyperspectral and the multispectral data respectively.

$$\hat{x}_i = x_i - \bar{x} \qquad \text{(Equation6)}$$

$$\hat{x}_i = \frac{x_i - x}{std(x)} \qquad \text{(Equation 7)}$$

The major aims for the data preprocessing are inclined to improve the data exploration, classification and calibration modelling by forcing the data to follow the Beers Lamberts law which suggests a linear relationship between the spectral measurements and the corresponding analytical analysis and is given by Equation 8 for transmittance measurements.

$$A_\lambda = -log_{10}(T) = \varepsilon_\lambda . I . c \qquad \text{(Equation 8)}$$

Where, A_λ is the absorbance (wavelength dependent), T represents transmittance, ε_λ is the molar absorptivity, I is the effective path length and c denotes the chemical concentrations.

In food data analysis, the most common preprocessing techniques are scatter correction and spectral derivatives in which the former represents the preprocessing operations such as Multiplicative Scatter Correction (MSC), Standard Normal variate (SNV) and normalization and the latter contains Norris-Willams (NS) derivatives and Savitzky-Golay (SG) polynomial derivative filters with both methods using smoothing prior to derivatization of the spectra.

MSC is the most commonly used preprocessing followed by SNV (Rinnan et al., 2009). MSC is aimed at removal of undesirable scatter effect from the data matrix prior to modelling stage and it constitutes two steps, the first of which is the estimation of the correction coefficients and in the second step the spectrum is corrected by applying the correction coefficients obtain in the first step.

Step 1 $$\boldsymbol{x}_{org} = b_o + b_{ref,1} . x_{ref} + e \qquad \text{(Equation 9)}$$

Step 2 $$\boldsymbol{x}_{corr} = \frac{x_{org} - b_0}{b_{ref,1}} = \boldsymbol{x}_{ref} + \frac{e}{b_{ref,1}} \qquad \text{(Equation 10)}$$

Where, $\boldsymbol{x}_{org}$ refers to the original sample spectra, $\boldsymbol{x}_{corr}$is the corrected spectra, $\boldsymbol{x}_{ref}$is the reference spectrum, e is the un-modeled part of the original spectrum and b_o and $b_{ref,1}$refer to the scalar quantities. The basic format of the SNV and normalization is similar to that of MSC.

Derivatives are used for the removal of both the additive and the multiplicative effects in the spectra with the first derivative only contributing towards the removal of the baseline and the second derivative towards the elimination of both baseline and linear trend. The estimation of the first derivative is done as the difference of the two successive spectral measurement points while the second derivative works with the calculation of the difference between the two successive points of the first derivative as shown in equations 11 and 12 respectively where x' refers to the first derivative and x'' refers to the second derivative.

$$x_i' = x_i - x_{i-1} \quad \text{(Equation 11)}$$

$$x_i'' = x_i' - x_{i-1}' = x_{i-1} - 2.x_i + x_{i+1} \quad \text{(Equation 12)}$$

2.8 Prediction and classification modelling approaches

In this chapter a few modelling approaches will be briefly introduced including, principle component analysis (PCA), multiple linear regression (MLR), principle component regression (PCR) and partial least squares regression (PLSR) approach. Also classification methods such as SIMCA and PLSDA will also be briefly explained.

2.8.1. Principle Component Analysis (PCA)

In PCA an **X** matrix of *r* rank is represented by a summation of *r* matrices of rank 1. Representing mathematically:

$$X = M_1 + M_2 + M_3 + M_4 + \cdots + M_r \quad \text{(Equation 13)}$$

These matrices $\boldsymbol{M_r}$ are an outer product of the loadings vector (p_r') and a scores vector (t_r). Hence equation 13 can be rewritten as:

$$X = t_1p_1' + t_2p_2' + t_3p_3' + t_4p_4' + \cdots + t_rp_r' \quad \text{(Equation 14)}$$

Equation 14 can also be represented as:

$$\boldsymbol{X = TP'} \quad \text{(Equation 15)}$$

In case of the PCA the angle cosines of the direction vector are known as loadings while projections of the sample points in the direction of the principle component are called scores.

2.8.2. Multiple Linear Regression (MLR)

MLR is quite similar to the simple regression, the only difference being the number of independent variables. In simple regression one independent variable is correlated with one dependent variable while in case of MLR many independent variables are attempted to correlate with a single dependent variable at the same time by using least squares method finding the smallest sum of the squares of the residuals. Therefore, MLR establishes a first order (linear) relationship between the characteristics measured from *m* number of independent variables (x_j where j=1 - *m*) and a dependent variable (*y*) hence mathematically depicting the relationship as:

$$y = b_1x_1 + b_2x_2 + \cdots + b_mx_m + e \quad \text{(Equation 16)}$$

Where, y is the dependent variable, x_1 to x_m are the independent variables, b_j are the coefficients and e is the residual or error term. Equation 16 can therefore also be represented as:

$$y = \sum_{j=1}^{m} b_j x_j + e \qquad \text{(Equation 17)}$$

MLR doesn't provide any unique solutions for the condition $m>n$ since in this case b will possess infinite solutions, all of them fitting the equation. In case of an impractical situation where $m = n$, the only unique solution for b is possible only if **X** (a matrix formed with n samples) has a full rank and can be mathematically expressed as:

$$e = y - \boldsymbol{X}b = 0 \qquad \text{(Equation 18)}$$

In case of $m<n$, i.e. the number of samples exceed the number of variables measured, a solution for b can be obtained by using the least squares method which minimizes the length of the residual vector e shown in equation 18. The least squares solution can therefore be expressed mathematically as:

$$b = (\boldsymbol{X}'\boldsymbol{X})^{-1}\boldsymbol{X}'y \qquad \text{(Equation 19)}$$

Hence equation 19 depicts a condition where MLR faces a frequent problem of collinearity since the inverse of **X'X** might not exist. Hence in this case it is imperative to have an equal number of samples (n) as the number of variables (m) by using various techniques for deleting insignificant variables in the condition $m>n$.

2.8.3. Principle Component Regression (PCR)

The basis for the proper elaboration of PCR can be established by understanding the working principle of PCA since in case of PCR the scores matrix represents the data matrix itself hence putting forward a possibility of developing a regression between the scores matrix against the dependent variables without any issues of matrix inversion. As mentioned earlier, in PCR the regression is done using the scores matrix **T** excluding the dimensions having small eigenvalues hence the transformation can be depicted as:

$$T = XP(= TP'P = TI_n) \qquad \text{(Equation 20)}$$

Therefore, equation 18 can be rearranged as:

$Y = TB + E\ (where, B_{hat} = (T'T)^{-1}T'Y)$ (Equation 21)

Hence equation 18 depicts that the variables in in the matrix **X** have been replaced by new variables that are orthogonal to each other spanning multidimensional space in **X**. Unlike the MLR in this case inverting T'T presents no problems since the scores are mutually orthogonal. Furthermore, collinearity problems are avoided by eliminating the score vectors with smaller eigenvalues also resulting in the reduction of noise in the data. The only issue facing the PCR is that some useful information for prediction purposes can be lost in the eliminated variables and some of the noise can be retained in the variables used for regression.

2.8.4. Partial Least Squares Regression (PLSR)

PLSR is a type of multivariate regression which is used to correlate the information in a data matrix **X** with the information in data matrix **Y** by taking into account the latent structures in both datasets. The datasets **X** and **Y** are decomposed into their latent structures iteratively and a regression model is developed between the scores of **X** and **Y** blocks. The concept of the PLS model can be demonstrated on the basis of outer and inner relations; the outer relations being **X** and **Y** blocks individually while for inner relations **X** and **Y** blocks are both linked. The outer relations in this case can be mathematically compared to PCA which in case of **X** block is:

$\boldsymbol{X = TP' + E} = \sum t_r p_r' + E$ (Equation 22)

Similarly, the outer relationship for the **Y** block can be written as:

$\boldsymbol{Y = UQ' + F} = \sum u_r q_r' + F$ (Equation 23)

The aim here is to describe **Y** in the best possible way and minimizing ||F|| while simultaneously achieving a meaningful relationship between **X** and **Y**. Hence the inner relationship (linking **X** and **Y**) can be achieved by plotting the scores of **X** block (t) and scores of **Y** block (u) for each component. The inner relation for a simple linear model can be given mathematically as:

$\hat{u} = b_r t_r$ (Equation 24)

where, $b_r = u_r' t_r / t_r' t_r$ and is the regression coefficient in case of the PLSR model.

The mixed relation can be given as $Y = TBQ' + F$ in which case ||F|| is minimized. Using the iterative method, the blocks receive each other's scores hence providing a better understanding of the inner relationship. Moreover, the orthogonality in the **X** scores is achieved by introducing weights. More

information on the PLSR can be achieved from (Geladi and Kowalski, 1986).

3. APPLICATIONS

Hyperspectral imaging has been used in the food industry for a number of goals including the evaluation of the water potential of leafy vegetables, measurement of plum quality, astringency assessment of persimmon, assessment of fruit ripening, detection of decayed peaches, early detection of bruises in peaches, detection of bruises in apples, yield estimation of mangoes, prediction of sugariness and hardness of melons, determination of moistures content and chromaticity of potato slices during drying and many other applications.

In a study conducted by Tung et al., 2018 the water potential of leafy vegetables was determined using hyperspectral imaging using Modified Partial Least Squares Regression (MPLSR) with an R^2 of 0.8 with simultaneously illustrating the distribution of water potential. Among the many mathematical pretreatments used, first derivative served as the best pretreatment resulting in the maximization of the correlation coefficient and the minimization of the SEC. It was concluded that hyperspectral imaging is a useful and reliable tool for the estimation of water stress of the leafy vegetables in terms of water potentials.

B. Li et al., 2018 used hyperspectral imaging for the measurement and prediction of the color, soluble solids content and firmness of plum fruits belonging to two different cultivars using partial least squares regression modelling. Individual PLSR models were developed for each cultivar followed by a combined model including both cultivars. In case of color measurement all the models were reliable for the hyperspectral images taken in Vis-NIR region and the correlation coefficient was found to be higher than 0.7 for individual and combined cases. On the other hand, the soluble solids content was reliably predicted with the hyperspectral images in the short wave NIR region with a correlation coefficient higher than 0.8.

Hyperspectral imaging has also been used for the astringency measurement of permission fruit using the hyperspectral images in the Vis-NIR range (Munera et al., 2017). 'Rojo Brillante' cultivar fruits were taken from three different commercial maturity stages and was treated with different CO_2 levels for attaining different astringency levels. PLS classification approaches were used for the classification of the fruits based on maturity levels and it was found out by the study that the 97.9% of the samples were correctly classified. Moreover, in the same study the flesh firmness was predicted with a correlation

coefficient of 0.8 while the soluble tannins after the CO_2 treatments which were distributed inside the fruit were illustrated by the hyperspectral images for the astringency measurements obtaining a correlation coefficient of 0.91.

J. Li et al., 2018 compared the short wave and long wave NIR systems for the detection of early bruises in peaches. Effective wavelengths were selected using the principle component analysis and a new segmentation approach named watershed segmentation approach was introduced which was found to better than the normally used segmentation approaches. The study revealed that using the short wave NIR system of hyperspectral images 96.5% of the bruised areas and 97.5% of the non-bruised areas were correctly classified. In another study, similar objectives were pursued by Huang et al., 2015 using the hyperspectral images in the Vis-NIR range where the weighing coefficients of the PC images were used for the determination of effective wavelengths i.e. 780, 850, 960 nm. Detection systems were developed for the static and online tests with the classification accuracies of 91.5% and 74.6% for static and online, respectively.

Sun et al., 2017 used the NIR based hyperspectral imaging system for estimation of texture and sweetness of melons. PLSR models proved to be promising for the reliable and most accurate prediction models with selective wavelengths based on the weighted regression coefficients. Hence each pixel of the images based on these selected wavelengths was used for the illustration of sweetness and hardness in the melon samples. Amjad et al., 2018 used hyperspectral imaging in the Vis-NIR region for the determination of the moisture content of potato slices of three different thicknesses. It was concluded by the study that the PLSR models with the reduced wavelengths was reliable to visualize and monitor moisture content during drying yielding the R^2 values between 0.93-0.98 and root mean square errors of 0.16-0.36 for the best models.

Lee et al., 2014 detected bruises under the pear skin using the hyperspectral imaging in the wavelength range of 950-1650 nm. For the bruise discrimination the classification algorithm applied was based on F value which finds the optimal waveband ratio. The best optimal waveband ratio classified the bruised surfaces with an accuracy of 92%. Li et al., 2016 developed hyperspectral a skin defect detection method using the band ratio ($Q_{781/848}$) integrated with image thresholding over the multicolored fruits. Various features for various defect types were detected by PC images either in the Vis-NIR region or the NIR

region or among the individual characteristic wavelengths. The study concluded that an overall accuracy of 96.6% was achieved for 145 samples for the nine defects under study.

Hyperspectral imaging was also used by B. Li et al., 2016 for the measurement of SSC, firmness and for the classification of the pears based on variety. Various algorithms such as principle component analysis, successive projections algorithm, partial least squares regression and fisher LDA were used for the prediction and classification purposes. The study concluded that for the prediction of firmness and SSC the SPA-PLS models were the best resulting in the correlation coefficient of 0.9977 for firmness and 0.9924 in case of the SSC prediction whereas a varietal classification accuracy of 95.56% was achieved using the Fisher LDA algorithm.

Rungpichayapichet et al., 2017 used hyperspectral imaging for mapping of the internal constituents including titratable acidity, TSS and firmness of mango also using hyperspectral images within the wavelength range of 450-998 nm followed by PLSR models. The study revealed a satisfactory and reliable correlation between the hyperspectral images and firmness and titratable acidity (R^2=0.81for both) while for the TSS the R^2 was lower up to 0.5. In order to visualize the spatial distribution of these models the prediction models were applied to each pixel of the hyperspectral images. Furthermore, hyperspectral imaging in the Vis-NIR range was used for the internal quality assessment of persimmon fruits (Munera et al., 2017). In this study ripeness and astringency levels of the fruits at three maturity stages were predicted using LDA, QDA and SVM. Moreover, PLSR was used to predict the firmness of the fruits. All classifiers successfully classified the three different fruits types based on the ripeness level whereas QDA yielded 95% correct classification based on the astringency levels. Moreover, PLSR model predicted the firmness yielding an R^2 of 0.80 and ratio of prediction deviation (RPD) of 1.86 hence concluding that hyperspectral imaging can serve as a useful tool for discriminating among various persimmon fruits of different maturity stages as well as prediction of firmness.

used hyperspectral imaging in the Vis-NIR and SWIR ranges for the detection of black spots (bruises) in potatoes since they are not visible to the human vision. Classification methods namely, PCA, PLSDA and SIMCA were used for the classification of the bruised potatoes with PLSDA serving as the best method (94% classification accuracy) within the SWIR range. It was also concluded that pixel based method yielded better results in PLSDA model in the SWIR range hence detecting blackspots in potatoes.

Hyperspectral imaging has also served as a useful tool for the detection of chilling injury in cucumbers (Cen et al., 2016). During the study reflectance and transmittance based hyperspectral images were acquired for chilled and normal cucumbers and classification models were developed for discriminating between chilled and normal cucumbers and also discriminating between severely chilled, lightly chilled and normal cucumber using supervised classification algorithms including naïve Bayes (NB), SVM and KNN. Out of all the methods used, SVM served as the best technique for classification between severely chilled, chilled and normal cucumbers with a classification accuracy of 100% using spectral information. Conclusively, hyperspectral imaging combined with multivariate and chemiometric techniques possesses a wide scope in the evaluation of food quality issues, adulteration problems and origin detection. Moreover, non-destructive techniques are rapid, reliable, economically feasible and convenient to use.

REFERENCES

Amjad, W., Crichton, S.O.J., Munir, A., Hensel, O., Sturm, B., 2018. Hyperspectral imaging for the determination of potato slice moisture content and chromaticity during the convective hot air drying process. Biosyst. Eng. 166, 170–183. https://doi.org/10.1016/J.BIOSYSTEMSENG.2017.12.001

Amodio, M.L., Capotorto, I., Chaudhry, M.M.A., Colelli, G., 2017. The use of hyperspectral imaging to predict the distribution of internal constituents and to classify edible fennel heads based on the harvest time. Comput. Electron. Agric. 134, 1–10. https://doi.org/10.1016/J.COMPAG.2017.01.005

Ariana, D.P., Lu, R., 2008. Quality evaluation of pickling cucumbers using hyperspectral reflectance and transmittance imaging: Part I. Development of a prototype. Sens. Instrum. Food Qual. Saf. 2, 144–151. https://doi.org/10.1007/s11694-008-9057-x

Ariana, D.P., Lu, R., 2008. Detection of internal defect in pickling cucumbers using hyperspectral transmittance imaging. Trans. ASABE 51, 705–713.

Bannon, D., Thomas, R., 2005. Harsh environments dictate design of imaging spectrometer. Laser Focus World 41, 93–+.

Chaudhry, M.M.A., Amodio, M.L., Babellahi, F., de Chiara, M.L.V., Amigo Rubio, J.M., Colelli, G., 2018. Hyperspectral imaging and multivariate accelerated shelf life testing (MASLT) approach for determining shelf life of rocket leaves. J. Food Eng. 238, 122–133. https://doi.org/10.1016/j.jfoodeng.2018.06.017

Dehariya, V.K., Shrivastava, S.K., Jain, R.C., 2010. Clustering of image data set using k-means and fuzzy k-means algorithms, in: Proceedings - 2010 International Conference on Computational Intelligence and Communication Networks, CICN 2010. pp. 386–391. https://doi.org/10.1109/CICN.2010.80

Dell'Endice, F., Nieke, J., Koetz, B., Schaepman, M.E., Itten, K., 2009. Improving radiometry of imaging spectrometers by using programmable spectral regions of interest. ISPRS J. Photogramm. Remote Sens. 64, 632–639. https://doi.org/10.1016/J.ISPRSJPRS.2009.05.007

Du, C.-J., Sun, D.-W., 2006. Learning techniques used in computer vision for food quality evaluation: a review. J. Food Eng. 72, 39–55. https://doi.org/10.1016/j.jfoodeng.2004.11.017

Geladi, P., Kowalski, B.R., 1986. Partial least-squares regression: a tutorial. Anal. Chim. Acta 185, 1–

17. https://doi.org/10.1016/0003-2670(86)80028-9

Gómez-Sanchis, J., Moltó, E., Camps-Valls, G., Gómez-Chova, L., Aleixos, N., Blasco, J., 2008. Automatic correction of the effects of the light source on spherical objects. An application to the analysis of hyperspectral images of citrus fruits. J. Food Eng. 85, 191–200. https://doi.org/10.1016/J.JFOODENG.2007.06.036

Gonzales, R.C., Wintz, P., 1987. Digital Image Processing (2Nd Ed.). Addison-Wesley Longman Publishing Co., Inc., Boston, MA, USA.

Gowen, A.A., O'Donnell, C.P., Taghizadeh, M., Cullen, P.J., Frias, J.M., Downey, G., 2008. Hyperspectral imaging combined with principal component analysis for bruise damage detection on white mushrooms [Agaricus bisporus), in: Journal of Chemometrics. Wiley-Blackwell, pp. 259–267. https://doi.org/10.1002/cem.1127

Gunasekaran, S., 1996. Computer vision technology for food quality assurance. Trends Food Sci. Technol. https://doi.org/10.1016/0924-2244(96)10028-5

Huang, W., Li, J., Wang, Q., Chen, L., 2015. Development of a multispectral imaging system for online detection of bruises on apples. J. Food Eng. 146, 62–71. https://doi.org/10.1016/J.JFOODENG.2014.09.002

Jayas, D.S., Singh, C.B., Paliwal, J., 2010. Hyperspectral Imaging for Food Quality Analysis and Control, Hyperspectral Imaging for Food Quality Analysis and Control. Academic. https://doi.org/10.1016/B978-0-12-374753-2.10015-2

Jiménez-Carvelo, A.M., Osorio, M.T., Koidis, A., González-Casado, A., Cuadros-Rodríguez, L., 2017. Chemometric classification and quantification of olive oil in blends with any edible vegetable oils using FTIR-ATR and Raman spectroscopy. LWT 86, 174–184. https://doi.org/10.1016/J.LWT.2017.07.050

Kaur, D., Kaur, Y., 2014. Various Image Segmentation Techniques : A Review. IJCSMC 3, 809–814.

Kim, M.S., Chen, Y.-R., Mehl, P., 2001. Hyperspectral reflectance and fluorescence imaging system for food quality and safety. Am. Soc. Agric. Eng. ISSN 44, 721–729. https://doi.org/10.13031/2013.6099

Lee, W.-H., Kim, M.S., Lee, H., Delwiche, S.R., Bae, H., Kim, D.-Y., Cho, B.-K., 2014. Hyperspectral

near-infrared imaging for the detection of physical damages of pear. J. Food Eng. 130, 1–7. https://doi.org/10.1016/J.JFOODENG.2013.12.032

Li, B., Cobo-Medina, M., Lecourt, J., Harrison, N., Harrison, R.J., Cross, J. V., 2018. Application of hyperspectral imaging for nondestructive measurement of plum quality attributes. Postharvest Biol. Technol. 141, 8–15. https://doi.org/10.1016/J.POSTHARVBIO.2018.03.008

Li, B., Hou, B., Zhang, D., Zhou, Y., Zhao, M., Hong, R., Huang, Y., 2016. Pears characteristics (soluble solids content and firmness prediction, varieties) testing methods based on visible-near infrared hyperspectral imaging. Optik (Stuttg). 127, 2624–2630. https://doi.org/10.1016/J.IJLEO.2015.11.193

Li, J., Chen, L., Huang, W., 2018. Detection of early bruises on peaches (Amygdalus persica L.) using hyperspectral imaging coupled with improved watershed segmentation algorithm. Postharvest Biol. Technol. 135, 104–113. https://doi.org/10.1016/J.POSTHARVBIO.2017.09.007

Li, J., Chen, L., Huang, W., Wang, Q., Zhang, B., Tian, X., Fan, S., Li, B., 2016. Multispectral detection of skin defects of bi-colored peaches based on vis–NIR hyperspectral imaging. Postharvest Biol. Technol. 112, 121–133. https://doi.org/10.1016/J.POSTHARVBIO.2015.10.007

Munera, S., Besada, C., Blasco, J., Cubero, S., Salvador, A., Talens, P., Aleixos, N., 2017. Astringency assessment of persimmon by hyperspectral imaging. Postharvest Biol. Technol. 125, 35–41. https://doi.org/10.1016/J.POSTHARVBIO.2016.11.006

Palmer, C., 2005. Diffraction Grating Handbook. J. Opt. Soc. Am. 46, 20–23. https://doi.org/10.1364/JOSA.46.000050

Peng, Y., Lu, R., 2008. Analysis of spatially resolved hyperspectral scattering images for assessing apple fruit firmness and soluble solids content. Postharvest Biol. Technol. 48, 52–62. https://doi.org/10.1016/J.POSTHARVBIO.2007.09.019

Qin, J., Lu, R., 2008. Measurement of the optical properties of fruits and vegetables using spatially resolved hyperspectral diffuse reflectance imaging technique. Postharvest Biol. Technol. 49, 355–365. https://doi.org/10.1016/j.postharvbio.2008.03.010

Reid, L.M., O'Donnell, C.P., Downey, G., 2006. Recent technological advances for the determination of food authenticity. Trends Food Sci. Technol. 17, 344–353.

https://doi.org/10.1016/j.tifs.2006.01.006

Rinnan, A., Berg, F. van den, Engelsen, S.B., 2009. Review of the most common pre-processing techniques for near-infrared spectra. Trends Anal. Chem. 28, 1201–1222. https://doi.org/10.1016/j.trac.2009.07.007

Rungpichayapichet, P., Nagle, M., Yuwanbun, P., Khuwijitjaru, P., Mahayothee, B., Müller, J., 2017. Prediction mapping of physicochemical properties in mango by hyperspectral imaging. Biosyst. Eng. 159, 109–120. https://doi.org/10.1016/J.BIOSYSTEMSENG.2017.04.006

Saleh Al-amri, S., Kalyankar, N., 2010. Image segmentation by using edge detection. Int. J. Comput. Sci. Eng. 02, 804–807.

Sapna Varshney, S., Rajpal, N., Purwar, R., 2010. Comparative study of image segmentation techniques and object matching using segmentation. 2009 Int. Conf. Methods Model. Comput. Sci. 1–6. https://doi.org/10.1109/ICM2CS.2009.5397985

Sun, D.-W., 2010. Hyperspectral imaging for food quality analysis and control. Academic.

Sun, M., Zhang, D., Liu, L., Wang, Z., 2017. How to predict the sugariness and hardness of melons: A near-infrared hyperspectral imaging method. Food Chem. 218, 413–421. https://doi.org/10.1016/J.FOODCHEM.2016.09.023

Trienekens, J., Zuurbier, P., 2008. Quality and safety standards in the food industry, developments and challenges. Int. J. Prod. Econ. 113, 107–122. https://doi.org/10.1016/j.ijpe.2007.02.050

Tung, K.-C., Tsai, C.-Y., Hsu, H.-C., Chang, Y.-H., Chang, C.-H., Chen, S., 2018. Evaluation of Water Potentials of Leafy Vegetables Using Hyperspectral Imaging. IFAC-PapersOnLine 51, 5–9. https://doi.org/10.1016/J.IFACOL.2018.08.052

Wu, D., Shi, H., Wang, S., He, Y., Bao, Y., Liu, K., 2012. Rapid prediction of moisture content of dehydrated prawns using online hyperspectral imaging system. Anal. Chim. Acta 726, 57–66. https://doi.org/10.1016/j.aca.2012.03.038

Wu, D., Sun, D.-W., 2013a. Advanced applications of hyperspectral imaging technology for food quality and safety analysis and assessment: a review—part II: applications. Innov. Food Sci. Emerg. Technol. 19, 15–28.

Wu, D., Sun, D.-W., 2013b. Advanced applications of hyperspectral imaging technology for food quality

and safety analysis and assessment: A review — Part I: Fundamentals. Innov. Food Sci. Emerg. Technol. 19, 1–14. https://doi.org/10.1016/J.IFSET.2013.04.014

Yang, C.-C., Kim, M.S., Kang, S., Cho, B.-K., Chao, K., Lefcourt, A.M., Chan, D.E., 2012. Red to far-red multispectral fluorescence image fusion for detection of fecal contamination on apples. J. Food Eng. 108, 312–319. https://doi.org/10.1016/J.JFOODENG.2011.08.008

Chapter 3

FRESH-CUT ROCKET QUALITY AND SHELF-LIFE: STATE OF THE ART

1. INTRODUCTION

Rocket leaves (*Diplotaxis tenufolia*) gained significant popularity in Europe especially in the Mediterranean countries as a leafy vegetable to be consumed in salads and is well known for its pungent smell and nutritional value. The name "rocket" serves as a collective name indicating a number of species belonging to the Brassicacea family all of which possess certain levels of pungent smell and pleasant bitter taste. Rocket leaves originated in the Mediterranean countries where common names include rucola, rughetta, roquette and others were used which were most probably descended from the Latin word 'roc' which meant 'rough' or 'harsh'.

A total of 3709 species and 338 genera are included in the Brassicacea family (Warwick et al., 2006); among these, perennial wall rocket or wild rocket (*Diplotaxis tenuifolia (L.)DC.*) and annual garden rocket or rocket salad (*Eruca satvia* Mill.) are of significant importance (Hall et al., 2012; Cavaiuolo and Ferrante, 2014). In case of the perennial rocket species the name *Diplotaxis* is derived from the Greek word 'diplos' meaning 'double' and 'taxis' meaning 'row' which refer to the seed arrangement inside the silique (Mohamedien, 1995). *Diplotaxis* plant is capable of achieving a height of 80cm and is characterized by lengthened leaves and tap root (Pratap and Gupta, 2010) possessing a woody stem base with hair present in the lower part (Mohamedien, 1995). The typical leaf is oblong, deeply lobed and fleshy, possessing sharp apexes. The germination of the rocket seeds occurs in autumn and the blooming that takes place after 28 days of germination is significantly impacted by the seasonal conditions (Kenigsbuch et al., 2009).

In case of *Eruca* the name refers to the pungent taste of the leaves and is derived from the Latin words 'uro' or 'urere' meaning 'to burn'. The pungency depends on the composition of the glucosinolate compounds (Mohamedien, 1995). A high morphological variability is observed with the species possessing round or serrated leaves (Hall et al., 2012). The *Eruca* plants possess the capability of achieving a height of 40cm with lyrate pinnatified leaves arranged as a rosette, having an enlarged

terminal lobes and slightly smaller lateral lobes (Hall et al., 2012; Pratap and Gupta, 2010). This species is characterized by a rigid hairy unbranched stem and a thin tap root. The leaves in this case might possess slight differences (smooth or round/lobed or serrated) based on the positioning along the stem achieving a maximum length of 20cm. For this species the seeds possess a brown color varying from yellowish brown to olive green color. On the other hand, both the species depict similar morphological attributes and a characteristic bitter taste (Halkier and Gershenzon, 2006).

2. NUTRITIONAL ATTRIBUTES OF ROCKET LEAVES

Out of the many rocket species *Diplotaxis tenufolia* and *Eruca satvia L.* are commercaially available as a result of consumer demand and are consumed either as fresh salad or mixed with other vegetables (Cavaiuolo and Ferrante, 2014). Rocket leaves are a rich source of a wide range of phytonutrients, including pro-vitamin A, vitamin C, glucosinolates, flavonoids, fiber, sulfur and potassium (Martínez-Sánchez et al., 2006a; Martínez-Sánchez et al., 2006b).

A wide range of health-related benefits are associated to the consumption of the nutrients present in the rocket leaves which are characterized by diuretic, anti-inflammatory, stimulant, depurative, hepatoprotective and stomathic activities. Also it has been proven that they are a glucosinolates and antioxidants prevent various types of cancer including colon (van Poppel et al., 1999; Seow et al., 2002), bladder (Paonessa et al., 2009), lung (London et al., 2000) and potentially breast and prostate cancers (Cohen et al., 2000; Kirsh et al., 2007).

Rocket leaves are a rich source of secondary metabolites which are significantly important for the tissue cell protection manifesting free-radical scavenging activity. A wide range of various biomolecules are found in the antioxidant derivate of the rocket flowers and leaves as a result of the oxidative stress response and senescence degenerative processes.

2.1. Carotenoids

Carotenoids formulate a portion of the composition of many fruits and vegetables and are natural fat-soluble pigments involved in primary metabolism. The wavelength rage of 400-500 nanometers (nm) characterize carotenoids in the visible region as a result of the light absorption with a characteristic orange color. More specifically in the plants carotenoids serve the purpose of accessory pigments transferring absorbed light to chlorophyll pigments which are further vitally involved in photosynthesis.

The role of carotenoids is also significant regarding the photo-protection of the cells due to the absorption and release of excess energy accumulated in the photosynthetic membrane. As for their pharmaceutic properties, they contribute to the prevention of cancers, eye disorders and cardiovascular diseases (Pacheco et al., 2013). Mevalonate pathway using the acetil-CoA or metabolic intermediates of glycolysis are responsible for the formulation of the carotenoids which are tetraterpenes and most of the vitamin A in the human diet is derived from carotenoids; this vitamin A being originated from β-cryptoxanthin, α-carotene and β-carotene (Rao and Rao, 2002). In case of the rocket leaves β-carotene and lutein are the most abundant carotenoids (Cavaiuolo and Ferrante, 2014). Moser et al., 2010 studied the composition of the rocket leaves and found out that β-carotene amount was 7.01 ± 1.04 mg 100 g^{-1} fresh weight (FW) in wild rocket (*Diplotaxis tenufolia*) and 7.96 ± 1.43 mg 100 g^{-1} FW in salad rocket (*Eruca sativa*), while the lutein amount was 5.82 ± 0.51 mg 100 g^{-1} FW in wild rocket and 7.44 ± 0.78 mg 100 g^{-1} FW in salad rocket. According to the information of the USDA, National nutrient database for standard reference, 2015, the total amount of carotenoids in the rocket leaves sums up to about 120 µg $100g^{-1}$ which is considered to be a significant amount keeping under consideration the recommended dietary allowance of 9700 µg day^{-1}.

2.2. Vitamin C

Anabolism in the human body lacks the presence of enzymes for the formulation of vitamin C, therefore vitamin C must be taken from foods (Niimura, 1994). Research works have proven that 90% of the vitamin C can be introduced in the human body with the consumption of fruits and vegetables (Lee and Kader, 2000). Proteins, lipids and carbohydrates that are prone to damage by free radicals and reactive oxygen species are protected by the vitamin C (Inzé et al., 2002). Furthermore, vitamin C has also been reported to be beneficial to prevent scurvy, in maintaining a healthy skin and gums and blood vessels (Nunes et al., 2013). Other significant biological functions carried out by vitamin C in the human body include collagen formulation, iron absorption, plasma cholesterol levels reduction, inhibition of nitrosoammine formation and enhanced immune system (Lee and Kader, 2000). Generally, vitamin C is referred to as ascorbic acid (AA) since it is a sum of the AA and its oxidative derivative, the L-dehydroascorbic acid (DHAA). The intestinal cells in the human body possess the potentiality to reduce the DHAA into AA leading to its permeation in the blood (Wilson, 2002), therefore, both AA and DHAA

are nutritionally important in the human diet. Various biosynthetic pathways such as D-mannose–L-galactose pathway, L-glucose pathway (Wolucka and Montagu, 2003), D-galacturonate pathway (Agius et al., 2003), and myo-inositol pathway (Lorence, 2004) are capable for the synthesis of the AA in plants. Rocket leaves are a rich source of vitamin C with a reported vitamin C content of 50mg 100^{-1} FW (Martínez-Sánchez et al., 2006a), but with high variation due to the growing conditions. The factors such as time of sowing and harvesting, light and temperature conditions significantly impact the vitamin C content of rocket leaves (Acikgoz, 2011). In this study Acikgoz, 2011 investigated the vitamin C of the rocket leaves grown in two different seasons namely, fall and spring and revealed that the rocket leaves grown in fall sowing time possessed a maximum vitamin C content of 57.41 mg of vitamin C 100^{-1} FW when grown in an unheated green house.

2.3 Phenolic Compounds

Phenolic compounds belong to a class of heterogeneous secondary metabolites, containing a phenolic group with a common basic structure corresponding to a hydroxyl group bound to an aromatic ring. Phenolic compounds play a significant role in plant defense mechanism, protecting them from herbivores and pathogen attack; simultaneously, they assist to attract pollinators and animals that are important for seed dispersion. The biosynthesis process of the phenolic compounds initiate through the shikimate pathway producing amino acids including phenylalanine the most significant intermediate and substrates for the phenylalanine-ammonia-lyase (PAL) which is a key enzyme for the production of several phenolic compounds. This enzyme acts as a catalyst to convert the phenylalanine in trans-cinnamic acid through releasing ammonia. Phenolic compounds include flavonoids, pigments synthesized through two separated pathways (malonic and shickimate), which can be subjected to oxidation into quinines (B.H., 2002). In case of *Diplotaxis tenufolia*, quercetin compounds were most abundantly found showing a total flavonoid content ranging from 4.68 to 19.81 g kg^{-1}. On the other hand, in case of *E. satvia* leaves, the primary group of phenolic compounds is represented by kampferol derivatives ranging from 8.47 to 26 g kg^{-1} corresponding to 77% to 88% of total phenols (Cavaiuolo and Ferrante, 2014; Pasini et al., 2011).

2.4 Glucosinolates

Glucosinolates (GLSs) are bioactive molecules found principally in Brassicacea family. GLSs as secondary metabolites also contribute towards the plant protection mechanisms by defending them

against the herbivores, pathogens, fungal diseases and pest infestation (Blažević and Mastelić, 2009). They also play a significant role in the sulphur and nitrogen metabolisms hence regulating the growth of the plants. As a result of tissue disruption and cell breakage, glucosinolates normally contained in the cell vacuole are converted into isothiocyanates (ITCs), thiocyanates, nitriles and sulfates in the cell cytosol via enzymatic reactions. It is due to the presence of these compounds which contain nitrogen (N) and sulphur (S) that the Brassicaceae family vegetables possess a pungent and sulphurous taste and a typical odor (Cavaiuolo and Ferrante, 2014). The enzymatic reaction occurs because of the myrosinase, which belongs to the hydrolase family. Research studies have shown that rocket leaves possess a high content of glucoraphanin (4-methylsulfinylbutyl-GLS) glucoerucin (4-methylthiobutyl-GLS) and dimeric 4-mercaptobutyl-GLS, whereas seeds and roots are rich in glucoerucin, and flowers mostly contain glucosativin (Cavaiuolo and Ferrante, 2014; Cataldi et al., 2007). The most abundant isothiocyanate found in rocket leaves erucin (4-methylthiobutyl isothiocyanate) is produced as a result of hydrolysis of glucoerucin. (Miyazawa et al., 2002).

3. FRESH-CUT ROCKET LEAVES: QUALITY AND SHELF-LIFE

Rocket leaves are usually available in the refrigerator shelves of the retail stores in modified atmosphere packages (MAP) to avoid wilting of the leaves due to water loss and generally possess a shelf-life of 9-14 days under different storage conditions and depending on the raw material quality (Martínez-Sánchez et al., 2006b; Nielsen et al., 2008; Løkke et al., 2012). They are commercially sold as whole leaves having a small section on the petiole that is exposed to oxidation hence leading to an enhanced postharvest shelf-life (Egea-Gilabert et al., 2009; Agius et al., 2002). The most important aspect effecting the shelf-life of rocket leaves is the storage temperature which is recommended to be as low as possible to attain best sensory and nutritional quality and an enhanced shelf life (Mastrandrea et al., 2017a); on the other side, it has been observed that in the open market shelves the temperature of the produce might reach approximately 10^{o}C (Koukounaras et al., 2007; Dixon et al., 2010) which can result in the rapid quality loss. The shelf-life of ready-to-eat rocket leaves is significantly related to the storage conditions and processing operations, which tend to accelerate the degradation of the rocket leaves, inducing wilting, discoloration, loss of nutritional properties, aroma and flavor (Koukounaras et al., 2009).

For the estimation of the limit of marketability, color can be considered as a prime factor and any changes

from the normal green color leads to the limiting marketability. Conventionally, rocket leaves are harvested twice or thrice per cultivation and are primarily utilized for the fresh-cut market. Mostly, they are minimally processed involving only the washing and packaging steps before they are delivered to the retail stores (Hall et al., 2013).

It has also been observed that the minimally processed vegetables are prone to faster physiological deterioration, biochemical changes and microbial degradation as compared to the intact produce (O'Beirne and Francis, 2003), as a result of the enhanced metabolic activity resulting in loss of typical color, texture and flavor (Mastrandrea, 2015; Varoquaux and Wiley, 1994). The reason for this rapid perishability of the fresh-cut produce is due to the lack of food processing methods applied to extend the shelf-life of the conventional food products therefore, the only strategy to prolong the life span of minimally processed fruits and vegetables is refrigerated storage.

Various studies have contributed to relate the quality parameters, storage conditions and shelf life of rocket leaves. Ferrante et al., 2004 studied the storage conditions for the fresh-cut leafy vegetables including rocket leaves at 4 to 5 ^{o}C correlating the effect of the storage conditions on the quality attributes. The color changes based on the total chlorophyll content, carotenoids and anthocyanins were monitored over a storage period of 12 days for storage at 4-5 ^{o}C with and without exposure to light. It was revealed by the study that leafy vegetables should be stored in darkness at low temperatures (<5 ^{o}C) to achieve a longer shelf life. In a study conducted by Martínez-Sánchez et al., 2006b the rocket leaves stored in air were compared to those in controlled atmosphere storage over a time span of 14 days and it was concluded that the rocket leaves stored in air lost the sensory and microbiological attributes for commecial distribution while out of a total of three controlled atmophere storage conditions the rocket leaves stored 5 kPa O_2 + 10 kPa CO_2 maintained the visual quality and microbiological quality traits. Edelenbos et al., 2017 demonstrated that the quality of the packaged rocket leaves varied between different growing seasons recommending low temperature storage for the color maintenance and shorter storage time spans for texture retention.

In another study conducted by Mastrandrea et al., 2016, the effects of temperature, cultivar and time of storage on ammonia accumulation in relation to color variation of rocket leaves was studied. Five different cultivars of rocket leave namely, 'Bellezia', 'Grazia', 'Letizia', 'Tricia', and 'Wild Thing' were

stored at three different temperatures i.e. 0, 5 or 10°C. In parallel the monitoring of visual scores, color (hue angle) and ammonia accumulation was conducted at an interval of each 4 or 8 days, based on the temperature of storage of the leaves. It was observed that leaf yellowing as a result of color loss was directly proportional to increasing temperature. At the same time the authors found out that for all storage conditions, an encouraging correlation between ammonia content and color changes was established. Ammonia content increased from 11-15 µg g-1 fresh weight (FW) to 150-220 at 0°C, 340-450 at 5°C and more than 590 µg g-1 FW at 10°C by the end of storage-life confirming the fact that storage temperature plays a significant role in ammonia accumulation. It was concluded that ammonia may be a good indicator of senescence in rocket leaves, since it correlated well to color change with storage temperature and time.

Mastrandrea et al., 2017 in another work investigated the volatile profile and quality of the rocket leaves as effected by improper atmosphere packaging subjecting rocket leaves to three different storage temperatures at 0, 5 and 15 ^{o}C over a 10 days storage period. Macro-perforated bags were used for rocket leaves storage aiming at prevention of modified atmosphere in the headspace for control samples. At 0^{o}C the ascorbic acid (AA) of the leaves retained throughout the storage time while a rapid loss of AA was observed for the leaves stored at higher storage temperatures owing the major losses in the AA, vitamin C and sensorial parameters to the low O_2 (0kP) and high CO_2 (25kP) concentrations. Also for the leaves stored at 0^{o}C the initial headspace fingerprint was best preserved as compared to leaves stored at higher temperatures where off-odors from dimethyl sulfide (DMS), dimethyl disulfides (DMDS) and other volatiles were produced hence varying the initial headspace fingerprint. It was concluded by the study that the improper packaging conditions resulted in decreasing the shelf-life of rocket leaves compared to storage in air. Additionally, it was also concluded that effect of modifying the gas composition for leaves stored at 0^{o}C did not add any beneficial effect in comparison to storage in air. In a similar study, Mastrandrea et al., 2017b, concluded that rocket leaves stored under non-isothermal conditions depicted higher levels of CO_2 concentrations and lower concentration of O_2 than those stored under isothermal conditions. Also an increased production of volatiles responsible of off-flavors (acetaldehyde and dimethyl sulfide) was observed for the leaves stored under non-isothermal conditions following temperature abuse. Conclusively, it was recommended that dimethyl sulfide and acetaldehyde possess

the potentiality to be effective markers for tracking the effect of temperature fluctuations on rocket during storage.

Possessing the ability for the adequate estimation of the shelf life of rocket leaves holds great significance in assisting in planning of produce logistics with fully automated distribution steps and better manage stocks. Amodio et al., 2015 attempted to utilize non-linear modelling approach for the estimation of the shelf life of rocket leaves. Rocket leaves were exposed to three different storage temperatures i.e. 0, 5 and 15 °C and the cumulative form of the Weibull equation combined with a log-logistic model were used for the fitting of experimental data over time of storage and for the investigation of temperature dependence of the degradation rates for various sensorial and physio-chemical attributes. The fitting accuracy of the Weibullian model was accessed by the correlation coefficients which ranged between 0.95 and 0.99 followed by traditional first-order kinetics. It was concluded that the log-logistic model not only accurately described the temperature dependence of the Weibull parameters but also accounted for the thermal history of the product. Additionally, a need for a different approach for the shelf life estimation considering more quality variable at the same time was also indicated in this work, since it was observed that fquality factors limiting the shelf-life may change depending on the temperature.

Degradation of the fresh-cut produce is in fact a multivariate phenomenon where different reactions take place at the same time. Multivariate data analysis algorithms/techniques are aimed at modelling the factors and responses in order to develop a relationship between the factors and responses for the extraction of useful information. This extracted information is quite useful to understand the system characteristics and also determines the variables contributing highly towards the quality changes.

In case of leafy vegetables, a number of studies have contributed towards the evaluation of quality parameters using the multivariate data analysis. Derossi et al., 2016 used the multivariate data analysis for the estimation of shelf-life of fresh-cut lettuce in which principle component analysis (PCA) was employed for the data acquired at three different storage temperatures, including different sensorial and physio-chemical attributes. A correlation was developed between the first PC and the time of storage. Multivariate degradation kinetics was studied and it was concluded that it was better elaborated by zero order reaction yielding an R^2 as high as 0.97 whereas the multivariate rate constant achieved a good fit using the log-logistic model. The shelf-life of the fresh-cut lettuce stored at 0, 5 and 15^{o}C was estimated

to be 12.4,10.4 and 3.7 days, respectively, providing an evidence that studying the multivariate approach can be useful in accurately describing the degradation phenomenon.

In another study, Toledo-Martín et al., 2017 used Vis-NIR spectroscopy for the prediction of glucosinolates and total phenolic content (TPC) in rocket leaves (*Eruca vesicaria*) using modified partial least squares regression (MPLS). The coefficients of determination in case of validation for both the parameters ranged from 0.59-0.84 characterizing equations with good to excellent quantitative information. The study also concluded using the MPLS loadings that cellulose and protein which are major cell components highly contributed in modelling equations for glucosinolates.

Edelenbos et al., 2017 used multivariate techniques (multispectral imaging) for the differentiation of rocket leaves based on seasons. The seasonal variation was assessed with multispectral imaging data as factors for color (570nm) and textural (780nm) measurements as responses. The data analysis showed that the color was better preserved in the spring season as compared to the summer season whereas, in case of temperatures the leaves stored at lower temperatures preserved green color better as compared to those at higher temperatures. For texture on the other hand, it was recommended that the lower storage time contributed towards a better texture of the leaves. Therefore, it was concluded that the multispectral imaging was a useful tool for the seasonal discrimination of rocket leaves based on color and texture.

It can be concluded for the aforementioned studies that the quality and shelf life of rocket leaves is a multivariate phenomenon and the need for the quality estimation and shelf life prediction using multivariate approaches is highly required. In addition, there is also space for non-destructive quality and shelf-life evaluation by means of spectral information.

REFERENCES

Acikgoz, F.E., 2011. The effects of different sowing time practices on Vitamin C and mineral material content for rocket (Eruca vesicaria subsp . sativa (Mill)). Sci. Res. Essays 6, 3127–3131. https://doi.org/10.5897/SRE10.779

Agius, F., González-Lamothe, R., Caballero, J.L., Muñoz-Blanco, J., Botella, M.A., Valpuesta, V., 2003. Engineering increased vitamin C levels in plants by overexpression of a D-galacturonic acid reductase. Nat. Biotechnol. 21, 177–181. https://doi.org/10.1038/nbt777

Agius, F., González-Lamothe, R., Caballero, J.L., Muñoz-Blanco, J., Botella, M.A., Valpuesta, V., 2002. Engineering increased vitamin C levels in plants by overexpression of a D-galacturonic acid reductase. https://doi.org/10.1038/nbt777

Amodio, M.L., Derossi, A., Mastrandrea, L., Colelli, G., 2015. A study of the estimated shelf life of fresh rocket using a non-linear model. J. Food Eng. 150, 19–28. https://doi.org/10.1016/j.jfoodeng.2014.10.030

B.H., H., 2002. The biochemistry and medical significance of the flavonoids, Pharmacology and Therapeutics.

Blažević, I., Mastelić, J., 2009. Glucosinolate degradation products and other bound and free volatiles in the leaves and roots of radish (Raphanus sativus L.). Food Chem. 113, 96–102. https://doi.org/10.1016/j.foodchem.2008.07.029

Cataldi, T.R.I., Rubino, A., Lelario, F., Bufo, S.A., 2007. Naturally occurring glucosinolates in plant extracts of rocket salad (Eruca sativa L.) identified by liquid chromatography coupled with negative ion electrospray ionization and quadrupole ion-trap mass spectrometry. Rapid Commun. Mass Spectrom. 21, 2374–2388. https://doi.org/10.1002/rcm.3101

Cavaiuolo, M., Ferrante, A., 2014. Nitrates and glucosinolates as strong determinants of the nutritional quality in rocket leafy salads. Nutrients. https://doi.org/10.3390/nu6041519

Cohen, J.H., Kristal, A.R., Stanford, J.L., 2000. Fruit and vegetable intakes and prostate cancer risk. J. Natl. Cancer Inst. 92, 61–68. https://doi.org/10.1093/jnci/92.1.61

Derossi, A., Mastrandrea, L., Amodio, M.L., De Chiara, M.L.V., Colelli, G., 2016. Application of multivariate accelerated test for the shelf life estimation of fresh-cut lettuce. J. Food Eng. 169, 122–

130. https://doi.org/10.1016/j.jfoodeng.2015.08.010

Dixon, M.S., Taylor, G., Zhang, F., Wagstaff, C., Rothwell, S.D., Fry, S.C., Clarkson, G.J.J., 2010. Modification of cell wall properties in lettuce improves shelf life. J. Exp. Bot. 61, 1239–1248. https://doi.org/10.1093/jxb/erq038

Edelenbos, M., Løkke, M.M., Seefeldt, H.F., 2017. Seasonal variation in color and texture of packaged wild rocket (Diplotaxis tenuifolia L.). Food Packag. Shelf Life 14, 46–51. https://doi.org/10.1016/j.fpsl.2017.08.005

Egea-Gilabert, C., Fernández, J.A., Migliaro, D., Martínez-Sánchez, J.J., Vicente, M.J., 2009. Genetic variability in wild vs. cultivated Eruca vesicaria populations as assessed by morphological, agronomical and molecular analyses. Sci. Hortic. (Amsterdam). 121, 260–266. https://doi.org/10.1016/j.scienta.2009.02.020

Ferrante, A., Incrocci, L., Maggini, R., Serra, G., Tognoni, F., 2004. Colour changes of fresh-cut leafy vegetables during storage, Agriculture & Environment.

Halkier, B.A., Gershenzon, J., 2006. BIOLOGY AND BIOCHEMISTRY OF GLUCOSINOLATES. Annu. Rev. Plant Biol. 57, 303–333. https://doi.org/10.1146/annurev.arplant.57.032905.105228

Hall, M.K.D., Jobling, J.J., Rogers, G.S., 2013. Influence of Storage Temperature on the Seasonal Shelf Life of Perennial Wall Rocket and Annual Garden Rocket. Int. J. Veg. Sci. 19, 83–95. https://doi.org/10.1080/19315260.2012.716387

Hall, M.K.D., Jobling, J.J., Rogers, G.S., 2012. SOME PERSPECTIVES ON ROCKET AS A VEGETABLE CROP: A REVIEW. degruyter.com 76, 21–41. https://doi.org/10.2478/v10032-012-0002-5

Inzé, D., Strain, J.J., Kanellis, A., Favell, D., Benzie, I.J.J., Fletcher, J., Sanmartin, M., Montagu, M. Van, Davey, M.W., Smirnoff, N., 2002. Plant L-ascorbic acid: chemistry, function, metabolism, bioavailability and effects of processing. J. Sci. Food Agric. 80, 825–860. https://doi.org/10.1002/(sici)1097-0010(20000515)80:7<825::aid-jsfa598>3.3.co;2-y

Kenigsbuch, D., Ovadia, A., Ivanova, Y., Chalupowicz, D., Maurer, D., Aharon, Z., Vinokur, Y., Aharoni, N., 2009. Wild rocket (Diplotaxis tenuifolia) mutant with late Flowering and delay in postharvest senescence. Acta Hortic. 830, 91–96. https://doi.org/10.17660/ActaHortic.2009.830.10

Kirsh, V.A., Peters, U., Mayne, S.T., Subar, A.F., Chatterjee, N., Johnson, C.C., Hayes, R.B., 2007. Prospective study of fruit and vegetable intake and risk of prostate cancer. J. Natl. Cancer Inst. 99, 1200–1209. https://doi.org/10.1093/jnci/djm065

Koukounaras, A., Siomos, A.S., Sfakiotakis, E., 2009. Impact of heat treatment on ethylene production and yellowing of modified atmosphere packaged rocket leaves. Postharvest Biol. Technol. 54, 172–176. https://doi.org/10.1016/j.postharvbio.2009.07.002

Koukounaras, A., Siomos, A.S., Sfakiotakis, E., 2007. Postharvest CO2 and ethylene production and quality of rocket (Eruca sativa Mill.) leaves as affected by leaf age and storage temperature. Postharvest Biol. Technol. 46, 167–173. https://doi.org/10.1016/j.postharvbio.2007.04.007

Lee, S.K., Kader, A.A., 2000. Preharvest and postharvest factors influencing vitamin C content of horticultural crops. Postharvest Biol. Technol. 20, 207–220. https://doi.org/10.1016/S0925-5214(00)00133-2

Løkke, M.M., Seefeldt, H.F., Edelenbos, M., 2012. Freshness and sensory quality of packaged wild rocket. Postharvest Biol. Technol. 73, 99–106. https://doi.org/10.1016/j.postharvbio.2012.06.004

London, S.J., Yuan, J.M., Chung, F.L., Gao, Y.T., Coetzee, G.A., Ross, R.K., Yu, M.C., 2000. Isothiocyanates, glutathione S-transferase M1 and T1 polymorphisms, and lung-cancer risk: A prospective study of men in Shanghai, China. Lancet 356, 724–729. https://doi.org/10.1016/S0140-6736(00)02631-3

Lorence, A., 2004. myo-Inositol Oxygenase Offers a Possible Entry Point into Plant Ascorbate Biosynthesis. PLANT Physiol. 134, 1200–1205. https://doi.org/10.1104/pp.103.033936

Martínez-Sánchez, A., Allende, A., Bennett, R.N., Ferreres, F., Gil, M.I., 2006a. Microbial, nutritional and sensory quality of rocket leaves as affected by different sanitizers. Postharvest Biol. Technol. 42, 86–97. https://doi.org/10.1016/J.POSTHARVBIO.2006.05.010

Martínez-Sánchez, A., Marín, A., Llorach, R., Ferreres, F., Gil, M.I., 2006b. Controlled atmosphere preserves quality and phytonutrients in wild rocket (Diplotaxis tenuifolia). Postharvest Biol. Technol. 40, 26–33. https://doi.org/10.1016/J.POSTHARVBIO.2005.12.015

Mastrandrea, L., 2015. Optimizing storage conditions for minimally processed rocket leaves: effect of temperature and gas conditions on aromatic profile, sensorial and nutritional quality.

Mastrandrea, L., Amodio, M.L., Cantwell, M.I., 2016. Modeling ammonia accumulation and color changes of arugula (Diplotaxis tenuifolia) leaves in relation to temperature, storage time and cultivar, in: Acta Horticulturae. pp. 275–282. https://doi.org/10.17660/ActaHortic.2016.1141.34

Mastrandrea, L., Amodio, M.L., de Chiara, M.L. V., Pati, S., Colelli, G., 2017a. Effect of temperature abuse and improper atmosphere packaging on volatile profile and quality of rocket leaves. Food Packag. Shelf Life 14, 59–65. https://doi.org/10.1016/J.FPSL.2017.08.004

Mastrandrea, L., Amodio, M.L., Pati, S., Colelli, G., 2017b. Effect of modified atmosphere packaging and temperature abuse on flavor related volatile compounds of rocket leaves (Diplotaxis tenuifolia L.). J. Food Sci. Technol. 54, 2433–2442. https://doi.org/10.1007/s13197-017-2685-6

Miyazawa, M., Maehara, T., Kurose, K., 2002. Composition of the essential oil from the leaves of Eruca sativa. Flavour Fragr. J. 17, 187–190. https://doi.org/10.1002/ffj.1079

Mohamedien, S., 1995. Rocket cultivation in Egypt, Rocket genetic resources network :Report of the first meeting, 13-15 November, 1994, Lisbon, Portugal.

Moser, B.R., Winkler-Moser, J.K., Shah, S.N., Vaughn, S.F., 2010. Composition and physical properties of arugula, shepherd's purse, and upland cress oils. Eur. J. Lipid Sci. Technol. https://doi.org/10.1002/ejlt.200900219

Nielsen, T., Bergström, B., Borch, E., 2008. The origin of off-odours in packaged rucola (Eruca sativa). Food Chem. 110, 96–105. https://doi.org/10.1016/J.FOODCHEM.2008.01.063

Niimura, Y., 1994. Evolution of Chemosensory Receptor Genes in Primates and Other Mammals, in: ASBMB. pp. 43–62. https://doi.org/10.1007/978-4-431-54011-3_4

Nunes, T.P., Martins, C.G., Faria, A.F., Bíscola, V., de Oliveira Souza, K.L., Mercadante, A.Z., Cordenunsi, B.R., Landgraf, M., 2013. Changes in total ascorbic acid and carotenoids in minimally processed irradiated Arugula (Eruca sativa Mill) stored under refrigeration. Radiat. Phys. Chem. 90, 125–130. https://doi.org/10.1016/j.radphyschem.2013.03.044

O'Beirne, D., Francis, G., 2003. Reducing the pathogen risk in MAP-prepared produce. Nov. food Packag. Tech.

Pacheco, T., Geraldes, C., Ferreira, A., Bíscola, V., Leani, K., Souza, D.O., Zerlotti, A., Rosana, B., 2013. Changes in total ascorbic acid and carotenoids in minimally processed irradiated Arugula (

Eruca sativa Mill) stored under refrigeration. Radiat. Phys. Chem. 90, 125–130. https://doi.org/10.1016/j.radphyschem.2013.03.044

Paonessa, J.D., Li, Y., Wong, M.K.K., Chen, S.C., Tang, L., Bhattacharya, A., Geng, F., Zhang, Y., 2009. Inhibition of bladder cancer development by allyl isothiocyanate. Carcinogenesis 31, 281–286. https://doi.org/10.1093/carcin/bgp303

Pasini, F., Verardo, V., Cerretani, L., Caboni, M.F., D'Antuono, L.F., 2011. Rocket salad (Diplotaxis and Eruca spp.) sensory analysis and relation with glucosinolate and phenolic content. J. Sci. Food Agric. 91, 2858–2864. https://doi.org/10.1002/jsfa.4535

Pratap, A., Gupta, S., 2010. Biology and Ecology of Wild Crucifers, in: Biology and Breeding of Crucifers. pp. 37–67. https://doi.org/10.1201/9781420086096.ch3

Rao, A. V, Rao, L.G., 2002. Carotenoids and human health. Pharmacol. Res. Off. J. Ital. Pharmacol. Soc. 49, 77–78.

Seow, A., Yuan, J., Sun, C., Berg, D. Van Den, Lee, H., Yu, M.C., 2002. Dietary isothiocyanates , glutathione S -transferase polymorphisms and colorectal cancer risk in the Singapore Chinese Health Study been inversely related to colorectal cancer risk , and this degradation products such as isothiocyanates (ITCs). These co. Carcinogenesis 23, 2055–2061.

Toledo-Martín, E.M., Font, R., Obregón-Cano, S., De Haro-Bailón, A., Villatoro-Pulido, M., Del Río-Celestino, M., 2017. Rapid and cost-effective quantification of glucosinolates and total phenolic content in rocket leaves by visible/near-infrared spectroscopy. Molecules 22. https://doi.org/10.3390/molecules22050851

van Poppel, G., Verhoeven, D.T.H., Verhagen, H., Goldbohm, R.A., 1999. Brassica Vegetables and Cancer Prevention. pp. 159–168. https://doi.org/10.1007/978-1-4757-3230-6_14

Varoquaux, P., Wiley, R.C., 1994. Biological and Biochemical Changes in Minimally Processed Refrigerated Fruits and Vegetables, in: Minimally Processed Refrigerated Fruits & Vegetables. Springer US, Boston, MA, pp. 226–268. https://doi.org/10.1007/978-1-4615-2393-2_6

Warwick, S.I., Francis, A., Al-Shehbaz, I.A., 2006. Brassicaceae: Species checklist and database on CD-Rom, in: Plant Systematics and Evolution. pp. 249–258. https://doi.org/10.1007/s00606-006-0422-0

Wilson, J.X., 2002. The physiological role of dehydroascorbic acid. FEBS Lett. 527, 5–9. https://doi.org/10.1016/S0014-5793(02)03167-8

Wolucka, B.A., Montagu, M., 2003. GDP-mannose 3{\textasciiacutex},5{\textasciiacutex}-epimerase forms GDP-L-gulose, a putative intermediate for the de novo biosynthesis of vitamin C in plants. J Biol Chem 278. https://doi.org/10.1074/jbc.M309135200

PART II: EXPERIMENTAL

OBJECTIVES

The major objectives of this doctoral thesis are to evaluate the potentiality of the non-destructive techniques including spectral profiles and hyperspectral images in the Vis-NIR (400-1000nm) and NIR (900-1700nm) ranges for the quality assessment, phytonutrient prediction, shelf life evaluation and prediction, and raw material discrimination of rocket leaves. Furthermore, wavelength selection for the model improvement will also be pursued followed by mapping of the changes in the phytonutrients over the storage period.

Chapter 4

HYPERSPECTRAL IMAGING AND MULTIVARIATE ACCELERATED SHELF LIFE TESTING (MASLT) APPROACH FOR DETERMINING SHELF LIFE OF ROCKET LEAVES

Authors: Muahmmad M.A. Chaudhry[1]; Maria L. Amodio[1]; Farahmand Babellahi[1]; Maria L. V. de Chiara[1], José M. Amigo Rubio[2]; Giancarlo Colelli[1]

[1]Dip.to di Scienze Agrarie, degli Alimenti e dell'Ambiente, Università di Foggia, Via Napoli 25, 71122 Foggia (Italy), corresponding author: marialuisa.amodio@unifg.it

[2]Dept. of Food Science (KU-FOOD), Chemometrics and Analytical Technologies CAT. Faculty of Sciences, University of Copenhagen. Rolighedsvej 30, DK-1958 Frederiksberg C. (Denmark)

ABSTRACT

The feasibility of using spectral profiles for the estimation of the shelf life of the rocket leaves was evaluated using a multivariate accelerated shelf life testing (MASLT) approach. Spectral changes over time were modeled by using principal component analysis (PCA) and as variation to the conventional method, partial least squares (PLS) method. Kinetic charts were built fitting the first principle component (PC1) and the first latent variable (LV1) scores versus time. In both cases, the kinetics were described by a first order reaction, obtaining R^2 values of 0.73, 0.94 and 0.95 for samples stored at 5, 10 and 15 ^oC, respectively. The spectra of samples judged unacceptable were used for the calculation of the cut-off value, estimated to be 3.955, leading to shelf life estimations of 9.8, 4.3 and 3.1 days for PCA based MASLT for the three temperatures, respectively. For PLS based MASLT the shelf life was 9.4, 4.5 and 3.3 days for samples stored at the three respective temperatures. Conclusively, shelf-life was correctly estimated by conventional MASLT using PCA and also with the newly proposed technique using LVs.

Keywords: PCA, PLS, cutoff, kinetic, appearance

1. INTRODUCTION

A significant increase has been observed in the consumption of minimally processed ready-to-eat foods in the last decades (Artés et al., 2009). This rapid rise in the consumption is a result of consumer preference for healthy, fresh, convenient, highly nutritive and appetizing food products (Ma et al., 2017; Oliveira et al., 2015).

Rocket leaves (*Diplotaxis tenuifolia*) are popular leafy vegetables especially in the Mediterranean countries, mostly preferred by consumers because of their pungent smell and strong flavour. Moreover, they are a rich source of health-promoting phytonutrients such as flavonoids, fiber, vitamin C and glucosinolates (Martínez-Sánchez et al., 2006, Cavaiuolo and Ferrante, 2014, Nurzyńska-Wierdak, 2015, Amodio et al., 2016). Normally rocket leaves are sold in packages after minimal processing operations including washing and drying due to which they are also prone to rapid degradation. Particularly, yellowing caused by chlorophyll degradation, wilting, and the production of off-odors are the main source of deterioration (Koukounaras, 2006, 2007, 2009; Nielsen et al., 2008). The shelf life of rocket leaves ranges between 7 to 14 days depending upon the raw material, handling, processing and especially the temperature of storage (Toivonen and Brummell, 2008).

At the market shelves, the consumer criteria for the selection of the leafy vegetables as rocket is the fresh appearance and green color (Løkke et al., 2012) and repurchase of the product depends on the quality at the consumption stage often evaluated by color, texture and flavor (Barrett et al., 2010). Freshness and green color are quick indicators of the fact that the product can sustain under prescribed conditions for a certain time.

The shelf life determination of any food product is usually conducted by monitoring the quality parameters most associated with time by developing kinetic models for deterioration under market and extreme conditions using accelerated shelf life testing methods (ASLT) (Labuza, 1982; Hough et al., 2006). In case of ASLT approach, the samples are subjected to severe storage conditions other than the market storage conditions and shelf life charts also known as kinetic charts are developed (Hough et al., 2006). Various studies have proved that ASLT approach is a useful tool for the rapid estimation of shelf life of fresh-cut produce, as apple (Amodio et al., 2015), melons (Amodio et al., 2012) even with the use of other empirical models as the Weibull model used on fresh-cut melons (Amodio et al., 2013) and fresh rocket leaves (M. L. Amodio et al., 2015a).

Degradation process of food products and particularly of fresh-cut produce is a multivariate phenomenon depending from several pre-harvest handling and storage factors, impacting on many quality attributes (Routray and Orsat, 2014; Torres-Contreras et al., 2014; Fernando Reyes et al., 2007). In this regard, spectral data, hyperspectral imaging and chemometric tools such as principal component analysis (PCA) may be usefully integrated into ASLT to formulate a new procedure named Multivariate Accelerated Shelf Life Testing (MASLT) (Bro and Smilde, 2014; Brereton, 2009; Labuza, 1982; Pedro and Ferreira, 2006).

The first step in MASLT procedure involves the kinetic description of the important degradation reactions based on the PC scores resulting from a PCA model, assuming that degradation reactions are the main sources of variation in the data set, and that PCA will explain the time-related phenomena. Usually, these are calculated using the zero order, first order and second order kinetics (Odriozola-Serrano et al., 2009; Amodio et al., 2015). Secondly, the temperature dependence of the rate constants is defined using the Arrhenius equation and the third step involves the calculation of shelf life. The MASLT approach has successfully been applied to various food products such as broccoli puree (Kebede et al., 2015), low-fat UHT milk (Richards et al., 2014), sunflower oil (Upadhyay and Mishra, 2015) and tomato paste (Pedro and Ferreira, 2006). This method was applied for the first time on fresh-cut produce by Derossi et al., 2016, who obtained an accurate description of the degradation phenomena occurring during the storage of fresh-cut lettuce at three different temperatures, monitoring several sensorial, physical and chemical changes over time. In the same way, MALST method was applied to estimate the shelf-life of fresh-cut pineapples (Amodio et al., 2016). Shelf-life estimation obtained with MALST method have been proved to be more reliable than ASLT, but generally, the application of these studies by processors is limited by the scarce possibility of carrying out specific quality analysis and collecting data. Therefore, many companies are looking for a possible alternative system for the evaluation of the quality and shelf-life in a faster, simple and eventually non-destructive way.

Hyperspectral imaging is a fast, reliable, objective, economical and non-destructive means of data collection. This technique is a combination or integration of imaging and spectroscopic techniques for the quantitative prediction of physical and chemical characteristics of the food samples as well as their spatial distribution.

Every product has, in fact, a specific spectral signature, which is a function of the structure of the sample, the moisture content, the particle size, the temperature of the sample and most importantly of its chemical composition (Workman and Shenk, 2004). In case of the green leaves, Vis-NIR region is retains all the information related to leaf pigments such as chlorophyll, anthocyanin and carotenoid content (Mishra et al., 2017), characterized by a strong absorption by these leafy pigments, particularly chlorophyll which are responsible for photosynthetic activity in plants (Feret et al., 2008). When spectral profiles are collected over time they can be used for the estimation of the quality changes and shelf life of the food products during storage (Gowen et al., 2008; Rajkumar et al., 2012; Løkke et al., 2013). Some applications include monitoring of the ripening of tomatoes (Polder and Heijden, 2010), or banana (Rajkumar et al., 2012), hence providing a promising opportunity for the collection of the information related to the quality of a product in the form of spectral responses as they retain most of the information related to the overall quality.

The objective of this study was to use the MASLT technique for the estimation of the shelf life of rocket leaves using the spectra as a quality attribute. In addition, an alternative method based on the use of partial least squares regression (PLSR) and latent variables (LV) instead of PCA and PC scores was also proposed.

2. MATERIALS AND METHODS

2.1 Experimental design and spectral acquisition

Washed and dried rocket leaves (*Diplotaxis tenuifolia*) were received in the postharvest laboratory of University of Foggia, after being processed in a commercial company. Drying was conducted with a drying tunnel, heating the product at 30 °C for 5 mins, and achieving about 95% of added water reduction. Upon arrival the rocket leaves were stored at 5 °C. Representative samples of 100 grams were packed in plastic clamshells and stored at three different temperatures (5 °C, 10 °C and 15 °C) in a humidified (99% RH) flow of air. Ten replicates were prepared for each storage temperature. Samples were taken for image acquisition and quality evaluation at 0, 3, 6, 8 and 10 days of storage following the same leaves over time.

A hyperspectral line scan scanner (Version 1.4, DV srl, Padova, Italy) equipped with a spectrograph, in the visible-near infrared (Vis-NIR) range of 400-1000 nm with a spatial resolution of 1000x2000 pixels and a spectral resolution of 5nm was used to acquire the images. Twenty leaves were taken for each

replicate in a single image and self-developed MATLAB (2012b, version 8.0.0.783) code was used for extracting the mean spectra of these leaves producing one spectrum per replicate. For the extraction of the mean spectrum, the original image was thresholded and the best contrast between the object and the background was found. Image thresholding was performed using the Otsu method, on the image depicting the best contrast between the foreground and background, corresponding to 795nm for the Vis-NIR and 1495nm for the NIR. A 2D binary image (mask) was obtained, with 0 value for the background and 1 for the leaves. This mask was imposed to extract the mean spectra of the pixels corresponding to the leaves. A total of 150 spectra were acquired, 50 from each storage temperature during 5 different days of acquisition (Figure 1). Figure 1a shows the mean spectra based on days of storage and 1b demonstrates the changes in the mean spectra based on the storage temperature plotted in PLS toolbox (version 7.5.2) supported by MATLAB.

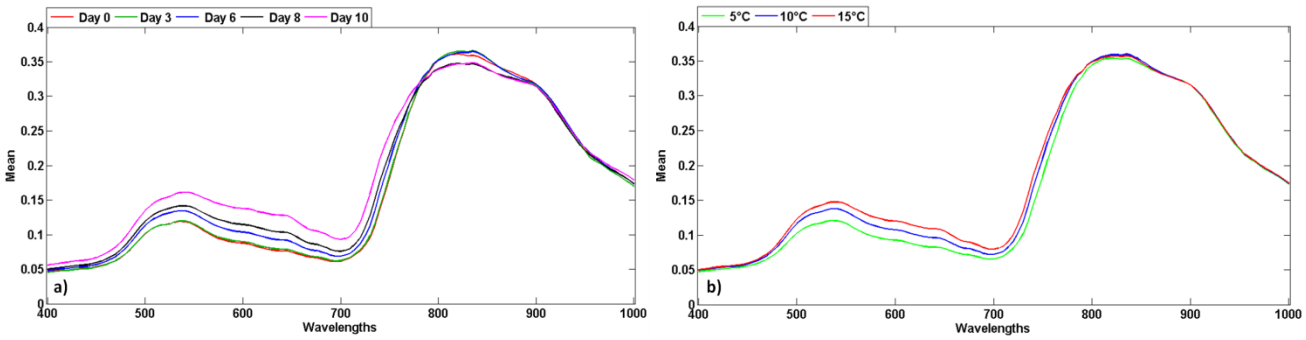

Figure 1. a) Mean spectra based on days of storage Day0 (red), Day3 (green), Day6 (blue), Day8 (black), Day10 (Violet); b) Mean spectra based on temperatures of storage 5 °C (green), 10 °C (blue), 15 °C (red)

Figure 1a shows the characteristic Vis-NIR reflectance spectra of the rocket leaves resulting from the leaf biochemical compounds such as chlorophyll, anthocyanins, carotenoids, water and cellulose in the wavelength range of 400-1000nm. In case of green leafy vegetables, the interaction between the plant leaves and electromagnetic radiation yields reflectance spectra in the Vis-NIR region which are mainly representative of the photosynthetic pigments such as chlorophyll and carotenoids (Mohd Asaari et al., 2018). Visually, a green plant spectral curve can be observed in the raw spectra with 550nm reflectance peak and 680nm absorbance peak caused by chlorophyll, a major color related pigment (Kong et al., 2016). The sharp rise in the spectra from 700nm corresponds to the red edge resulting from two special

optical properties of plant tissue, the high internal leaf scattering resulting in large NIR reflectance and low red reflectance as a result of chlorophyll absorption (Horler et al., 1983).

2.2 Sensory analysis

Rocket leaves were evaluated by a panel of experts for changes in appearance, including freshness, color and dehydration, during the storage period. Since appearance is the most important quality attribute for the selection of the product at the retail sites for the consumers, the appearance scores were given a scale from 0 to 5 and these sensory evaluations were carried out on each acquisition day. In case of appearance scores, rocket leaves with uniform dark green color with fresh and turgid appearance were given score 5, fresh rocket leaves with a slight loss of turgidity obtained an appearance score of 4, rocket leaves with a significant loss of turgidity and an apparent loss of color (limit of marketability) were set at an appearance score of 3, leaves with significant senescence with the passage of storage time having wrinkled and yellowish blades received an appearance score of 2 and the spoiled rocket leaves with severe wilting, significant yellowing and decay symptoms were given a score value of 1 (M. L. Amodio et al., 2015).

2.3 Multivariate Accelerated Shelf Life Testing (MALST) Approach

An elaboration of the MASLT algorithm used in this study is presented, and for the sake of convenience, conventional algebraic symbology is followed, where matrices will be represented by boldface upper case letters, vectors with bold face lower case letters, scalar quantities with italic lower case, italic subscripts denote case letters and sequences.

In the first step, a matrix **X (m**x**n)** where **m**=150 and **n**=121, was formulated representing the quality changes in the rocket attributes at three different storage temperatures (5, 10 and 15 °C) with **m** being the number of data points collected during storage on Days 0, 3, 6, 8 and 10 respectively with 10 replicates from each storage temperature and **n** being the vector of variables or spectra in a wavelength range of 400-1000nm (Figure 2). Auto-scaling the data is a necessary consideration when various univariate quality attributes with different scales are simultaneously under study (Pedro and Ferreira, 2006; Derossi et al., 2016) and in case where spectral profiles are serving as property attributes, normalization of the data is important for which mean centering was done.

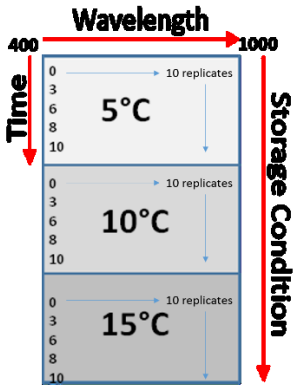

Figure 2. Data Matrix (mxn) with Time=m, Wavelength=n at the 3 Storage Conditions (5, 10, 15 °C)

Secondly, PCA was performed on the data matrix **X** after data mean centering (Figure 3). PCA describes the data by projecting it on a new set of axis in the multivariate space. Principal components are linear combinations of the original variables and each one accounts for the direction of maximum variability in the data (Bro and Smilde, 2014). The loading plots of the time related PCs were observed for the selection of the best variables and the elimination of those who did not contribute to any information in the PCA model resulting in the elimination of the wavelength range from 800-1000nm. For each storage temperature, the scores matrix (**S**) of every i^{th} time related PC were plotted against the storage time to formulate kinetic plots also known as shelf life charts, describing the changes of the PC scores as a function of time. For these time related PCs, reaction order and multivariate kinetic parameters were determined. After the estimation of the multivariate constants, the Arrhenius equation (Labuza, 1982) was used for estimating their temperature dependence for each kinetic model.

Quality degradation kinetics can be represented by the equation 1:

$$-\frac{dQ}{dt} = kQ^n \qquad \text{(Equation 1)}$$

Where Q is the measured quality attribute, t represents time, n is the reaction order and k is the reaction or degradation rate.

The reaction rates are significantly temperature dependent, higher the storage temperature the faster the degradation. Therefore, to associate or describe the temperature dependence of the degradation rates, Arrhenius equation is used.

$$\ln(k) = \ln k_{T_{ref}} - \frac{E_a}{RT} \qquad \text{(Equation 2)}$$

Where, Ea is the activation energy, R is the universal gas constant with a constant value of 8.314 J/mol, Tref is the reference temperature usually in shelf life studies is the market shelf temperature of any food product.

The most important and significant aspect of the MASLT technique is the selection of the cut-off criteria for the property under study. In case of study evaluating different quality parameters, individual reference limits are chosen for each quality index, and cut-off criteria (t_c) is calculated as the maximum acceptable value of the vector **t** (Pedro and Ferreira, 2006; Derossi et al., 2016).

$$\mathbf{t} = \mathbf{x_a} * \mathbf{L} \qquad \text{(Equation 3)}$$

$$t_c = \text{Max}(\mathbf{t}) \qquad \text{(Equation 4)}$$

Where $\mathbf{x_a}$ is the row vector containing the auto-scaled values of the reference limits of each quality attribute that define the threshold of acceptability of the product, while **L** is the loading matrix of the time-related PCs at the market storage conditions.

In this study, the spectra of samples judged unacceptable was used for the calculation of the cut-off value. For visualization of degradation with the passage of storage time for leaves stored at different temperatures, 5 random leaves were collected from the replicates of each acquisition time and were processed in Hypertools (Mobaraki and Amigo, 2018). The images were spatially binned, masked and augmented with each row representing a single acquisition time (Figure 5).

2.4 Partial Least squares regression (PLSR)

A slight modification of the MALST algorithm was also proposed in this study by developing PLS models for the spectra against time of storage. PLSR works by maximizing the covariance between the linear functions of the information included in the **X** (**m**x**n**) matrix and the corresponding vector of storage time in the **m** (ter Braak and de Jong, 1998; Dunn et al., 1989). Random subset cross validation was applied in this case. Firstly, a PLS model to predict days of storage was developed after mean centering the **X** data and auto-scaling **m** using the PLS toolbox. Then the LVs were taken as properties and were plotted against time to formulate shelf life charts. The rest of the procedure remained the same as the conventional MASLT application. In this case, only mean centering was done for data normalization. The model reliability was accessed by the values of R^2 calibration and R^2 cross validation

and also by the root mean square errors.

3. RESULTS AND DISCUSSION

3.1 Principal Component Analysis and PC relationship with time

PCA of the normalized data in the wavelength range of 400-1000nm resulted in two PCs covering maximum variance in the data where, PC1 accounted for only 88.24% of the total variability over the entire wavelength range constituting 121 variables. After the removal of the variables not contributing to the model from the preliminary PCA, (MacGregor and Kourti, 1995; Saavedra et al., 2013) a total of 2 PCs accounted for 98.99% of the total variability in the data in the wavelength range of 400-800nm. In this case, PC1 explained maximum variability of 96.27% followed by the PC2 which accounted for only 2.72% of the total data variability (Figure 3).

Plot of PC1 vs PC2 scores clearly indicated as the main source of variance on PC1 was related to time (Figure 3a). Figure 3b depicts the change in the PC1 scores for the samples stored at three different temperatures over the storage time. The degradation rate of the rocket leaves stored at 5 °C is much lower than those stored at 10 °C and 15 °C, which as expected, indicates that storage temperature had a significant impact on the shelf life of the rocket leaves. Temperature is, in fact, the most important factor affecting the quality of fresh produce. Low temperature is essential to maintain an optimal product quality because it reduces several physiological activities, such as transpiration, which causes weight loss, and respiration. Senescence can induce chemical and enzymatic changes that may cause tissue softening, pigment loss, ripening and discoloration (Brosnan and Sun, 2001). Moreover, low temperature also reduces the growth rate of spoilage microorganisms on surfaces of vegetable tissues (Rediers et al., 2009; Ukuku and Sapers, 2007). These changes in the PC scores may be directly related to the leaf pigments which are responsible for the color in the rocket leaves since the spectra responses vary with the change in color of the leaves in the Vis-NIR range, as a result of the loss of chlorophyll over the storage period. As shown in the sample score plot in Figure 3b, spectral signatures of the leaves at each acquisition time varied with the temperature of storage. From Figure 3a and 3b it can also be observed that up to day 3 all the samples at the three different storage temperatures possessed similar scores and therefore similar quality attributes. Regarding appearance, in fact, until day 3 all the leaves possessed a visual score value above 3 and were still marketable, as can be seen in Figure 4. Starting from day 6 of storage, significant quality differences can be observed in the samples stored at different temperatures.

Therefore, PC scores possess the capability to mark the days of storage during which significant quality changes occur for the samples stored at different storage temperatures. Also in the case of samples stored in modified atmosphere packaging at 5, 10 and 15 °C, differences in appearance score were higher starting from the 6^{th} day of storage (Amodio et al., 2015), as well as difference in the overall sensorial quality. In the same study, it was found that appearance scores limited the shelf life of the leaves stored at 5 °C, estimated in 7.3 days while an increase in the temperature affected the loss of ascorbic acid more than the appearance and off-odor scores.

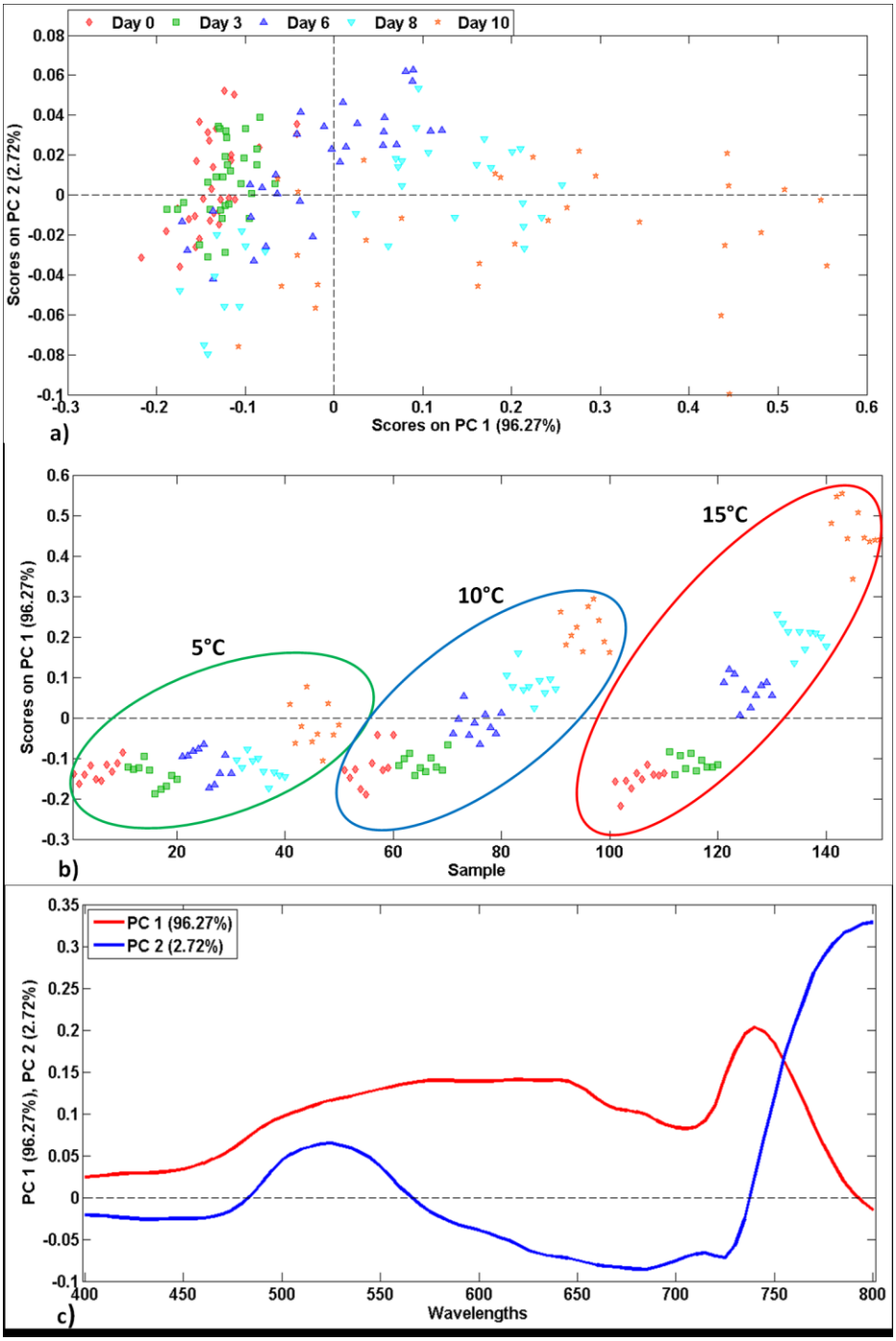

Figure 3. PC scores plots in the wavelength range of 400-800nm: a) PC1 vs PC2 for days of storage (0, 3, 6, 8, 10); b) PC1 variation of the samples at 5 (green ellipse), 10 (blue ellipse) and 15 °C (red ellipse) respectively; c) PC Loadings PC1 (red) PC2 (blue)

Figure 3c depicts the importance of the variables for the model; all the loadings of the PC1 model above the threshold contributed weight to the model. Since the considered wavelength range is 400-800nm, this is mainly accounting for the color changes related to the pigments of the rocket leaves such as chlorophyll and carotenoids therefore, the PC1 and PC2 loadings correspond to the chlorophyll absorption at 670nm in case of PC1 and the peak at 535nm corresponds to the anthocyanins absorption. The spectral profiles in the NIR region from 800-1000nm are mostly related to the changes in dry matter and textural properties. Moreover, the mid NIR region is usually depicting changes based on the water content as this region is based on the high influence by water (Sánchez et al., 2011).

As for leaf pigments, chlorophyll compounds absorb in the blue and red regions, corresponding to the wavelength peak at 430 and 670 nm for Chlorophyll a, and 460 and 640 nm for chlorophyll b. Carotenoid peak ranges from 470 to 530 nm, whereas anthocyanins has a maximum absorbance at 530 nm. Based on previous research works both the carotenoid and chlorophyll absorbance decreased with the storage time due to the senescence of the leaves (Gitelson and Merzlyak, 1994; Ferrante et al., 2004). Figure 1a shows lowest reflectance values in the region from 650-670nm for samples at Day0, which means that the leaves possess significant chlorophyll content which with the passage of storage time decreased resulting in higher reflectance (low absorption) values at the end of storage period. This transition from the green to yellow color as a result of chlorophyll breakdown, associated to senescence, results in increased reflectance values.

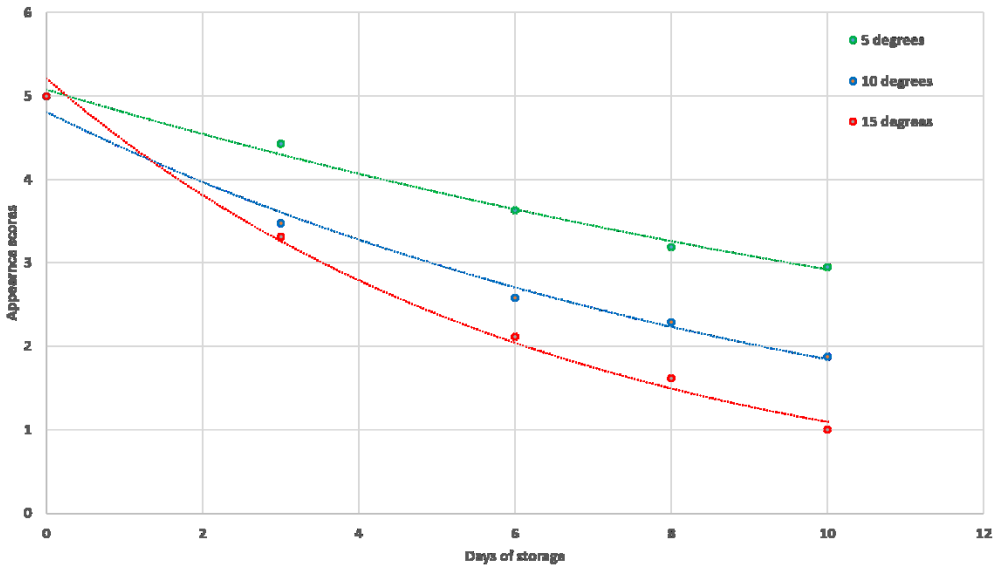

Figure 4. Changes in the appearance scores of fresh rocket leaves stored at 5 ºC (green), 10 ºC (blue) and 15 ºC (red) over time

From Figure 4 it can be observed that leaves stored at 15 °C showed the highest degradation, followed by samples at 10 ºC and 5 ºC; this is a result of color changes and leaf dehydration and wilting.

Figure 5 represents the variability of the PC Scores in the leaves stored at 5, 10 and 15 °C. As can be seen, the color changes in each row (each acquisition time) at 5 °C are not visually different, but in case of 10 and 15 °C higher changes can be observed. As for 10 °C, starting from the 3rd row corresponding to the 6th day of storage, slight changes in the score colors can be observed. In case of 15 °C, the leaves in row 3 are clearly showing a significant variation of the score values when compared to those at 5 °C and 10 °C. This is totally comparable to the PCA results of the spectra in Figure 3b where the score sample plot depicts maximum score changes at 15 °C. So Figure 5 is an image visualization of the trend of the score changes, obtained using randomly chosen leaves which has been expressed in Figure 3b for the samples stored at all three temperatures. The differences in the Figures 5a, 5b and 5c can be directly related to the quality of the leaves. While Figure 3b shows a plot of the samples against the time related PC1, Figure 5 shows the relative maps of the leaves stored at all the three different temperatures over a time span of 10 storage days. The PC1 score values correspond to the color changes in the leaves from dark green to yellow over the storage period, which can also be depicted in the PC scores plot along the

PC1 axis in Figure 3a. According to the Figure 3b all the samples at Day1 of storage have the same score values hence they possess the same freshness and green color as can also be observed for the samples of Day1 for all samples in Figure 5. Since the degradation rate at different temperatures is different, clear quality changes (transition from dark green towards yellowish color) were observed for the samples stored at 10 °C and 15 °C after 6 days of storage, especially for the samples stored at 15 °C.

3.2 Multivariate modeling and shelf life estimation

Table 1 shows the results obtained by applying non-linear fitting to PC1 scores against time; based on R^2 values, results of first order fitting, particularly when a pre exponential factor was also included in the equation were better than those of the zero order reactions. First order kinetics explained the PC1 score changes with time with an R^2 of 0.73 at 5, 0.94 at 10, and 0.95 at 15°C for the variables in the range of 400-800nm. The reason for this low value of R^2 in case of 5ºC can be attributed to the fact that the degradation rate at this temperature was slower as compared to 10 and 15ºC. A_0 refers to the pre exponential factor, and was estimated in similar values among different temperatures, being 3.849, 3.831 and 3.776, respectively at 5, 10 and 15 °C

Table 1. First order kinetic parameters of PC1 scores as a function of time for fresh rocket leave samples stored at 5, 10 and 15°C using the equation $A=A_0*e^{(-kt)}$

Wavelength Range 400-800nm							
Temperature		**Estimate**	**Std. error**	**t-value**	**p-level**	**Conf limits**	**R^2**
5°C	A_0	3.849	0.030	126.570	0.000001	3.753-3.947	0.73
	k_m	0.008	0.004	1.825	0.16	-0.006-0.022	
10°C	A_0	3.831	0.043	87.299	0.000003	3.692-3.971	0.94
	k_m	0.033	0.006	4.870	0.01	0.011-0.055	
15°C	A_0	3.776	0.071	52.478	0.00001	3.547-4.005	0.95
	k_m	0.058	0.011	5.276	0.01	0.023-0.094	

Looking also at the confidence values for A_0 values, it can be concluded that all the samples had the same quality attributes upon the beginning of the shelf life estimation and that the variance of overall quality

of the fresh samples did not affect the degradation kinetics. On the other hand, a progressive increase in the value of the multivariate rate constants is seen with the increasing temperature which at 5°C increased with a value of $0.008d^{-1}$, at 10°C with a value of $0.033d^{-1}$ and at 15°C it increased with a value of $0.058d^{-1}$. From the confidence intervals, a significant difference can be observed between samples stored at 5 and 15°C, with an increase of ~7.2 fold in the degradation rate of the appearance scores. Derossi et al., 2016 found higher multivariate rate constants with values increasing with the increasing temperature for fresh-cut lettuce stored in MAP at 0, 5 and 15°C, but this may be explained with the higher sensitivity of lettuce to browning and quality degradation due to mechanical damages induced with the cutting (Murata et al., 2004) and to the effect of modified atmosphere which at higher temperature may result in improper gas composition and in off-flavor development (Mastrandrea et al., 2017). On the other side, observed values for k_m at 5 and 15°C were very similar to the value obtained by Amodio et al. (2015) when fitting color score kinetic, evaluated sensorially with the same scale system from 5 to 1. These authors reported values of 0.019 and 0.047, at 5 and 15°C, respectively, fitting the kinetic curve with a Weibull model. Considering that shape factor values were not very different from 1 (1.34), a rough comparison of the constant can be done, and thus it can be hypothesized that observed variations were closely related to the color changes. The decrease in the values of the PC scores with the passage of storage time in the wavelength range of 400-800nm is indicative of the transition from green color to yellowish as a result of the loss of chlorophyll which at 15ºC is the highest (Figure 5c) followed by 10ºC (Figure 5b) and 5ºC (Figure 5a) and color changes can only be observed in the region from 550-700nm.

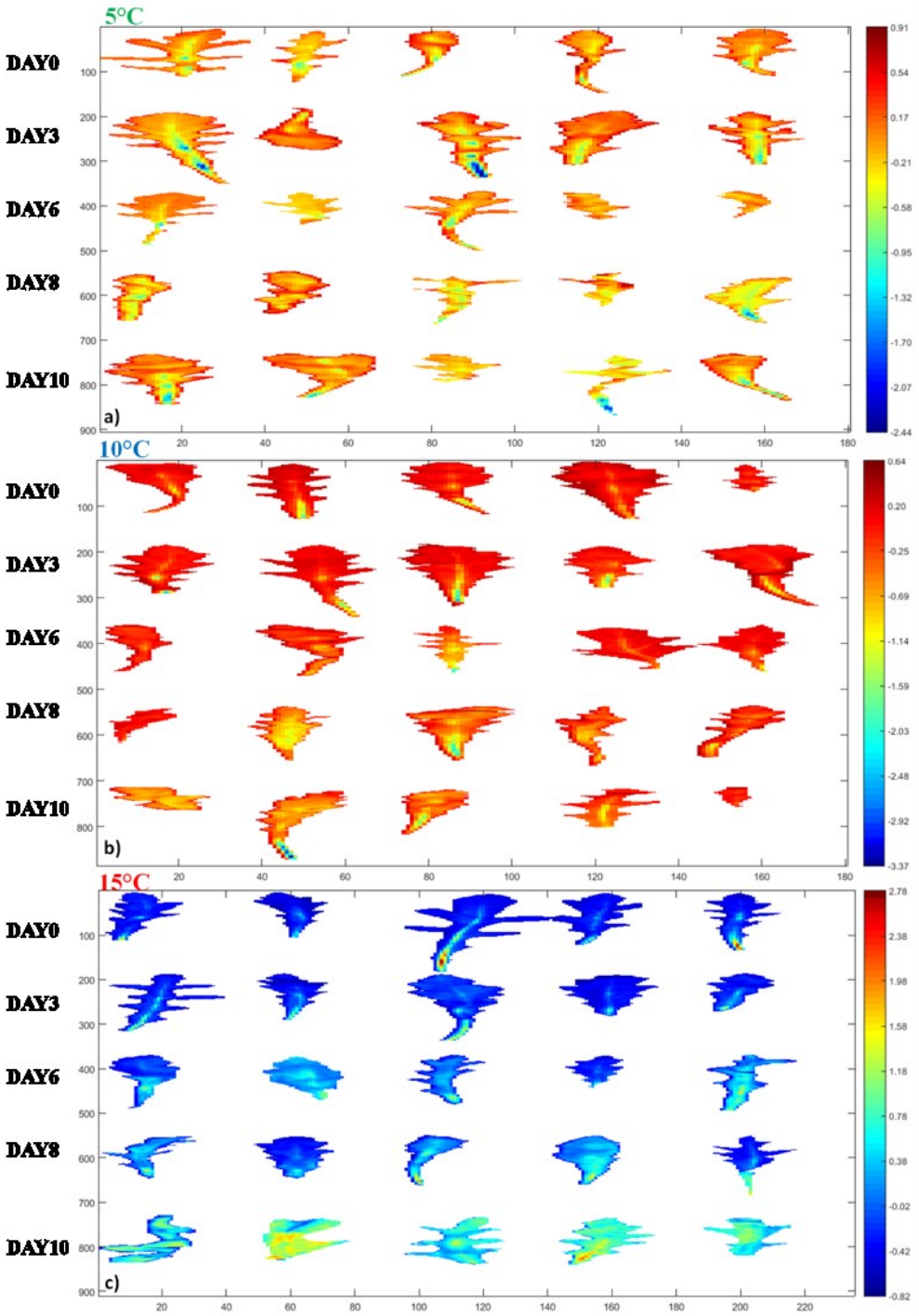

Figure 5. Variability in PC1 scores over storage) a) 5°C b) 10°C c)15°C in a wavelength range of 400-800nm.

The multivariate kinetic parameters (k_m, α_m, E_a) calculated using PC scores as properties after various data pretreatments and utilizing two different spectral ranges, are shown in Table 2. These kinetic parameters were obtained after the exponential fitting of the time related PC scores with time of storage using the equation $A=A_0*e^{(-kt)}$.

Table 2. First order kinetic parameters as a result of exponential modeling of PC1 scores as a function of time for fresh rocket leave samples stored at 5, 10 and 15°C using the equation $A=A_0*e^{(-kt)}$

Wavelength range (400-1000 nm)						
PC#	Variance explained (%)	Pretreatment	Storage Temperature (°C)	Multivariate rate constant (k_m)	Acceleration factor (α_m)	Activation Energy (E_a)
1st	88.92	Mean Centering	05	0.0024	…	120.91
			10	0.0085	3.54	
			15	0.0147	6.13	
Wavelength range (400-800 nm)						
PC#	Variance explained (%)	Pretreatment	Storage Temperature (°C)	Multivariate rate constant (k_m)	Acceleration factor (α_m)	Activation Energy (E_a)
1st	96.37	Mean Centering	05	0.0022	…	124.88
			10	0.0082	3.73	
			15	0.0143	6.5	

From Table 2 it can be seen that the dependence of the rate constant (k_m) on the temperature of storage is clearer in case of mean centered data both for the 121 variables used (400-1000nm) and 81 variables (400-800nm) after the spectral cropping. Other data pre-treatments were applied, but a clear difference between the rate constants could not be observed in those cases, since, by extensively preprocessing the data, the baseline effects related to the product degradation cannot be observed (Pedro and Ferreira, 2009), therefore the spectral data were only normalized.

In case of the full wavelength range, the rate constant changed from $0.0024d^{-1}$ to $0.0085d^{-1}$ and $0.0147d^{-1}$, respectively for 5, 10, and 15°C, depicting the change in the rate constants with respect to temperature. Similarly, after the omission of the undesired variables, the variance explained by PC1 increased but still there was not a significant difference between the rate constant and acceleration factor values from those of the total 121 variables under study. The activation energy calculated for 121 variables was 120.91 kJ/mol whereas for 81 selected variables it was 124.88 kJ/mol. Also in this case the comparison with value found by Derossi et al., 2016 for fresh-cut lettuces, confirmed that degradation reactions in rocket leaves were much slower than for fresh-cut lettuce, requiring much higher E_a.

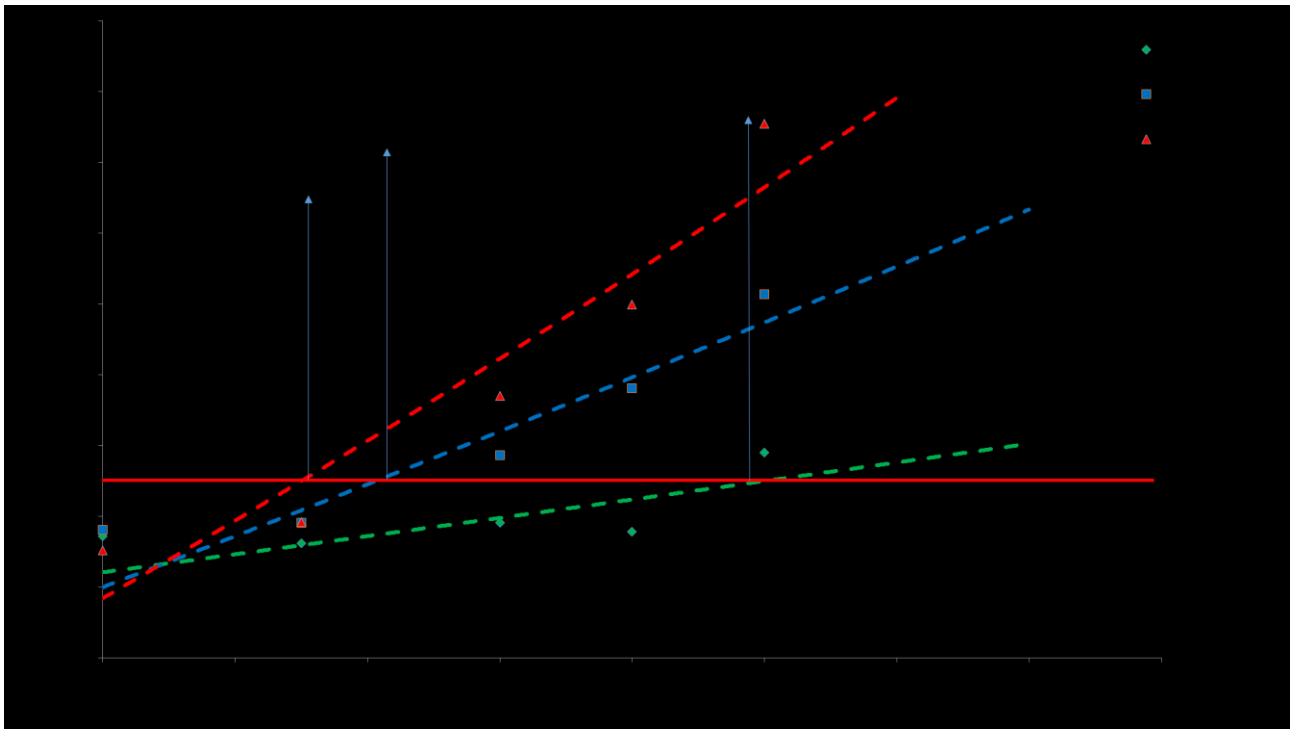

Figure 6. PC1 scores as a function of time for rocket leaves stored at 5°C (green), 10°C (blue) and 15°C (red). Red full-line represent the shelf-life cut-off value.

In Figure 6, PC1 scores for each temperature were plotted against time in order to estimate the shelf-life. The cut off criterion was calculated based on the number of days needed to reach score 3, corresponding to the marketability limit, applied to the kinetic at 15°C. This is in line with the MASLT theory of using the maximum acceptable values among shelf-life limit of considered attributes. The spectrum of the

unacceptable sample as vector $\mathbf{x_a}$ and the loadings of the time related PC were taken and using equation 4 the cutoff criteria was calculated to be 3.955. These appearance score values were in agreement with the studies conducted by Amodio et al., 2015 and Mastrandrea et al., 2017 in which the rocket leaves reached the limit of marketability (appearance score 3) on the third day of storage when stored at 15°C. Estimated values of shelf life were similar to those reported by Amodio et al., 2015 and were lower when compared to values reported by Koukounaras et al., 2007, but this can bedue to the difference in raw material possibly related with the cultivar, the season, and the number of cutting (Seefeldt et al., 2012; Koukounaras et al.,2007; Martínez-sánchez et al., 2008). Moreover this study was conducted in humidified air flow storage of the leaves and the same leaves were followed over time, being more prone to mechanical damage during image acquisitions.

Generally shelf-life of wild rocket leaves stored at 0°C was extended to about 3 days if compared to storage at 4°C and 6 days compared to storage at 7°C (Hall et al., 2013). Amodio et al., (2015) reported value of 7.3, 5.8 and 3.7 days for samples stored at 0, 5 and 15 °C, respectively, when appearance score was used as marketability limit. In the same study, the shelf life was of 12.6, 10.4 and 3.1 when calculated on texture score, and even higher if calculated on the ascorbic acid losses. The authors, showed, in fact that appearance score was the limiting factor for shelf life at 0 and 5°C, but that at 15°C, ascorbic acid content, followed by the texture, were more critically contributing to the marketability, because the degradation rates of these attributes increased with temperature more than the appearance and off-odor. These findings confirm the needing of a multivariate approach for shelf-life estimation. When MALST method was applied on fresh-cut lettuce, it was found that the degradation of samples stored at 15°C was mainly attributed to the off-odor rather than to the appearance score and color score, which, on the other hand, were the most determinant for samples stored at 0 and 5°C, respectively (Derossi et al., 2016).

3.3 PLSR for the estimation of days of storage and shelf life

This method is a slight modification of the MASLT approach. In this case instead of doing a PCA, a PLS model was developed for the prediction of days of storage from the spectra acquired during the storage period at all three storage temperatures. The spectra were mean centered and PLS regression model for days of storage in the full wavelength range resulted in an R^2_{cal} of 0.86 and R^2_{cv} of 0.83 with the RMSC of 1.32 and RMSECV of 1.48. The first latent variable (LV) accounted for 88.82% of the variance and

the second LV described 8.31% of the variance in the data. Variables having minimal or negligible weight in the PLS model as shown in the loading plots were removed, resulting also in this case, in the elimination of the variables from 800-1000nm. PLS regression model for prediction of days of storage was developed again with 81 variables from 400-800nm after data normalization (Figure 7).

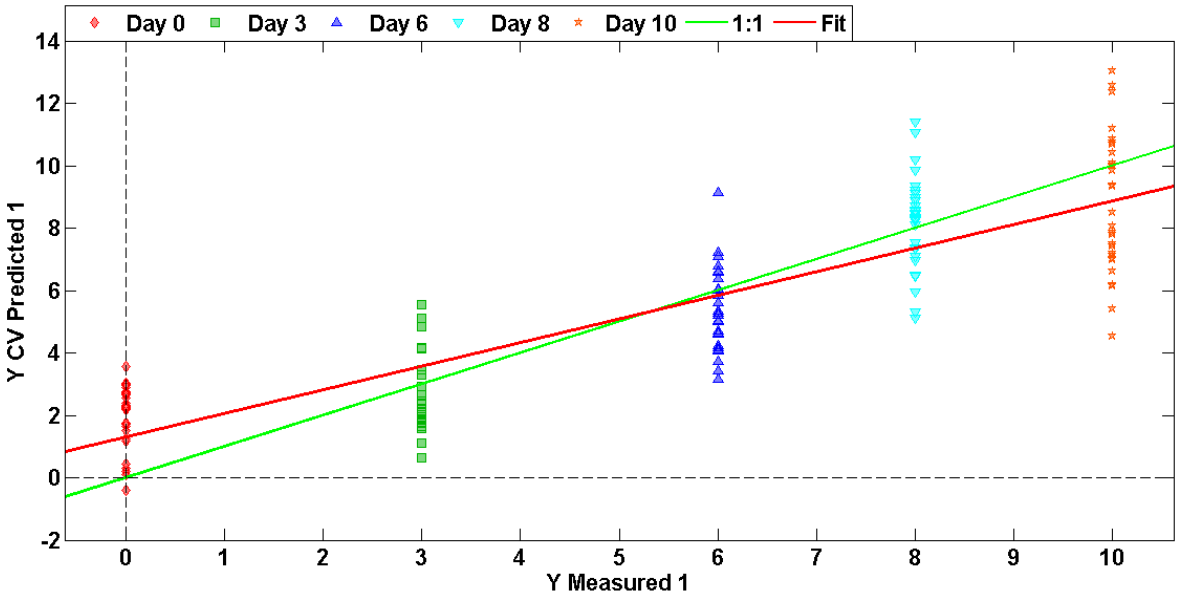

Figure 7. PLS regression model for prediction of days of storage in the wavelength range of 400-800nm; Day0 (red), Day3 (green), Day6 (blue), Day8 (light blue), Day 10 (orange).

LV1 explained 96.25% of the covariance, whereas LV2 only accounted for 2.69% of the covariance in the data. The plot of LV1 versus LV2 shows the variability of the LV scores along the LV1 axis (Figure 8a). The cause of this variability can be found in the differences of the Y values due to the different storage temperatures. Figure 8b depicts the loadings of LV1 and LV2.

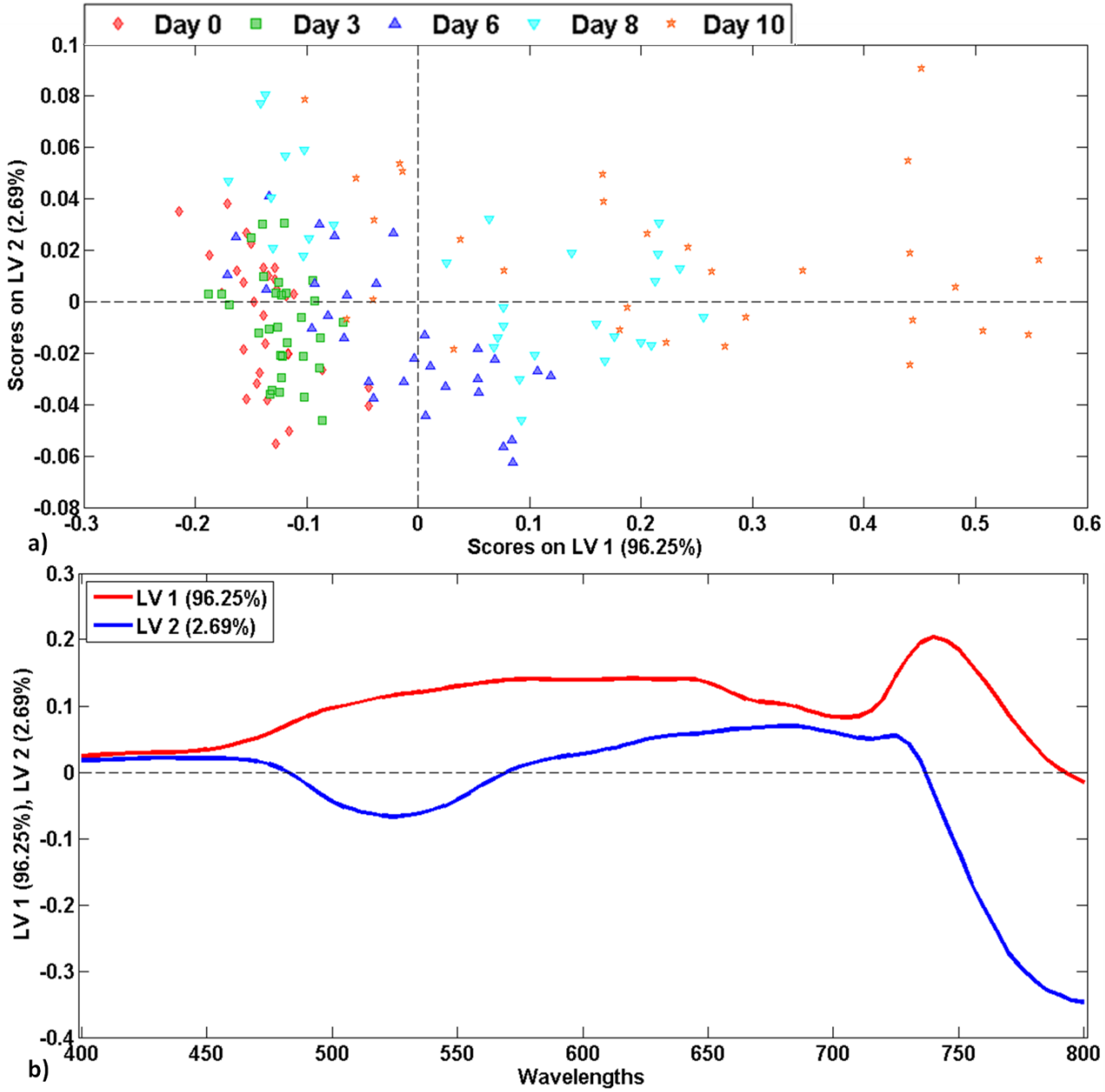

Figure 8. LV plots in the wavelength range of 400-800nm; a) LV1 vs LV2 score variability for days of storage (0, 3, 6, 8, 10); b) LV loadings LV1 (red) LV2 (blue).

Compared to the PCA in Figure 3a a similar dependence of LV values with time of storage can be observed; the changes in the spectral properties are evident in this case as well. For this reason, this can

also be considered as a new MASLT approach and its results can be compared to the conventional MASLT based on PCA. As expected, LV1 was found to be time related and the loadings of LV1 and PC1 possessed negligible difference. Both the LV1 and PC1 loading profiles hold similarity with the mean centered spectral profiles, hence explaining maximum covariance and variance, respectively.

Table 3. Estimated A_0 and slope k_m values resulting from the regression analysis of storage time and LV1 scores

Wavelength range (400-800 nm)							
Temperature		**Estimate**	**Std. error**	**t-value**	**p-level**	**Conf. limits**	**R^2**
5	A_0	3.849	0.029	128.814	0.000001	3.754-3.944	0.74
	k_m	0.008	0.004	1.919	0.15	-0.005-0.021	
10	A_0	3.831	0.044	86.470	0.000003	3.689-3.972	0.94
	k_m	0.033	0.006	4.842	0.01	0.011-0.054	
15	A_0	3.775	0.072	51.784	0.00001	3.543-4.007	0.95
	k_m	0.058	0.011	5.218	0.01	0.023-0.095	

If compared to Table 1, the results obtained by applying non-linear fitting to the LV1 against time using the first order kinetics are not significantly different as the PC scores approach in the conventional MASLT studies (see Table 3). LV1 score changes with time resulted in an R^2 of 0.74 at 5°C, slightly higher than the R^2 obtained in the case of PC scores at the same storage temperature, 0.94 at 10°C and 0.95 at 15°C, similar to those of the PC approach. The A_0 values for all three temperatures is almost similar in this case and negligibly different from those of the PC scores for each storage temperature. Moreover, the multivariate rate constant values are exactly the same in both cases, with the increasing temperature which at 5°C was $0.008d^{-1}$, at 10°C was $0.033d^{-1}$ and at 15°C was $0.058d^{-1}$. If compared to the A_0 values in Table 1 it can be seen that the results of the PLS regression coupled with the MASLT analysis are the same as the conventional MASLT approach. Also in this case the negligible differences in the A_0 values signify that the leaves in the start of the analysis had the same quality attributes which deteriorated with the passage of time at different rates stored at different temperatures.

Table 4. First order kinetic parameters as a result of exponential modeling of LV1 scores as a

function of time for fresh rocket leave samples stored at 5, 10 and 15°C using the equation $A=A_0*e^{(-kt)}$

Wavelength range (400-800 nm)						
LV#	Co-variance explained (%)	Pretreatment	Storage Temperature (°C)	Multivariate rate constant (k_m)	Acceleration factor (α_m)	Activation Energy (E_a)
1st	96.25	Mean Centering	05	0.0023	…	121.95
			10	0.0082	3.57	
			15	0.0143	6.22	

The kinetic charts were developed for the LV scores at each storage temperature against the days of storage (Figure 9).

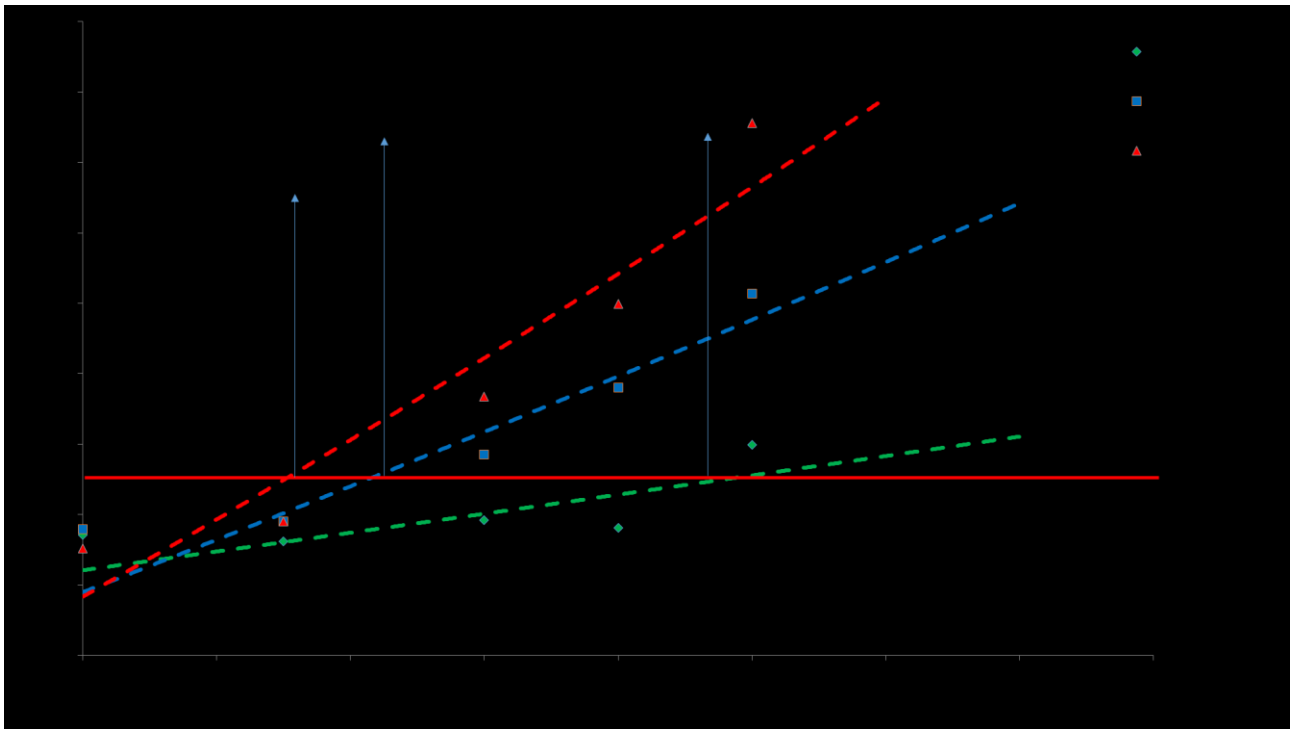

Figure 9. LV1 scores as a function of time Figure 6. PC1 scores a for rocket leaves stored at 5°C

(green), 10°C (blue) and 15°C (red). Red full-line represent the shelf-life cut-off value.

If compared to Figure 6, in which the PC1 scores were plotted as a function of time, it can be observed that the results are not very different. Equation 4 was used for the calculation of cutoff criteria using the unacceptable spectrum and the loadings matrix of the time related LVs, and these cutoff criteria possessed negligible difference from that of the PC scores approach. The estimate of shelf life in this case for samples stored at all three temperatures had minute differences but was still better as compared to the PCA, 3.3 days, 4.5 days and 9.4 days at 5, 10 and 15°C.

Comparing Figure 6 and Figure 9, as well as Table 4 and Table 2, it is clear that LV can be used as an alternative approach for the shelf life estimation in the MASLT method since the differences in the values of the rate constants, of the activation energy, as well as of shelf-life estimation are not significant. The advantage of using this approach instead of using a PCA is that it would be much more flexible for further validation experiments. In fact, while PCA distribution of variables may be more sensitive to other sources of variation, a PLS prediction model based on days of storage will be more robust since PLS takes into consideration the covariance between the spectral profiles and the predictor values. Hence, the co-variability of the spectra with respect to days of storage are more accurately represented by PLS. This will facilitate the comparison of data obtained with new samples, just by plotting them versus the regression line plot, without the need of re-running a PCA every time, and also the adding of new calibration data into the model.

4. CONCLUSIONS

For the first time a multivariate approach using the spectral fingerprints for the estimation of the shelf life of fresh cut rockets was used. The changes in the spectra with the passage of storage time for the samples stored at three different temperatures served as the property under study. Comparing the MASLT approach with the conventional ASLT methods the use of PCA yielded valuable information regarding the variables contributing towards the weight in the model and accounting for the quality losses of the product. It was highlighted that the wavelength range of 550-700nm held great significance while estimating shelf life based on appearance scores. The conventional MASLT approach using the PC scores was also compared with a new method using PLS and LV for the development of the kinetic or shelf life charts. Comparing both the approaches it was concluded that no significant difference exists between the results yielded by both the techniques.

On the other side, the PLS model can be more robust as compared to a PCA model with the allowance of new samples to be added in the calibration and can serve as a tool for better validation. MASLT approach with PLS can enable the processors to better estimate the shelf life of their products and access the market with better product quality by improving the logistics.

REFERENCES

Amodio, M.L., Derossi, A., Colelli, G., 2013. Modelling sensorial and nutritional changes to better define quality and shelf life of fresh-cut melons. Journal of Agricultural Engineering 43, 6. doi:10.4081/jae.2013.e6

Amodio, M.L., Derossi, A., Mastrandrea, L., Colelli, G., 2015a. A study of the estimated shelf life of fresh rocket using a non-linear model. Journal of Food Engineering 150, 19–28. doi:10.1016/j.jfoodeng.2014.10.030

Amodio, M.L., Derossi, A., Mastrandrea, L., Colelli, G., 2015b. A study of the estimated shelf life of fresh rocket using a non-linear model. Journal of Food Engineering 150, 19–28. doi:10.1016/j.jfoodeng.2014.10.030

Amodio, M.L., Derossi, A., Mastrandrea, L., Colelli, G., 2015c. A study of the estimated shelf life of fresh rocket using a non-linear model. Journal of Food Engineering 150, 19–28. doi:10.1016/j.jfoodeng.2014.10.030

Amodio, M.L., Dollo, L., Colantuono, F., Colelli, G., 2015. Degradation patterns for external and internal quality attributes of fresh-cut apples. Acta Horticulturae 175–182. doi:10.17660/ActaHortic.2015.1091.21

Amodio, M.L., Dollo, L., Rinaldi, R., Colelli, G., 2012. Degradation patterns for external and nutritional quality parameters of fresh-cut “cantaloupe” melons. Acta Horticulturae 641–647. doi:10.17660/ActaHortic.2012.934.85

Amodio, M.L., Ferrante, A., Rogers, H., Colelli, G., 2016. A QUAFETY approach to quality monitoring and prediction for fresh-cut produce, in: Acta Horticulturae. pp. 1–12. doi:10.17660/ActaHortic.2016.1141.1

Artés, F., Gómez, P., Aguayo, E., Escalona, V., Artés-Hernández, F., 2009. Sustainable sanitation techniques for keeping quality and safety of fresh-cut plant commodities. Postharvest Biology and Technology 51, 287–296. doi:10.1016/J.POSTHARVBIO.2008.10.003

Barrett, D.M., Beaulieu, J.C., Shewfelt, R., 2010. Color, Flavor, Texture, and Nutritional Quality of Fresh-Cut Fruits and Vegetables: Desirable Levels, Instrumental and Sensory Measurement, and the Effects of Processing. Critical Reviews in Food Science and Nutrition 50, 369–389.

doi:10.1080/10408391003626322

Brereton, R., 2009. Chemometrics for Pattern Recognition (Google eBook). doi:10.1002/9780470746462

Bro, R., Smilde, A.K., 2014. Principal component analysis. Anal. Methods 6, 2812–2831. doi:10.1039/C3AY41907J

Brosnan, T., Sun, D., 2001. Precooling techniques and applications for horticultural products-a review. International Journal of Refrigeration 24, 154–170.

Cavaiuolo, M., Ferrante, A., 2014. Nitrates and glucosinolates as strong determinants of the nutritional quality in rocket leafy salads. Nutrients. doi:10.3390/nu6041519

Derossi, A., Mastrandrea, L., Amodio, M.L., De Chiara, M.L.V., Colelli, G., 2016. Application of multivariate accelerated test for the shelf life estimation of fresh-cut lettuce. Journal of Food Engineering 169, 122–130. doi:10.1016/j.jfoodeng.2015.08.010

Derossi, A., Mastrandrea, L., Amodio, M.L., De Chiara, M.L.V., Colelli, G., 2016. Application of multivariate accelerated test for the shelf life estimation of fresh-cut lettuce. Journal of Food Engineering 169, 122–130. doi:10.1016/j.jfoodeng.2015.08.010

Dunn, W.J., Scott, D.R., Glen, W.G., 1989. Principal components analysis and partial least squares regression. Tetrahedron Computer Methodology 2, 349–376. doi:10.1016/0898-5529(89)90004-3

Feret, J., François, C., Asner, G., … A.G.-R. sensing of, 2008, U., n.d. PROPECT-4 and 5- Advances in the leaf optical properties model separating photosynthetic pigments.pdf. Elsevier.

Fernando Reyes, L., Emilio Villarreal, J., Cisneros-Zevallos, L., 2007. The increase in antioxidant capacity after wounding depends on the type of fruit or vegetable tissue. Food Chemistry 101, 1254–1262. doi:10.1016/J.FOODCHEM.2006.03.032

Ferrante, A., Incrocci, L., Maggini, R., Serra, G., Tognoni, F., 2004. Colour changes of fresh-cut leafy vegetables during storage. Journal of Food, Agriculture & Environment Journal of Food Agriculture & Environment 22, 40–44.

Gitelson, A., Merzlyak, M.N., 1994. Spectral Reflectance Changes Associated with Autumn Senescence of Aesculus hippocastanum L. and Acer platanoides L. Leaves. Spectral Features and Relation to Chlorophyll Estimation. Journal of Plant Physiology 143, 286–292. doi:10.1016/S0176-

1617(11)81633-0

Gowen, A.A., O'Donnell, C.P., Taghizadeh, M., Gaston, E., O'Gorman, A., Cullen, P.J., Frias, J.M., Esquerre, C., Downey, G., 2008. Hyperspectral imaging for the investigation of quality deterioration in sliced mushrooms (Agaricus bisporus) during storage. Sensing and Instrumentation for Food Quality and Safety 2, 133–143. doi:10.1007/s11694-008-9042-4

Hall, M.K.D., Jobling, J.J., Rogers, G.S., 2013. Influence of Storage Temperature on the Seasonal Shelf Life of Perennial Wall Rocket and Annual Garden Rocket. International Journal of Vegetable Science 19, 83–95. doi:10.1080/19315260.2012.716387

Horler, D.N.H., Dockray, M., Barber, J., 1983. The red edge of plant leaf reflectance. International Journal of Remote Sensing 4, 273–288. doi:10.1080/01431168308948546

Hough, G., Garitta, L., Gómez, G., 2006. Sensory shelf-life predictions by survival analysis accelerated storage models. Food Quality and Preference 17, 468–473. doi:10.1016/j.foodqual.2005.05.009

Kebede, B.T., Grauwet, T., Magpusao, J., Palmers, S., Michiels, C., Hendrickx, M., Van Loey, A., 2015. Chemical changes of thermally sterilized broccoli puree during shelf-life: Investigation of the volatile fraction by fingerprinting-kinetics. Food Research International 67, 264–271. doi:10.1016/j.foodres.2014.10.017

Kong, W., Liu, F., Zhang, C., Zhang, J., Feng, H., 2016. Non-destructive determination of Malondialdehyde (MDA) distribution in oilseed rape leaves by laboratory scale NIR hyperspectral imaging. Scientific Reports 6. doi:10.1038/srep35393

Koukounaras, A., Siomos, A.S., Sfakiotakis, E., 2009. Impact of heat treatment on ethylene production and yellowing of modified atmosphere packaged rocket leaves. Postharvest Biology and Technology 54, 172–176. doi:10.1016/J.POSTHARVBIO.2009.07.002

Koukounaras, A., Siomos, A.S., Sfakiotakis, E., 2007. Postharvest CO2 and ethylene production and quality of rocket (Eruca sativa Mill.) leaves as affected by leaf age and storage temperature. Postharvest Biology and Technology 46, 167–173. doi:10.1016/J.POSTHARVBIO.2007.04.007

Koukounaras, A., Siomos, A.S., Sfakiotakis, E., 2006. 1-Methylcyclopropene prevents ethylene induced yellowing of rocket leaves. Postharvest Biology and Technology 41, 109–111. doi:10.1016/J.POSTHARVBIO.2006.01.018

Labuza, T., 1982. Shelf-life dating of foods.

Løkke, M.M., Seefeldt, H.F., Edelenbos, M., 2012. Freshness and sensory quality of packaged wild rocket. Postharvest Biology and Technology 73, 99–106. doi:10.1016/j.postharvbio.2012.06.004

Løkke, M.M., Seefeldt, H.F., Skov, T., Edelenbos, M., 2013. Color and textural quality of packaged wild rocket measured by multispectral imaging. Postharvest Biology and Technology 75, 86–95. doi:10.1016/J.POSTHARVBIO.2012.06.018

Ma, L., Zhang, M., Bhandari, B., Gao, Z., 2017. Recent developments in novel shelf life extension technologies of fresh-cut fruits and vegetables. Trends in Food Science & Technology 64, 23–38. doi:10.1016/J.TIFS.2017.03.005

MacGregor, J.F., Kourti, T., 1995. Statistical process control of multivariate processes. Control Engineering Practice 3, 403–414. doi:10.1016/0967-0661(95)00014-L

Martínez-sánchez, A., Gil-izquierdo, A., Gil, M.I., Ferreres, F., 2008. Article A Comparative Study of Flavonoid Compounds , Vitamin C , and Antioxidant Properties of Baby Leaf Brassicaceae Species A Comparative Study of Flavonoid Compounds , Vitamin C , and Antioxidant Properties of Baby Leaf. Society. doi:10.1021/jf072975

Martínez-Sánchez, A., Marín, A., Llorach, R., Ferreres, F., Gil, M.I., 2006. Controlled atmosphere preserves quality and phytonutrients in wild rocket (Diplotaxis tenuifolia). Postharvest Biology and Technology 40, 26–33. doi:10.1016/J.POSTHARVBIO.2005.12.015

Mastrandrea, L., Amodio, M.L., de Chiara, M.L. V., Pati, S., Colelli, G., 2017. Effect of temperature abuse and improper atmosphere packaging on volatile profile and quality of rocket leaves. Food Packaging and Shelf Life 14, 59–65. doi:10.1016/J.FPSL.2017.08.004

Mishra, P., Shahrimie, M., Asaari, M., Herrero-Langreo, A., Lohumi, S., En Diezma, B., Scheunders, P., 2017. Close range hyperspectral imaging of plants: A review. Biosystems Engineering 164, 49–67. doi:10.1016/j.biosystemseng.2017.09.009

Mobaraki, N., Amigo, J.M., 2018. HYPER-Tools. A graphical user-friendly interface for hyperspectral image analysis. Chemometrics and Intelligent Laboratory Systems 172, 174–187. doi:10.1016/j.chemolab.2017.11.003

Mohd Asaari, M.S., Mishra, P., Mertens, S., Dhondt, S., Inzé, D., Wuyts, N., Scheunders, P., 2018.

Close-range hyperspectral image analysis for the early detection of stress responses in individual plants in a high-throughput phenotyping platform. ISPRS Journal of Photogrammetry and Remote Sensing 138, 121–138. doi:10.1016/j.isprsjprs.2018.02.003

MURATA, M., TANAKA, E., MINOURA, E., HOMMA, S., 2004. Quality of Cut Lettuce Treated by Heat Shock: Prevention of Enzymatic Browning, Repression of Phenylalanine Ammonia-lyase Activity, and Improvement on Sensory Evaluation during Storage. Bioscience, Biotechnology, and Biochemistry 68, 501–507. doi:10.1271/bbb.68.501

Nielsen, T., Bergström, B., Borch, E., 2008. The origin of off-odours in packaged rucola (Eruca sativa). Food Chemistry 110, 96–105. doi:10.1016/J.FOODCHEM.2008.01.063

Nurzyńska-Wierdak, R., 2015. Protein nutritional value of rocket leaves and possibilities of its modification during plant growth. Turkish Journal of Agriculture and Forestry 39, 1023–1028. doi:10.3906/tar-1412-6

Odriozola-Serrano, I., Soliva-Fortuny, R., Martín-Belloso, O., 2009. Influence of storage temperature on the kinetics of the changes in anthocyanins, vitamin C, and antioxidant capacity in fresh-cut strawberries stored under high-oxygen atmospheres. Journal of Food Science 74, C184–C191. doi:10.1111/j.1750-3841.2009.01075.x

Oliveira, M., Abadias, M., Usall, J., Torres, R., Teixidó, N., Viñas, I., 2015. Application of modified atmosphere packaging as a safety approach to fresh-cut fruits and vegetables – A review. Trends in Food Science & Technology 46, 13–26. doi:10.1016/J.TIFS.2015.07.017

Pedro, A.M.K., Ferreira, M.M.C., 2009. The use of near-infrared spectroscopy and chemometrics for determining the shelf-life of products. Applied spectroscopy 63, 1308–1314. doi:10.1366/000370209789806830

Pedro, A.M.K., Ferreira, M.M.C., 2006a. Multivariate accelerated shelf-life testing: A novel approach for determining the shelf-life of foods. Journal of Chemometrics 20, 76–83. doi:10.1002/cem.995

Pedro, A.M.K., Ferreira, M.M.C., 2006b. Multivariate accelerated shelf-life testing: A novel approach for determining the shelf-life of foods. Journal of Chemometrics 20, 76–83. doi:10.1002/cem.995

Polder, G., Heijden, G. van der, 2010. Measuring Ripening of Tomatoes Using Imaging Spectrometry, in: Hyperspectral Imaging for Food Quality Analysis and Control. Elsevier, pp. 369–402.

doi:10.1016/B978-0-12-374753-2.10012-7

Rajkumar, P., Wang, N., EImasry, G., Raghavan, G.S.V., Gariepy, Y., 2012a. Studies on banana fruit quality and maturity stages using hyperspectral imaging. Journal of Food Engineering 108, 194–200. doi:10.1016/J.JFOODENG.2011.05.002

Rajkumar, P., Wang, N., EImasry, G., Raghavan, G.S.V., Gariepy, Y., 2012b. Studies on banana fruit quality and maturity stages using hyperspectral imaging. Journal of Food Engineering 108, 194–200. doi:10.1016/J.JFOODENG.2011.05.002

Rediers, H., Claes, M., Peeters, L., Willems, K.A., 2009. Evaluation of the cold chain of fresh-cut endive from farmer to plate. Postharvest Biology and Technology 51, 257–262. doi:10.1016/j.postharvbio.2008.07.017

Richards, M., De Kock, H.L., Buys, E.M., 2014. Multivariate accelerated shelf-life test of low fat UHT milk. International Dairy Journal 36, 38–45. doi:10.1016/j.idairyj.2013.12.012

Routray, W., Orsat, V., 2014. Variation of phenolic profile and antioxidant activity of North American highbush blueberry leaves with variation of time of harvest and cultivar. Industrial Crops and Products 62, 147–155. doi:10.1016/j.indcrop.2014.08.020

Saavedra, J., Cordova, A., Galvez, L., Quezada, C., Navarro, R., 2013. Principal component analysis as an exploration tool for kinetic modelling of food quality: a case study of dried apple cluster snacks. Journal of Food Engineering 119, 229–235.

Sánchez, M.T., De la Haba, M.J., Guerrero, J.E., Garrido-Varo, A., Pérez-Marín, D., 2011. Testing of a local approach for the prediction of quality parameters in intact nectarines using a portable NIRS instrument. Postharvest Biology and Technology 60, 130–135. doi:10.1016/j.postharvbio.2010.12.006

Seefeldt, H.F., Løkke, M.M., Edelenbos, M., 2012. Effect of variety and harvest time on respiration rate of broccoli florets and wild rocket salad using a novel O2 sensor. Postharvest Biology and Technology 69, 7–14. doi:10.1016/J.POSTHARVBIO.2012.01.010

ter Braak, C.J.F., de Jong, S., 1998. The objective function of partial least squares regression. Journal of Chemometrics 12, 41–54. doi:10.1002/(SICI)1099-128X(199801/02)12:1<41::AID-CEM500>3.0.CO;2-F

Toivonen, P.M.A., Brummell, D.A., 2008. Biochemical bases of appearance and texture changes in fresh-cut fruit and vegetables. Postharvest Biology and Technology 48, 1–14. doi:10.1016/J.POSTHARVBIO.2007.09.004

Torres-Contreras, A.M., Nair, V., Cisneros-Zevallos, L., Jacobo-Velázquez, D.A., 2014. Plants as biofactories: Stress-induced production of chlorogenic acid isomers in potato tubers as affected by wounding intensity and storage time. Industrial Crops and Products 62, 61–66. doi:10.1016/J.INDCROP.2014.08.018

Ukuku, D.O., Sapers, G.M., 2007. Effect of time before storage and storage temperature on survival of Salmonella inoculated on fresh-cut melons. Food Microbiology 24, 288–295. doi:10.1016/j.fm.2006.04.007

Upadhyay, R., Mishra, H.N., 2015. Multivariate Analysis for Kinetic Modeling of Oxidative Stability and Shelf Life Estimation of Sunflower Oil Blended with Sage (Salvia officinalis) Extract Under Rancimat Conditions. Food and Bioprocess Technology 8, 801–810. doi:10.1007/s11947-014-1446-z

Workman, J.; Shenk, J., 2004. Understanding and using the near-infrared spectrum as an analytical method, in: Near-Infrared Spectroscopy in Agriculture. pp. 3–10.

Chapter 5

SPECTRAL FINGERPRINTING AND HYPERSPECTRAL IMAGING FOR THE PREDICTIONAND MAPPING OF PHYTONUTRIENTS IN MINIMALLY PROCESSED ROCKET LEAVES (*Diplotaxis tenuifolia*) DURING STORAGE

Muahmmad M.A. Chaudhry[a], Maria L. Amodio[a], José M. Amigo Rubio[b], Maria L. V. de Chiara[a], Farahmand Babellahi[a], Giancarlo Colelli[a]
[a] Dip.to di Scienze Agrarie, degli Alimenti e dell'Ambiente, Universita di Foggia, Via Napoli, 25, 71122 Foggia (Italy)
[b] Dept. of Food Science (KU-FOOD), Chemometrics and Analytical Technologies CAT. Faculty of Sciences, University of Copenhagen, Rolighedsvej 30, DK 1958Frederiksberg C. (Denmark)
* Corresponding author: marialuisa.amodio@unifg.it

Abstract

The potential of hyperspectral imaging in the visible and near infrared regions was investigated for the prediction and mapping of Vitamin C, ascorbic acid (AA), dehydroascorbic acid (DHAA), antioxidant activity and phenols in wild rocket (*Diplotaxis tenuifolia)* over a storage span of 12 days at 5°C. Hyperspectral images of the wild rocket leaves were acquired in the Vis-NIR (400-1000nm) and the NIR (900-1700nm) ranges followed by Partial least squares regression (PLSR) using different data pretreatments and wavelength selection. The model reliability was checked by the root mean square error (RMSE) and R^2 values. Among the predicted parameters Vitamin C, AA, antioxidant activity and phenols were predicted satisfactorily in the NIR range. 1st derivative followed by mean centering served as the best spectral pretreatment in each case. The PLSR models for Vitamin C yielded an R^2 of 0.76 in external prediction (RMSEP of 10.905 over a range of 15.80 to 123.33 mg/100g) while for AA, with the same data pretreatment the R^2 value in external prediction was 0.73 with a RMSEP of 10.249 over a range of 7.97 to 109.38 mg/100g. The R^2 value for antioxidant activity was 0.76 in external prediction (RMSEP of 16.022 over a range of 54.26 to 192.15 mg Trolox/100g) while for phenols, external prediction yielded an R^2 of 0.78 with a RMSEP of 13.816 over a range of 83.53 to 200.92 mg of gallic acid/100g. The prediction maps for the parameters were calculated to follow the changes over the storage period. More reliable results were acquired in the NIR range as compared to the Vis-NIR range.

Keywords: NIR, PLSR, wavelength selection, prediction, hyperspectral image mapping

1. INTRODUCTION

Leafy vegetables have always served as a significant source of health promoting elements in human diet as they are an enormous reserve of active chemical compounds and are the cheapest and widely available source of fiber, proteins, vitamins, phenolic compounds, antioxidants and minerals (Gibson et al., 2012). Along with aiding the consumers in meeting their optimum nutrient requirements they also act in the prevention of various morbid conditions (Lampe, 1999; Mann, 2001; He et al., 2006; Webb and Villamor, 2008). Therefore, the consumption of minimally processed ready-to-eat fruit and vegetable has significantly boosted in the last decades (Artés, Gómez, Aguayo, Escalona, & Artés-Hernández, 2009), since they are perceived as healthy, convenient, highly nutritive and appetizing (Oliveira et al., 2015; Ma et al., 2017)..

In the Mediterranean countries, rocket leaves (*Diplotaxis tenuifolia*) with its pungent smell and strong flavour, lies among the most popular leafy vegetables mostly consumed as stand-alone salads or as a part of mixed salad products. The rocket leaves are a rich source of phytonutrients such as fiber, Vitamin C, flavonoids and glucosinolates which are widely known for their positive impacts on human health (Cavaiuolo and Ferrante, 2014; Nurzyńska-Wierdak, 2015). The nutritional value of the wild rocket leaves and its degradation with the passage of the shelf life depends on the pre-harvest practices, postharvest handing, processing and storage conditions (Toivonen and Brummell, 2008; Cefola and Pace, 2015). After minimal processing operations (most commonly in this case, washing and drying), the rocket leaves are available packaged in plastic bags in the retail stores. Particularly, yellowing caused by chlorophyll degradation, wilting, and the production of off-odors are the main sources of deterioration for this product (Nielsen et al., 2008; Koukounaras et al., 2009; Løkke et al., 2012; Chaudhry et al., 2018).

The degradation process in fruits and vegetables also results in the degradation of the phytonutrients and many studies have taken into account the changes in the vitamin C, ascorbic acid (AA), antioxidant capacity, phenols and anthocyanins (Amodio, Derossi, Mastrandrea, & Colelli, 2015; Derossi, Mastrandrea, Amodio, De Chiara, & Colelli, 2016a). The kinetics of AA degradation is effected by

temperature, pH, enzymes, oxygen, metallic catalysers and light (Santos & Silva, 2008; Pérez-Balibrea, Moreno, & García-Viguera, 2008). The effect of storage time and temperature on vitamin C degradation of rocket leaves has been reported by (Kim and Ishii, 2007; Spadafora et al., 2016; Mastrandrea et al., 2017). Kim & Ishii, 2007 observed that the vitamin C content was significantly affected during the storage of the rocket leaves at both 4ºC and 15ºC and also it was reported that the vitamin C content was higher in the leaves with roots and leaves only in case of 4ºC as compared to 15ºC regardless of the storage time. In the same study it was also observed that the rocket leaves stored without roots showed better results during storage at 4ºC in terms of freshness and weight loss. Moreover, Spadafora et al., 2016 also reported a rapid decrease in the vitamin C content of rocket leaves stored at higher temperatures. In this study it was concluded that the vitamin C depletion rate was higher for rocket leaves stored at 10ºC at all time-points but this difference was particularly significant at the ninth day of storage. At the end of the storage period the rocket leaves stored at 5ºC retained more vitamin C as compared to the leaves stored at 10ºC. Particularly, Mastrandrea, Amodio, de Chiara, Pati, & Colelli, 2017 reported that the leaves stored at 0ºC both in air and in modified atmosphere packaging (MAP) did not show any changes in the AA content but those stored at 5ºC air portrayed slight decrease in the AA content with the passage of storage time while a progressive and rapid decrease was observed in the AA content degradation at 15ºC both in case of samples stored in air and in MAP. Changes in AA content during storage of rocket leaves were also studied by (Cavaiuolo, Cocetta, Bulgari, Spinardi, & Ferrante, 2015a) which observed a slight increase in the AA content in the initial days of storage. In another study a comparison of the changes in the AA and vitamin C content was made for the rocket leaves stored at 4ºC in controlled atmosphere (CA) with those stored in air concluding that the AA content remained unaltered in the CA and also increased at the end of the storage while the ascorbic acid (AA) content degraded in the leaves stored in air (Martínez-Sánchez, Marín, Llorach, Ferreres, & Gil, 2006a). Moreover, a decrease in the total antioxidant capacity was observed during the storage period which was more significant for the samples stored in air. The phenolic content in the leaves also portrayed a decrease with the passage of storage time regardless of the storage atmosphere.

All the above studies rely on chemical methods for the quantification of the phytonutrients that are time consuming, require skilled personnel and they are expensive to conduct. As an alternative rapid, and

cheaper means of measuring nutritional quality may facilitate the access to this information also to processing companies and finally to the consumer. Hyperspectral imaging is a technique that integrates imaging and spectroscopy for the quantification and prediction of physical attributes and chemical compounds in food samples along with the mapping of their spatial distribution in the sample (Elmasry et al., 2012; Y.-Y. Pu et al., 2015; Huang et al., 2014). Every food product has, in fact, a specific spectral fingerprint, depending on the sample structure, the moisture content, the particle size, the temperature of the sample and most importantly of its chemical composition (Osorio, Haughey, Elliott, & Koidis, 2014). Most commonly, during the storage period, these spectral profiles are collected from the hyperspectral images which later integrated with multivariate tools can be used as a powerful tool for the estimation of the quality and shelf life of the food products during storage (Gowen et al., 2008; Løkke et al., 2013).

The potentiality of the hyperspectral imaging and spectral fingerprinting combined with multivariate analysis has been widely recognized for the prediction of various chemical constituents, contaminant, detection of defects, safety inspection, in fresh fruits and vegetables such as strawberries (Nagata et al., 2005; Tallada et al., 2006), apples (ElMasry, Wang, Vigneault, Qiao, & ElSayed, 2008), cucumbers (Liu, Chen, Wang, Chan, & Kim, 2004), lychee fruits (H. Pu, Liu, Wang, & Sun, 2015), wheat grains ;(Vigneau, Ecarnot, Rabatel, & Roumet, 2011), and spinach leaves (C. D. Everard, Kim, & Lee, 2014a). Many research works have concentrated on the non-destructive evaluation of leafy vegetables particularly spinaches (Diezma et al., 2013; Tewey et al., 2017; Lara et al., 2013; Zhang et al., 2017; Cho et al., 2017; Everard et al., 2014; Lunadei et al., 2012; Yang et al., 2017), lettuce (Derossi et al., 2016; Xue and Yang, 2009), and rocket leaves (Toledo-Martín et al., 2017; Løkke et al., 2013b; Giovenzana et al., 2015; Chaudhry et al., 2018). Among leafy vegetables most of the research works have implemented hyperspectral or multispectral techniques for the quality evaluation of spinach leaves including detection of Escherichia coli (Siripatrawan, Makino, Kawagoe, & Oshita, 2011) where Vis-NIR hyperspectral imaging was used to establish a correlation between the hyperspectral data and the number of *E. Coli* which varied from 5.1 to 7.4 Log (CFU/g) in the four sub-groups for different initial inoculated concentrations of *E. Coli* (K12). Diezma et al., 2013b and to discriminate between the fresh, degrading and degraded spinach leaves over the storage period. In another study (C. D. Everard, Kim, & Lee, 2014b) hyperspectral imaging in the visible-NIR and florescence regions was used for the fecal detection

on the spinach leaves up to 1:10 dilution level with 100% accuracy. Moreover, for rocket leaves Løkke et al., 2013b used CIELAB obtained from multispectral imaging for achieving a correlation with the sensory evaluation based on color and texture. It was observed that a more reliable color evaluation was achieved using the CIELAB multispectral image data whereas the selective wavelengths in the NIR region resulted in the reliable description of textural variations. Kokalj, Prikeržnik, & Kreft, 2016 used FTIR spectroscopy for detecting the rocket contamination with the common groundsel leaves and obtained 100% correct classification. Moreover, Chaudhry et al., 2018 used hyperspectral imaging in the Vis-NIR range for followed by the multivariate accelerated shelf life testing approach (MASLT) for the non-destructive shelf life estimation of stored rocket leaves. It was concluded by the study that wavelength range between 550–700 nm significantly contributed towards the shelf life estimation based on appearance scores. The changes in the appearance scores were also mapped over the storage time for all storage temperatures. NIRS was also employed by Villatoro-Pulido et al., 2012 for the prediction of mineral composition of the rocket leaves in the wavelength range of 400-2500nm using modified partial least squares regression (MPLS). For the model simplification wavelength selection was done and it was found out that the wavelengths in the regions between 500–700, 1100–1300, 1400 and 1900–2400 nm were significantly important for the prediction of minerals with R^2 values ranging between 0.39-0.78 for various minerals. Villatoro-Pulido et al., 2012 also used the Vis-NIR spectroscopy for the quantification of total phenolic content (TPC) and glucosinolates in the rocket leaves using MPLS regression with R^2 values ranging between 0.59 to 0.84 depicting reliable quantification results. Nevertheless, none of the studies have attempted to quantify and predict the phytonutrient changes over time in leafy vegetables particularly rocket leaves using spectral profiles and map these changes over time using hyperspectral imaging.

The objective of this study is to correlate the spectral information acquired over time with the changes in vitamin C content, antioxidant activity, AA, DHAA and phenols over the storage period and map the concentration profiles over time, by using hyperspectral images in the visible and NIR ranges using Partial Least Squares Regression (PLSR). To this aim a new approach was introduced in order to correct errors due to the pixel by pixel prediction based on prediction model obtained with mean spectra of leaf regions.

2. MATERIALS AND METHODS

2.1. Experimental design and spectral acquisition

Washed and dried rocket leaves (*Diplotaxis tenuifolia*) were received in the postharvest laboratory of University of Foggia, Italy. Representative samples were weighted; distributed into 100g batches, packed into plastic clamshells and stored at 5^{o}C under humidified air flow. Fifteen replicates comprising 20 leaves each were acquired on each acquisition interval over a span of 12 days of storage. Hyperspectral image acquisition and reference analysis of the samples was done on 0, 2, 5, 7, 9 and 12 days of storage. Prior to the analysis the leaves were kept at room temperature.

For the acquisition of the hyperspectral images, a hyperspectral line scan scanner (Version 1.4, DV srl, Padova, Italy) equipped with two spectrographs, one in the visible near infrared (Vis-NIR) region and the other in the near infrared region (NIR) were used. The spatial resolution of the Vis-NIR spectrograph was 2000x1000 pixels with a spectral resolution of 5nm over a wavelength range of 400-1000nm while the spatial resolution of NIR spectrograph was 623x320 pixels and a spectral resolution similar to Vis-NIR spectrograph over a wavelength of 900-1700nm.

Self-developed MATLAB codes were used for image thresholding and the extraction of the average spectra of twenty leaves from each replicate based on the best contrast between the object and the background followed by masking and the same procedure was followed for each acquisition interval. A total of 90 spectra both in the NIR and Vis-NIR ranges were collected to formulate the dataset.

2.2 Chemical analysis

2.2.1 Total phenolic content and antioxidant activity evaluation

Total phenolic content and antioxidant activity were determined according to Singleton and Rossi (1965) and Brand-Williams et al., (1995) with minor modifications. Three grams of leafy tissues representing the leaves of one replicate (one image) were homogenized in 2mM sodium fluoride methanol:water solution (80:20) for 1 minute and centrifuged at 5°C and 12,000 rpm for 5 minutes. The total phenol content was expressed as mg of gallic acid equivalent (GAE) 100^{-1} g fresh weight. The antioxidant activity was reported as mg Trolox equivalent antioxidant activity (TEAC) 100 g^{-1} FW. Readings were made at 725 nm, against a blank after 2 h standing for phenolic content and at 515 nm after 24 h standing for antioxidant activity using a UV-1700 Shimadzu spectrophotometer (Jiangsu, China).

2.2.2 Vitamin C analysis

Three grams of fresh rocket tissues representing the leaves of one replicate (one image) were homogenized with 10 mL of MeOH/H_2O (5:95) plus citric acid (21 g L^{-1}) with EDTA (0.5 g L^{-1}). The homogenate was filtered through cheesecloth and a C18 Bakerbond SPE column (Waters, Milford, MA, USA). AA and DHAA contents were determined as described by Zapata and Dufour, (1992), with some modifications. The HPLC analysis was achieved after derivatization of DHAA into the fluorophore 3-(1,2-dihydroxyethyl) furol [3,4-b] quinoxaline-1-one (DFQ), with 1,2-phenylenediamine dihydrochloride (OPDA). Samples of 20 µl were analyzed with an Agilent 1200 Series HPLC. The HPLC system consisted of a G1312A binary pump, a G1329A autosampler, a G1315B photodiode array detector from Agilent Technologies (Waldbronn, Germany). Separations of DFQ and AA were achieved on a Zorbax Eclipse XDB- C18 column (150 mm × 4.6 mm; 5 µm particle size; Agilent Technologies, Santa Clara, CA, USA). The mobile phase was MeOH/H_2O (5:95 v/v) containing 5mM cetrimide and 50mM potassium dihydrogen phosphate at pH 4.5. The flow rate was 1 mL min^{-1}. AA and DHAA contents were expressed as mg of ascorbic or dehydroascorbic acid per 100 g of fresh weight (mg 100 g^{-1}).

2.3. Partial Least Squares Regression (PLSR)

Prediction models for the desired parameters were developed using the PLS algorithm in the PLS toolbox (Eigenvector Research Inc., version 7.2.5) working under MATLAB 2012b (version 8.0.0.783, The mathworks, MA, USA) as well as in HYPER-Tools (Version 2.0). The spectral dataset was divided into calibration set and validation set based on the 70/30 ration with 70% of the samples in the calibration dataset and 30% of the samples reserved for external validation from the replicates of each acquisition interval. For the development of the PLSR calibration models internal cross validation was done using the random subset cross validation. The accuracy of the calibration models was accessed by visualizing the R^2 in calibration, R^2 cross validation and the root mean square error for calibration (RMSEC) and cross-validation (RMSECV). After the formulation of the best calibration model the external dataset was used for the prediction of the desired constituent.

After the development of prediction models, the mapping of the internal constituents was done by introducing a brand new approach based on the selection of pixels in the image according to the calibration range. PLSR models were developed within the calibration range based on the spectra

acquired from the average of the leaves in an image, standing to the consideration that the mean spectrum of that particular image corresponds to the averages of the vitamin C content of all the leaves in that image. Therefore, it is normal that when the PLSR calibration model developed with the mean spectra of all the leaves of all the replicates is applied to a new image for pixel by pixel prediction, some of the pixels may fall out (below or above) of the calibration range. Moreover, since the prediction can be certain only if the obtained values are within the calibration range, the pixels with concentrations that falls out of the calibration range should not be considered. Also keeping under consideration the confidence level, the root mean square error of calibration (RMSEC) in the model, the calibration range can be spanned from the minimum of the calibration range minus the RMSEC until the maximum of the calibration range plus the RMSEC. All the pixels with prediction values outside this range were excluded from the concentration map and were depicted separately both for above and below calibration range with the passage of storage time.

3. RESULTS AND DISCUSSION

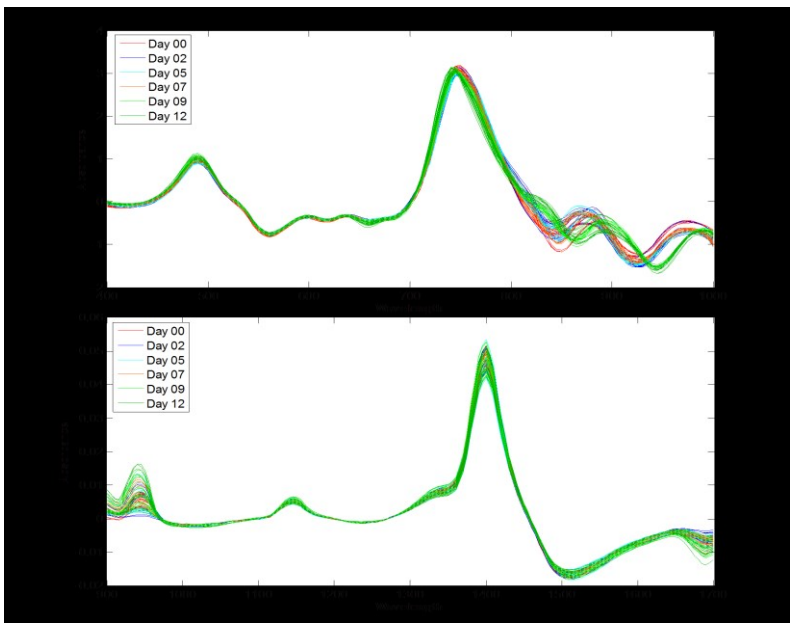

Figure 1. a) 1st Derivative of Vis-NIR spectra b) 1st Derivative of NIR spectra Day 0 (red), Day 2 (blue), Day 5 (cyan), Day 7 (pink), Day 9 (light green) and Day 12 (green)

In table 1 are shown the mean values and respective range of composition for the main chemical constituents analyzed in this study. The variation in the minimum and the maximum range of values for

the chemical parameters were determined over a storage span of 12 days at the intervals of 0, 2, 5, 7, 9 and 12 days. Mastrandrea, Amodio, de Chiara, Pati, & Colelli, 2017b also found similar values of vitamin C in fresh rocket leaves with a much higher amount of AA and a low amount of DHAA, hence showing that the rocket leaves in the start of the storage period possess a significantly higher amount of AA as compared to DHAA. Moreover, in a similar study regarding vitamin C content Martínez-Sánchez, Marín, Llorach, Ferreres, & Gil, 2006b also showed that the predominant form of vitamin C at the beginning of the storage time was AA in rocket leaves as compared to DHAA. The also confirmed that a significant decrease in the AA content was recorded after six days of storage ultimately decreasing the vitamin C content of the rocket leaves stored both in air and in controlled atmosphere.

Figure 1a and 1b, shows the pre-processed (1st derivative) Vis-NIR and NIR spectra, respectively. The VIS-NIR peaks correspond to the color related properties of rocket leaves and the leaf reflectance as affected by chlorophyll *a*, chlorophyll *b* and β-carotene, in the region of 400-700nm (Chaudhry et al., 2018a). On the other hand, in case of NIR spectra, the reflectance signal is dominated by the leaf water content. In figure 1b the peaks observed between 900-1000nm and 1400-1500nm are located in the third overtone region the beginning of the first overtone region, respectively, both predominantly affected by water absorption. (Workman, 2003; Sasic and Ozaki, 2011). In these regions most of the peaks identified by H. Yang & Irudayaraj, 2002 can be found for vitamin C in powdered mixtures and solutions (1000, 1210, 1360, 1457, 1579 and 1651 nm); the same author also reported one peak at 840 nm related to vitamin C. Therefore, in this regard, it can be inferred that only one peak for vitamin C can be observed in the Vis-NIR region while all the other peaks are located in the NIR region from 900-1700nm. Moreover, the region between 1300-1700nm held great significance also for the other compounds analyzed in this study, since the correlations between the spectra and the corresponding concentration in this wavelength region were higher than in the VIS-NIR region.

The PLSR models yielded, reliable results for the Vitamin C content, AA, phenols and antioxidant activity in NIR range while results obtained for DHAA were not satisfying. After the development of these models, the most significant variables were selected based on the loading weights for each parameter and simplified PLSR models were developed.

Table 1. Range values and statistical distribution of Chemical Parameters

Chemical Parameter	Min	Max	Mean	Standard Deviation
Vitamin C	15.80	123.33	66.39	22.94
Ascorbic Acid (AA)	7.97	109.38	55.83	20.53
Dehydroascorbic Acid (DHAA)	5.01	19.45	11.23	3.43
Antioxidant Activity	54.26	192.15	113.72	35.30
Phenols	83.53	200.92	136.06	29.79

Table 2 shows the calibration results for the parameters in the NIR range in terms of R^2, root mean square error of calibration and random block cross validation. Individual calibration models were developed for each parameter. Different preprocessing techniques were attempted including mean centering, derivatization, SNV, MSC and their combinations. The best models obtained resulted from the combination of 1st derivatives followed by data mean centering in the NIR range which was also reported by Pissard et al., 2013 while measuring similar parameters in apples.

Table 2. Calibration statistics for the PLSR modelling of the internal constituents in fresh cut rocket leaves (Dev= derivative, MC= mean centering

		NIR range (900-1700nm)					
Parameter	Pretreatment	No. of variables	LVs	R^2_{cal}	RMSEC	R^2_{cv}	RMSECV
Vitamin C	1st Dev+MC	161	8	0.80	10.129	0.71	12.184
	1st Dev+MC	75	6	0.80	10.263	0.73	11.903
	1st Dev+MC	**55**	**5**	**0.80**	**10.149**	**0.74**	**11.727**
AA	1st Dev+MC	161	6	0.82	8.301	0.77	9.615
	1st Dev+MC	68	6	0.82	8.312	0.77	9.636

	1st Dev+MC	**39**	**6**	**0.81**	**8.377**	**0.77**	**9.438**
DHAA	2nd Dev+MC	161	2	0.17	2.978	0.10	3.119
	1st Dev+MC	93	3	0.22	2.887	0.13	3.060
Phenols	1st Dev+MC	**161**	**5**	**0.80**	**12.909**	**0.75**	**14.488**
	1st Dev+MC	80	7	0.79	13.261	0.72	15.344
Antioxidant activity	1st Dev+MC	161	5	0.77	15.324	0.74	16.651
	1st Dev+MC	91	6	0.79	14.876	0.74	16.531
	1st Dev+MC	**77**	**8**	**0.82**	**13.544**	**0.75**	**16.375**

In case of vitamin C, the calibration dataset comprised of 70 samples and the external validation was done with 12 samples. Figure 2a shows the PLSR calibration results for the vitamin C over a storage period of 12 days. The calibration model developed with a total of 161 variables in the NIR range yielded R^2_{cal} of 0.80 and R^2_{cv} of 0.71 with the RMSEC and RMSECV of 10.129 and 12.184 mg/100g f.w, respectively which was very similar to the laboratory error (9.179 mg/100g f.w) hence confirming the reliability of the calibration model. Optimal wavelength selection not only simplified the calibration model but also resulted in enhancing the performance in cross validation with R^2_{cv} of 0.74 and RMSECV of 11.727 mg/100g f.w.

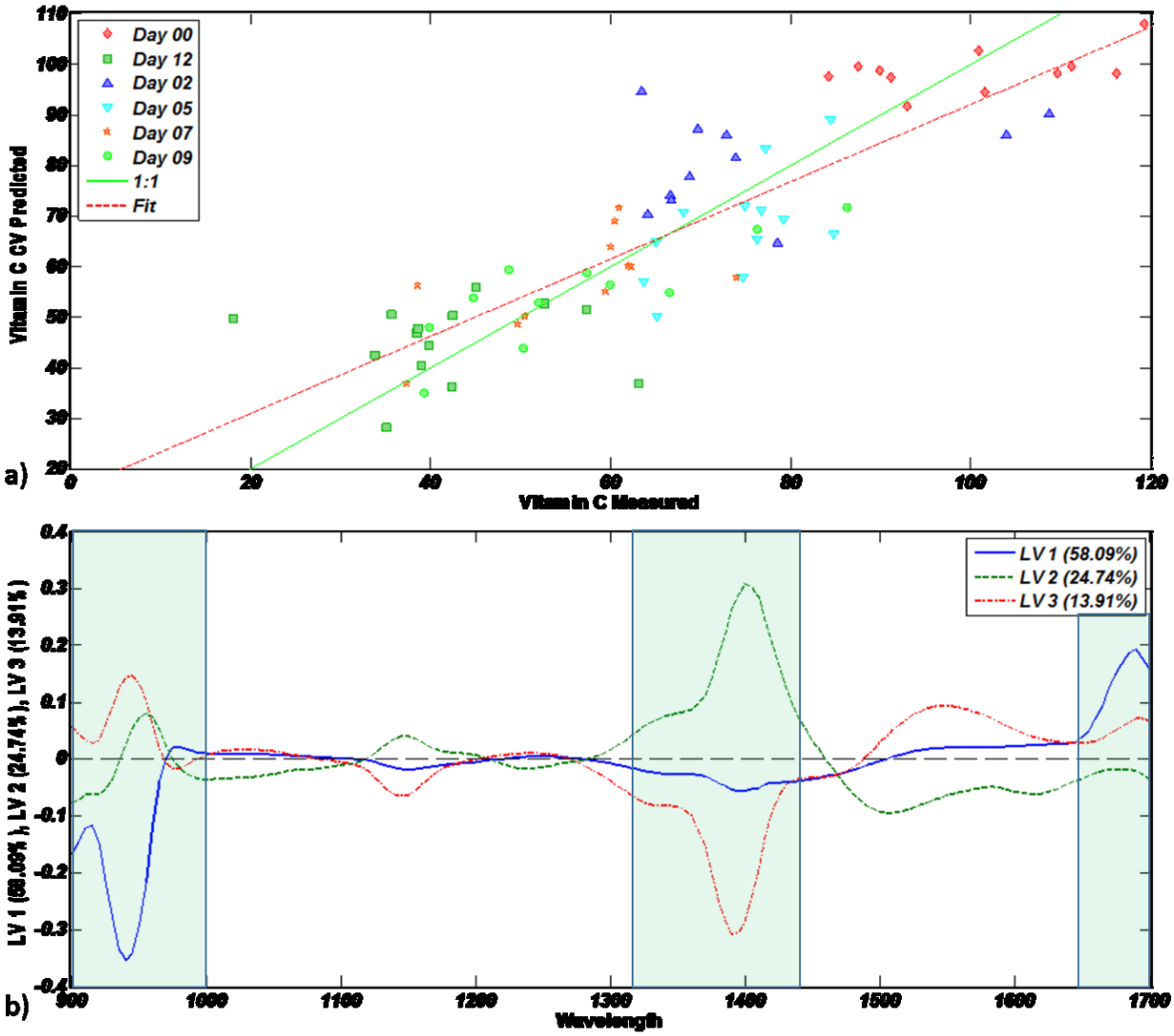

Figure 2. a) PLS regression plot for Vitamin C measured vs Vitamin C predicted in the NIR range b) Loadings plots for LV1, LV2 and LV3. Highlighted green regions represent the variables selected for final calibration model

It can be observed that the wavelength regions from 900-1000nm, 1300-1500nm and 1650-1700nm hold the most significant weight in the model for quantification of vitamin C and therefore, the variable reduction did not impact the model performance.

In this model for the prediction of vitamin C in the NIR region a total of 55 variables highlighted in green in the loadings plot were utilized ranging from 900-1000nm, 1315-1435nm and 1650-1700nm. External

validation allowed to obtain R^2_{pred} of 0.76 with a RMSEP of 10.905 mg/100g f.w. The best prediction results are summed in Table 3 for all the parameters.

Table 3. Prediction statistics for the PLSR modelling of fresh cut rocket leaves

Parameter	**Preprocessing**	**Wavelength Range (nm)**	**LVs**	R^2_{cal}	**RMSEC**	R^2_{cv}	**RMSECV**	R^2_{pred}	**RMSEP**
Vitamin C	1st Dev+MC	900-1000 1300-1500 1650-1700	5	0.80	10.149 mg/100g	0.74	11.727	0.76	10.905
AA	1st Dev+MC	900-1000 1295-1480 1655-1700	6	0.81	8.377 mg/100g	0.77	9.438	0.73	10.249
Phenols	1st Dev+MC	900-1700	5	0.80	12.909 Mg gallic acid/100g	0.75	14.488	0.78	13.816
Antioxidant activity	1st Dev+MC	900-970 1285-1540 1655-1700	8	0.82	13.544 Mg Trolox/100g	0.75	16.375	0.76	16.022

Applying this model pixel by pixel to the images, a prediction map of the vitamin C content during storage could be obtained as shown in figure 3. It is worth mentioning that the pixels located above and below calibration range are not included in the prediction map (figure 3) but are separately shown in figure 4d and 4e.

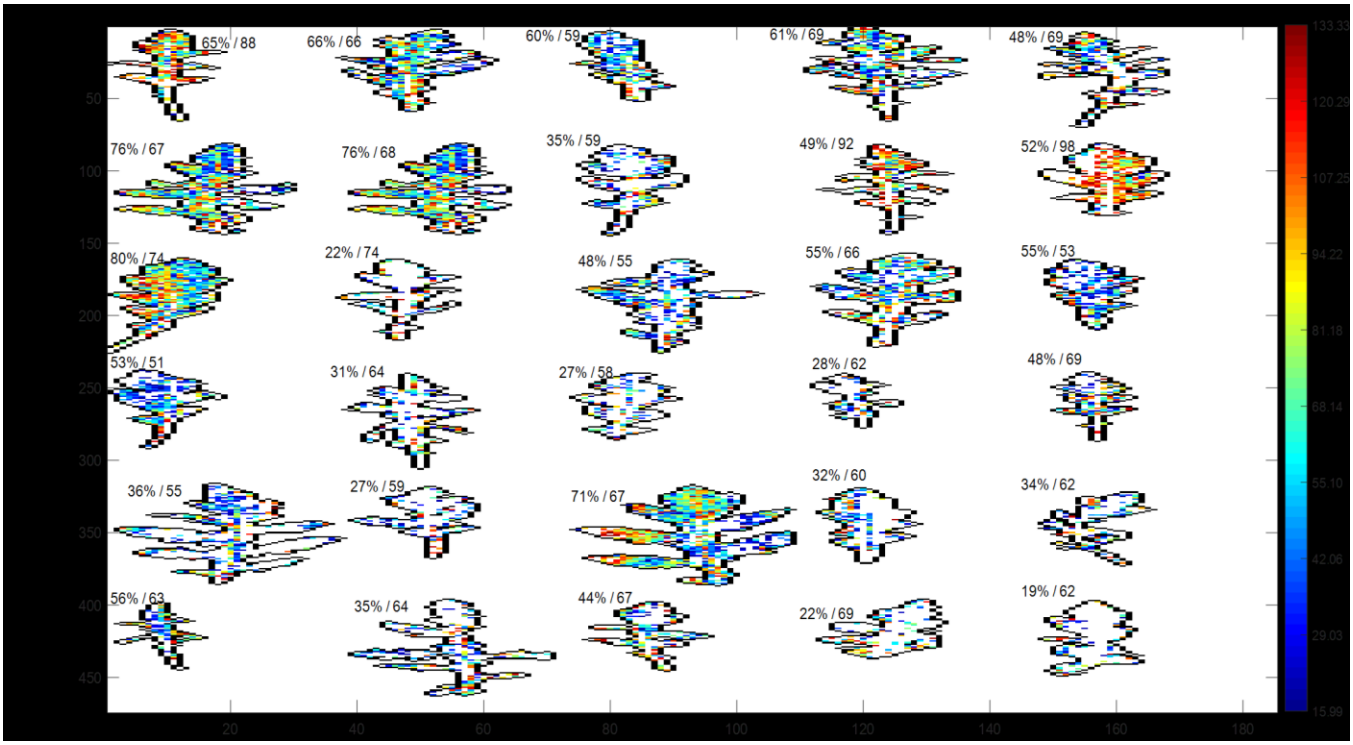

Figure 3. PLS prediction map for Vitamin C with each row corresponding to Day 0, Day 2, Day 5, Day 7, Day 9 and Day 12 / For each leaf, first number: percent pixels predicted within calibration range; second number: average concentration of vitamin C on predicted pixels

Figure 3 demonstrates, 5 random leaves chosen from the replicates of each storage time in order to visualize the changes in Vitamin C over the storage period, where each row represents leaves from each acquisition interval. As can be observed, prediction values ranged between 15.8-123.33 mg/100g f.w. for vitamin C, with many pixels higher than calibration range (133.35-670.40 mg/100g f.w.), and even with negative values for the pixels lying below the calibration range (-326.43-15.92 mg/100g f.w.). Moreover, each leaf in figure 3 is labelled by two numbers, first one being the percentage of the pixels predicted for each leaf within the calibration range and the second number represents the average concentration of Vitamin C on the pixels falling within the calibration range. It can be observed that both average vitamin C and AA contents slightly increased in the initial days, especially at the second acquisition interval and then decreased with time; similar results were reported by Cavaiuolo, Cocetta, Bulgari, Spinardi, & Ferrante, 2015b in which the AA content increased at initial days of storage and then decreased later during the entire storage span. These results are also compliant to those reported by Martínez-Sánchez, Allende, Bennett, Ferreres, & Gil, 2006 and Amodio et al., 2015 which revealed that

the rocket leaves when stored in the continuous air flow tend to decrease the AA and vitamin C content even at lower temperatures during storage time. Moreover, the calibration models for DHAA were also developed but the correlation between the spectra and the DHAA values was not encouraging which led to the conclusion that the calibration and prediction models for vitamin C possessed a slightly lower accuracy as compared to the PLSR models for AA because of the fact that vitamin C was determined using both AA and DHAA.

For phenolic content the PLSR model were developed yielding an R^2_{cal} of 0.80 with RMSEC of 12.909 mg of gallic acid 100g^{-1} and R^2_{cv} of 0.75 with RMSECV 14.488 mg of gallic acid 100g^{-1} (refer to S4a) with all 161 variables (refer to S4b). The reliability of the calibration model was accessed with external validation yielding R^2_{pred} of 0.78 and RMSEP of 13.816 mg of gallic acid 100g^{-1}. Figure 7 shows the changes in the phenolic content of the rocket leaves over the 12 day storage period within the calibration range (77.37 to 229.89 mg of gallic acid 100g^{-1}). Moreover, the in case of phenols also the percentage of pixels detected within the calibration range decreased with the passage of storage time and so did the average phenolic content.

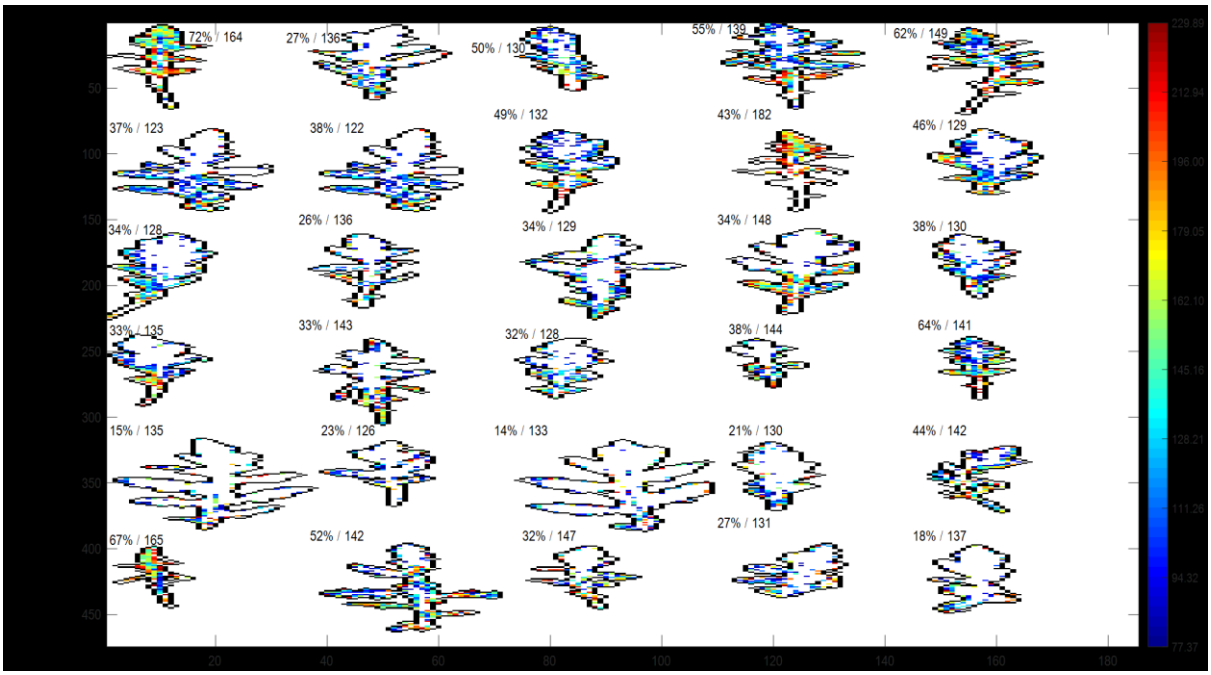

Figure 7. PLS prediction map for Phenols with each row corresponding to Day 0, Day 2, Day 5, Day 7, Day 9 and Day 12 / For each leaf, first number: percent pixels predicted within calibration

range; second number: average concentration of phenols on predicted pixels

The percentage of the pixels within the calibration range for the phenols is shown in S5a which decreases over the storage period followed by a decrease in the average phenol content depicted by S5b. Additionally, the maps for the pixels within (77.37 to 229.89 mg of gallic acid $100g^{-1}$), above (229.93 to 626.96 mg of gallic acid $100g^{-1}$) and below (-278.34 to 77.35 mg of gallic acid $100g^{-1}$) the calibration range for the phenolic content are represented by S5c, S5d and S5e, respectively. Furthermore, S6 depicts the number of pixels in each leaf representing the concentration of predicted phenols by each pixel in the map.

For antioxidant activity the final calibration model contained 77 variables ranging from 900-970nm, 1285-1540nm and 1655-1700nm yielding R^2_{cal} of 0.82 and R^2_{cv} of 0.75 with RMSEC and RMSECV being 13.544 and 15.675 mg Trolox $100g^{-1}$, respectively (refer to S7a) with first 3 LVs explaining 97.12% co-variance in the data. The chosen wavelength regions are highlighted in green regions (refer to S7b). The external validation resulted in an R^2_{pred} value of 0.76 with a RMSEP of 16.022 mg Trolox $100g^{-1}$. Figure 8 shows the prediction map for the changes in the antioxidant activity over time of storage. It can be observed that the average content of the antioxidant activity decreases with time (also refer to S8b) which can be more related to the leaf structure and chemical composition than the storage conditions since Martínez-Sánchez, Allende, et al., 2006 studied the storage of rocket leaves in controlled atmosphere as well as air flow and concluded that the antioxidant capacity decreased regardless of the storage conditions. Other studies have also revealed that the variation of the antioxidant activity in plants can be a result of the changes in the phenolic profiles (Lattanzio, Cicco, & Linsalata, 2005; Lattanzio et al., 2005), with the ellagic acid (Marie E. Olsson et al., 2004) with anthocyanins (Wang & Lin, 2000), and also with ascorbic acid changes (Cocci et al., 2006). Therefore, the percentage of detected pixels for antioxidant activity decreased with time followed by a decrease in the antioxidant activity. The pixels within (45.49 to 206.43 mg of gallic acid $100g^{-1}$ refer to S8c), above (206.46 to 816.33 mg of gallic acid $100g^{-1}$ refer to S8d) and below (-452.34 to 45.48 mg of gallic acid $100g^{-1}$ refer to S8e) the calibration range for the antioxidant activity showed the same trend as vitamin C and AA that is the percentage of pixels within the calibration range decreased over the storage period while those below the calibration range increased (refer to S8a and S8e).

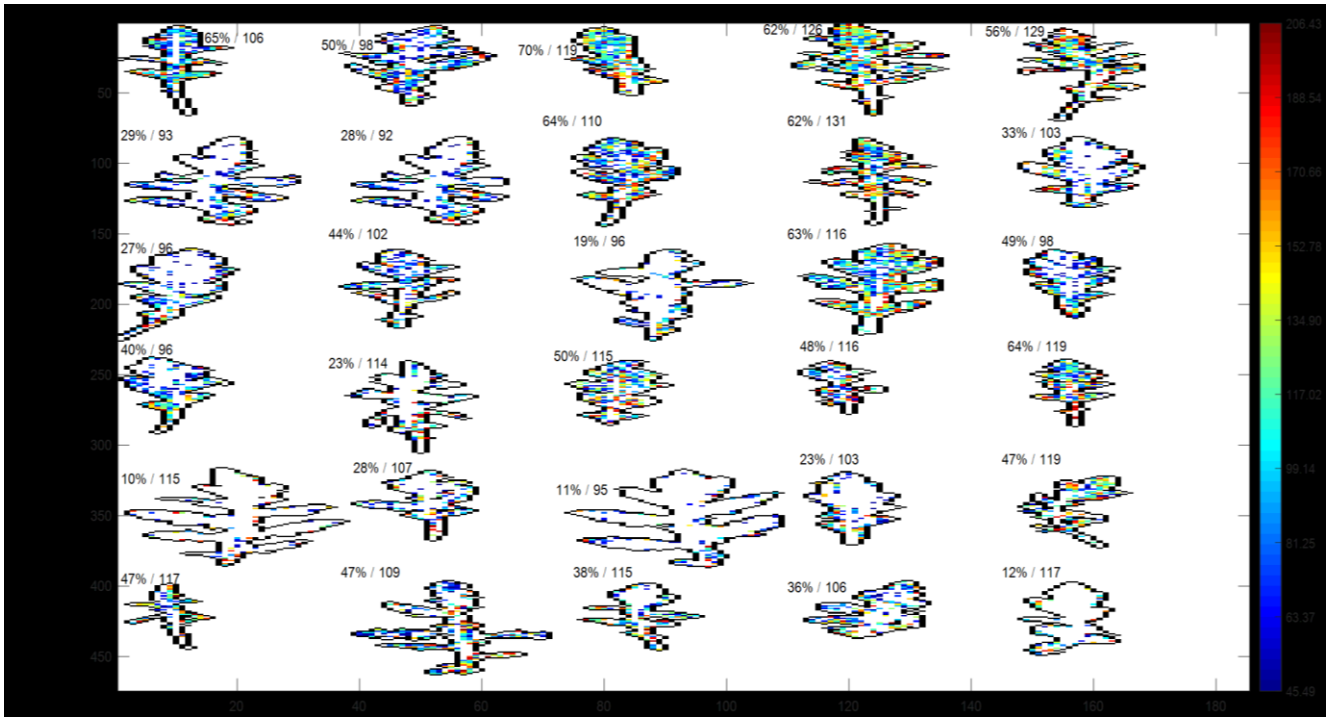

Figure 8. PLS prediction map for Antioxidant activity with each row corresponding to Day 0, Day 2, Day 5, Day 7, Day 9 and Day 12 / For each leaf, first number: percent pixels predicted within calibration range; second number: average concentration of antioxidant activity on predicted pixels

Moreover, S9 depicts the histograms representing the association of the number of pixels with the antioxidant activity concentration in each leaf over the storage period. Similar, trend was observed as the phenols in this case as well.

4. CONCLUSIONS

The potential application of spectral fingerprints and hyperspectral images in the NIR region, together with multivariate data analysis, has proven the potential to predict and map phytonutrients in fresh cut rocket leaves, provided that predicted values are included in the calibration range. A new method was, in fact, developed in order to overcome the prediction error due to the unavoidable process of using average spectra for the calibration model and individual pixels for the image prediction. It was shown that the number of pixels detected within the calibration range decreased with the passage of storage time with a simultaneous increase in the pixels below the calibration range hence reducing the capability of

the PLSR model to predict the corresponding phytonutrient. In this way, hyperspectral images revealed that the central part of the leaves lose vitamin C content faster as compared to the leaf edges or in other words the vitamin C starts degrading from the center of the leaf. Furthermore, the PLSR models in this case were very sensitive to the number of samples and their performance can be further enhanced with increasing the number of the samples in the calibration sets. Conclusively, NIR combined with hyperspectral imaging can be a very informative tool for studying the changes in the phytonutrient content during storage.

REFERENCES

Amodio, M. L., Derossi, A., Mastrandrea, L., & Colelli, G. (2015). A study of the estimated shelf life of fresh rocket using a non-linear model. *Journal of Food Engineering*, *150*, 19–28. https://doi.org/10.1016/J.JFOODENG.2014.10.030

Artés, F., Gómez, P., Aguayo, E., Escalona, V., & Artés-Hernández, F. (2009). Sustainable sanitation techniques for keeping quality and safety of fresh-cut plant commodities. *Postharvest Biology and Technology*, *51*(3), 287–296. https://doi.org/10.1016/J.POSTHARVBIO.2008.10.003

Brand-Williams, W., Cuvelier, M., & Berset, C. (1995). Use of a free radical method to evaluate antioxidant activity. *LWT - Food Science and Technology*, *28*(1), 25–30. https://doi.org/10.1016/S0023-6438(95)80008-5

Cavaiuolo, M., Cocetta, G., Bulgari, R., Spinardi, A., & Ferrante, A. (2015a). Identification of innovative potential quality markers in rocket and melon fresh-cut produce. *Food Chemistry*, *188*, 225–233. https://doi.org/10.1016/J.FOODCHEM.2015.04.143

Cavaiuolo, M., Cocetta, G., Bulgari, R., Spinardi, A., & Ferrante, A. (2015b). Identification of innovative potential quality markers in rocket and melon fresh-cut produce. *Food Chemistry*, *188*, 225–233. https://doi.org/10.1016/j.foodchem.2015.04.143

Cavaiuolo, M., & Ferrante, A. (2014). Nitrates and glucosinolates as strong determinants of the nutritional quality in rocket leafy salads. *Nutrients*. https://doi.org/10.3390/nu6041519

Cefola, M., & Pace, B. (2015). Application of Oxalic Acid to Preserve the Overall Quality of Rocket and Baby Spinach Leaves during Storage. *Journal of Food Processing and Preservation*, *39*(6), 2523–2532. https://doi.org/10.1111/jfpp.12502

Chaudhry, M. M. A., Amodio, M. L., Babellahi, F., de Chiara, M. L. V., Amigo Rubio, J. M., & Colelli, G. (2018a). Hyperspectral imaging and multivariate accelerated shelf life testing (MASLT) approach for determining shelf life of rocket leaves. *Journal of Food Engineering*, *238*, 122–133. https://doi.org/10.1016/j.jfoodeng.2018.06.017

Chaudhry, M. M. A., Amodio, M. L., Babellahi, F., de Chiara, M. L. V., Amigo Rubio, J. M., & Colelli, G. (2018b). Hyperspectral imaging and multivariate accelerated shelf life testing (MASLT) approach for determining shelf life of rocket leaves. *Journal of Food Engineering*, *238*, 122–133. https://doi.org/10.1016/j.jfoodeng.2018.06.017

Cho, H., Baek, I., Oh, M., Kim, S., Lee, H., & Kim, M. S. (2017). Characterization of E coli biofim formations on baby spinach leaf surfaces using hyperspectral fluorescence imaging. In *spiedigitallibrary.org* (p. 102170X). https://doi.org/10.1117/12.2264826

Cocci, E., Rocculi, P., Romani, S., and, M. D. R.-P. B., & 2006, undefined. (n.d.). Changes in nutritional properties of minimally processed apples during storage. *Elsevier*. Retrieved from https://www.sciencedirect.com/science/article/pii/S0925521405002632

Derossi, A., Mastrandrea, L., Amodio, M. L., De Chiara, M. L. V., & Colelli, G. (2016a). Application of multivariate accelerated test for the shelf life estimation of fresh-cut lettuce. *Journal of Food Engineering*, *169*, 122–130. https://doi.org/10.1016/j.jfoodeng.2015.08.010

Derossi, A., Mastrandrea, L., Amodio, M. L., De Chiara, M. L. V., & Colelli, G. (2016b). Application of multivariate accelerated test for the shelf life estimation of fresh-cut lettuce. *Journal of Food Engineering*, *169*, 122–130. https://doi.org/10.1016/j.jfoodeng.2015.08.010

Diezma, B., Lleó, L., Roger, J. M., Herrero-Langreo, A., Lunadei, L., & Ruiz-Altisent, M. (2013a). Examination of the quality of spinach leaves using hyperspectral imaging. *Postharvest Biology and Technology*, *85*, 8–17. https://doi.org/10.1016/j.postharvbio.2013.04.017

Diezma, B., Lleó, L., Roger, J. M., Herrero-Langreo, A., Lunadei, L., & Ruiz-Altisent, M. (2013b). Examination of the quality of spinach leaves using hyperspectral imaging. *Postharvest Biology and Technology*, *85*, 8–17. https://doi.org/10.1016/J.POSTHARVBIO.2013.04.017

Elmasry, G., Kamruzzaman, M., Sun, D.-W., & Allen, P. (2012). Principles and Applications of Hyperspectral Imaging in Quality Evaluation of Agro-Food Products: A Review. *Critical Reviews in Food Science and Nutrition*, *52*(11), 999–1023. https://doi.org/10.1080/10408398.2010.543495

ElMasry, G., Wang, N., Vigneault, C., Qiao, J., & ElSayed, A. (2008). Early detection of apple bruises on different background colors using hyperspectral imaging. *LWT - Food Science and Technology*, *41*(2), 337–345. https://doi.org/10.1016/j.lwt.2007.02.022

Everard, C. D., Kim, M. S., & Lee, H. (2014a). A comparison of hyperspectral reflectance and fluorescence imaging techniques for detection of contaminants on spinach leaves. *Journal of Food Engineering*, *143*, 139–145. https://doi.org/10.1016/j.jfoodeng.2014.06.042

Everard, C. D., Kim, M. S., & Lee, H. (2014b). A comparison of hyperspectral reflectance and fluorescence imaging techniques for detection of contaminants on spinach leaves. *Journal of Food Engineering*, *143*, 139–145. https://doi.org/10.1016/J.JFOODENG.2014.06.042

Everard, C., Kim, M., & Lee, H. (2014). A comparison of hyperspectral reflectance and fluorescence imaging techniques for detection of contaminants on spinach leaves. *Journal of Food Engineering*, *143*. https://doi.org/10.1016/j.jfoodeng.2014.06.042

Gibson, A., Edgar, J. D., Neville, C. E., Gilchrist, S. E., McKinley, M. C., Patterson, C. C., … Woodside, J. V. (2012). Effect of fruit and vegetable consumption on immune function in older people: a randomized controlled trial. *American Journal of Clinical Nutrition*, *96*(6), 1429–1436. https://doi.org/10.3945/ajcn.112.039057

Giovenzana, V., Beghi, R., Civelli, R., & Guidetti, R. (2015). Trends in Food Science & Technology Optical techniques for rapid quality monitoring along minimally processed fruit and vegetable chain. *Trends in Food Science & Technology*, *46*(2), 331–338. https://doi.org/10.1016/j.tifs.2015.10.006

Gowen, A. A., O'Donnell, C. P., Taghizadeh, M., Gaston, E., O'Gorman, A., Cullen, P. J., … Downey, G. (2008). Hyperspectral imaging for the investigation of quality deterioration in sliced mushrooms (Agaricus bisporus) during storage. *Sensing and Instrumentation for Food Quality and Safety*, *2*(3), 133–143. https://doi.org/10.1007/s11694-008-9042-4

He, F., Nowson, C., & MacGregor, G. (2006). Fruit and vegetable consumption and stroke: meta-analysis of cohort studies. *The Lancet*. Retrieved from

https://www.sciencedirect.com/science/article/pii/S0140673606680690

Huang, H., Liu, L., & Ngadi, M. (2014). Recent Developments in Hyperspectral Imaging for Assessment of Food Quality and Safety. *Sensors*, *14*(4), 7248–7276. https://doi.org/10.3390/s140407248

Kim, S. J., & Ishii, G. (2007). Effect of storage temperature and duration on glucosinolate, total vitamin C and nitrate contents in rocket salad (Eruca sativa Mill.). *Journal of the Science of Food and Agriculture*, *87*(6), 966–973. https://doi.org/10.1002/jsfa.2787

Kokalj, M., Prikeržnik, M., & Kreft, S. (2016). FTIR spectroscopy as a tool to detect contamination of rocket (Eruca sativa and diplotaxis tenuifolia) salad with common groundsel (senecio vulgaris) leaves. *Journal of the Science of Food and Agriculture*, *97*(7), 2238–2244. https://doi.org/10.1002/jsfa.8034

Koukounaras, A., Siomos, A. S., & Sfakiotakis, E. (2009). Impact of heat treatment on ethylene production and yellowing of modified atmosphere packaged rocket leaves. *Postharvest Biology and Technology*, *54*(3), 172–176. https://doi.org/10.1016/J.POSTHARVBIO.2009.07.002

Lampe, J. W. (1999). Health effects of vegetables and fruit: assessing mechanisms of action in human experimental studies. *The American Journal of Clinical Nutrition*, *70*(3), 475s–490s. https://doi.org/10.1093/ajcn/70.3.475s

Lara, M. A., Lleó, L., Diezma-Iglesias, B., Roger, J. M., & Ruiz-Altisent, M. (2013). Monitoring spinach shelf-life with hyperspectral image through packaging films. *Journal of Food Engineering*, *119*(2), 353–361. https://doi.org/10.1016/j.jfoodeng.2013.06.005

Lattanzio, V., Cicco, N., & Linsalata, V. (2005). ANTIOXIDANT ACTIVITIES OF ARTICHOKE PHENOLICS. *Acta Horticulturae*, (681), 421–428. https://doi.org/10.17660/ActaHortic.2005.681.59

Liu, Y., Chen, Y.-R., Wang, C. Y., Chan, D. E., & Kim, M. S. (2004). Development of hyperspectral imaging technique for the detection of chilling injury in cucumbers. In *elibrary.asabe.org* (p. 18). https://doi.org/10.1117/12.597550

Løkke, M. M., Seefeldt, H. F., & Edelenbos, M. (2012). Freshness and sensory quality of packaged wild rocket. *Postharvest Biology and Technology*, *73*, 99–106. https://doi.org/10.1016/j.postharvbio.2012.06.004

Løkke, M. M., Seefeldt, H. F., Skov, T., & Edelenbos, M. (2013a). Color and textural quality of packaged wild rocket measured by multispectral imaging. *Postharvest Biology and Technology*, *75*, 86–95. https://doi.org/10.1016/j.postharvbio.2012.06.018

Løkke, M. M., Seefeldt, H. F., Skov, T., & Edelenbos, M. (2013b). Color and textural quality of packaged wild rocket measured by multispectral imaging. *Postharvest Biology and Technology*, *75*, 86–95. https://doi.org/10.1016/J.POSTHARVBIO.2012.06.018

Lunadei, L., Diezma, B., Lleó, L., Ruiz-Garcia, L., Cantalapiedra, S., & Ruiz-Altisent, M. (2012). Monitoring of fresh-cut spinach leaves through a multispectral vision system. *Postharvest Biology and Technology*, *63*(1), 74–84. https://doi.org/10.1016/J.POSTHARVBIO.2011.08.004

Ma, L., Zhang, M., Bhandari, B., & Gao, Z. (2017). Recent developments in novel shelf life extension technologies of fresh-cut fruits and vegetables. *Trends in Food Science & Technology*, *64*, 23–38. https://doi.org/10.1016/J.TIFS.2017.03.005

Mann, J. I. (2001). Diet and risk of coronary heart disease and type 2 diabetes. *Lancet*, *360*, 783–789. Retrieved from https://www.sciencedirect.com/science/article/pii/S0140673602099014

Marie E. Olsson, *,†, Jimmy Ekvall, ‡, Karl-Erik Gustavsson, †, Jessica Nilsson, §, Deepa Pillai, §, Ingegerd Sjöholm, #, … Nyman‡, M. G. L. (2004). Antioxidants, Low Molecular Weight Carbohydrates, and Total Antioxidant Capacity in Strawberries (Fragaria × ananassa): Effects of Cultivar, Ripening, and Storage. https://doi.org/10.1021/JF030461E

Martínez-Sánchez, A., Allende, A., Bennett, R. N., Ferreres, F., & Gil, M. I. (2006). Microbial, nutritional and sensory quality of rocket leaves as affected by different sanitizers. *Postharvest Biology and Technology*, *42*(1), 86–97. https://doi.org/10.1016/J.POSTHARVBIO.2006.05.010

Martínez-Sánchez, A., Marín, A., Llorach, R., Ferreres, F., & Gil, M. I. (2006a). Controlled atmosphere

preserves quality and phytonutrients in wild rocket (Diplotaxis tenuifolia). *Postharvest Biology and Technology*, *40*(1), 26–33. https://doi.org/10.1016/J.POSTHARVBIO.2005.12.015

Martínez-Sánchez, A., Marín, A., Llorach, R., Ferreres, F., & Gil, M. I. (2006b). Controlled atmosphere preserves quality and phytonutrients in wild rocket (Diplotaxis tenuifolia). *Postharvest Biology and Technology*, *40*(1), 26–33. https://doi.org/10.1016/J.POSTHARVBIO.2005.12.015

Martínez-Sánchez, A., Marín, A., Llorach, R., Ferreres, F., & Gil, M. I. (2006c). Controlled atmosphere preserves quality and phytonutrients in wild rocket (Diplotaxis tenuifolia). *Postharvest Biology and Technology*, *40*(1), 26–33. https://doi.org/10.1016/J.POSTHARVBIO.2005.12.015

Mastrandrea, L., Amodio, M. L., de Chiara, M. L. V., Pati, S., & Colelli, G. (2017a). Effect of temperature abuse and improper atmosphere packaging on volatile profile and quality of rocket leaves. *Food Packaging and Shelf Life*, *14*, 59–65. https://doi.org/10.1016/J.FPSL.2017.08.004

Mastrandrea, L., Amodio, M. L., de Chiara, M. L. V., Pati, S., & Colelli, G. (2017b). Effect of temperature abuse and improper atmosphere packaging on volatile profile and quality of rocket leaves. *Food Packaging and Shelf Life*, *14*, 59–65. https://doi.org/10.1016/J.FPSL.2017.08.004

Nagata, M., Tallada, J. G., Kobayashi, T., & Toyoda, H. (2005). NIR hyperspectral imaging for measurement of internal quality in strawberries. In *2005 ASAE Annual Meeting* (p. 1).

Nielsen, T., Bergström, B., & Borch, E. (2008). The origin of off-odours in packaged rucola (Eruca sativa). *Food Chemistry*, *110*(1), 96–105. https://doi.org/10.1016/J.FOODCHEM.2008.01.063

Nurzyńska-Wierdak, R. (2015). Protein nutritional value of rocket leaves and possibilities of its modification during plant growth. *Turkish Journal of Agriculture and Forestry*, *39*(6), 1023–1028. https://doi.org/10.3906/tar-1412-6

Oliveira, M., Abadias, M., Usall, J., Torres, R., Teixidó, N., & Viñas, I. (2015). Application of modified atmosphere packaging as a safety approach to fresh-cut fruits and vegetables – A review. *Trends in Food Science & Technology*, *46*(1), 13–26. https://doi.org/10.1016/J.TIFS.2015.07.017

Osorio, M. T., Haughey, S. A., Elliott, C. T., & Koidis, A. (2014). Evaluation of methodologies to

determine vegetable oil species present in oil mixtures: Proposition of an approach to meet the EU legislation demands for correct vegetable oils labelling. *Food Research International*, *60*, 66–75. https://doi.org/10.1016/j.foodres.2013.12.013

Pérez-Balibrea, S., Moreno, D. A., & García-Viguera, C. (2008). Influence of light on health-promoting phytochemicals of broccoli sprouts. *Journal of the Science of Food and Agriculture*, *88*(5), 904–910. https://doi.org/10.1002/jsfa.3169

Pissard, A., Fernández Pierna, J. A., Baeten, V., Sinnaeve, G., Lognay, G., Mouteau, A., … Lateur, M. (2013). Non-destructive measurement of vitamin C, total polyphenol and sugar content in apples using near-infrared spectroscopy. *Journal of the Science of Food and Agriculture*, *93*(2), 238–244. https://doi.org/10.1002/jsfa.5779

Pu, H., Liu, D., Wang, L., & Sun, D. W. (2015). Soluble Solids Content and pH Prediction and Maturity Discrimination of Lychee Fruits Using Visible and Near Infrared Hyperspectral Imaging. *Food Analytical Methods*, 235–244. https://doi.org/10.1007/s12161-015-0186-7

Pu, Y.-Y., Feng, Y.-Z., & Sun, D.-W. (2015). Recent Progress of Hyperspectral Imaging on Quality and Safety Inspection of Fruits and Vegetables: A Review. *Comprehensive Reviews in Food Science and Food Safety*, *14*(2), 176–188. https://doi.org/10.1111/1541-4337.12123

Santos, P. H. S., & Silva, M. A. (2008, November 21). Retention of vitamin C in drying processes of fruits and vegetables - A review. *Drying Technology*. https://doi.org/10.1080/07373930802458911

Sasic, S., & Ozaki, Y. (2011). *Raman, infrared, and near-infrared chemical imaging*. Retrieved from https://books.google.it/books?hl=en&lr=&id=DQqB97nREOEC&oi=fnd&pg=PP10&dq=Weyer,+L.+and+Lo,+S.-C.+(2002)+Spectra-Structure+Correlations+in+the+Near-infrared,+In+Handbook+of+Vibrational+Spectroscopy,+Vol.+3,+Wiley,+U.K.,+pp.+1817-1837.+&ots=VketjW2sRX&sig=

Singleton, V. L., Rossi, J. A., & Jr, J. (1965). COLORIMETRY OF TOTAL PHENOLICS WITH PHOSPHOMOYBDIC-PHOSPHOTUNGSTIC ACID REAGENTS. *Am J Enol Viticult.*, (16), 144–158. Retrieved from http://www.ajevonline.org/content/16/3/144.short

Siripatrawan, U., Makino, Y., Kawagoe, Y., & Oshita, S. (2011). Rapid detection of Escherichia coli contamination in packaged fresh spinach using hyperspectral imaging. *Talanta*, *85*(1), 276–281. https://doi.org/10.1016/J.TALANTA.2011.03.061

Spadafora, N. D., Amaro, A. L., Pereira, M. J., Müller, C. T., Pintado, M., & Rogers, H. J. (2016). Multi-trait analysis of post-harvest storage in rocket salad (Diplotaxis tenuifolia) links sensorial, volatile and nutritional data. *Food Chemistry*, *211*, 114–123. https://doi.org/10.1016/j.foodchem.2016.04.107

Tallada, J. G., Nagata, M., & Kobayashi, T. (2006). Non-destructive estimation of firmness of strawberries (Fragaria x ananassa Duch.) using NIR hyperspectral imaging. *Environmental and Control Biology*, *44*(4), 245–255.

Tewey, K., Lefcourt, A., Tasch, U., Shilts, P., & Kim, M. (2017). Hyperspectral, time-resolved, fluorescence imaging system for large sample sizes: Part II. Detection of fecal contamination on spinach. Retrieved from https://elibrary.asabe.org/abstract.asp?aid=48593

Toivonen, P. M. A., & Brummell, D. A. (2008). Biochemical bases of appearance and texture changes in fresh-cut fruit and vegetables. *Postharvest Biology and Technology*, *48*(1), 1–14. https://doi.org/10.1016/J.POSTHARVBIO.2007.09.004

Toledo-Martín, E. M., Font, R., Obregón-Cano, S., De Haro-Bailón, A., Villatoro-Pulido, M., & Del Río-Celestino, M. (2017). Rapid and cost-effective quantification of glucosinolates and total phenolic content in rocket leaves by visible/near-infrared spectroscopy. *Molecules*, *22*(5). https://doi.org/10.3390/molecules22050851

Vigneau, N., Ecarnot, M., Rabatel, G., & Roumet, P. (2011). Potential of field hyperspectral imaging as a non destructive method to assess leaf nitrogen content in Wheat. *Field Crops Research*, *122*(1), 25–31. https://doi.org/10.1016/j.fcr.2011.02.003

Villatoro-Pulido, M., Moreno Rojas, R., Muñoz-Serrano, A., Cardeñosa, V., Amaro López, M. Á., Font, R., & Del Río-Celestino, M. (2012). Characterization and prediction by near-infrared reflectance of mineral composition of rocket (Eruca vesicaria subsp. sativa and Eruca vesicaria subsp. vesicaria).

Journal of the Science of Food and Agriculture, *92*(7), 1331–1340. https://doi.org/10.1002/jsfa.4694

Wang, S. Y., & Lin, H.-S. (2000). Antioxidant Activity in Fruits and Leaves of Blackberry, Raspberry, and Strawberry Varies with Cultivar and Developmental Stage. *Journal of Agricultural and Food Chemistry*, *48*(2), 140–146. https://doi.org/10.1021/jf9908345

Webb, A. L., & Villamor, E. (2008). Update: Effects of Antioxidant and Non-Antioxidant Vitamin Supplementation on Immune Function. *Nutrition Reviews*, *65*(5), 181–217. https://doi.org/10.1111/j.1753-4887.2007.tb00298.x

Workman, J. (2003). NIR spectral characteristics. *NIR Newa*, *14*(1;2), 10–21. https://doi.org/10.1255/nirn.710

Xue, L., & Yang, L. (2009). Deriving leaf chlorophyll content of green-leafy vegetables from hyperspectral reflectance. *ISPRS Journal of Photogrammetry and Remote Sensing*, *64*(1), 97–106. https://doi.org/10.1016/j.isprsjprs.2008.06.002

Yang, H.-Y., Inagaki, T., Ma, T., & Tsuchikawa, S. (2017). High-Resolution and Non-destructive Evaluation of the Spatial Distribution of Nitrate and Its Dynamics in Spinach (Spinacia oleracea L.) Leaves by Near-Infrared Hyperspectral Imaging. *Frontiers in Plant Science*, *8*. https://doi.org/10.3389/fpls.2017.01937

Yang, H., & Irudayaraj, J. (2002). Rapid determination of vitamin C by NIR, MIR and FT-Raman techniques. *Journal of Pharmacy and Pharmacology*, *54*(9), 1247–1255. https://doi.org/10.1211/002235702320402099

ZAPATA, S., & DUFOUR, J. -P. (1992). Ascorbic, Dehydroascorbic and Isoascorbic Acid Simultaneous Determinations by Reverse Phase Ion Interaction HPLC. *Journal of Food Science*, *57*(2), 506–511. https://doi.org/10.1111/j.1365-2621.1992.tb05527.x

Zhang, C., Wang, Q., Liu, F., He, Y., & Xiao, Y. (2017). Rapid and non-destructive measurement of spinach pigments content during storage using hyperspectral imaging with chemometrics.

Measurement: Journal of the International Measurement Confederation, *97*, 149–155. https://doi.org/10.1016/j.measurement.2016.10.058

SUPPLIMENTARY MATERIAL

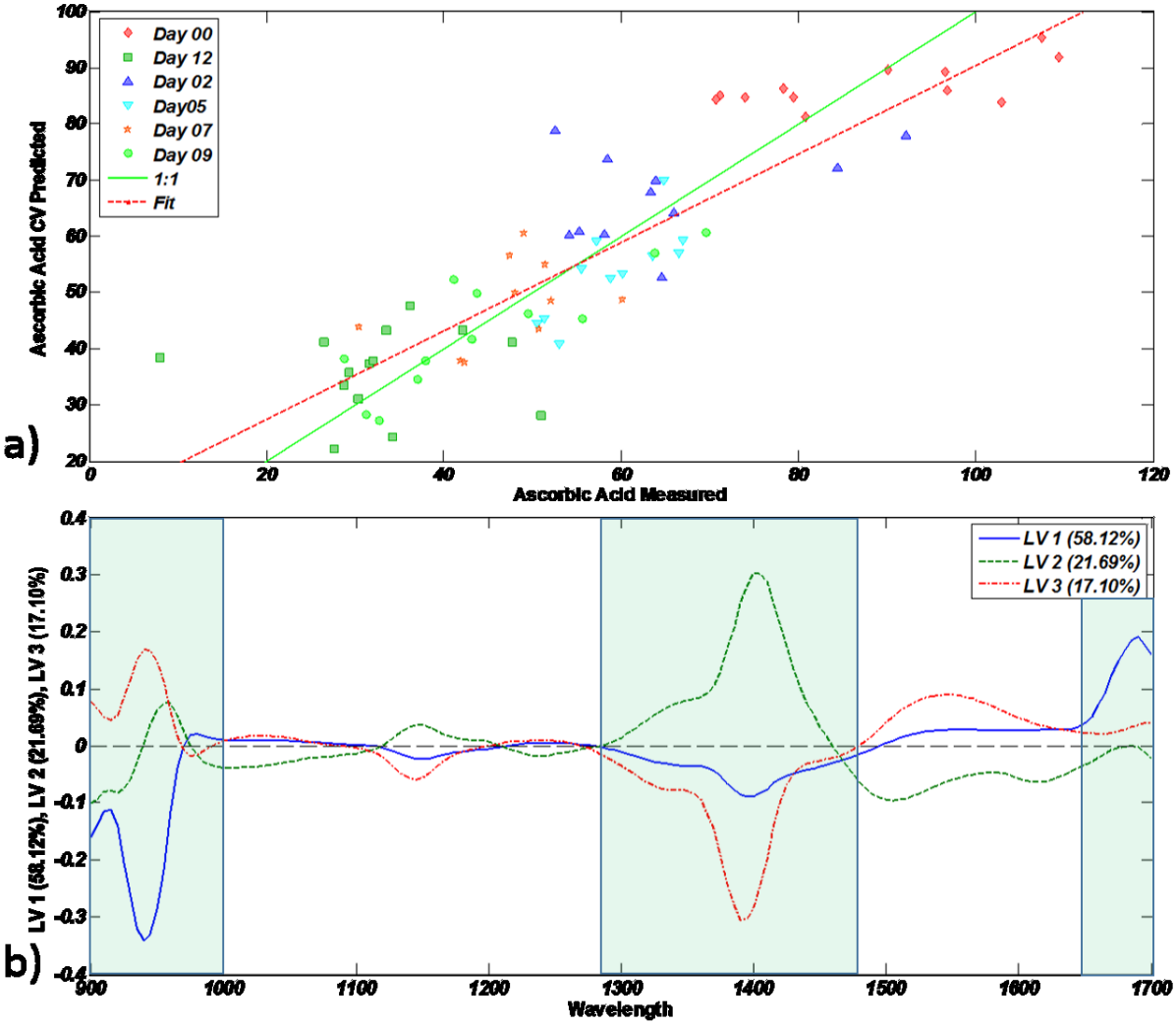

S1 (a) PLS regression plot for ascorbic acid measured vs ascorbic acid predicted (b) Loadings plots for LV1 (58.12%), LV2 (21.69%) and LV3 (17.10%). Highlighted green regions represent the variables selected for final calibration model

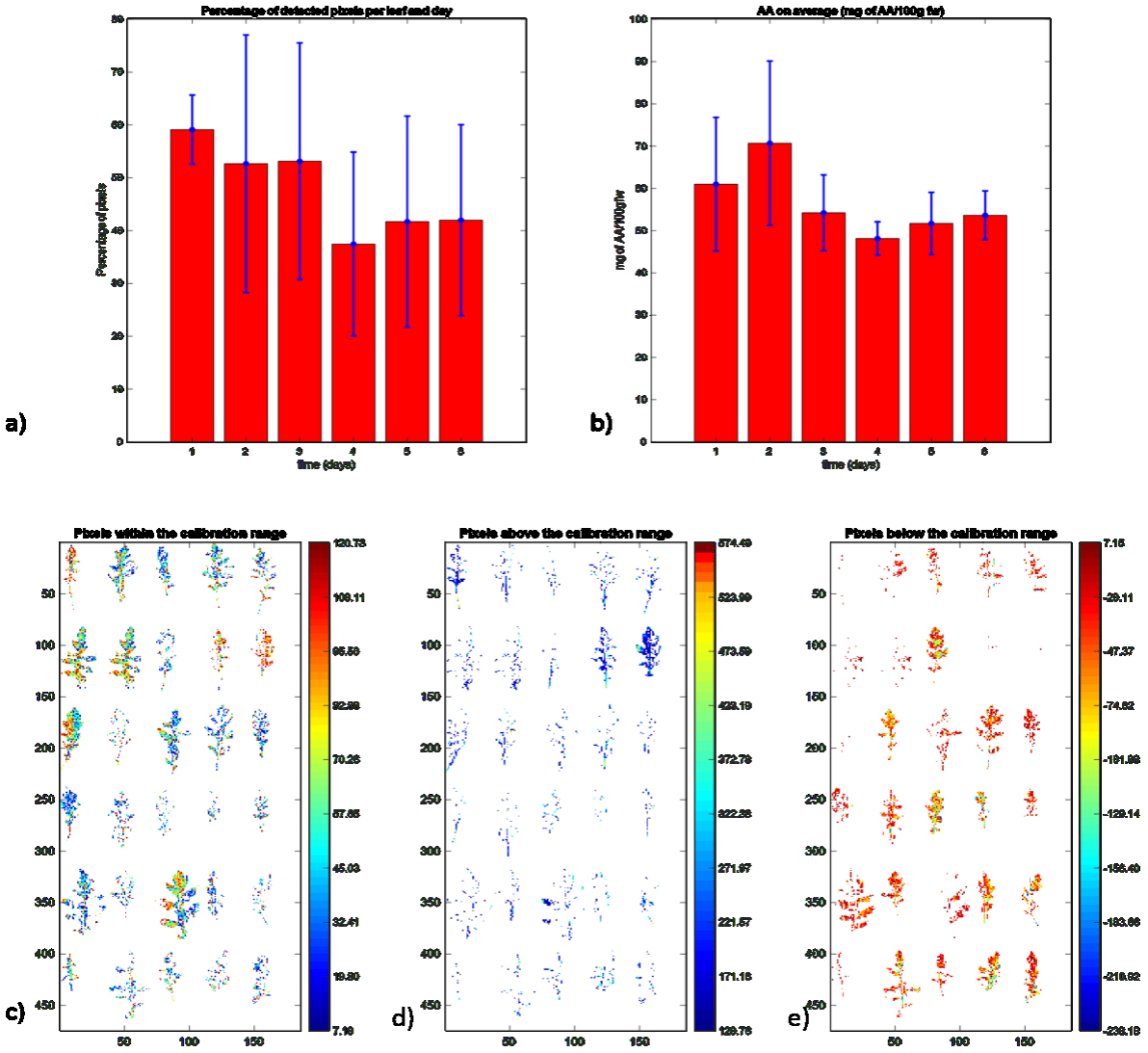

S2. a) Percentage of detected pixels and standard deviation pre leaf w.r.t days of storage for AA b) AA on average c) pixels within calibration range d) pixels above calibration range e) pixels below calibration range (time in days refers to the 6 acquisition intervals i.e. Days 0, 2, 5, 7, 9, 12)

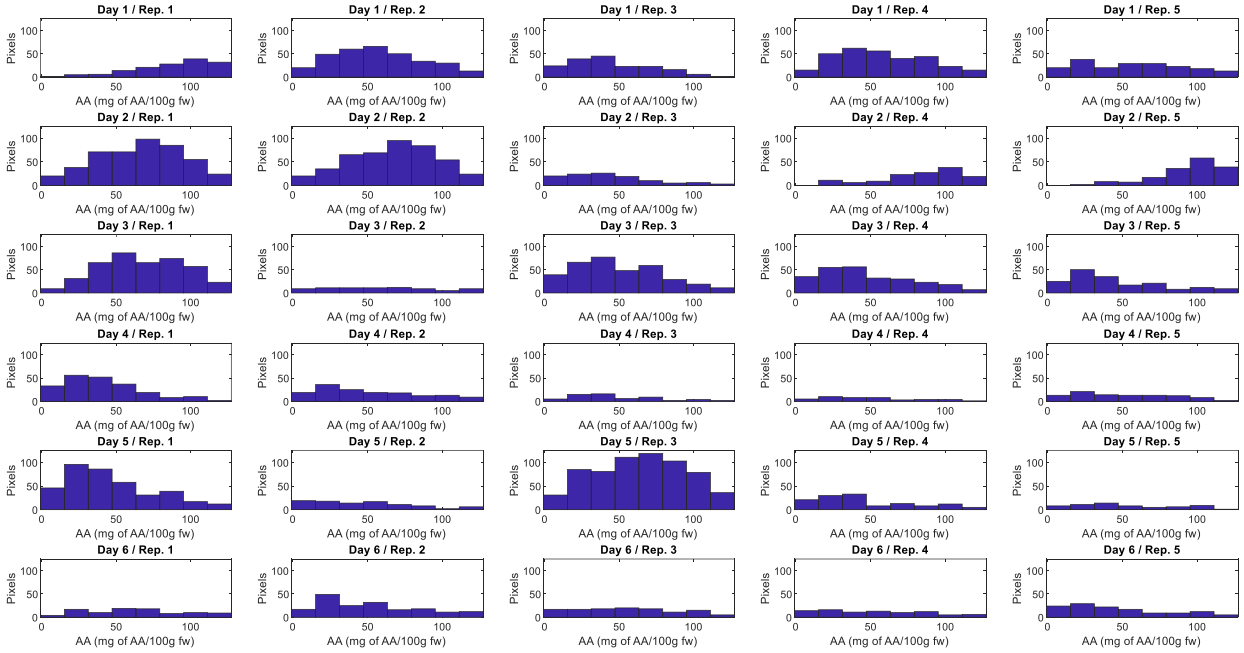

S3. Histograms of AA content of the leaves representing number of pixels with respect to AA concentration (Day1, 2, 3, 4, 5, 6 refers to the 6 acquisition intervals i.e. Days 0, 2, 5, 7, 9, 12)

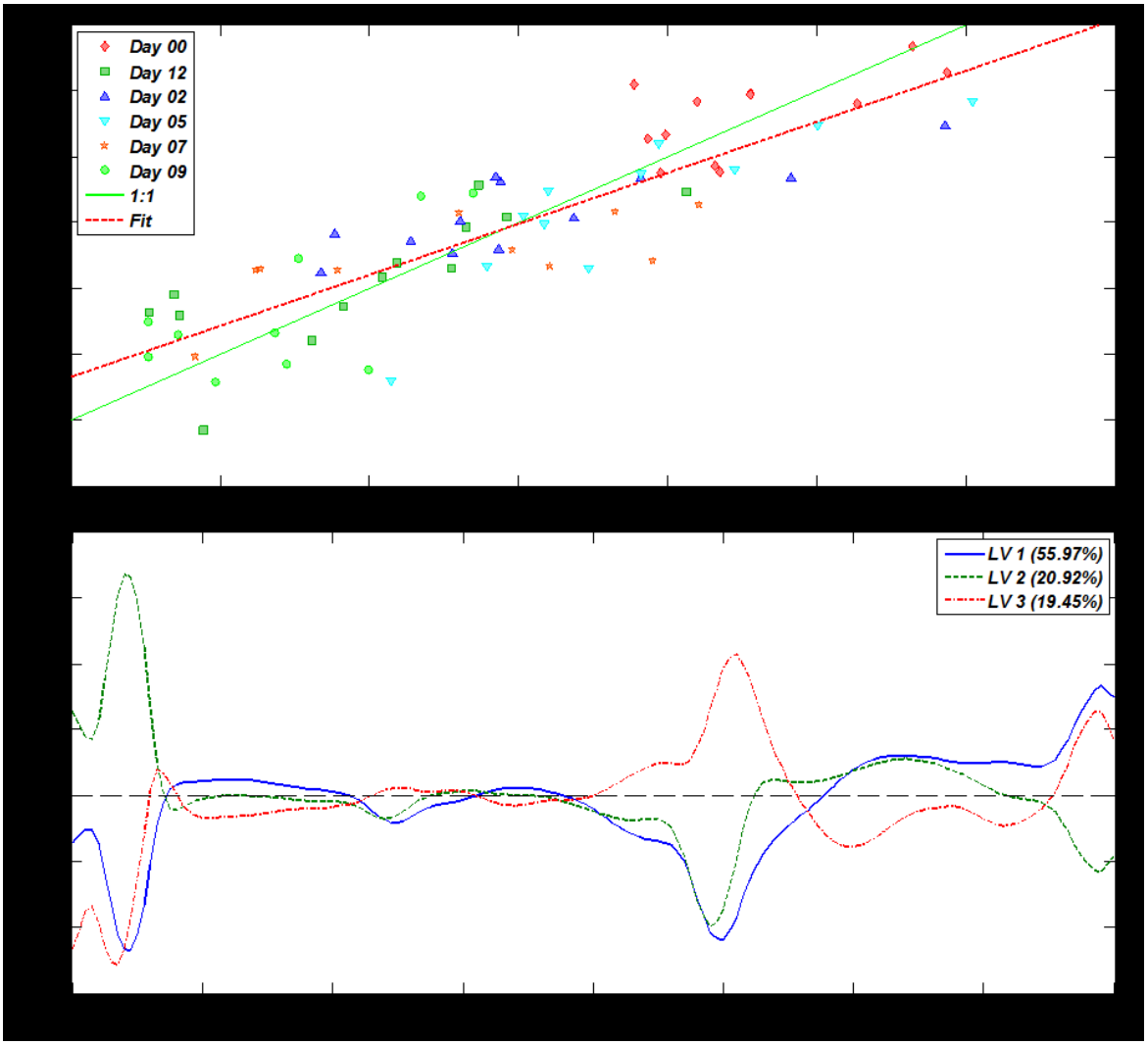

S4. a) PLS regression plot for Phenols measured vs Phenols predicted b) Loadings plots for LV1, LV2 and LV3

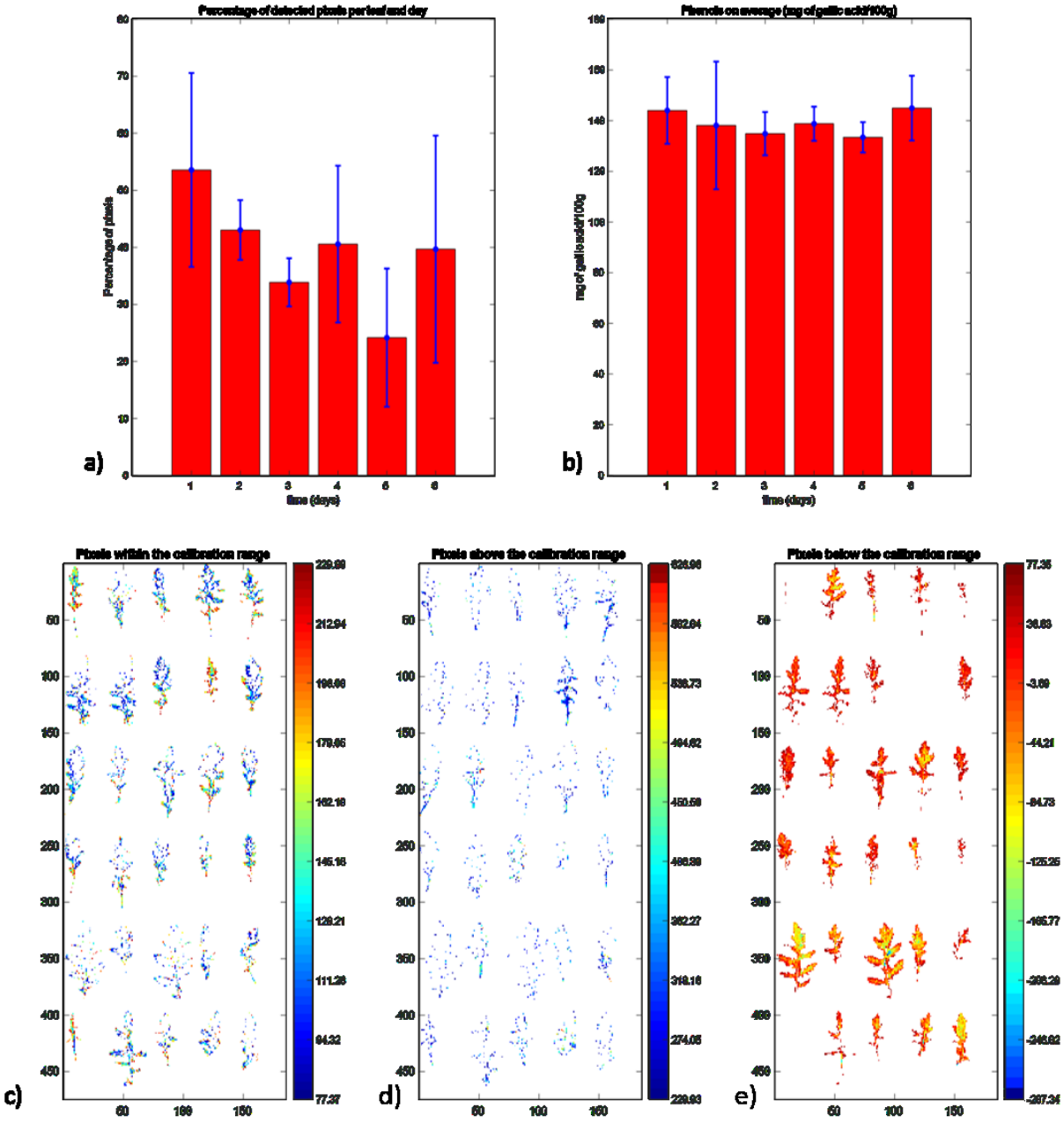

S5. a) Percentage of detected pixels and standard deviation pre leaf w.r.t days of storage b) Phenols on average c) pixels within calibration range d) pixels above calibration range e) pixels below calibration range (time in days refers to the 6 acquisition intervals i.e. Days 0, 2, 5, 7, 9, 12)

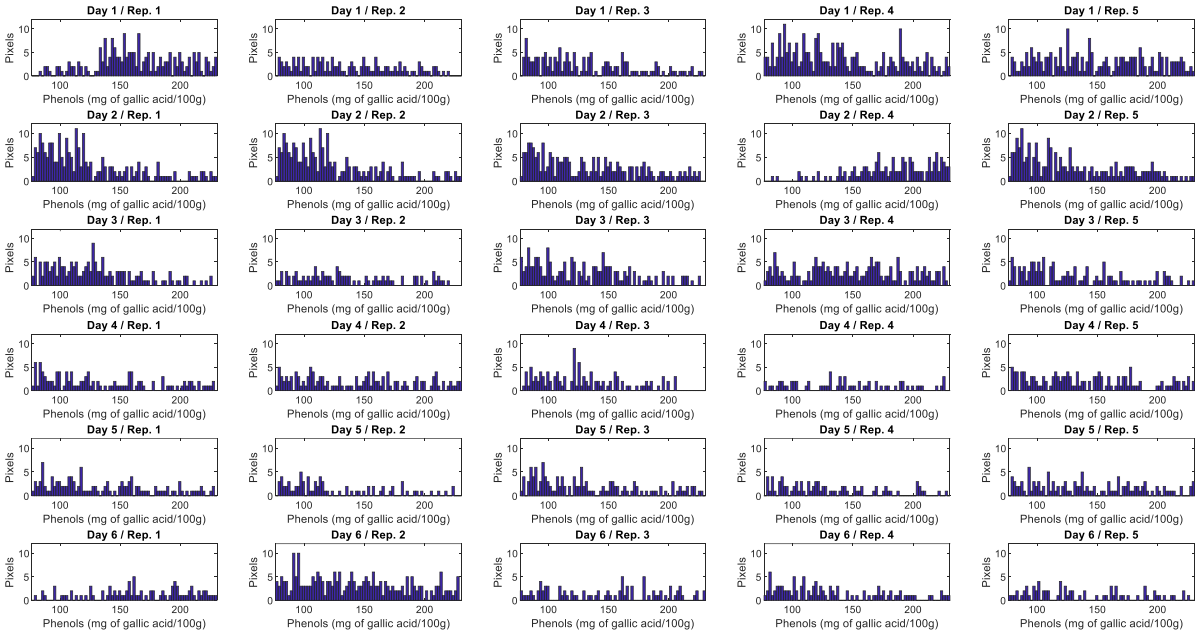

S6. Histograms of Phenols detected in leaves with respect to the pixels detected (Day1, 2, 3, 4, 5, 6 refers to the 6 acquisition intervals i.e. Days 0, 2, 5, 7, 9, 12)

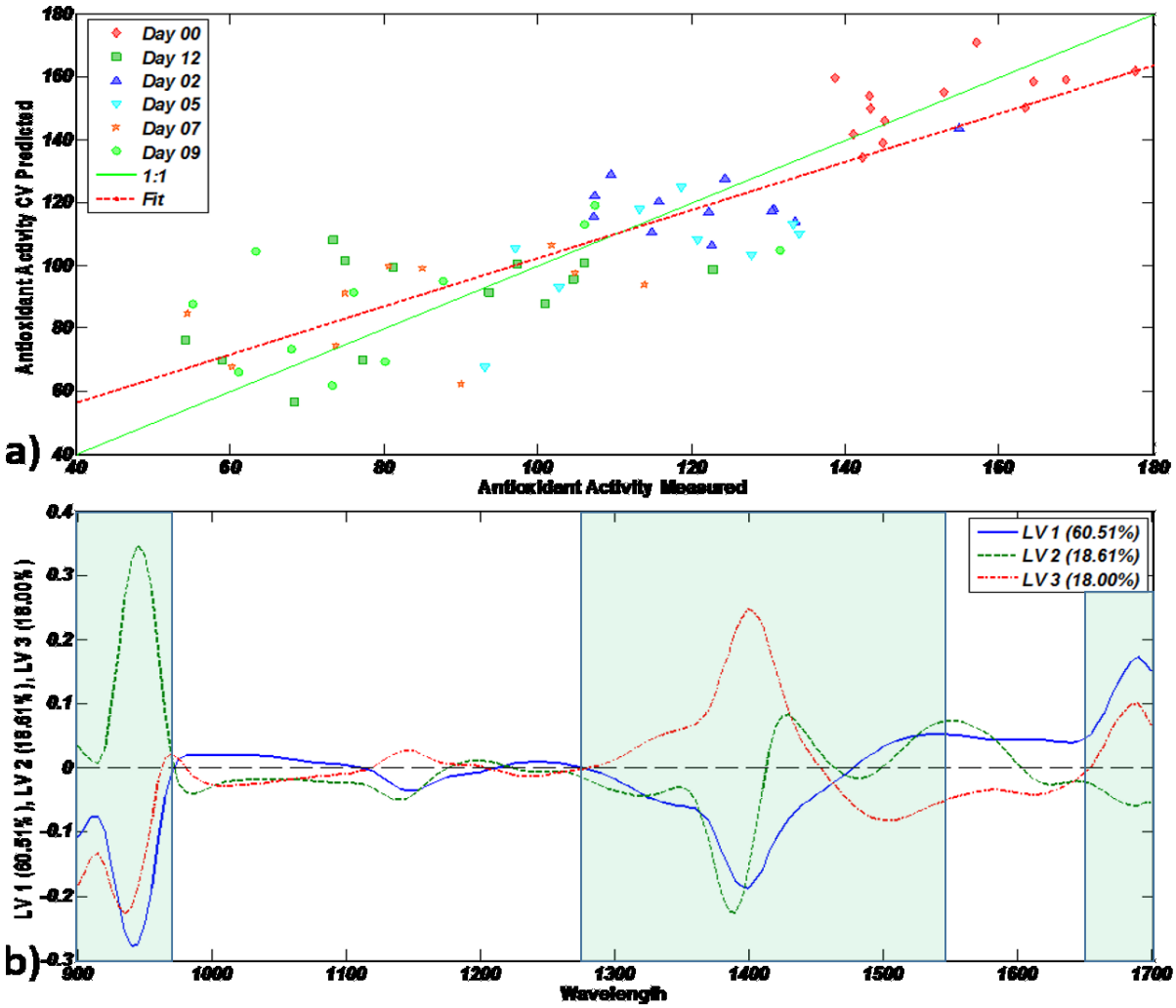

S7. (a) PLS regression plot for antioxidant activity measured vs antioxidant activity predicted (b) Loadings plots for LV1, LV2 and LV3. Highlighted green regions represent the variables selected for final calibration model

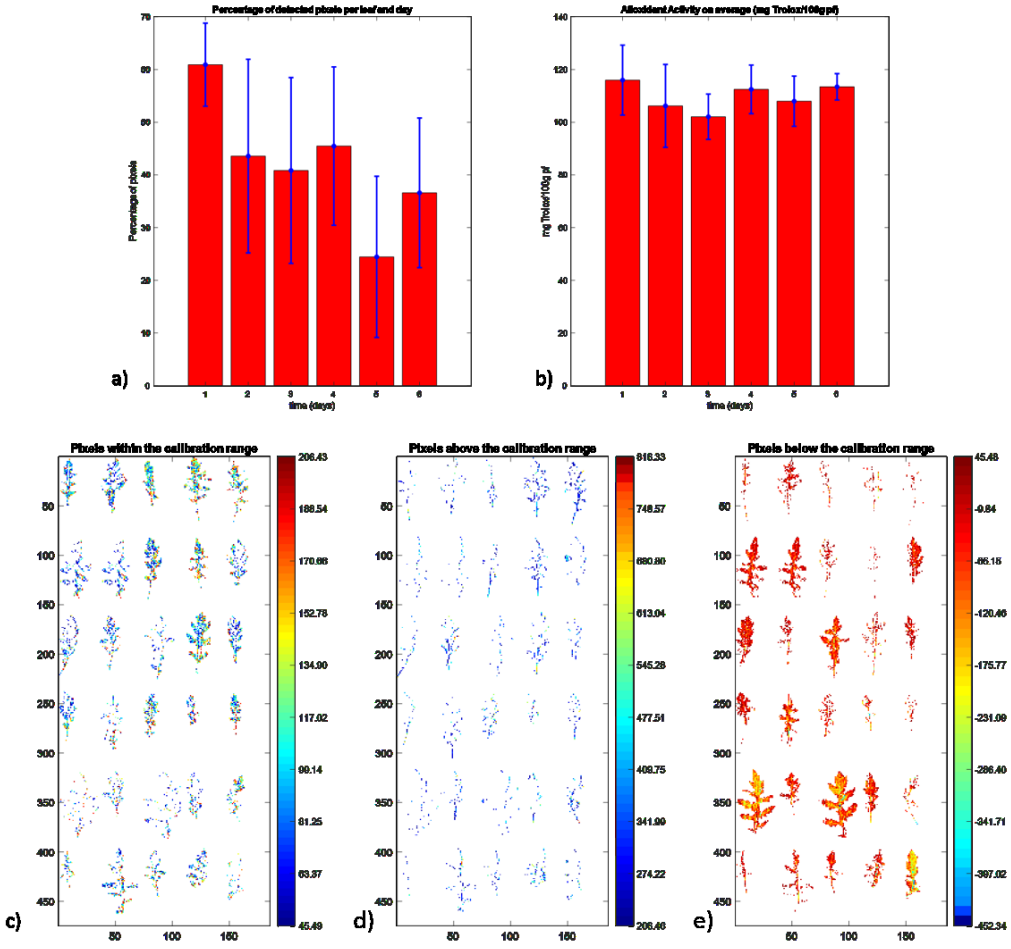

S8. a) Percentage of detected pixels and standard deviation pre leaf w.r.t days of storage for antioxidant activity b) antioxidant activity on average c) pixels within calibration range d) pixels above calibration range e) pixels below calibration range (time in days refers to the 6 acquisition intervals i.e. Days 0, 2, 5, 7, 9, 12)

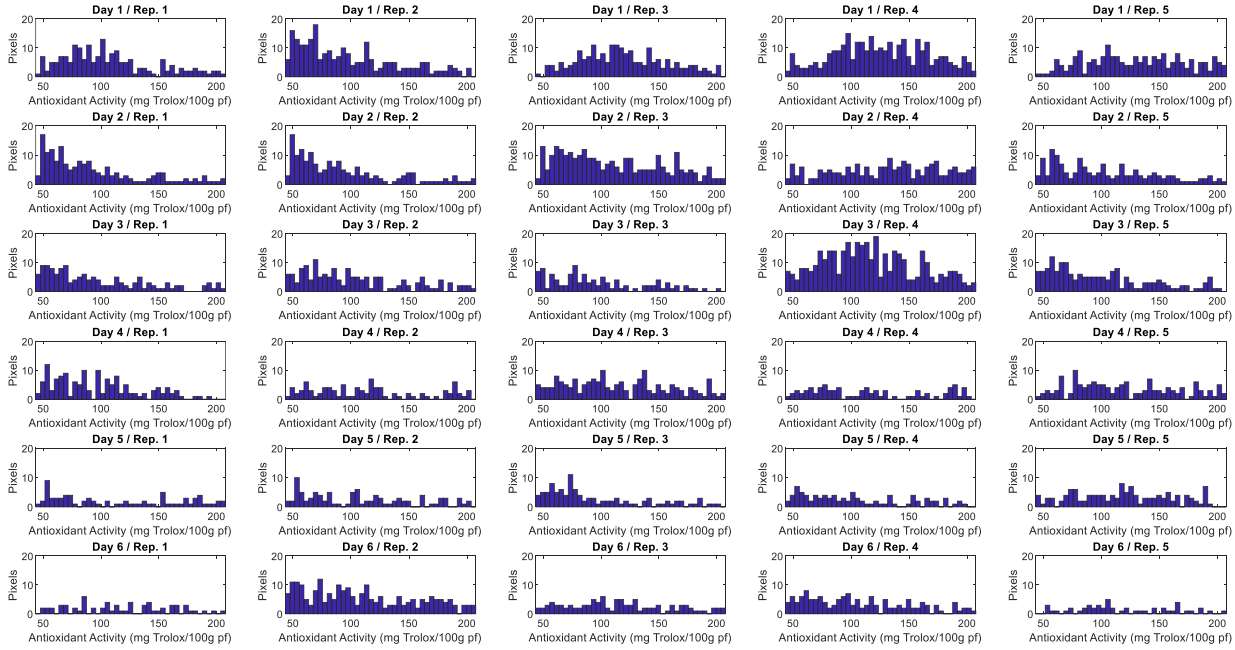

S9. Histograms of antioxidant activity detected in leaves with respect to the pixels detected (Day1, 2, 3, 4, 5, 6 refers to the 6 acquisition intervals i.e. Days 0, 2, 5, 7, 9, 12)

Chapter 6

POTENTIALITY OF NEAR INFRARED SPECTROSCOPY FOR ROCKET LEAVES (*Diplitaxis tenufolia*) CHARACTERIZATION: RAW MATERIAL DISCRIMINATION AND PHYTONUTRIENT MODELING

Abstract

The potentiality of spectral profiles in the NIR region for the classification of rocket raw material and global modelling of vitamin C content was investigated. Partial Least Squares Discriminant Analysis (PLSDA) with mean centering as data pretreatment was used for the classification of rocket leaves belonging to three different seasons of harvest namely spring, summer and autumn with a non-error rate (NER) of 94% both in calibration and validation. Moreover, partial least squares regression (PLSR) models for the prediction of vitamin C, ascorbic acid (AA), phenols and antioxidant activity were formulated using the spectral information from the hyperspectral images acquired in the NIR spectral range from 900-1700 nm with selective variables. The best data pretreatments in this case were first derivative followed by mean centering. Vitamin C prediction model resulted in R^2_{cal} of 0.77, R^2_{cv} of 0.70 and R^2_{pred} of 0.65 with RMSEC, RMSECV and RMSEP of 8.70, 9.92 and 12.42 mg of vitamin C $100g^{-1}$ f.w, respectively. In case of AA the R^2_{pred} was 0.72 with a RMSEP of 12.81 mg of AA $100g^{-1}$ f.w. PLSR prediction models for phenols and antioxidant activity showed R^2_{pred} of 0.70 and 0.61 with RMSEP of 18.70 mg of gallic acid $100g^{-1}$ and 25.65 mg of Trolox $100g^{-1}$, respectively. Conclusively, spectral information retrieved from the hyperspectral images using selected variables revealed good potentiality for quality assessment of rocket leaves, suggesting a possible implementation for raw material inspection and characterization in the NIR range.

Keywords: classification, prediction, phytonutrients, shelf-life, PLSR, PLSDA

1. INTRODUCTION

Leafy vegetables have always served as a significant source of health promoting elements in human diet as they are an enormous reserve of active chemical compounds and are the cheapest and widely available source of fiber, proteins, vitamins, phenolic compounds, antioxidants and minerals (Gibson et al., 2012). Therefore, the consumption of minimally processed ready-to-eat fruit and vegetable has significantly boosted in the last decades (Artés et al., 2009), since they are perceived as healthy, convenient, highly nutritive and appetizing (Oliveira et al., 2015; Ma et al., 2017).

In the Mediterranean countries, rocket leaves (*Diplotaxis tenuifolia*) with its pungent smell and strong flavor, lies among the most popular leafy vegetables, mostly consumed as stand-alone salads or as a part of mixed salad products. The rocket leaves are a rich source of phytonutrients such as fiber, Vitamin C, flavonoids and glucosinolates which are widely known for their positive impacts on human health (Cavaiuolo and Ferrante, 2014; Nurzyńska-Wierdak, 2015). The nutritional value of the wild rocket leaves and its degradation with the passage of the shelf life depends on the pre-harvest practices, postharvest handing, processing and storage conditions (Toivonen and Brummell, 2008; Cefola and Pace, 2015). After minimal processing operations (most commonly in this case, washing and drying), the rocket leaves are available packaged in plastic bags in the retail stores. Particularly, yellowing caused by chlorophyll degradation, wilting, and the production of off-odors are the main sources of deterioration for this product (Nielsen et al., 2008; Koukounaras et al., 2009; Løkke et al., 2012; Chaudhry et al., 2018). Moreover, the degradation process in fruits and vegetables also results in the degradation of the phytonutrients specially the degradation of nutrients, such as vitamin C has been reported over storage time (Kim and Ishii, 2007; Spadafora et al., 2016; Mastrandrea et al., 2017). Kim & Ishii, 2007 observed that the vitamin C content was significantly affected during the storage of the rocket leaves at both 4ºC and 15ºC and also it was reported that the vitamin C content was higher in the leaves with and without roots in case of 4ºC as compared to 15ºC regardless of the storage time. Moreover, Spadafora et al., 2016 also reported a rapid decrease in the vitamin C content of rocket leaves stored at high temperatures. Mastrandrea, Amodio, de Chiara, Pati, & Colelli, 2017 reported that the leaves stored at 0ºC both in air and in modified atmosphere packaging (MAP) did not show any changes in the AA content but those stored at 5ºC air portrayed slight decrease in the AA content with the passage of storage time while a

rapid decrease was observed in the AA content degradation at 15ºC both in case of samples stored in air and in MAP. On the other side, other authors reported that AA remained unaltered in rocket leaves stored in controlled atmosphere (CA) at 4 °C, while it degraded in the leaves stored in air (Martínez-Sánchez et al., 2006b). In the same way, the reduction of total antioxidant capacity was also significant for the samples stored in air, whereas the phenolic content decreased with the passage of storage time regardless of the storage atmosphere. Changes in AA content during storage of rocket leaves were also studied by (Cavaiuolo et al., 2015) which observed a slight increase in the AA content in the initial days of storage. Moreover, it was also revealed by Mastrandrea et al., 2017b that improper MAP contributed towards the loss of appearance and degradation of vitamin C hence resulting in a shorter shelf life of rocket leaves stored at 5ºC and 15ºC in improper MAP as compared to those stored in air. The study also specified that the appearance score loss and vitamin C degradation occurred at low O_2 (0 kPa) and at high CO_2 (25 kPa) in the modified atmosphere packages.

Near infrared spectroscopy (NIRS) has gained wide attention in the food sector due to its potentiality to attain fingerprints of the various products as a result of the interaction between light and the molecular structure of food since every product has a different fingerprint indicating its contrast with the others (Workman and Shenk, 2004), being the results of the different pre-harvest factors, which also affect its final quality and composition. Hyperspectral imaging devices are being used in the food research sector in a bid to evaluate the quality, class, authenticity, adulteration or fraud in a rapid and non-destructive way (ElMasry & Sun, 2010; Yoon et al., 2011; Lorente et al., 2012). Chemiometric techniques and particularly discriminant analysis are the statistical tools used for analyzing differences between various samples or groups of samples relative to a number of variables simultaneously. Soft independent modelling of class analogy (SIMCA), partial least squares discriminant analysis (PLSDA), artificial neural networks (ANN), discriminant analysis (DA) and support vector machine (SVM) have commonly been used in scientific studies addressing discrimination among fruit and vegetable belonging to different quality classes. Oliveri et al., 2011 discussed different class modelling methods for addressing the types of potential problems rising during studies related to food authentication. Moreover, for the prediction of the nutritional value partial least squares regression (PLSR) models are used which are internally

cross-validated and the accuracy of these models is ensured with external validation (Geladi and Kowalski, 1986). But there is a need of making the state of the art for the use of spectral information and chemiometric tools for prediction as well as discrimination purposes. In this case the transition from the hyperspectral to the multispectral approaches is gaining significance resulting is model simplification and process rapidness. None of the studies have yet used the reduced wavelengths for the classification of the rocket raw materials and global prediction of the internal phytonutrients over the storage period. The objective of this study was to discriminate between different rocket raw materials using the PLSDA and development of global PLSR models for the prediction of the internal composition of the phytonutrients utilizing a reduced wavelength range with variables constituting weights in the model for the model simplification.

2. MATERIALS AND METHODS

2.1 Experimental design and spectral acquisition

Washed and dried rocket leaves (*Diplotaxis tenuifolia*) were received in the postharvest laboratory of the University of Foggia (Italy) from 3 different raw material quality leaves over a time span of two years, season/year namely, September 2017 (raw material 1 referred as RM1 in the text), March 2018 (raw material 2 (RM2)) and July 2018 (raw material 3 (RM3)). For each experiment the representative samples were weighted, distributed into 100g batches, packed into plastic clamshells and stored at 5ºC under humidified air flow. Ten to fifteen replicates of >20 leaves each were acquired on each acquisition interval (for each experiment) over a span of shelf life of rocket leaves ranging between 8-12 days. Hyperspectral image acquisition followed by sensorial and reference analysis of the different raw materials was conducted over the storage period for the leaves of each season.

For each individual experiment the acquisition of the hyperspectral images was done using a hyperspectral line scan scanner (Version 1.4, DV srl, Padova, Italy) equipped with a spectrograph, in the near infrared region (NIR). The spatial resolution of NIR spectrograph was 623x320 pixels with a spectral resolution of 5nm over a wavelength range of 900-1700nm.

Self-developed MATLAB codes were used for image thresholding and the extraction of the average spectra of each replicate based on the best contrast between the object and the background followed by masking. Two different objectives were pursued; firstly, the principle component analysis (PCA) was utilized for the discrimination of rocket raw materials using reference analysis values of the first ten

replicates for each season followed by the PCA analysis of spectral datasets in the NIR range. Whereas, a separate dataset for the global classification and prediction modelling was formulated utilizing 146 samples of rocket leaves with different raw material quality RM1, RM2 and RM3 in the NIR range (146x161). The wavelength ranges used for the prediction of the phytonutrients in Chapter 5 were kept under consideration during variable reduction.

2.2 Chemical Analysis

2.2.1 Vitamin C reference analysis

For each individual experiment, three grams of fresh rocket tissues representing the leaves of one replicate (one image) were homogenized with 10 mL of MeOH/H_2O (5:95) plus citric acid (21 g L^{-1}) with EDTA (0.5 g L^{-1}). The homogenate was filtered through cheesecloth and a C18 Bakerbond SPE column (Waters, Milford, MA, USA). AA and DHAA contents were determined as described by Zapata and Dufour, (1992), with some modifications. The HPLC analysis was achieved after derivatization of DHAA into the fluorophore 3-(1,2-dihydroxyethyl) furol [3,4-b]quinoxaline-1-one (DFQ), with 1,2-phenylenediamine dihydrochloride (OPDA). Samples of 20 µl were analyzed with an Agilent 1200 Series HPLC. The HPLC system consisted of a G1312A binary pump, a G1329A auto-sampler, a G1315B photodiode array detector from Agilent Technologies (Waldbronn, Germany). Separations of DFQ and AA were achieved on a Zorbax Eclipse XDB- C18 column (150 mm × 4.6 mm; 5 µm particle size; Agilent Technologies, Santa Clara, CA, USA). The mobile phase was MeOH/H_2O (5:95 v/v) containing 5mM cetrimide and 50mM potassium dihydrogen phosphate at pH 4.5. The flow rate was 1 mL min^{-1}. AA and DHAA contents were expressed as mg of ascorbic or dehydroascorbic acid 100 g^{-1} of f.w (mg 100 g^{-1}).

2.2.2 Total phenolic content and antioxidant activity evaluation

Total phenolic content and antioxidant activity were determined according to Singleton and Rossi (1965) and Brand-Williams et al., (1995) with minor modifications. Three grams of leafy tissues representing the leaves of one replicate (one image) were homogenized in 2mM sodium fluoride methanol:water solution (80:20) for 1 minute and centrifuged at 5°C and 12,000 rpm for 5 minutes. The total phenol content was expressed as mg of gallic acid equivalent (GAE) 100 g^{-1} fresh weight (f.w). The antioxidant activity was reported as mg Trolox equivalent antioxidant activity (TEAC) 100 g^{-1} f.w. Readings were made at 725 nm, against a blank after 2 h standing for phenolic content and at 515 nm after 24 h standing

for antioxidant activity using a UV-1700 Shimadzu spectrophotometer (Jiangsu, China).

2.3 Multivariate analysis

A PCA model including samples of different raw materials was performed separately on the spectra of the Vis-NIR and the NIR range as well as the reference analysis values for the preliminary data exploration. The data acquired using the hyperspectral imaging device were in this way reduced to few variables, called Principal components (Bro and Smilde, 2014) which are a linear combination of the original variables. For the classification of the samples belonging to different raw materials over their storage period, partial least squares discriminant analysis (PLSDA) was conducted on the NIR spectral dataset in the NIR range which were then reduced to 30 variables after wavelength selection. In this case the model accuracy was evaluated based on the sensitivity and the specificity values. Moreover, in the second methodology the pixels belonging to the corresponding classes were used for the development of a PLSDA prediction model in Hypertools (Mobaraki et al., 2018). Five-fold spatial binning of the hyperspectral image with the dimensions 1869x320x161 was done reducing the image size to 374x64x161. Furthermore, the spectral cropping was done for the reduction of the variables from a total of 161 to 30 variables which were related to vitamin C related regions in the NIR range resulting in a final image of the size 374x64x30 for conducting a pixel based PLSDA analysis.

Prediction models for the desired parameters were developed using the PLS algorithm in the PLS toolbox (Eigenvector Research Inc., version 7.2.5) working under MATLAB 2012b (version 8.0.0.783, MathWorks, MA, USA). The spectral dataset was divided into calibration set and validation sets using the Kennard stone algorithm. For the development of the PLSR calibration models random subset internal cross validation was applied. The accuracy of the calibration models was accessed by visualizing the coefficient of determination in calibration (R^2_{cal}), coefficient of determination in cross validation (R^2_{cv})and the root mean square error for calibration (RMSEC) and cross-validation (RMSECV). After the formulation of the best calibration models the external dataset was used for the prediction of the desired constituent.

3. RESULTS AND DISCUSSION

3.1 Raw material classification

Figure 1a shows the preprocessed NIR spectra of the three different rocket raw materials (RM1, RM2 and RM3) over their storage period in the full wavelength range comprising of 161 variables.

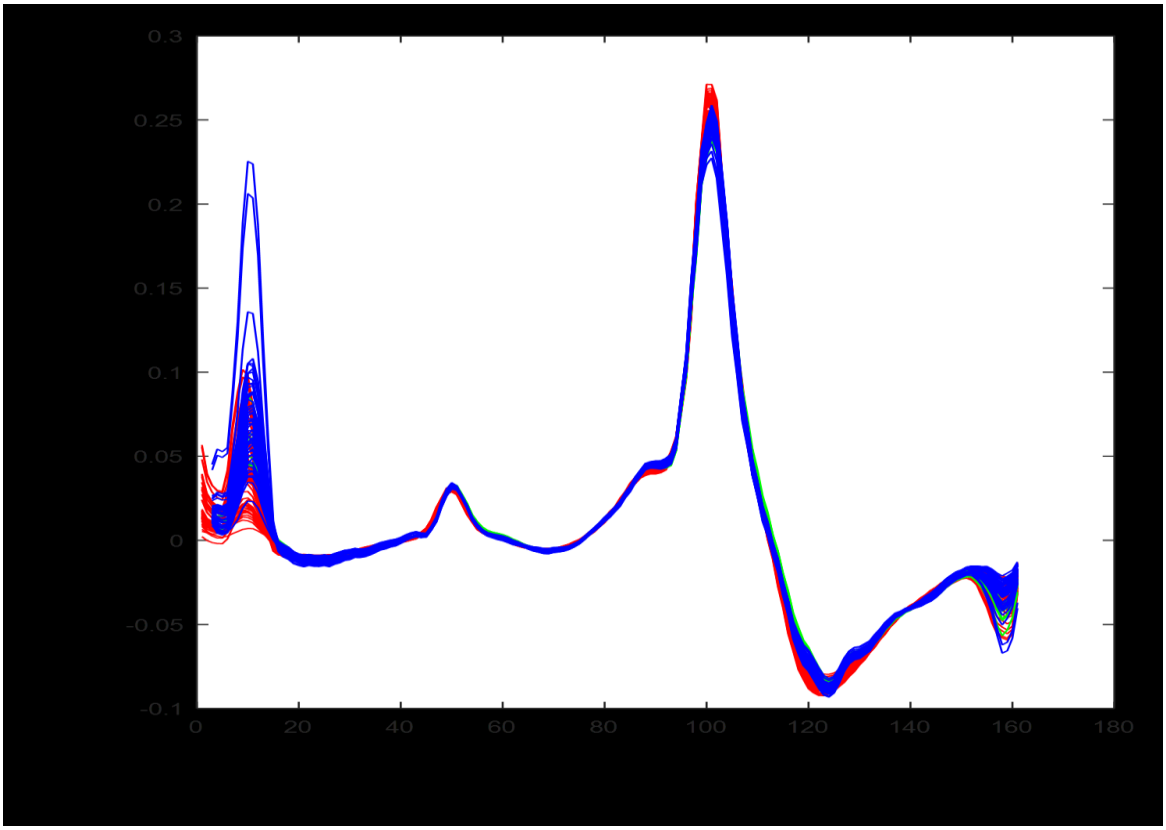

Figure 1. Preprocessed (SNV+ 1st derivative) NIR spectra (Red color = RM1, Green color = RM2, Blue color = RM3)

For the initial data exploration, a PCA was conducted and a clear discrimination of the data was obtained as shown in figure 2a with the first principle component (PC) explaining 86.64% and the second PC explaining 6.10% of the total variance in the data. PC1 discriminated the data based in the year of harvest since the RM1 samples belonged to year 2017 while RM2 and RM3 belonged to the year 2018. The loadings plot (figure 2b) for the PCA also demonstrated potential for the discrimination in the regions from 900-1000nm, 1300-1450nm and 1500nm onwards.

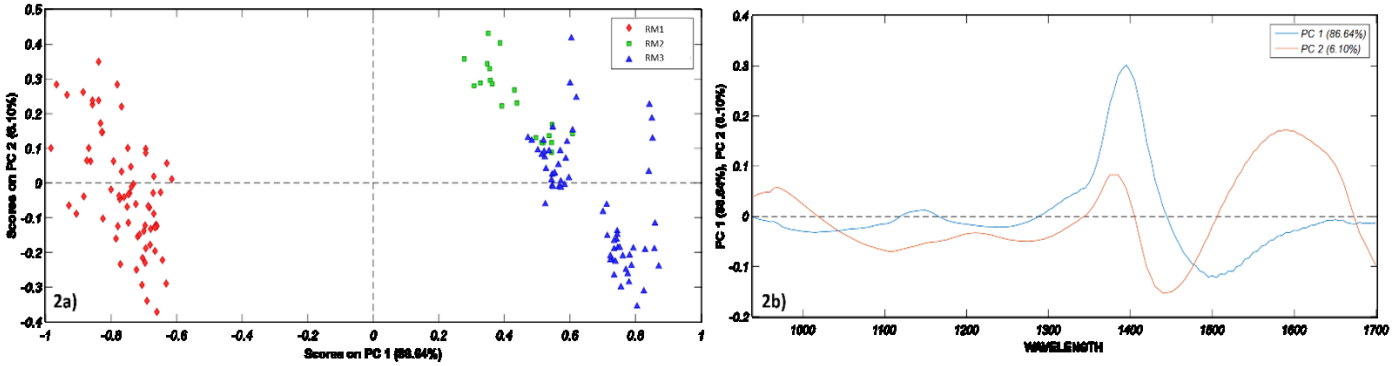

Figure 2. a) Scores plot for PCA based on season of harvest b) Loading plot for PCA based on season of harvest

For the exploration of the chemical parameters responsible for the discrimination of raw material in the NIR range a second PCA was conducted with the destructive quality parameters obtained on the initial samples. The PCA yielded a good discrimination based on 3 PCs resulting in the elaboration of 52.46%, 14.08% and 9.92% variance in the data for the respective PCs. Based on the PCA it was observed that vitamin C held significance as compared to other variables as can be seen in figure 3. It can be observed that chlorophyll a and chlorophyll b formulated a cluster whereas another cluster can be observed with soluble solids content (SSC), yeasts and moulds, firmness and mesophilic bacteria. Moreover, pH and NH4 g^{-1} were found to have a close relationship. Based on this PCA it was deduced that vitamin C content can be a reliable indicator for the raw material discrimination.

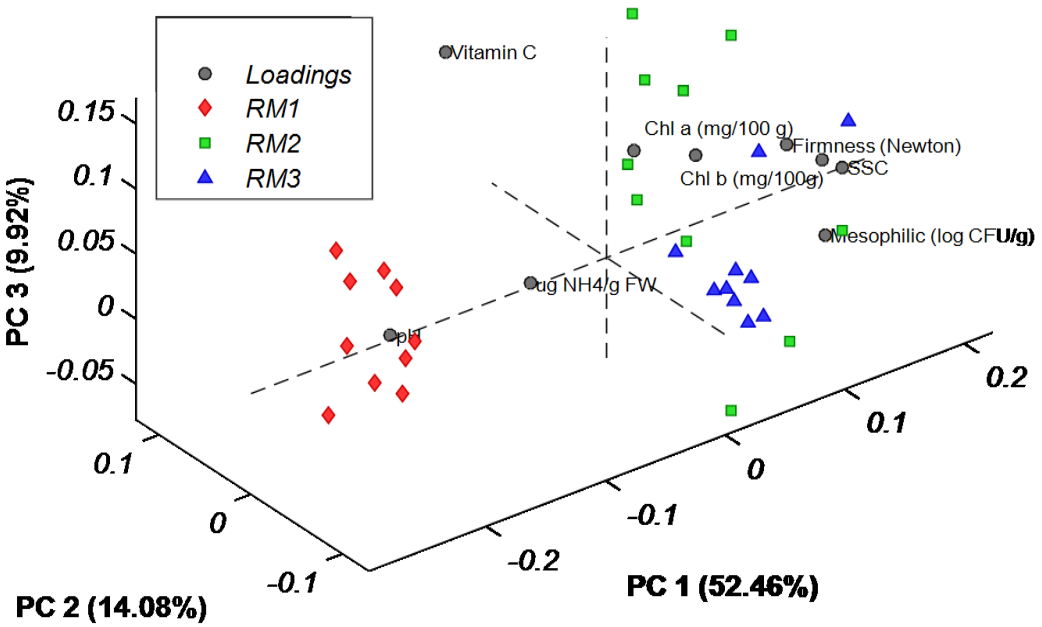

Figure 3. PCA for the reference values of raw material on first day of storage

Therefore, based on the loading weights of the spectral based PCA model, a PLSDA model was formulated in the NIR range from 900-1700nm based on the vitamin C sensitive peaks i.e. 945-980nm, 1350-1410nm and 1660-1700nm having 30 variables in total. These wavelength ranges were used since in the NIR range these regions are highly effected with the vitamin C content (Malegori et al., 2016). The PLSDA modelling was utilized using two different approaches firstly, on the spectral dataset and secondly, PLSDA was applied on the pixels of the hyperspectral image. In case of the spectral based PLSDA, the calibration set comprised of 108 samples while the external validation set contained 36 samples. The data was mean-centered followed by random subset cross validation. Table 1 shows the confusion matrix for the spectral based PLSDA. The model performance was evaluated based on the non-error rate which is an average of the sensitivity calculated over the various classes, and gives an overall idea of the goodness of the classification.

Table 1. Confusion table for sensitivities and specificities for the classes summer, spring and autumn in calibration, cross validation and prediction

Calibration	*CV*	*Actual Class*			*N*	**Global**	
		SUMMER	***SPRING***	***AUTUMN***		**SENS**	**SPEC**
Predicted as Class	***SUMMER***	51	0	0	52	98	100
	SPRING	1	11	0	11	100	98
	AUTUMN	0	0	45	45	100	100
TOTAL					**108**	Non error rate = 99.33%	
Cross Validation	***CV***	***Actual Class***			***N***	**Global**	
		SUMMER	***SPRING***	***AUTUMN***		**SENS**	**SPEC**
Predicted as Class	***SUMMER***	49	0	0	52	94	100
	SPRING	3	11	0	11	100	96
	AUTUMN	0	0	45	45	100	100
TOTAL					**108**	Non error rate = 98%	
Prediction	***CV***	***Actual Class***			***N***	**Global**	
		SUMMER	***SPRING***	***AUTUMN***		**SENS**	**SPEC**
Predicted as Class	***SUMMER***	10	0	0	12	83	100
	SPRING	2	3	0	3	100	93
	AUTUMN	0	0	21	21	100	100
TOTAL					**36**	Non error rate = 94.33%	

The PLSDA model in this yielded 6 latent variables (LVs) with the first two LVs explaining 98% of the covariance in the data. From the confusion matrix it can be seen that out of the 108 samples in the calibration dataset spring and autumn datasets were classified with 100% accuracy while in case of summer class only one sample was misclassified as spring class. Similarly, in case of cross validation 100% accuracy was achieved for the classification of spring and autumn classes whereas 3 samples of summer class were misclassified in the spring class. The external prediction resulted in the non-error rate of 94.33% with sensitivity values of the summer, spring and autumn values to be 83%, 100% and 100% respectively. In addition, the areas under the receiver operating characteristic (ROC) curves (data not shown) were close to 1 for this classification model, which is an indication of excellent classification.

The PLSDA classification model accuracy in this case was also evaluated based on the sensitivity, specificity and NER values. Table 2 shows the sensitivities and specificities of the pixels belonging to three different classes in calibration and cross validation.

Table 2. Confusion table for sensitivities and specificities for the pixels belonging to classes summer, spring and autumn in calibration and cross validation

Calibration	*CV*	*Actual Class*				**Global**	
		AUTUMN	***SPRING***	***SUMMER***	***UNASSIGNED***	**SENS**	**SPEC**
Predicted as Class	***AUTUMN***	2473	17	8	373	99	100
	SPRING	0	2122	202	255	91	96
	SUMMER	5	239	3259	271	93	96
NON-ERROR RATE						94.33%	
Cross Validation	***CV***	***Actual Class***				**Global**	
		AUTUMN	***SPRING***	***SUMMER***	***UNASSIGNED***	**SENS**	**SPEC**
Predicted as Class	***AUTUMN***	2482	15	8	366	99	100
	SPRING	0	2123	205	251	91	96
	SUMMER	4	242	3261	267	93	96
NON-ERROR RATE						94.66%	

The PLSDA model based on the pixels of the classes retrieved from the hyperspectral image comprised of 5 LVs with the first LV explaining 41.38% (figure 4a) and the second LV explaining 22.28% (figure 4b) of the covariance in the data. The classification accuracy in calibration and random subset cross validation was depicted by NER of 94.33% and 94.66%, respectively. The classified pixels during the calibration were then used to develop a classification map for the prediction mapping of the three classes as shown in figure 4c.

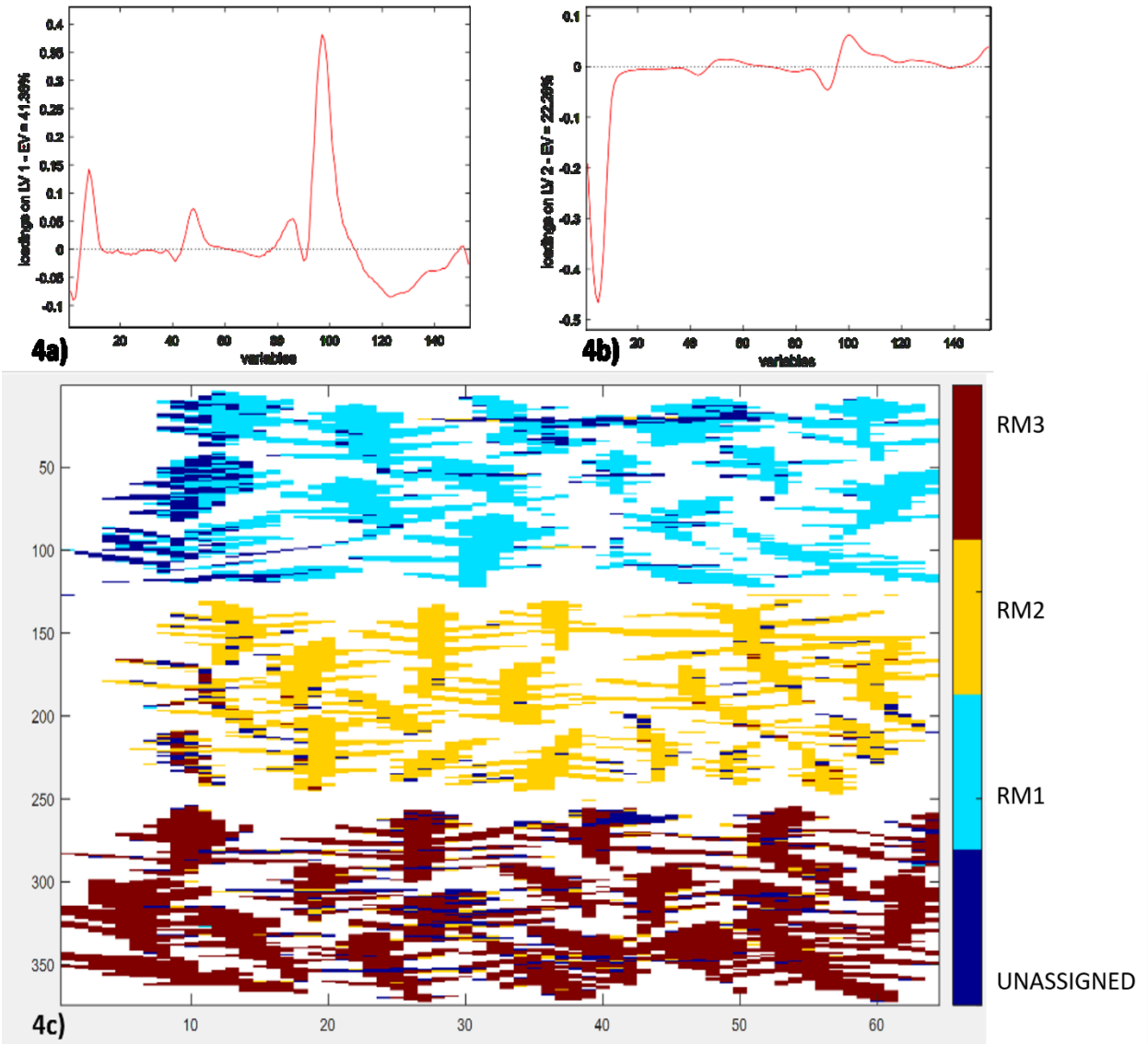

Figure 4. PLSDA classification map for the classification of RM1 (cyan colored pixels), RM2 (yellow colored pixels), RM3 (red colored pixels); the pixels not assigned to any class are colored blue

3.2 Global Modelling of Phytonutrients

Table 3 shows the means and the ranges of the composition of the phytonutrients globally modelled in this study. The determination of the variation in the minimum and maximum was conducted over the storage period of rocket leaves.

Table 3. Range values and statistical distribution of Chemical Parameters for the reference vector developed for global PLSR modelling (summer, spring, autumn)

Chemical Parameter	Min	Max	Mean	Standard Deviation
Vitamin C	15.80	123.33	59.51	19.02
Ascorbic Acid (AA)	7.77	109.38	45.33	20.41
Antioxidant Activity	54.26	225.98	127.35	33.94
Phenols	83.53	251.26	142.40	32.18

Various research studies have demonstrated that at the beginning of the storage time of rocket leaves AA is the principle form of vitamin C which slowly converts to dehydroascorbic acid over the storage span (Martínez-Sánchez, Marín, Llorach, Ferreres, & Gil, 2006b). Since the rocket leaves possess a storage life ranging between approximately 7-14 days; it has been revealed by Martínez-Sánchez, Marín, Llorach, Ferreres, & Gil, 2006b that a significant decrease in the AA occurs after six days of storage ultimately leading to a lower vitamin C content for rocket leaves stored in various conditions. Similarity in the range of vitamin C values were also encountered by Mastrandrea, Amodio, de Chiara, Pati, & Colelli, 2017b confirming a significantly higher amount of AA on the initial day of storage as compared to a much lower amount of dehydroascorbic acid.

It can be observed in figure1 that the leaf water content highly affected the reflectance signal, particularly for the peaks between 900-1000nm which correspond to the third overtone region hence corresponding to the O-H bonds and the peaks between 1400-1500nm which correspond to the first overtone region corresponding to the O-H and N-H bonds with water absorption between 1400 1450 nm (Workman, 2003; Sasic and Ozaki, 2011). Moreover, Malegori et al., 2016 also found region between 7200-6700cm^{-1} which corresponds to 1428-1492nm to be effective for studying most characteristic vitamin C absorbance for acerola fruit and Liu et al., 2006 also revealed that the region between 1428-1492nm is significantly influenced by vitamin C absorption possessing a broad band at approximately 1428nm. On the other hand, in a study based on powdered mixtures and solutions, H. Yang & Irudayaraj, 2002 found that for vitamin C in powdered mixtures and solutions the peaks can be found around 1000, 1210, 1360, 1457, 1579 and 1651 nm. Moreover, the same author also demonstrated that one peak for vitamin C can

also be observed at 840 nm.

As for prediction models, PLSR was applied for Vitamin C content, AA, phenols and antioxidant activity in NIR range of 900-1700nm keeping under consideration the wavelengths utilized for this aim in Chapter 5. Table 4 shows the calibration statistics of the PLSR models for the phytonutrients measured over the storage time in fresh-cut rocket leaves.

Table 4. Calibration statistics for global PLSR models for phytonutrients in fresh-cut rocket leaves

Parameter	Pretreatment	No. of variables	LVs	R^2_{cal}	RMSEC	R^2_{cv}	RMSECV
Vitamin C	1st Dev+MC	30	10	0.77	8.70	0.70	9.92
AA	1st Dev+MC	59	9	0.78	9.09	0.72	10.31
Phenols	1nd Dev+MC	109	10	0.69	17.47	0.60	19.85
Antioxidant-Activity	1st Dev+MC	86	8	0.72	15.75	0.61	18.96

Kennard stone algorithm was used for the splitting of the samples in the calibration and validation datasets. In this case a logical vector is created and allocates TRUE (1) and FALSE (0) values to the samples in the dataset based on maximum variability. The samples allocated TRUE formulate the external validation set while the samples allocated FALSE formulate the calibration dataset. In case of vitamin C, the calibration dataset contained 108 samples and the external validation was conducted with 36 samples. The PLSR calibration results for the vitamin C over a storage period of 12 days are shown in figure 5. A number of various data pretreatments were used but the best pretreatment was concluded to be 1st derivative accompanied by data mean centering. The calibration model developed with a total of 30 variables and 10 LVs in the NIR range yielded R^2_{cal} of 0.77 and R^2_{cv} of 0.70 with the RMSEC and RMSECV of 8.70 and 9.92 mg of vitamin C $100g^{-1}$ f.w, respectively which was very similar to the laboratory error (9.179 mg of vitamin C $100g^{-1}$ f.w) hence confirming the reliability of the global PLSR calibration model. The 30 variables selected for the formulation of the vitamin C calibration model included wavelength ranges from 930-970nm, 1420-1500nm and 1660-1700nm. An external prediction

set comprising of 36 samples was used to evaluate the performance of the global PLSR model which yielded R^2_{pred} of 0.65 with a RMSEP of 12.43 mg of vitamin C 100g^{-1} f.w (Table 5).

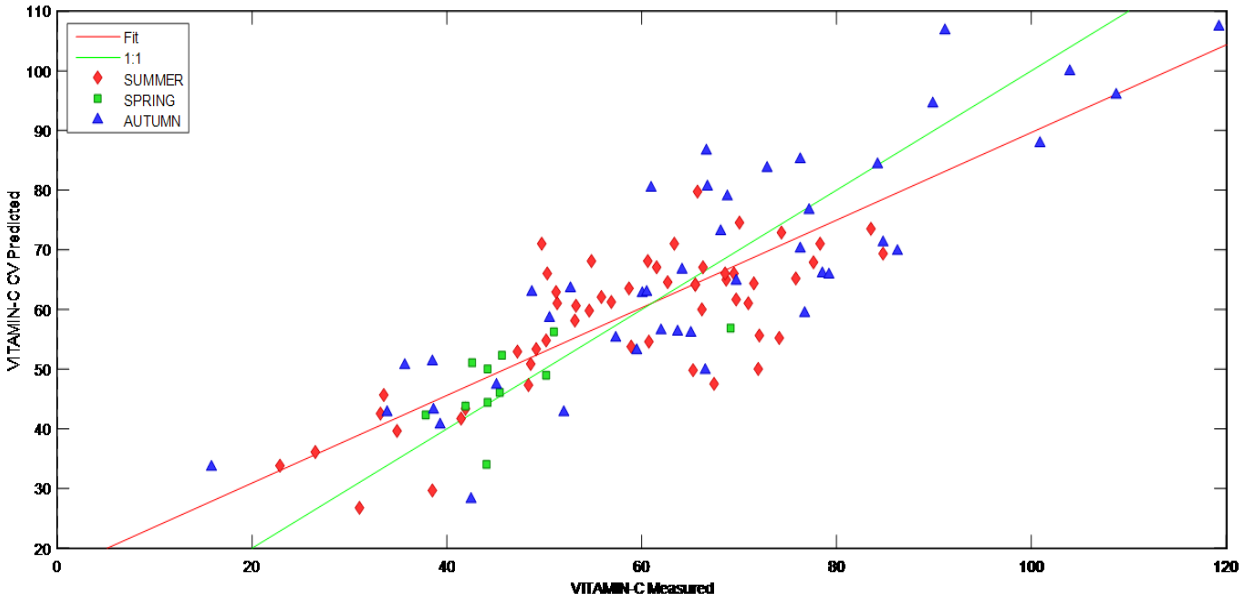

Figure 5. Global PLS regression model plot for Vitamin C measured vs Vitamin C predicted in the selected NIR ranges

Similar wavelengths are reported to be used for prediction and mapping of the vitamin C content in acerola fruits by Malegori et al., 2016 where 7200-6700cm^{-1} was most significantly related to vitamin C changes. In a similar study, Liu et al., 2006 recommended that the wavenumber regions between 7200-6700nm are most sensitive to vitamin C changes and hence it was confirmed that the global PLSR model for the vitamin C prediction yielded reliable R^2 values as well as RMSEs for vitamin C calibration.

The calibration dataset for AA contained 108 samples 30 samples comprised the external validation set. Global PLSR calibration results for AA are depicted in figure 6. A total of 59 variables and 9LVs in the NIR range were used for the formulation of the global PLSR model for AA after pretreating the spectral dataset with 1st derivative and mean centering resulting in the model statistics in the form of R^2_{cal} of 0.78 and R^2_{cv} of 0.72 with the RMSEC and RMSECV of 9.09 and 10.31 mg of AA 100g^{-1} f.w, respectively. The global calibration model for AA was developed utilizing the wavelength ranges from 900-1000nm, 1340-1500nm and 1660-1700nm selected based on the loading plots with the variables possessing maximum weights in the model. An external prediction set containing of 30 samples was utilized for the

performance evaluation of the global PLSR model for AA which yielded R^2_{pred} of 0.72 with a RMSEP of 12.82 mg of AA 100g^{-1} f.w. as shown in table 5.

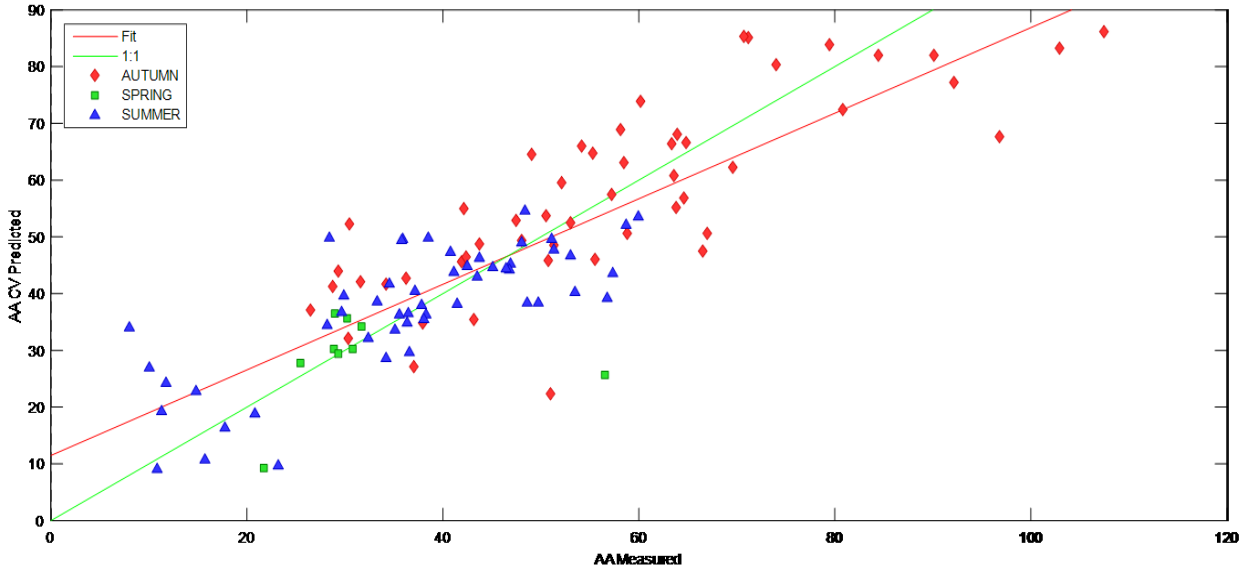

Figure 6. Global PLS regression model plot for AA measured vs AA predicted in the selected NIR ranges

Similar results were obtained for the prediction of AA in bell peppers by Ignat et al., 2012 in which the AA was predicted with a RMSECV of 11.4-14.6%. In this study, Vis-NIR and SWIR mini-spectrometers were used for the measurement of the AA content. In case of the SWIR range (850-1888nm) the AA was predicted yielding an R^2_{cal} of 0.75 with 8 LVs accompanied by RMSEC of 12.6 mg of AA 100g^{-1}.

For phenolic content the Kennard Stone algorithm was used to generate calibration and validation sets comprising 134 samples in the calibration and leaving 50 samples for the external prediction. Global PLSR models were developed using various data pretreatments but the best pretreatment in this case was 1st derivative flowed by mean centering of the data. A total of 109 variables were used for the calibration development yielding an R^2_{cal} of 0.69 with RMSEC of 17.47 mg of gallic acid 100g^{-1} and R^2_{cv} of 0.60 with RMSECV of 19.85 mg of gallic acid 100g^{-1}. These 109 variables comprised of wavelength ranges from 900-970nm, 1095-1170nm and 1330-1700nm. The reliability of the calibration model was accessed with external validation done with 50 samples yielding R^2_{pred} of 0.70 and RMSEP of 18.70 mg of gallic acid 100g^{-1} (Table 5). Figure 7 shows the global calibration plot for the phenolic content of the rocket

leaves over the storage period of rocket leaves for the three different seasons.

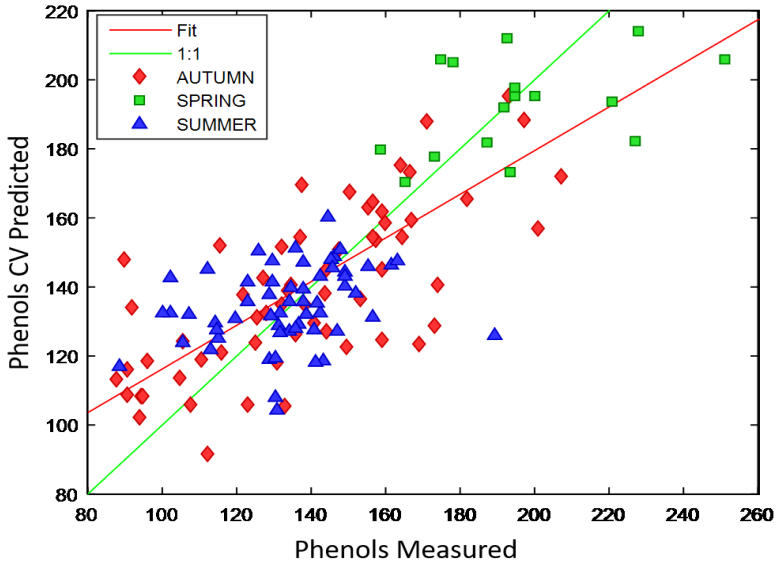

Figure 7. Global PLS regression model plot for Phenols measured vs Phenols predicted in the selected NIR ranges

In case of the antioxidant activity, a total of 86 variables were used including the wavelength ranges from 900-970nm, 1250-1550nm and 1655-1700nm. The global calibration model with a total of 8 LVs yielded R^2_{cal} of 0.72 and R^2_{cv} of 0.61 with RMSEC and RMSECV being 15.75 and 18.96 mg Trolox 100g^{-1}, respectively. The external validation resulted in an R^2_{pred} value of 0.61 with a RMSEP of 25.65 mg Trolox 100g^{-1}. A close observation of the PLSR results for antioxidant activity shows that the RMSEP is quite high and hence decreases the reliability of the model. It can be due to the reason that the variation in the content of antioxidant activity with the passage of storage time is related to the leaf structure and chemical composition than the storage conditions therefore during various storage periods the leaves specially in autumn and spring the leaves would have maintained their structure not leading to a constant decrease in the antioxidant activity. Martínez-Sánchez, Allende, et al., 2006 concluded that the antioxidant capacity decreased regardless of the storage conditions in case of rocket leaves. But it is quite possible that the rate of decrease of antioxidant activity may vary among various quality raw materials, harvest times and seasons. Other studies have also revealed that the variation of the antioxidant activity in plants can be a result of the changes in the phenolic profiles (Lattanzio, Cicco, & Linsalata, 2005;

Lattanzio et al., 2005), with the ellagic acid (Marie E. Olsson et al., 2004) with anthocyanins (Wang and Lin, 2000), and also with ascorbic acid changes (Cocci et al., 2006).

Table 5 shows the prediction results for the vitamin C, AA, phenols and antioxidant activity.

Table 5. Prediction statistics for the global PLSR modelling of fresh cut rocket leaves

Parameter	No. of predicted samples	Wavelength Range (nm)	LVs	R^2_{pred}	RMSEP
Vitamin C	1st Dev+MC	900-1000 1300-1500 1650-1700	10	0.65	12.43
AA	1st Dev+MC	900-1000 1295-1480 1655-1700	9	0.72	12.82
Phenols	1st Dev+MC	900-1700	10	0.78	18.70
Antioxidant activity	1st Dev+MC	900-970 1285-1540 1655-1700	8	0.76	25.65

4. CONCLUSIONS

Hyperspectral imaging in the NIR range was used for the classification of rocket raw materials and global prediction of the changes in the phytonutrients in rocket leaves belonging to three different quality standards. The classification models were simplified by using variable reduction. It was concluded that the vitamin C sensitive regions in the NIR range were effective for the classification of the rocket leaves based on raw material (season of harvest as well) yielding classification accuracies as high as 94%. Moreover, for the prediction of the plant phytonutrients global PLSR models with appropriate variable selection techniques assisted in model simplification but also the model reliability was enhanced due to increasing the variability in the calibration dataset. Conclusively, NIR range accompanied by the wavelength selection can serve as a reliable tool for the sorting of rocket leaves based on the raw material quality and prediction of the internal constituents.

REFERENCES

Artés, F., Gómez, P., Aguayo, E., Escalona, V., Artés-Hernández, F., 2009. Sustainable sanitation techniques for keeping quality and safety of fresh-cut plant commodities. Postharvest Biol. Technol. 51, 287–296. https://doi.org/10.1016/J.POSTHARVBIO.2008.10.003

Brand-Williams, W., Cuvelier, M., Berset, C., 1995. Use of a free radical method to evaluate antioxidant activity. LWT - Food Sci. Technol. 28, 25–30. https://doi.org/10.1016/S0023-6438(95)80008-5

Cavaiuolo, M., Cocetta, G., Bulgari, R., Spinardi, A., Ferrante, A., 2015. Identification of innovative potential quality markers in rocket and melon fresh-cut produce. Food Chem. 188, 225–233. https://doi.org/10.1016/J.FOODCHEM.2015.04.143

Cavaiuolo, M., Ferrante, A., 2014. Nitrates and glucosinolates as strong determinants of the nutritional quality in rocket leafy salads. Nutrients. https://doi.org/10.3390/nu6041519

Cefola, M., Pace, B., 2015. Application of Oxalic Acid to Preserve the Overall Quality of Rocket and Baby Spinach Leaves during Storage. J. Food Process. Preserv. 39, 2523–2532. https://doi.org/10.1111/jfpp.12502

Chaudhry, M.M.A., Amodio, M.L., Babellahi, F., de Chiara, M.L.V., Amigo Rubio, J.M., Colelli, G., 2018. Hyperspectral imaging and multivariate accelerated shelf life testing (MASLT) approach for determining shelf life of rocket leaves. J. Food Eng. 238, 122–133. https://doi.org/10.1016/j.jfoodeng.2018.06.017

Cocci, E., Rocculi, P., Romani, S., and, M.D.R.-P.B., 2006, undefined, n.d. Changes in nutritional properties of minimally processed apples during storage. Elsevier.

ElMasry, G., Sun, D., 2010. Meat quality assessment using a hyperspectral imaging system. imaging food Qual. Anal. ….

Geladi, P., Kowalski, B.R., 1986. Partial least-squares regression: a tutorial. Anal. Chim. Acta 185, 1–17. https://doi.org/10.1016/0003-2670(86)80028-9

Gibson, A., Edgar, J.D., Neville, C.E., Gilchrist, S.E., McKinley, M.C., Patterson, C.C., Young, I.S., Woodside, J. V., 2012. Effect of fruit and vegetable consumption on immune function in older people: a randomized controlled trial. Am. J. Clin. Nutr. 96, 1429–1436.

https://doi.org/10.3945/ajcn.112.039057

Kim, S.J., Ishii, G., 2007. Effect of storage temperature and duration on glucosinolate, total vitamin C and nitrate contents in rocket salad (Eruca sativa Mill.). J. Sci. Food Agric. 87, 966–973. https://doi.org/10.1002/jsfa.2787

Koukounaras, A., Siomos, A.S., Sfakiotakis, E., 2009. Impact of heat treatment on ethylene production and yellowing of modified atmosphere packaged rocket leaves. Postharvest Biol. Technol. 54, 172–176. https://doi.org/10.1016/J.POSTHARVBIO.2009.07.002

Lattanzio, V., Cicco, N., Linsalata, V., 2005. ANTIOXIDANT ACTIVITIES OF ARTICHOKE PHENOLICS. Acta Hortic. 421–428. https://doi.org/10.17660/ActaHortic.2005.681.59

Liu, H., Xiang, B., Qu, L., 2006. Structure analysis of ascorbic acid using near-infrared spectroscopy and generalized two-dimensional correlation spectroscopy. J. Mol. Struct. 794, 12–17. https://doi.org/10.1016/J.MOLSTRUC.2006.01.028

Løkke, M.M., Seefeldt, H.F., Edelenbos, M., 2012. Freshness and sensory quality of packaged wild rocket. Postharvest Biol. Technol. 73, 99–106. https://doi.org/10.1016/j.postharvbio.2012.06.004

Lorente, D., Aleixos, N., Gómez-Sanchis, J., 2012. Recent advances and applications of hyperspectral imaging for fruit and vegetable quality assessment. Food Bioprocess.

Ma, L., Zhang, M., Bhandari, B., Gao, Z., 2017. Recent developments in novel shelf life extension technologies of fresh-cut fruits and vegetables. Trends Food Sci. Technol. 64, 23–38. https://doi.org/10.1016/J.TIFS.2017.03.005

Marie E. Olsson, *,†, Jimmy Ekvall, ‡, Karl-Erik Gustavsson, †, Jessica Nilsson, §, Deepa Pillai, §, Ingegerd Sjöholm, #, Ulla Svensson, ⊥, Björn Åkesson, § and, Nyman‡, M.G.L., 2004. Antioxidants, Low Molecular Weight Carbohydrates, and Total Antioxidant Capacity in Strawberries (Fragaria × ananassa): Effects of Cultivar, Ripening, and Storage. https://doi.org/10.1021/JF030461E

Martínez-Sánchez, A., Allende, A., Bennett, R.N., Ferreres, F., Gil, M.I., 2006a. Microbial, nutritional and sensory quality of rocket leaves as affected by different sanitizers. Postharvest Biol. Technol. 42, 86–97. https://doi.org/10.1016/J.POSTHARVBIO.2006.05.010

Martínez-Sánchez, A., Marín, A., Llorach, R., Ferreres, F., Gil, M.I., 2006b. Controlled atmosphere

preserves quality and phytonutrients in wild rocket (Diplotaxis tenuifolia). Postharvest Biol. Technol. 40, 26–33. https://doi.org/10.1016/J.POSTHARVBIO.2005.12.015

Mastrandrea, L., Amodio, M.L., de Chiara, M.L. V., Pati, S., Colelli, G., 2017a. Effect of temperature abuse and improper atmosphere packaging on volatile profile and quality of rocket leaves. Food Packag. Shelf Life 14, 59–65. https://doi.org/10.1016/J.FPSL.2017.08.004

Mastrandrea, L., Amodio, M.L., de Chiara, M.L. V., Pati, S., Colelli, G., 2017b. Effect of temperature abuse and improper atmosphere packaging on volatile profile and quality of rocket leaves. Food Packag. Shelf Life 14, 59–65. https://doi.org/10.1016/J.FPSL.2017.08.004

Nielsen, T., Bergström, B., Borch, E., 2008. The origin of off-odours in packaged rucola (Eruca sativa). Food Chem. 110, 96–105. https://doi.org/10.1016/J.FOODCHEM.2008.01.063

Nurzyńska-Wierdak, R., 2015. Protein nutritional value of rocket leaves and possibilities of its modification during plant growth. Turkish J. Agric. For. 39, 1023–1028. https://doi.org/10.3906/tar-1412-6

Oliveira, M., Abadias, M., Usall, J., Torres, R., Teixidó, N., Viñas, I., 2015. Application of modified atmosphere packaging as a safety approach to fresh-cut fruits and vegetables – A review. Trends Food Sci. Technol. 46, 13–26. https://doi.org/10.1016/J.TIFS.2015.07.017

Oliveri, P., Di Egidio, V., Woodcock, T., Downey, G., 2011. Application of class-modelling techniques to near infrared data for food authentication purposes. Food Chem. 125, 1450–1456. https://doi.org/10.1016/j.foodchem.2010.10.047

Singleton, V.L., Rossi, J.A., Jr, J., 1965. COLORIMETRY OF TOTAL PHENOLICS WITH PHOSPHOMOYBDIC-PHOSPHOTUNGSTIC ACID REAGENTS. Am J Enol Viticult. 144–158.

Spadafora, N.D., Amaro, A.L., Pereira, M.J., Müller, C.T., Pintado, M., Rogers, H.J., 2016. Multi-trait analysis of post-harvest storage in rocket salad (Diplotaxis tenuifolia) links sensorial, volatile and nutritional data. Food Chem. 211, 114–123. https://doi.org/10.1016/j.foodchem.2016.04.107

Toivonen, P.M.A., Brummell, D.A., 2008. Biochemical bases of appearance and texture changes in fresh-cut fruit and vegetables. Postharvest Biol. Technol. 48, 1–14. https://doi.org/10.1016/J.POSTHARVBIO.2007.09.004

Wang, S.Y., Lin, H.-S., 2000. Antioxidant Activity in Fruits and Leaves of Blackberry, Raspberry, and

Strawberry Varies with Cultivar and Developmental Stage. J. Agric. Food Chem. 48, 140–146. https://doi.org/10.1021/jf9908345

Workman, J., Shenk, J., 2004. Understanding and using the near-infrared spectrum as an analytical method. Near-infrared Spectrosc.

Yoon, S., Park, B., Lawrence, K., Windham, W., 2011. Line-scan hyperspectral imaging system for real-time inspection of poultry carcasses with fecal material and ingesta. Electron. ….

ZAPATA, S., DUFOUR, J. -P, 1992. Ascorbic, Dehydroascorbic and Isoascorbic Acid Simultaneous Determinations by Reverse Phase Ion Interaction HPLC. J. Food Sci. 57, 506–511. https://doi.org/10.1111/j.1365-2621.1992.tb05527.x

Chapter 7

POTENTIALITY OF VIS-NIR SPECTROSCOPY FOR THE SHELF LIFE PREDICTION OF ROCKET LEAVES (*Diplotaxis tenufolia*) BASED ON RAW MATERIAL QUALITY

Muahmmad M.A. Chaudhry[a], Maria L. Amodio[a], José M. Amigo Rubio[b], Maria L. V. de Chiara[a], Farahmand Babellahi[a], Giancarlo Colelli[a]

[a] Dip.to di Scienze Agrarie, degli Alimenti e dell'Ambiente, Universita di Foggia, Via Napoli, 25, 71122 Foggia (Italy)

[b] Dept. of Food Science (KU-FOOD), Chemometrics and Analytical Technologies CAT. Faculty of Sciences, University of Copenhagen, Rolighedsvej 30, DK 1958Frederiksberg C. (Denmark)

* Corresponding author: marialuisa.amodio@unifg.it

Abstract

The potentiality of the Vis-NIR hyperspectral imaging for the prediction of the rocket raw material shelf-life was investigated along with the identification of the reference parameters contributing significantly towards shelf life estimation. Hyperspectral images in the range of 400-750nm were acquired for five different rocket raw materials were acquired followed by extraction of the spectral profiles. Partial least squares regression (PLSR) models were developed for correlating the initial spectral response of the raw materials to the marketability limit as assessed by sensorial evaluation. PLSR models were also developed for the prediction of shelf-life by establishing a correlation between the initial reference analysis and the shelf-life for each rocket raw material. Principle component analysis (PCA) was used for exploration of the reference analysis variables with the first 2 PCs explaining 70.13% of the total variance in the data. PLSR models were developed for the selected reference analysis variables resulting from the PCA model loading weights. The PLSR models in this case resulted in an R^2_{cal} of 0.83 accompanied by RMSEC of 0.51 days and an R^2_{cv} of 0.79 with RMSECV of 0.57 days. In case of the spectral based PLSR calibration models the potential shelf life of the rocket raw materials was predicted yielding an R^2_{cal} of 0.99 and R^2_{cv} of 0.99 followed by RMSEC and RMSECV of 0.10 days and 0.11 days,

respectively. Hence it was concluded that the spectral profiles are a more reliable tool for the prediction of the potential shelf-life of different rocket raw materials as compared to reference analysis variables.
Keywords: raw material, shelf-life, PLSR, prediction, hyperspectral

1. INTRODUCTION

Minimally processed ready to eat foods have demonstrated a significant increase in terms of consumption in the last decades. The rising demand of these food products is a corollary to the consumer concern regarding fresh, convenient, nutritive, appetizing and healthy food products (Ma et al., 2017).

Rocket leaves (*Diplotaxis tenuifolia*) have gained significant popularity particularly in the Mediterranean countries, due to their pungent smell and strong flavor and are usually preferred by consumers in their diet since they are a rich source of health promoting phytonutrients such as flavonoids, fiber, vitamin C and glucosinolates (Martínez-Sánchez et al., 2006; Amodio et al., 2016). After minimal processing steps such as washing and drying, rocket leaves are found on the retail stores in modified atmosphere packages (MAP). Due to minimal processing they are also prone to rapid degradation. The degradation symptoms appear in the form of yellowing resulting from the degradation of chlorophyll, wilting due to water loss, off-odor production and degradation of flavor related volatile compounds (Koukounaras et al., 2009; Nielsen et al., 2008; Mastrandrea et al., 2017). A number of factors including raw material quality, handling, processing steps and storage temperature significantly impact the shelf life of rocket leaves which generally ranges between 7 to 14 days (Toivonen and Brummell, 2008).

The consumer criteria for the selection of rocket leaves at retail stores includes fresh like appearance and green color while development of the consumer trust regarding repurchasing, relies on the quality of the product during consumption which is usually attributed to color, texture and flavor (Løkke et al., 2012; Barrett et al., 2010). Particularly, the shelf life is the time span during which the produce retains freshness and is saleable to the ultimate consumer. It is a critical phenomenon in the fresh cut industry since from the potential shelf-life depends on the possibility of an easy distribution of the product and its general salability, also in consideration of the fact that commercial agreement with

distributors very often ensure that unmarketable products are sorted out prior to the processing stage. Various techniques have been used in different research works for the estimation and monitoring of the shelf life of rocket leaves using various pretreatments of raw materials and storage conditions, and evaluating the effect of the relevant parameters on the ultimate shelf life of the rocket leaves (Koukounaras et al., 2006; Martínez-Sánchez et al., 2006; Kalio, 2008). Recent studies have also considered raw material quality in relation to the ultimate quality of the stored rocket leaves. Edelenbos et al., 2017 demonstrated that the quality of the packaged rocket leaves varied between different growing seasons recommending low temperature storage for the color maintenance and shorter storage time spans for texture retention. In a study conducted by Martínez-Sánchez et al., 2006 the rocket leaves stored in air were compared to those in controlled atmosphere storage over a time span of 14 days and it was concluded that the rocket leaves stored in air lost the sensory and microbiological attributes for commecial distribution while out of a total of three controlled atmophere storage conditions the rocket leaves stored 5 kPa O_2 + 10 kPa CO_2 maintained the visual quality and microbiological quality traits. On the other hand, Amodio et al., 2015 worked with the development of non-linear models for the prediciton of the shelf life of rocket leaves. In this case the temperature dependence of the various sensorial, chemical and physical parameters of the rocket leaves were studied fitting the experimental data over time. Weibullian model was compared with the traditional zero and first order kinetics concluding that the Weibull-log logistic model best described the quality variaiton in fresh rocket leaves. It was also recommended that the limitinig factor for shelf life significantly varied with respect to the temperature of storage as well as the thermal history of the product.

Various multivariate approaches have also been applied for the estimation of the shelf life of the fresh-cut produce including accelerated shelf life testing approach for as apples (M.L. Amodio et al., 2015), lettuce (Derossi et al., 2016), melons (Amodio et al., 2012) , also using non-linear modelling used on fresh-cut melons (Amodio et al., 2013), and rocket leaves (Amodio et al., 2015) and monitoring of volatile organic compounds for shelf life monitoring of rocket leaves (Spadafora et al., 2018).

Chaudhry et al., 2018 used hyperspectral imaging accompnied by MALST approch for the estimation

of th shelf life of fresh-cut rocket leaves using the time related principle components (PCs) and latent variables (LVs) and the cut-off criteria formulated resulted in the shelif life estimation of 9.4, 4.5 and 3.3 days for the rocket leaves stored at respective temperatures.

All the available studies, predict shelf-life based on storage data fitting, but none of the them have attempted to predict the shelf life only based on raw material quality, as requested from both processor and distributors. Since the processors and producers interact with the raw material at the reception points of the processing plants and it is imperative to formulate a methodology to predict the shelf life of the raw materials based on quality.

The objective of this study was to predict potential shelf-life of different rocket raw material using two alternative approaches; firstly, characterizing produce quality and defining critical quality parameters for shelf-life prediction, secondly, using hyperspectral images and multivariate approach to formulate shelf-life prediciton models.

2. MATERIALS AND METHODS

2.1 Experimental design and spectral acquisition

Minimally processed rocket leaves (*Diplotaxis tenuifolia*) were received in the postharvest laboratory of University of Foggia from different harvest seasons over a time span of two years. Immediately after recieveing, the rocket leaves were transferred to a storage room at 5°C. Plastic clamshells were used to package 100 grams (g) of representative rocket samples (10 replicates for each raw material upon arrival) followed by storage at 5°C in plastic continers with humidified air flow circulation. Hyperspectral images of all the replicates were taken on the initial day of storage along with other quality parameters and over the storage life which ranged from approximately 5-12 days depending on the initial quality of the raw materials and the season of harvest. Each replicate acquired comprised of a minimum of twenty leaves in a single image.

For the hyperspectral image acquisition, a hyperspectral line scan scanner (Version 1.4, DV srl, Padova, Italy) equipped with a spectrograph, in the visible- near infrared (Vis-NIR) range of 400-1000 nm with a spatial resolution of 1000x2000 pixels and a spectral resolution of 5nm was used with the leaves of each image, producing one spectrum per replicate. The mean spectrum was extracted by thresholding the image to find the best contrast between the object of interest and the

background. The initial 10 spectra of the 5 different raw materials (RM) named RM1: summer 2017, RM2: summer 2017, RM3: autumn 2017, RM4: spring 2018 and RM5: summer 2018, were aquired resulting in the formulaiton of a spectral dataset of 50 samples x 71 variables with quality traits differing from raw material to raw material

2.2 Sensorial and Physico-Chemical Analysis

2.2.1 Sensory analysis

Sensory evaluation for the rocket leaves was done by a panel of experts for assessing changes in appearance, including color, freshness, and dehydration, over the entire storage span on a scale from 1 to 5. In case of appearance scores (Amodio et al., 2015), rocket leaves with uniform dark green color with fresh and turgid appearance were given score 5, fresh rocket leaves with a slight loss of turgidity obtained an appearance score of 4, rocket leaves with a significant loss of turgidity and an apparent loss of color (marketability limit) were set at an appearance score of 3, leaves with significant senescence with the passage of storage time having wrinkled and yellowish blades received an appearance score of 2 and the spoiled rocket leaves with severe wilting, significant yellowing and decay symptoms were given a score value of 1.

2.2.2 Soluble solids content, titratable acidity, and pH

Soluble solids content (SSC) was measured on homogenized samples diluted with water using a digital hand refractometer (Atago, Japan). One gram of puree was then used to measure the pH, with an automatic titrator (T50 M Terminal, Mettler Toledo, Switzerland).

2.2.3 Determination of the microbial load

For microbiological enumeration, five grams of rocket leaves from each replicate was weighted, diluted (1:10) with 45 ml of saline solution (NaCl 8.6 g L^{-1}), and homogenized in a blender (Bag Mixer, Interscience, Saint-Nom-la-Bretéche, France) for 2 minutes. Then, samples were submitted to tenfold serial dilution. Mesophilic microorganism were enumerated by plate counting on Plate Count Agar (PCA) and incubated at 25 °C for 48 h. Yeasts and moulds were plated on Potato Dextrose Agar (PDA) (Oxoid) added with chloramphenicol (100 mg L^{-1}) and incubated at 30 °C for 48 h.

2.2.4 Ammonia determination

The determination of ammonia was done using a colorimetric method (Nason and WHITTEN, 1970) using a Shimadzu UV-1700 PharmaSpec spectrophotometer. 4 g of rocket leaves were cut and then frozen at a -80 °C until analysis. Tissue was homogenized with 20mL distilled water for 1 min, and a 0.5 mL aliquot was centrifuged for 10 min at 14000 g at 5 °C. A 0.5 mL was added to a solution of nitroprusside with phenol and alkaline hypochlorite in a reaction mixture which was incubated at 37 °C for 15 min; color development was measured at 635nm. Ammonium sulfate was used as a standard.

2.2.5 Chlorophyll determination

1 g of frozen rocket leaf samples were weighed into 25 mL of methanol and kept in the dark for 24 hours at room temperature. 15mL methanol was then added and kept for another 24 hours and repetead until no green pigments were found on the leaves. The extracts were then separated and the absorbance was read at resolution of 1 nm using Shimadzu UV-1700 spectrophotometer. Chlorophyll was determined as the maximum absorbance at 666nm, 653 nm and 470 nm and the amount of pigments were calculated for chlorophyll a, chlorophyll b and total chlorophyll according to the methods of (Wellburn, 1994).

2.2.6 Firmness determination

The texture variations among the initial replicates of the different raw materials were determined on five grams of leaves with an Instron Universal Testing Machine (model 3340), equipped with a Kramer cell. The leaves were placed in the Kramer shear cell equipped with 5 blades and extruded with the crosshead at a speed of 50 mm min-1. Texture was measured as the maximum peak force and expressed in Newton (N).

2.3 Multivariate analysis

A principle component analysis (PCA) was done to explore the relationship between the reference variables. On the other hand, partial least squares regression (PLSR) modelling was used for the shelf life prediction of the different rocket raw materials under study using two different approaches. Firstly, PSLR was applied to the reference analysis data as variables against the marketability limit to achieve a shelf life prediction and secondly, spectral profiles of each raw material were used as

variables under study for the shelf life prediciton based on marketability limit. The model reliability was accessed by the values of R^2 in calibration and R^2 in cross validation and also by the root mean square errors in calibration and cross validation. PCA and PLSR modlelling was conducted using PLS toolbox (version 7.5.2) supported by MATLAB 2015a (version 8.5.0.197.613).

3. RESULTS AND DISCUSSION

3.1 Raw material characterization

Figure 1 shows the mean values of the different reference analysis conducted for five different rocket raw materials on the initial 10 replicates for each. It can be clearly observed that the values of the reference analysis for the five different raw materials vary since the raw materials are not of the same quality neither they come from the same season of harvest.

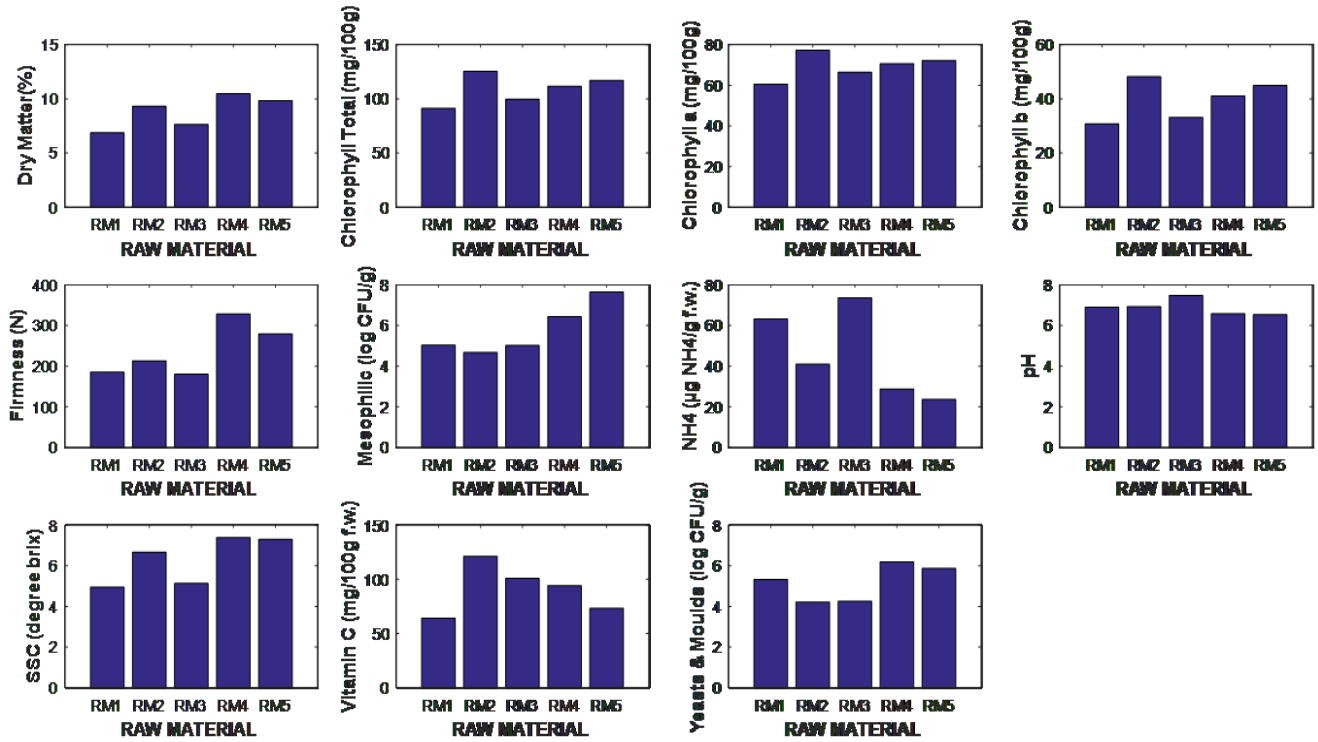

Figure 1. Mean vales of the reference analysis for raw material 1 (RM1), RM2, RM3, RM4 and RM5

Figure 2 shows the preprocessed spectra in the Vis-NIR range (400-750nm) of the rocket raw materials with 2a depicting the preprocessed spectral data and 2b representing the mean preprocessed spectra of

the 5 differrent raw materials. The Vis-NIR peaks correspond to the color related properties of rocket leaves as affected by chlorophyll *a*, chlorophyll *b* and β-carotene (Chaudhry et al., 2018). In case of the Vis-NIR spectral range, the characteristic reflectance spectra of the rocket leaves result from the leaf biochemical compounds such as chlorophyll, anthocyanins, carotenoids, water and cellulose. In case of green leafy vegetables, the interaction between the plant leaves and electromagnetic radiation yields reflectance spectra in the Vis-NIR region which are mainly representative of the photosynthetic pigments such as chlorophyll and carotenoids (Mohd Asaari et al., 2018). Visually, a green plant spectral curve can be observed in the raw spectra with 550 nm reflectance peak and 680 nm absorbance peak caused by chlorophyll, a major color related pigment (Kong et al., 2016). Approximately around 700 nm, the reflectance signal in case of the leaves depicts a sharp rise of around 40–50% which is a result of the scattering of light with the leaf cell structure, mainly within the mesophyll (Mishra et al., 2017).

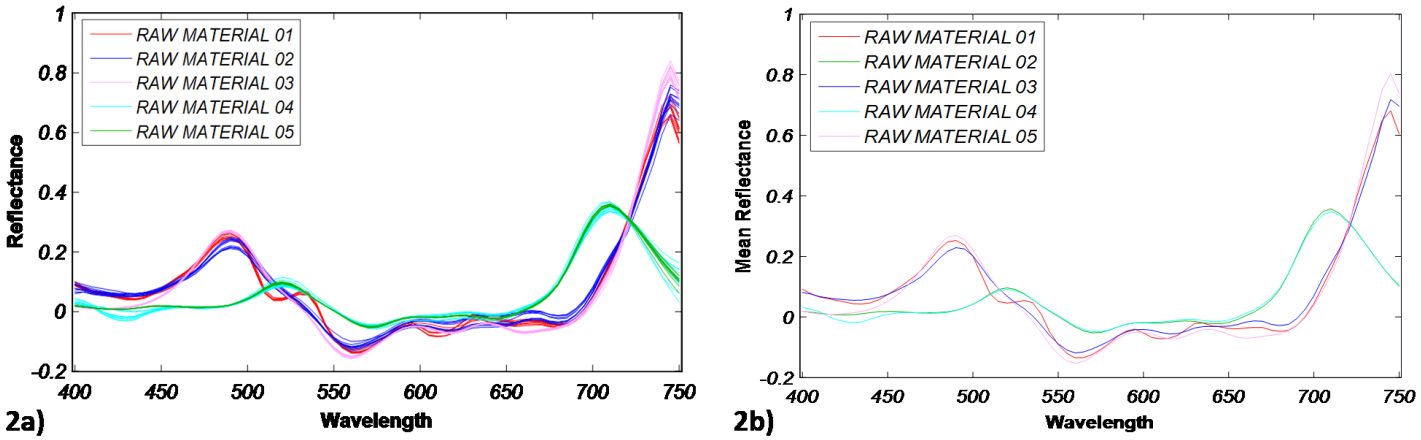

Figure 2. a) Preprocessed spectra (SNV+1st Derivative) for RAW MATERIAL(RM) in the Vis-NIR range (400-750nm) b) mean spetra for each RM in the Vis NIR range (400-750nm)

The PCA model for the quality reference parameters yielded 78.23% of total variance with 3 PCs; the first PC accounting for 47.30% while the second and third PCs explained 22.83% and 8.10% of the total variance, respectively. The loadings from the PCA model were used for the selection of the most significant variables portraying differences among the raw materials and contributing towards describing shelf life. Prior to conducting the PCA, the data were autoscaled.

After the variable selection based on the loading weights the PCA model was reduced to 6 variables, namely, mesophilic bacteria, yeasts and moulds, pH, SSC, chlorophyll b and dry matter (DM). In this

case with a dataset containing 50 samples and 6 variables a second PCA model was formulated resulting in 2 PCs with the first PC explaining 63.58% and the second PC explaining 18.74% of the total variance in the data as shown in figure 3.Figure 3a shows the scores/loadings bi-plot and figure 3b shows the loadings for the variables. As can be seen in the loadings plot, mesophilic bacteria and yeasts and moulds hold significant weights; it has been revealed by the previous studies that fresh-cut produce possess a neutral pH, and are a rich source of sugars and phytochemicals which are prone to be metabolized by bacteria hence these foods are an ideal media for microbial growth if handeled incorrectly (Rico et al., 2007).

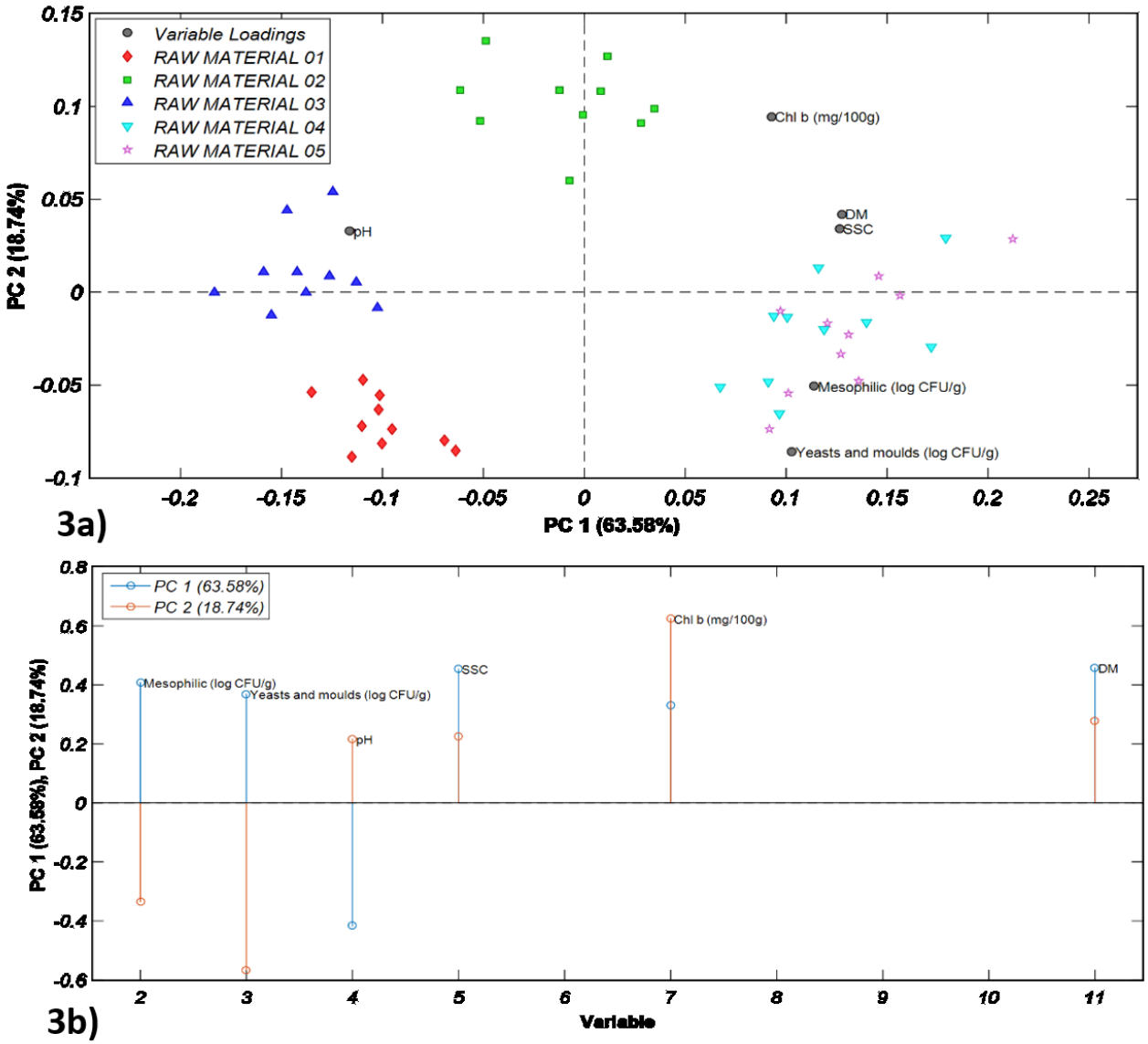

Figure 3. a) Scores/loadings bi-plot for PC1 and PC2 for reduced variables b) Loadings plot for PCA model for reduced variables

On the PC1 axis DM and SSC were among the most significant variables in the positive direction while in the negitive region pH was noteworthy. On the other hand in case of the PC2 axis chlorophyll b and yeasts and moulds carried greater significance in the positive and negative regions respectively. As per the sensorial analysis by a panel of experts the shelf life of the rocket leaves was determined for each raw material plotting the visual scores against the days of storage (data not shown) until they reach the

marketability limit (score value of 3). In this case RM1 and RM2 took 9.4 and 9.3 days respectively to reach the marketablity limit. RM3, RM4 and RM5 showed a shorter storability with a shelf-life of 8, 6.9 and 6.3 days, respectively. The initial quality of the raw materials in this study can be compared to those of Martínez-Sánchez et al., 2006a which showed high initial mesophilic load of 5.35 log CFU g^{-1} whereas for the yeasts and moulds RM4 and RM5 showed significantly higher values as comapred to the latter. Moreover, RM4 and RM5 also showed a significantly higher mesophilic load as compared to the other raw materials which can be contributing factor for lower storability for RM4 and RM5. Ferrante et al., 2004 studied the shelf life of rocket leaves and demonstrated that fresh-cut rocket leaves possess a short shelf life in which case the leaf yellowing initiates within 4 to 8 days of storage even at lower storage temperatures i.e. 5 °C. Spadafora et al., 2016 revealed that the leaves stored at three different temperatures showed slight increase in the microbial loads till day 6 of storage; but it is important to note that the initial microbial count was significantly lower ~1.2 log CFU g^{-1} as compared to those of present study. Moreover, the differences between the mesophilic count and yeasts and moulds for the RM1, RM2, RM3, RM4 and RM5 can also be due to the fact that the season of growth for all raw materials is different since Yahya et al., 2019 demonstrated that the bacterial loads of summer produce is higher compared to winter produce.

3.2 Shelf-life prediction

For the prediction of the shelf life based on the initial reference analysis of the five different raw materials, PLSR models were developed (Table 1).

Table 1. Calibration statistics for the PLSR models developed for the shelf life prediction of rocket raw materials

PLSR models based on reference analysis (50 samples x 6 variables)							
Parameter	Pretreatment	No. of vars	LVs	R^2_{cal}	RMSEC	R^2_{cv}	RMSECV
Prediction of shelf life	Auto-scaling	6	3	0.83	0.51	0.79	0.57
PLSR models based on Vis-NIR spectra in the range of 400-750nm (50 samples x 71 variables)							
Prediction of shelf life	Log(1/R) + SNV + mean centering	71	6	0.99	0.10	0.99	0.11

The dataset utilized for the PLSR model based on the reference analysis results comprised of 50 samples and 6 variables. Accuracy of the model was evaluated based on the coefficient of determination in calibration (R^2_{cal}), coefficient of determination in cross validation (R^2_{cv}), root mean square error of calibration (RMSEC) and root mean square error of cross validation (RMSECV). The PLSR model for the prediction of the shelf life contained three latent variables (LVs) with the first LV explaining 62.80% of the co-variance in the data while the second and third LVs explained 14.18% and 11.97% of the co-variance , respectively. Figure 4a demonstrates the calibration plot for the PLSR model debveloped while figure 4b shows the loadings plot for the variables included in the PLSR model.

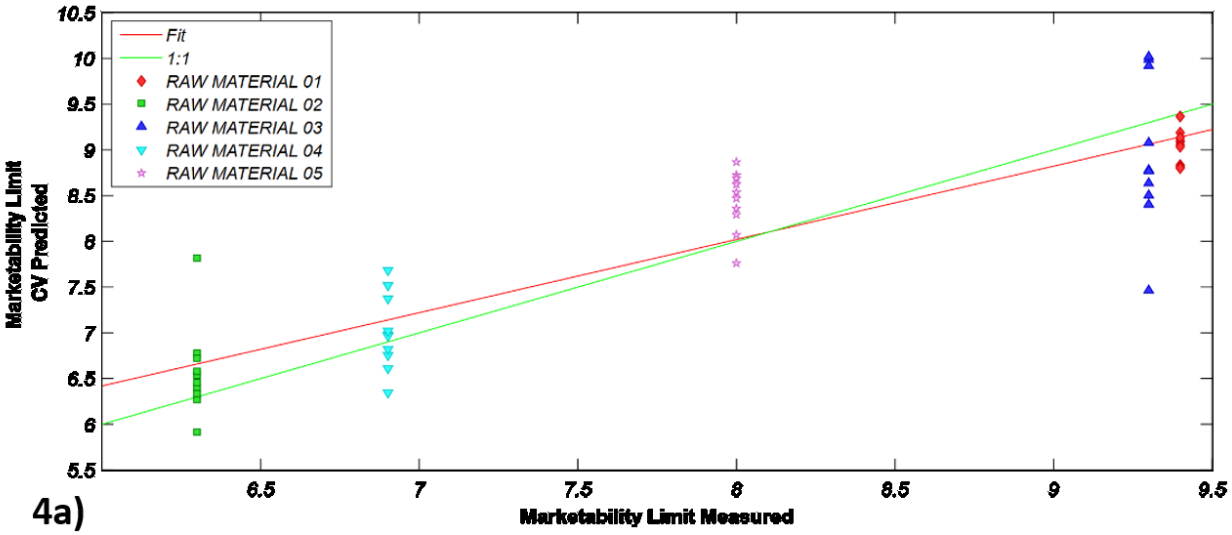

4a)

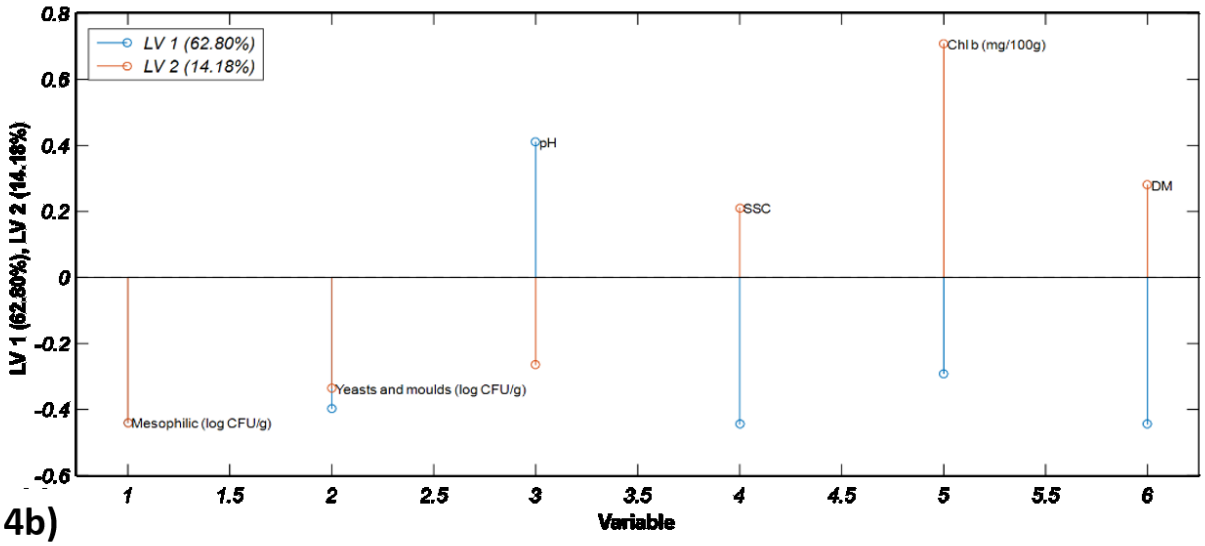

4b)

Figure 4. a) Calibration plot for tshelf-life measured vs shelf-life predicted b) Loadings plot of LV1 and LV2 for the variables involved in the PLSR model

As for prediction based on spectral data, after preprocessing (transformation from reflectance to absorbance+ SNV+mean centering) the PLSR model resulted in a significant difference as compared to the one formulated based on the reference values. In this case the model contained six LVs with the first LV explained already 96.28% of the co-variance in the data followed by the second LVs explaining 2.81% of the co-variance. The model accuracy was accessed by the R^2_{cal} which was 0.99 accompnied by RMSEC of 0.10 days followed by an R^2_{cv} of 0.99 with a RMSECV of 0.11 days (Table 1). Figure 5a and 5b depicts the calibraiton plot and the loading plots, respectively for the spectral based PLSR model.

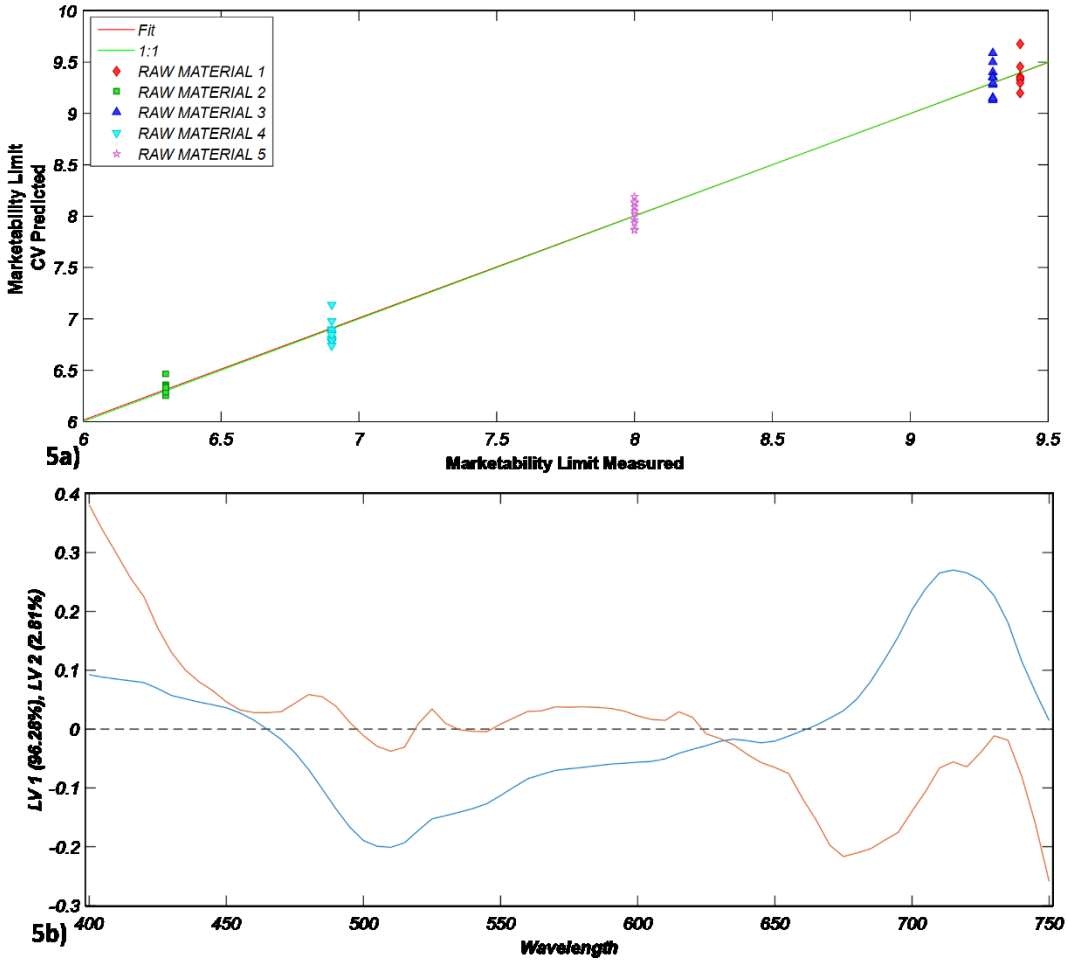

Figure 5. a) Calibration plot for the marketability limit measured vs marketability limit

predicted based on spectral profiles b) Loadings plot of LV1 and LV2 for the for the included wavelength range

Shelf life determination based on the spectral profiles in the Vis-NIR region has been attempted in a recent work by Chaudhry et al., 2018 (refer to Chapter 4),but in this case authors applied a Multivariate Accelerated Shelf Life Test (MASLT) collecting spectral profiles over the storage period of rocket stored at 3 different temperatures. The authors reported a shelf life of 9.4 days at 5 °C, with root mean square errors of 1.32 and 1.48 in calibration and cross validation, using a spectral range from 400-800 nm, but in this case the shelf life estimaiton was possible only by modeling storage data and the study did not compare different raw materials. On the other hand, similar results for the shelf life were found by M. L. Amodio et al., 2015 using weibull models where the shelf life for the rocket leaves stored at 5 ºC was estimated to be 5.8 days. To our knowledge, none of the studies have based shelf-life predicion only on raw material quality. Comparing both PLSR models in this study, i.e. the reference analysis based PLSR and the spectral based PLSR model, it can be observed that the RMSEC and RMSECV in of spectral based PSLR model is quite low hence proving that spectral informaiton of the raw materials can be a useful tool for the prediciton of potential shelf life of the raw material under consideration. Moreover, the accuracy of the spectral based PLSR model can be enhanced by using a greater number of samples from various seasons and harvest times.

4. CONCLUSIONS

For the first time a multivariate approach has been implemented for the prediction of the potential shelf-life of rocket leaves based on the raw material quality. The most significant quality variables contributing towards shelf life of the raw materials were mesophilic count, yeasts and moulds, pH, SSC, chlorophyll b and DM. PLSR models using these reference variables resulted in adequate shelf life prediction based on raw material quality. Moreover, a secondary approach using the spectral profiles of different raw materials was also used for the prediction of shelf-life potential implementing PLSR modelling which yielded a reliable prediction error of about 0.1 day. These results would be very important both for the producers and processors for making logistic decisions and ensuring product quality along all the market chain.

REFERENCES

Amodio, M.L., Derossi, A., Colelli, G., 2013. Modelling sensorial and nutritional changes to better define quality and shelf life of fresh-cut melons. J. Agric. Eng. 43, 6. https://doi.org/10.4081/jae.2013.e6

Amodio, M. L., Derossi, A., Mastrandrea, L., Colelli, G., 2015. A study of the estimated shelf life of fresh rocket using a non-linear model. J. Food Eng. 150, 19–28. https://doi.org/10.1016/j.jfoodeng.2014.10.030

Amodio, M.L., Dollo, L., Colantuono, F., Colelli, G., 2015. DEGRADATION PATTERNS FOR EXTERNAL AND INTERNAL QUALITY ATTRIBUTES OF FRESH-CUT APPLES. Acta Hortic. 175–182. https://doi.org/10.17660/ActaHortic.2015.1091.21

Amodio, M.L., Dollo, L., Rinaldi, R., Colelli, G., 2012. DEGRADATION PATTERNS FOR EXTERNAL AND NUTRITIONAL QUALITY PARAMETERS OF FRESH-CUT "CANTALOUPE" MELONS. Acta Hortic. 641–647. https://doi.org/10.17660/ActaHortic.2012.934.85

Amodio, M.L., Ferrante, A., Rogers, H., Colelli, G., 2016. A QUAFETY approach to quality monitoring and prediction for fresh-cut produce, in: Acta Horticulturae. pp. 1–12. https://doi.org/10.17660/ActaHortic.2016.1141.1

Barrett, D.M., Beaulieu, J.C., Shewfelt, R., 2010. Color, Flavor, Texture, and Nutritional Quality of Fresh-Cut Fruits and Vegetables: Desirable Levels, Instrumental and Sensory Measurement, and the Effects of Processing. Crit. Rev. Food Sci. Nutr. 50, 369–389. https://doi.org/10.1080/10408391003626322

Chaudhry, M.M.A., Amodio, M.L., Babellahi, F., de Chiara, M.L.V., Amigo Rubio, J.M., Colelli, G., 2018a. Hyperspectral imaging and multivariate accelerated shelf life testing (MASLT) approach for determining shelf life of rocket leaves. J. Food Eng. 238, 122–133. https://doi.org/10.1016/j.jfoodeng.2018.06.017

Chaudhry, M.M.A., Amodio, M.L., Babellahi, F., de Chiara, M.L.V., Amigo Rubio, J.M., Colelli, G., 2018b. Hyperspectral imaging and multivariate accelerated shelf life testing (MASLT) approach for determining shelf life of rocket leaves. J. Food Eng. 238, 122–133. https://doi.org/10.1016/j.jfoodeng.2018.06.017

Derossi, A., Mastrandrea, L., Amodio, M.L., De Chiara, M.L.V., Colelli, G., 2016. Application of multivariate accelerated test for the shelf life estimation of fresh-cut lettuce. J. Food Eng. 169, 122–130. https://doi.org/10.1016/j.jfoodeng.2015.08.010

Edelenbos, M., Løkke, M.M., Seefeldt, H.F., 2017. Seasonal variation in color and texture of packaged wild rocket (Diplotaxis tenuifolia L.). Food Packag. Shelf Life 14, 46–51. https://doi.org/10.1016/j.fpsl.2017.08.005

Ferrante, A., Incrocci, L., Maggini, R., Serra, G., Tognoni, F., 2004. Colour changes of fresh-cut leafy vegetables during storage, Agriculture & Environment.

Kalio, H., 2008. The effect of film wrapping and nitrogen flushing of produce atmosphere on the storage quality of lettuce. Agric. J.

Kong, W., Liu, F., Zhang, C., Zhang, J., Feng, H., 2016. Non-destructive determination of Malondialdehyde (MDA) distribution in oilseed rape leaves by laboratory scale NIR hyperspectral imaging. Sci. Rep. 6. https://doi.org/10.1038/srep35393

Koukounaras, A., Siomos, A.S., Sfakiotakis, E., 2009. Impact of heat treatment on ethylene production and yellowing of modified atmosphere packaged rocket leaves. Postharvest Biol. Technol. 54, 172–176. https://doi.org/10.1016/J.POSTHARVBIO.2009.07.002

Koukounaras, A., Siomos, A.S., Sfakiotakis, E., 2006. 1-Methylcyclopropene prevents ethylene induced yellowing of rocket leaves. Postharvest Biol. Technol. 41, 109–111. https://doi.org/10.1016/J.POSTHARVBIO.2006.01.018

Løkke, M.M., Seefeldt, H.F., Edelenbos, M., 2012. Freshness and sensory quality of packaged wild rocket. Postharvest Biol. Technol. 73, 99–106. https://doi.org/10.1016/J.POSTHARVBIO.2012.06.004

Ma, L., Zhang, M., Bhandari, B., Gao, Z., 2017. Recent developments in novel shelf life extension technologies of fresh-cut fruits and vegetables. Trends Food Sci. Technol. 64, 23–38. https://doi.org/10.1016/J.TIFS.2017.03.005

Martínez-Sánchez, A., Allende, A., Bennett, R.N., Ferreres, F., Gil, M.I., 2006a. Microbial, nutritional and sensory quality of rocket leaves as affected by different sanitizers. Postharvest Biol. Technol. 42, 86–97. https://doi.org/10.1016/J.POSTHARVBIO.2006.05.010

Martínez-Sánchez, A., Marín, A., Llorach, R., Ferreres, F., Gil, M.I., 2006b. Controlled atmosphere preserves quality and phytonutrients in wild rocket (Diplotaxis tenuifolia). Postharvest Biol. Technol. 40, 26–33. https://doi.org/10.1016/J.POSTHARVBIO.2005.12.015

Mastrandrea, L., Amodio, M.L., Pati, S., Colelli, G., 2017. Effect of modified atmosphere packaging and temperature abuse on flavor related volatile compounds of rocket leaves (Diplotaxis tenuifolia L.). J. Food Sci. Technol. 54, 2433–2442. https://doi.org/10.1007/s13197-017-2685-6

Mishra, P., Shahrimie, M., Asaari, M., Herrero-Langreo, A., Lohumi, S., En Diezma, B., Scheunders, P., 2017. Close range hyperspectral imaging of plants: A review. Biosyst. Eng. 164, 49–67. https://doi.org/10.1016/j.biosystemseng.2017.09.009

Mohd Asaari, M.S., Mishra, P., Mertens, S., Dhondt, S., Inzé, D., Wuyts, N., Scheunders, P., 2018. Close-range hyperspectral image analysis for the early detection of stress responses in individual plants in a high-throughput phenotyping platform. ISPRS J. Photogramm. Remote Sens. 138, 121–138. https://doi.org/10.1016/j.isprsjprs.2018.02.003

Nason, A., WHITTEN, B.K., 1970. Analytical biochemistry., Analytical Biochemistry. [Elsevier, etc.].

Nielsen, T., Bergström, B., Borch, E., 2008. The origin of off-odours in packaged rucola (Eruca sativa). Food Chem. 110, 96–105. https://doi.org/10.1016/J.FOODCHEM.2008.01.063

Rico, D., Martín-Diana, A.B., Barat, J.M., Barry-Ryan, C., 2007. Extending and measuring the quality of fresh-cut fruit and vegetables: a review. Trends Food Sci. Technol. 18, 373–386. https://doi.org/10.1016/j.tifs.2007.03.011

Spadafora, N.D., Amaro, A.L., Pereira, M.J., Müller, C.T., Pintado, M., Rogers, H.J., 2016. Multi-trait analysis of post-harvest storage in rocket salad (Diplotaxis tenuifolia) links sensorial, volatile and nutritional data. Food Chem. 211, 114–123. https://doi.org/10.1016/j.foodchem.2016.04.107

Spadafora, N.D., Cammarisano, L., Rogers, H.J., Müller, C.T., 2018. Using volatile organic compounds to monitor shelf-life in rocket salad. Acta Hortic. 1299–1306. https://doi.org/10.17660/ActaHortic.2018.1194.183

Toivonen, P.M.A., Brummell, D.A., 2008. Biochemical bases of appearance and texture changes in fresh-cut fruit and vegetables. Postharvest Biol. Technol. 48, 1–14. https://doi.org/10.1016/J.POSTHARVBIO.2007.09.004

Wellburn, A.R., 1994. The Spectral Determination of Chlorophylls a and b, as well as Total Carotenoids, Using Various Solvents with Spectrophotometers of Different Resolution. J. Plant Physiol. 144, 307–313. https://doi.org/10.1016/S0176-1617(11)81192-2

Yahya, H.N., Lignou, S., Wagstaff, C., Bell, L., 2019. Changes in bacterial loads, gas composition, volatile organic compounds, and glucosinolates of fresh bagged Ready-To-Eat rocket under different shelf life treatment scenarios. Postharvest Biol. Technol. 148, 107–119. https://doi.org/10.1016/J.POSTHARVBIO.2018.10.021

GENERAL CONCLUSIONS

For the first time a multivariate approach using the spectral fingerprints for the estimation of the shelf life of fresh cut rockets was used. The changes in the spectra with the passage of storage time for the samples stored at three different temperatures served as the property under study. Comparing the MASLT approach with the conventional ASLT methods the use of PCA yielded valuable information regarding the variables contributing towards the weight in the model and accounting for the quality losses of the product. It was highlighted that the wavelength ranges of 550-700nm held great significance while estimating shelf life based on appearance scores. The conventional MASLT approach using the PC scores was also compared with a new method using PLS and LV for the development of the kinetic or shelf life charts. Comparing both the approaches it was concluded that no significant difference exists between the results yielded by both the techniques. On the other side, the PLS model can be more robust as compared to a PCA model with the allowance of new samples to be added in the calibration and can serve as a tool for better validation. MASLT approach with PLS can enable the processors to better estimate the shelf life of their products and access the market with better product quality by improving the logistics.

The potential application of spectral fingerprints and hyperspectral images in the NIR region, together with multivariate data analysis, has proven the potential to predict and map phytonutrients in fresh cut rocket leaves, provided that predicted values are included in the calibration range. A new method was, in fact, developed in order to overcome the prediction error due to the unavoidable process of using average spectra for the calibration model and individual pixels for the image prediction. It was shown that the number of pixels detected within the calibration range decreased with the passage of storage time with a simultaneous increase in the pixels below the calibration range hence reducing the capability of the PLSR model to predict the corresponding phytonutrient. In this way, hyperspectral images revealed that the central part of the leaves lose vitamin C content faster as compared to the leaf edges or in other words the vitamin C starts degrading from the center of the leaf. Furthermore, the PLSR models in this case were very sensitive to the number of samples and their performance can be further enhanced with increasing the number of the samples in the calibration sets. Conclusively, NIR combined with hyperspectral imaging can be a very informative tool for studying the changes in the phytonutrient content during storage.

The future research perspectives in the domain of non-destructive analysis should be focused on simplifying the existing models by reducing the number of variables (hence orienting the hyperspectral imaging to multispectral imaging) to facilitate the industry for online implementation of the sorting systems on the basis of nutritional value and furthermore exploring the possibilities of employing these techniques for the development of new methods for nutritional compounds as has been proposed in Chapter 5 of the thesis.

Since the food industry is oriented towards acquiring simple, rapid, reliable and cost effective methods addressing their concerns regarding quality or origins of their products; it has been demonstrated by the research studies in this thesis that spectral information accompanied by multivariate and chemiometric methods possess the capability for the discrimination among the crops in accordance with the product history since each sample is comprised of a different fingerprint NIR spectrum which consists of a unique and characteristic pattern of radiation, hence suggesting that samples having similar spectra may be discriminated by other physically and/or chemically different samples. But for a reliable classification based on unsupervised or supervised classification methods the number of samples used to develop a discrimination model holds great significance. Therefore, it is imperative to have a dataset with a wide variability of samples for achieving a PLSDA or PCA model with utmost reliability.